THE RELATIONSHIP BETWEEN POROSITY AND THERMAL CONDUCTIVITY OF CONCRETE

A dissertation submitted in accordance with the requirements for the degree of

DOCTOR OF PHILOSOPHY

IN

CIVIL ENGINEERING

BY

Esmaiel Ganjian, B.Sc. (Hons.), M.Sc. (Eng.)

Department of Civil Engineering

The University of Leeds.

December 1990

UNIVERSITY LIBRARY LEEDS

A B S T R A C T

This thesis reports the details and results of an experimental study into the effect of porosity on the thermal conductivity of lightweight and normal-weight concretes. The concretes were made from either Pellite, limestone or quartzitic coarse aggregates, with or without air-entraining agent. Their density varied from 1550 to 2350 kg/m^3 and their porosity from 10 to 39 per cent.

The thermal conductivity of all the concretes was measured in accordance with B.S. 874: 1988, using a plain hot-plate technique and the total porosity and pore size distribution of each mix were determined using vacuum saturation and Mercury Intrusion Porosimetry.

Micromorphological changes were additionally assesed by:

a) using thermal analysis methods to monitor lime and non-evaporable water content of mortars and also to monitor the carbonation process by quantitative evaluation on mortar samples.

b) assessment of the depth of carbonation on concrete cubes.

c) using Scanning Electron Microscopy on coarse aggregates and mortar samples.

For characterization purposes, the experimental programme also involved studying the properties of fresh concrete, such as workability and air content and other engineering properties of hardened concretes, such as compressive strength.

The results obtained from the individual tests were statistically analysed using a standard 'Statistical Analysis System' (SAS) package. This enabled detailed examination of the relationship between the different properties to be assessed. Resulting from this, a model was developed which enabled the thermal cocductivity of a concrete to be estimated knowing its dry density,total porosity and median pore diameter.

The findings of this investigation confirm that in general, the thermal conductivity of concretes are directly related to density and inversely related to porosity and pore diameter and that density and total porosity have the highest coefficient of correlation respectively.

CONTENTS

		Page
Abstract		(II)
Table of Contents		(IV)
List of Tables		(IX)
List of Figures		(XI)
List of Plates		(XVII)
Acknowledgements		(IXX)
Abbreviations		(XX)

CHAPTER ONE :

INTRODUCTION

1.1	Applications of thermal properties in concrete structures	(1)
1.2	Objective and scope of the study	(4)

CHAPTER TWO :

REVIEW OF LITERATURE

2.1	Introduction to heat conduction and thermal conductivity of materials	(7)
2.2	Mechanisms of heat transfer in porous materials	(10)
2.3	Factors effecting the thermal conductivity of materials	(13)
	2.3.1 Density	(13)
	2.3.2 Moisture content	(15)
	2.3.3 Porosity and pore characteristics	(18)
	2.3.4 Mineral composition and solid structure	(24)
	2.3.5 Temperature	(26)
2.4	Determination of porosity	(28)
2.5	Theoretical models for determining the thermal conductivity of porous materials	(30)
2.6	Specific models for calculating the thermal conductivity of concrete	(38)
2.7	Mechanisms of moisture migration in moist specimens	(42)
2.8	Pores and porous structure of hydrated cement	(45)

CHAPTER THREE :

CHARACTERISTICS OF THE MATERIALS USED IN THE INVESTIGATION

3.1 Introduction (48)

3.2 Materials (49)

3.2.1 Cement (49)
3.2.2 Coarse aggregates (50)
3.2.3 Fine aggregate (51)
3.2.4 Admixture (51)

3.3 Laboratory preparation of aggregates (53)

CHAPTER FOUR :

MIX DESIGN AND CHARACTERISTICS OF FRESH CONCRETE

4.1 Introduction (55)

4.2 Selection of materials (56)

4.3 Mix design method (57)

4.4 Mixing, curing and conditioning (61)

4.5 Properties of fresh concrete (64)

4.5.1 Workability (64)
4.5.2 Air content (66)

CHAPTER FIVE :

THERMAL CONDUCTIVITY MEASUREMENT

5.1 Introduction (68)

5.1.1 Plain hot-plate apparatus (71)
5.1.2 Test procedure (79)

5.2 Calibration of plain hot-plate apparatus (81)

5.3 Preliminary investigations and results (84)

5.3.1 Investigation into surface contact problems (84)
5.3.2 Results and trends (88)

5.4 Tolerance of apparatus and experimental error (92)

5.5 Moisture correction factors (96)

5.5.1 Introduction (96)
5.5.2 Experimental procedure for moisture factor determination (99)
5.5.3 Results and trends of moisture factors (101)

CHAPTER SIX :

ENGINEERING AND MICROSTRUCTURAL TESTS OF MORTAR AND CONCRETE

6.1 Introduction (112)

6.2 Cube compressive strength (113)

6.3 Measurement of total porosity (114)

6.3.1 Vacuum saturation (114)

6.3.1.1 Apparatus (115)

6.3.1.2 Experimental procedure (116)

6.4 Pore size distribution measurement (119)

6.4.1 Mercury porosimetry method (120)

6.4.2 Mercury porosimetry apparatus (121)

6.4.3 Sources of error in mercury porosimetry (125)

6.4.4 Sample preparation and test procedure (125)

6.5 Microscopic observation (129)

6.5.1 Specimen preparation (129)

CHAPTER SEVEN :

DEGREE OF HYDRATION AND CARBONATION

7.1 Hydration of cement (130)

7.2 Thermal analysis methods (134)

7.2.1 A quantitative determination of calcium hydroxide content from TG results (135)

7.2.2 Determination of non-evaporable water (136)

7.3 Apparatus and procedure (139)

7.4 Carbonation (142)

7.4.1 Experimental methods to monitor carbonation (143)

CHAPTER EIGHT :

P R E S E N T A T I O N O F R E S U L T S

8.1 Introduction (145)

8.2 Thermal conductivity results for 'A' curing condition (145)

8.3 Pore size distribution and total porosity results using Mercury Intrusion Porosimetry (MIP) (147)

8.3.1 Repeatability of data (147)

8.3.2 MIP results (147)

8.4 Vacuum saturation results (166)

8.5 Thermogravimetry results (170)

8.6 Depth of carbonation results (172)

8.7 SEM results (173)

8.8 Compressive strength results (173)

CHAPTER NINE :

D I S C U S S I O N A N D A N A L Y S I S O F R E S U L T S

9.1 Thermal conductivity (175)

9.2 Mercury porosimetry (182)

9.2.1 Coarse aggregate (186)

9.3 Vacuum saturation (201)

9.4 Thermogravimetry (209)

9.5 Depth of carbonation (211)

9.6 Interpretation of SEM results (212)

9.7 Strength results (221)

9.8 Relationship between thermal conductivity and parameters studied (225)

9.9 Development of a model to predict thermal conductivity of concretes (236)

9.10 Validation of experimental models given in the literature (241)

CHAPTER TEN :

CONCLUSIONS AND RECOMMENDATIONS FOR FURTHER RESEARCH

10.1 Conclusions (244)

10.2 Recommendations for further research (251)

REFERENCES (253)

APPENDIX I Slabs mould (277)

APPENDIX II Foil-type thermocouples, construction and calibration (278)

APPENDIX III Selected thermal conductivity print-outs (282)

APPENDIX IV Selected TG and DTG's results (283)

APPENDIX V Cube compressive strength results (286)

LIST OF TABLES

Table		Page
2.1	Standard curve values published by Arnold	(14)
2.2	Jakob moisture factors	(17)
2.3	Typical values of thermal conductivity of concrete	(26)
3.1	Properties of Ordinary Portland Cement used	(49)
3.2	Oxide composition of Pelletised blast furnace slag	(51)
3.3	Sieve analysis for coarse aggregates	(54)
3.4	Sieve analysis for fine aggregates	(54)
4.1	Composition of mixes made	(59)
4.2	Mean dry density and total porosity of mixes made at 'A' curing condition	(60)
4.3	Summary of curing and conditioning regimes	(63)
4.4	Fresh properties of mixes	(67)
5.1	Summary results of surface contact methods	(88)
5.2	Comparison between B.S. 874: 1988 and achieved tolerances	(92)
5.3	Long term stability of plain-hot plate apparatus using Siporex specimens	(95)
5.4	Mix composition and bulk dry density of slab specimens selected	(99)
5.5	Thermal conductivity results	(102)
5.6	Regression equation relating λ to mc per cent by volume	(103)
5.7	Comparison of thermal conductivity value corrected to 3% moisture content by volume	(108)
5.8	Summary of thermal conductivity data corrected to 3% moisture content by volume	(110)
5.9	Summary of thermal conductivity data corrected to 5% moisture content by volume	(111)
8.1	Thermal conductivity of concrete specimens at 3% m.c. by volume	(146)

8.2 Summary of MIP results for mortars and coarse aggregates (149)

8.3 Results of vacuum saturation tests (166)

8.4 The degree of hydration and carbonation results for mortar mixes (170)

8.5 Results of the depth of carbonation for concretes (172)

8.6 Summary of cube compressive strength results for concretes (174)

9.1 Standard deviation of total porosity and median pore diameter for the eight mortar mixes which were cured successively in 'A' to 'E' curing conditions. (183)

9.2 Mean and standard deviation of successively cured mixes (202)

9.3 Comparison of calculated MIP and vacuum saturation porosities of concretes. (207)

9.4 Summary of thermal conductivity, dry density, porosity and median pore diameter results for concretes studied (232)

9.5 Comparison of experimental models in the literature (242)

V.I Cube compressive strength results for concretes (286)

LIST OF FIGURES

Figure		Page
2.1	Graph showing λ versus porosity at 100°C	(21)
2.2	Thermal conductivity of lightweight concrete in relation to temperature and moisture content by weight	(27)
2.3	Parallel and series arrangments	(31)
2.4	Combination of series and parallel model	(33)
2.5	Cubes model for calculating thermal conductivity of concrete by Method 2.	(39)
3.1	Photograph of typical Pellite aggregate	(52)
5.1	Photograph of inside hot plate showing layout of heating element	(73)
5.2	Photograph of cold plate showing reversing spiral circulation system on the left and flat surface of completed cold plate on the right	(73)
5.3	Diagram of plain Hot-plate Apparatus and typical thermocouple arrangements on specimen surfaces	(77)
5.4	Photograph of opened insulating cabinet	(78)
5.5	Photograph of the Hot-plate Apparatus and Insulating Cabinet with controlling equipment and the micro-computer	(78)
5.6	Heat loss vs. mean sample temperature for rig calibration using glass fibre slabs	(83)
5.7	Thermal conductivity vs. moisture content for different densities studied	(105)
5.8	Moisture factors vs. density and moisture content	(106)
6.1	Photograph of vacuum saturation apparatus	(118)
6.2	Schematic diagram of vacuum saturation apparatus	(118)
6.3	Photograph of mercury porosimeter apparatus	(124)
7.1	Typical thermogravimetry and the derivative thermogravimetry curves	(138)
7.2	Schematic diagram of TG-750 showing the components	(141)

7.3 Depth of carbonation on a cross section of a concrete cube after carbonation (144)

8.1 Cumulative volume vs. pore diameter for mortar: mix A, W/C= 0.8 (151)

8.2 Incremental pore volume vs. pore diameter for mortar: mix A, W/C= 0.8 (151)

8.3 Cumulative volume vs. pore diameter for mix proportion A, B and C with W/C= 0.8 (152)

8.4 Cumulative volume vs. pore diameter for mortars sieved from Pellite concretes on 2.36mm sieve (153)

8.5 Cumulative volume vs. pore diameter for mortar: mix A, W/C= 0.53 (154)

8.6 Incremental pore volume vs. pore diameter for mortar: mix A, W/C= 0.53 (154)

8.7 Cumulative volume vs. pore diameter for air entrained mortar: mix A, W/C= 0.43 (155)

8.8 Incremental pore volume vs. pore diameter for air entrained mortar: mix A, W/C= 0.43 (155)

8.9 Cumulative volume vs. pore diameter for mortar: mix B, W/C= 0.56 (156)

8.10 Incremental pore volume vs. pore diameter for mortar: mix B, W/C= 0.56 (156)

8.11 Cumulative volume vs. pore diameter for mortar: mix C, W/C= 0.90 (157)

8.12 Incremental pore volume vs. pore diameter for mortar: mix C, W/C= 0.90 (157)

8.13 Cumulative volume vs. pore diameter for mortar: mix C, W/C= 0.95 (158)

8.14 Incremental pore volume vs. pore diameter for mortar: mix C, W/C= 0.95 (158)

8.15 Cumulative volume vs. pore diameter for air-entrained mortar: mix C, W/C= 0.90 (159)

8.16 Incremental pore volume vs. pore diameter for air-entrained mortar: mix C, W/C= 0.90 (159)

8.17 Cumulative volume vs. pore diameter for sieved mortar: mix C, W/C= 1.29 (160)

8.18 Incremental pore volume vs. pore diameter for sieved mortar: mix C, W/C= 1.29 (160)

8.19 Cumulative volume vs. pore diameter for air-entrained mortar: mix C, W/C= 1.29 (161)

8.20 Incremental pore volume vs. pore diameter for air-entrained mortar: mix C, W/C= 1.29 (161)

8.21 Cumulative volume vs. pore diameter for selected mixes (162)

8.22 Cumulative volume vs. pore diameter for quartzitic aggregates of different sizes (163)

8.23 Incremental pore volume vs. pore diameter for quartzitic aggregates for different sizes (163)

8.24 Cumulative volume vs. pore diameter for limestone aggregates of different sizes (164)

8.25 Incremental pore volume vs. pore diameter for limestone aggregates of different sizes (164)

8.26 Cumulative volume vs. pore diameter for Pellite aggregates of different sizes (165)

8.27 Incremental pore volume vs. pore diameter for Pellite aggregates of different sizes (165)

9.1 Bar chart representation of thermal conductivity for concretes with same total W/C ratio (179)

9.2 Bar chart representation of thermal conductivity for concretes with same free W/C ratio (179)

9.3 Bar chart representation of thermal conductivity for A and B proportion concretes with same total W/C ratio (180)

9.4 Bar chart representation of thermal conductivity for selected concretes (180)

9.5 Bar chart representation of thermal conductivity for selected concretes (181)

9.6 Bar chart representation of pore volume for mortar: mix A, W/C= 0.53 (188)

9.7 Bar chart representation of pore volume for air entrained mortar: mix A, W/C= 0.43 (189)

9.8 Bar chart representation of pore volume for mortar: mix B, W/C= 0.56 (190)

9.9 Bar chart representation of pore volume for mortar: mix C, W/C= 0.90 (191)

9.10 Bar chart representation of pore volume for mortar: mix C, W/C= 0.95 (192)

9.11 Bar chart representation of pore volume for air-entrained mortar: mix C, W/C= 0.90 (193)

9.12 Bar chart representation of pore volume for sieved mortar: mix C, W/C= 1.29 (194)

9.13 Bar chart representation of pore volume for air-entrained sieved mortar: mix C, W/C= 1.29 (195)

9.14 Cumulative volume vs. pore diameter for mortar mix proportions A and B (which are the same). (196)

9.15 Incremental pore volume vs. pore diameter for mortar mix proportions A and B (196)

9.16 Cumulative volume vs. pore diameter for mortar mix proportion C (197)

9.17 Incremental pore volume vs. pore diameter for mortar mix porportion C (197)

9.18 Cumulative volume vs. pore diameter for mortars sieved from Pellite concretes (198)

9.19 Incremental pore volume vs. pore diameter for mortars sived from Pellite concretes (198)

9.20 Cumulative volume vs. pore diameter for air-entrained mortars (199)

9.21 Incremental pore volume vs. pore diameter for air-entrained mortars (199)

9.22 Cumulative volume vs. pore diameter for selected mortars (200)

9.23 Incremental pore volume vs. pore diameter for selected mortars (200)

9.24 Bar chart representation of total porosity for selected concretes (205)

9.25 Bar chart representation of total porosity for selected concretes (205)

9.26 Bar chart representation of total porosity for selected concretes (206)

9.27 Bar chart representation of total porosity for selected concretes (206)

9.28 Compressive strength vs. age for 65% RH, 20°C cured concretes (223)

9.29 Compressive strength vs. age for 65% RH, 20°C cured concretes (223)

9.30 Compressive strength vs. age for 65% RH, 20°C cured concretes (224)

9.31 Thermal conductivity at 3% m.c. vs. density (233)

9.32 Three-dimensional scatter graph of thermal conductivity vs. density and total porosity for different concretes studied (234)

9.33 Thermal conductivity vs. total porosity for the 24 concretes studied (235)

9.34 Thermal conductivity vs. median pore diameter for the 24 concretes studied (235)

9.35 Three-dimensional surface graph of thermal conductivity vs. density and the ratio of median pore diameter to total porosity (239)

9.36 Three-dimensional surface graph of thermal conductivity vs. density and reciprocal of total porosity using Eqn. 9.15 (240)

I.1 Photograph of steel mould, square head rammer (used to compact the concrete slabs) and a typical concrete slab (277)

II.1 Photograph of electric arc welder and argon gas bottle (279)

II.2 Miniature roller designed to flatten the beads to 0.035mm thickness. The chrome plated drum rollers are 55mm in diameter, made of mild-steel (280)

II.3 Photograph of thermocouple's bare wires on the right, bead joined by arc welding in the centre and after flattening, calibrating and mounting on adhesive tape on the left (281)

LIST OF PLATES

Plate		Page
9.1	General view of the fracture surface of quartzitic aggregate magnification x 200	(214)
9.2	General view of the fracture surface of quartzitic aggregate magnification x 1900	(214)
9.3	General view of the fracture surface of quartzitic aggregate magnification x 5750	(215)
9.4	General view of the fracture surface of limestone aggregate magnification x 200	(215)
9.5	General view of the fracture surface of limestone aggregate magnification x 1900	(216)
9.6	General view of the fracture surface of limestone aggregate magnification x 5750	(216)
9.7	General view of the fracture surface of Pellite aggregate magnification x 27	(217)
9.8	General view of the fracture surface of Pellite aggregate magnification x 1900	(217)
9.9	General view of the fracture surface of Pellite aggregate showing a close-up view of an area marked in Plate 9.8 magnification x 5750	(218)
9.10	SEM micrograph illustrating a typical fracture surface of mortar mix number 20 (Magnification x 1920). The C-S-H gel (honeycomb morphology) are visible in this micrograph	(218)
9.11	SEM micrograph illustrating a typical fracture surface of mortar mix number 21 (Magnification x 1900). The massive calcium hydroxide deposits grown through regions of C-S-H gel is clearly seen.	(219)
9.12	Finer structural details of mortar mix number 20 showing ettringite structure (Magnification x 5750).	(219)
9.13	Coarser structural details of mortar mix number 20 (Magnification x 27)	(220)

9.14 Coarse structural details of mortar mix number 21 showing a typical air-entrained mortar fracture surface (Magnification x 27) (220)

A C K N O W L E D G E M E N T S

The author wishes to express his sincere gratitude to Mr. J.G.Cabrera, Reader in Civil Engineering Materials and Dr. J.A.Tinker, Lecturer in Civil Engineering for their supervision and guidence throughout the course of this study and most importantly for their critical reading of this text.

The author also wishes to acknowledge the valuable help rendered by the technical staff of the departments of Civil Engineering, Earth Science, Mining and Ceramics during the various stages of the project.

The author extends his appreciation to those colleagues who have helped by discussing the matter arising throughout this research and expresses with deep appreciation, the understanding and encouragement given by his parents and his wife during the course of his studies at Leeds University. Further thanks must go also to my wife Maryam for her preparation of the text and excellent standard of typing.

Final thanks must go to god for making all things possible.

ABBREVIATIONS

ACI	American Concrete Institute
AMD	Amendment
Å	Angstrom, 10^{-10}m
BS(BSI)	British Standards Institution
CIBSE	Charted Institute of Building Services Engineers
cc	centimetre cube
Creep room	Laboratory controlled room at 65±5% RH and 20±1 °C
CV	Coefficient of variation
DIN	Deutsches Institut für Normung (German standards)
DTG	Differential Thermal Gravimetry
emf	electro-motive force
Fog room	Laboratory controlled room at 95±5% RH and 20±1 °C
F ratio	The ratio produced by dividing MS(Model) by MS Error
λ	Thermal conductivity (W/mK)
mc (MC)	Moisture Content (%)
MIP	Mercury Intrusion Porosimetry
MS	Mean Square
MPD	Median Pore Diameter (Micron)
RH	Relative Humidity
$\sqrt{MSE}$	root Mean Square Error
SAS	Computer package program 'Statistical Analysis System'
SEM	Scanning Electron Microscopy
SG	Specific Gravity
TC	Thermal Conductivity
TG	Thermogravimetry
vol.	Volume
VS	Vacuum Saturation
W/C	Water- Cement ratio

CHAPTER ONE

INTRODUCTION

1.1 Applications of thermal properties in concrete structures

Concrete in many types and forms has been used extensively in all manner of constructions for many years mainly because of its versatility to shape and ease of production. It s thermal performance has not however, until recently (since the advent of the fuel crisis in 1973), been a primary consideration, particularly in relation to overall structural performance and energy conservation. However the increasing awareness of energy conservation and heat transfer control coupled with the introduction of basic standards of the performance and the continued increase in the use of concretes in civil engineering applications such as construction of buildings, roads, dams, mass pour concretes, storage tanks etc. has focused more attention on the evaluation of its thermal properties.

There is no doubt that in the immediate future, there will be a considerable increase in the activity directed towards the measurement of the thermal conductivity of all types of concretes both by direct measurement and by calculation. The results from these will be useful in

selecting materials for the construction of buildings, roads, underground power cables, pipelines, fabrication of walls of furnaces and perhaps design of solar energy storage and cryogenic liquid storage tanks.

The study of the thermal performance of concretes is becoming increasingly important with the recent developments in science and engineering. Calculations of heat dissipation from underground nuclear explosions or determination of heat losses from underground steam and hot water pipes requires knowledge of the thermal properties of concretes, soils and rocks.

Realistic thermal performance values for concretes are required not only to solve problems in civil engineering but also in many geophysical and meteorological applications. Besides the usual applications in thermal design, this knowledge is also of great importance to evaluate the thermal effects arising in massive structures exposed to a variable thermal fields. For example, concrete dams exhibit large temperature variations that induce thermal stresses, often in the same order of magnitude as those induced by external loads. Modern analytical techniques allow a sufficiently accurate evaluation of the spatial and temporal temperature distribution, provided that the thermal properties of the material are well known.

Because of the foregoing reasons, the measurement of thermal conductivity of lightweight and normal-weight density concretes is becoming increasingly important. The study of the effect of pore structure on thermal conductivity of concrete can help in explaining the variations which exists

between thermal performances of different types of concretes.

At the outset it has to be realized that the term 'concrete' covers a very wide range of materials, and, in consequence, a wide range of thermal performance. Moreover, for any type of concrete there are different density ranges and constituents, each of which can affect the thermal performance to a greater or lesser extent.

1.2 Objective and Scope of the study

All engineering materials have a certain amount of porosity. The amount of pore-phase present plays an important role among the many factors which influence a material's physical properties. A particular property of interest is thermal conductivity. The influence of air content on thermal conductivity is such that in reported data, where the pore characteristics of the material have not been specified, results are meaningless for comparison with other data or as an indication of a material property.

The effect of porosity on thermal conductivity has been studied by many investigators and numerous attempts have been made to derive simplified relationships to assess the complex effects of pore volume and pore structure. It has been correctly realized that not only the volume pore fraction but also the size, shape, orientation and type of entrained gas in the pores have a considerable effect on the thermal conductivity. However, no formulae are known that represent reasonably, the effect of porosity on thermal conductivity.

The main objective of this research therefore, is to investigate the relationships that may exist between thermal conductivity and pore structure with particular reference to the range of concrete densities most commonly found in building and civil engineering work i.e. lightweight and normal-weight density concretes. The pore structure can be defined by volume of pores (porosity), pore size distribution (median pore diameter) and composition of the material

forming the pore network (hydrated cement and carbonated fraction).

The programme of work was formulated after carrying out a literature survey. The survey revealed that the amount of published data on the effect of total porosity and microstructural properties of concrete, on thermal conductivity is rather scarce. Hence investigations into the thermal conductivity of different types of concrete with varying porosities and strengths were carried out.

For the purpose of the investigation twenty-four different mixes were designed and test specimens produced. The concrete specimens contained either Pellite, limestone or quartz aggregates, with or without air-entraining agent (Febcrete), their density varied from 1550 to 2350 kg/m^3 and porosity from 10 to 39 per cent.

The thermal conductivity of all the concretes was measured in accordance with B.S. 874: 1988[1], using a plain hot-plate technique and the total porosity and pore size distribution of each mix were determined using vacuum saturation and Mercury Intrusion Porosimetry.

The measured values of thermal conductivity and porosity were statistically examined. From this, a mathematical model was developed relating thermal conductivity to dry density, total porosity and median pore diameter. Existing experimental models for calculating the thermal conductivity of concretes were also examined using data from some of the concretes studied.

For characterization purposes, the experimental programme also involved measuring the properties of fresh

concrete and other engineering properties of hardened concrete, such as compressive strength. Comparisons of degree of hydration using mortars were also made by monitoring calcium hydroxide content and by non-evaporable water content using thermal analysis methods. This was done to differentiate the nature of the material forming the pore walls of different concretes.

Throughout the literature survey, little information was found regarding the change in thermal conductivity of concretes due to carbonation. Because of this, the carbonation process of concretes was monitored and compared against each other by assessment of the depth of carbonation on concrete cubes and by quantitative evaluation on mortar samples.

Finally, use was made of Scanning Electron Microscopy in an attempt to establish whether the pore structure and morphology of hydrated cement gel in different mixes were different. The S.E.M. was also used for the study of the micromorphology and analysis of aggregates particles.

CHAPTER TWO

REVIEW OF LITERATURE

In this chapter, important aspects of heat conduction through concrete are reviewed. When undertaking the literature survey on concretes and mortars, thermal conductivity and its relation to density, moisture content and porosity; very few references specific to the overall topic area were found. Fortunately however, the individual parameters have been investigated to varying extents in isolation to each other and a survey of each is presented. This will serve as a basis for understanding the relationship between the parameters considered in the study.

2.1 Introduction to heat conduction and thermal conductivity of materials

Heat conduction, considered at the atomic level is due to the elastic impacts of molecules in gases and due to longitudinal oscillations of molecules in solids. From a phenomenological point of view, it means the exchange of heat between contiguous bodies or parts of a body which are at different temperatures. The basic law of heat conduction is in complete analogy to the law of electrical conduction and according to Max Jakob [2], is

$$Q = \lambda \frac{A\ \Delta t}{L} \qquad \text{...(2.1)}$$

where:

Q = Rate of heat flow (W)

A = Area of slab (m^2)

Δt = Temperature difference between the faces (K)

L = Thickness of slab (m)

λ = Thermal conductivity (W/mK)

It originates from Biot [3] dating back to 1804 but is generally called Fourier' s equation, because Fourier [4] used it as a fundamental equation in his analytic theory of heat.

Thermal Conductivity is a physical property which expresses the ability of the material to conduct heat. It is defined in B.S.874:Pt1:1986 [5] as ' the heat flux density under steady-state conditions divided by the temperature gradient in the direction of heat flow '. The term 'Thermal Conductivity' (λ) is defined in B.S.874:1973 [6], as ' the quantity of heat in the 'steady state' conditions passing in unit time through an area forming part of a slab of uniform material of infinite extent and with flat and parallel faces. It is proportional to the area A and to the temperature difference between the faces, and inversely proportional to the thickness of the slab '. It is technically a difficult property to measure to any degree of accuracy, requiring sophisticated equipment and trained operating personnel. Thermal conductivity is measured in joules per second per square metre of area of body when the temperature difference is 1 K per metre of thickness of the body, i.e. W/mK.

Thermal conductivity is a characteristic property of a material and its value may depend on; density, moisture content, pore structure, shape of the solid particle, temperature and composition of the material, type of material

and type of entrained gas in the material. (see section 2.3)

At normal temperatures the thermal conductivity of solids covers a range of five orders of magnitude, from 0.02 W/mK for the best insulants such as foamed polyurethane to 2000 W/mK for the best conductors such as diamond. This very wide range is attributed to the factors mentioned above.

Civil engineering materials may be generally considered as multi-phase materials, that is, mixtures of gases and solid bodies. The thermal conductivity of these materials typically varies from 0.02 W/mK for foamed polyurethane to 3.1 W/mK for gravel aggregate concretes. Metals, which are used less extensively, have conductivity values between 100 to 1000 W/mK. Thermal insulation is achieved by encapsulating still air and since the conductivity of 'still' convection-free air is about 0.025 W/mK [7] at normal temperatures, this is the lowest value attainable by most insulants.

2.2 Mechanisms of heat transfer in porous materials

Heat may be thought of as the kinetic energy of motion (translational, rotational, or vibrational) of ions or molecules. It is usual to consider three methods of heat transfer: conduction, convection, and radiation. They have in common that a temperature difference must exist and that heat is always transferred in the direction of decreasing temperature. On the other hand they differ entirely in the physical mechanisms and laws by which they are governed.

In *conduction*, energy (heat) is transferred by the mechanism of interaction between two particles (e.g., ions and molecules), one with a greater amount of energy and the other with a lesser amount of energy, in such a way that some energy is passed from one to the other. In the case of a gas, one molecule may strike another molecule with less kinetic energy and impart some of its energy to the second molecule. In the case of a solid, an atom with a certain amount of vibrational energy will tend to transmit some of this energy to a neighbouring ion with less energy through the bond connecting them. In *convection*, [2,8,9] heat is transferred by the actual movement of particles with a given energy to another part of the system where the particles have less energy on the average. In *Radiation*, [2,8,10] heat is transferred by the emission or absorption of radiant energy between particles or surfaces.

Thermal conductivity of a porous material is a complex property, since all three mechanisms of heat transmission can play a role. Some heat is conducted through the solid component and some through the gas in the pores.

Convection also occurs in any gas pockets large enough to support circulation currents, these generally must be greater than 3 mm in size [11] for any significant convection to occur. Finally, radiation can travel from one surface to another in each pore, and some radiation may even travel through the solid if it is partially transparent to infrared [12].At temperatures found in concretes that are under consideration in this work, i.e around 20°C, the radiation component can generally be ignored and although it may become significant at very low densities or at high temperatures, it is generally small compared with the conduction component.

Since a porous material exhibits a complex thermal transfer pattern when subjected to a thermal gradient, the method of analysis used to measure the heat transfer rate is generally adapted to the particular case being considered. By electing to measure one particular heat transfer mechanism certain less important factors are neglected compared to dominant ones, i.e. in the case of measuring thermal conductivity, radiation and convection is sometimes ignored depending on the case being considered. Even for two substances composed of the same solid material in the same type of arrangement, a difference in pore size or density can change the relative importance of various mechanisms of heat transfer. This can be to such an extent that the conductivity of one will fail to correlate with an analysis that fits the other.

It should be emphasized at this point, that since all the three mechanisms of heat transfer are acting at the same time during thermal conductivity measurement and it is

difficult to differentiate between the three mechanisms, the measured 'λ' would be 'apparent' rather than a true value.

The mechanisms of heat transfer through concrete within the ambient temperature range may be generalised as:

A) Solid conduction- this depends upon the fraction of the solid component. It is important because the conductivity of the solid is much higher than that of air. Typically, the solid conductivity value lies in the range 0.2 W/mK for polymers, to 4 W/mK for granite, compared with the conductivity of air which is approximately 0.025 W/mK.

B) Gas conduction- in pores smaller than a few millimetres diameter, gas convection cannot occur and the transfer of heat through the gas in the pores depends only on collisions between the molecules within the pores and the gas conductivity is that of still air. The radiation component can generally be ignored because the temperature difference within the pore walls is small at ambient temperature and is generally small compared with the conduction component. Since the volume of air entrained in concretes is significantly less than the solid fraction, the thermal conductivity of the solid phase is a principal factor in determining the overall conductivity. However the manner in which the air is entrained in concrete can influence the overall conductivity.

2.3 Factors effecting the thermal conductivity of materials

Thermal conductivity is a characteristic physical property of a material and its value may depend on many factors as mentioned in section 2.1, these factors are elaborated in the following sections;

2.3.1 Density

The thermal conductivity (λ) of engineering materials is directly related to bulk dry density. λ increasing as the density increases because less air is entrapped within the material.

In 1949 Jakob [2], published a curve relating the density of a wide range of inorganic materials to thermal conductivity corrected to 3 percent moisture content. Arnold, in 1970, [13] published an updated version of the same curve and values obtained from it, which are given in Table 2.1, are proposed as 'standard' values of thermal conductivity for a given density. It can be seen from Table 2.1 that as density increases so does λ. The increase being more pronounced at higher densities.

Table (2.1)

Standard curve values published by Arnold[13]

Dry density (kg/m^3)	λ at 3% m.c. by volume (W/mK)
200	0.111
400	0.148
600	0.185
800	0.234
1000	0.295
1200	0.381
1400	0.516
1600	0.664
1800	0.874
2000	1.132
2200	1.452
2400	1.846

In the absence of specific test information, it is accepted practice for engineers and designers to refer to the standard values or curve for conductivity data. Difficulties arise when trying to determine the thermal conductivity of different concrete materials from a standard curve because, for a given density, the relationship may be invalid due to the specific inherent properties of the concrete such as, different constituent solids, internal pore structure, porosity and type of entrained gas.

2.3.2 Moisture content

It has long been recognised that the thermal conductivity of engineering materials is directly related to moisture content and increases with it. Not only are some of the gaps in the solid matrix occupied by water which is about 24 times more conductive than 'still' air $\left[\lambda_{air} \simeq 0.025 W/mK \right.$ and $\left. \lambda_{water} \simeq 0.6\ W/mK \right]$, but also additional latent heat can be transferred across the air spaces by an evaporation-condensation process. The relative effect of moisture becomes increasingly important as the conductivity decreases, that is as the density of the material is decreased and the porosity is increased.

When a porous material is moist, the analysis of heat transfer becomes complicated because Fourier's heat conduction equation (equation 2.1) is limited since it assumes that the heat flux is uniform throughout the thickness. During steady state heat transfer measurement on materials containing water, moisture migrates to the cold side of the specimen when a temperature gradient is applied across its faces. The cause of this is the vapour flow induced in the unfilled pores of the materials by the temperature differences existing across them due to the over-all temperature gradient [14] acting on the specimen. The evaporation-condensation which takes place, results in an augmented energy transfer of latent heat across the pores which is one cause of the apparent increased heat transmission that can occur when moisture is present. The other principal cause of increased heat transfer is due to

the replacement of the air in pores and capillaries with water. All engineering materials have a natural porosity, that is to say, they have air-filled pores which may show great variation in both character and size. If the air in the pores is replaced by moisture the value of the thermal conductivity of these materials increases considerably. Gases other than air in the pores also affect the conductivity. Similar migration cannot take place in a saturated material since there are no unfilled pores.

Loudon [15] suggests that the measured λ-value under a moisture gradient may well be as little as half the 'true' value for uniformly distributed moisture. Despite the practical problems encountered during measurement, a number of general curves relating λ to moisture content have been proposed; Krischer and Rohnalter [14] in 1940 reported thermal measurements on moist brick materials (fired clay slabs), which stimulated thoughts on the processes of heat transmission through moist granular materials, concretes as well as bricks. Krischer (1941) [16] showed that the main mode of heat transfer across moist pores at elevated temperatures is by vapour diffusion and that at the temperatures of building materials in practice, λ is affected appreciably by moisture and only to a small extent by temperature. In 1949, Jakob [2] proposed curves relating density to λ and moisture content to λ for a wide range of inorganic materials. In order to enable thermal conductivity to be expressed at different moisture content (by vol.), he established a list of moisture factors which are given in the C.I.B.S.E. Guide A3, 1980[7] and are reproduced in Table 2.2.

Table (2.2)

Jakob moisture factors

M.C. % by Vol.	1	3	5	10	15	20	25
Moisture factors	1.3	1.6	1.75	2.1	2.35	2.55	2.75

Jakob suggested that the relationships may be in error for particular materials by about ±15 % but later work [17] shows that errors are greater than this. The curves are, nevertheless, useful for rough estimates of the thermal conductivity of masonry material and are still fairly widely adopted today.

In German DIN standards, a linear moisture curve is assumed, the conductivity increasing by 6% for each 1% increase in moisture content by volume. The slope is significantly less than that of the Jakob curve over the standard range, but good agreement is obtained for concretes over a limited density range.

In general the λ-value of concrete cannot be measured at a precise moisture content, but it is normally determined in the equilibrium 'air-dry' state, usually containing 1 to 5 percent moisture content by volume, after the samples have been conditioned to constant weight in a controlled laboratory environment of 20°C, 65% R.H.. This is in accordance with the British Standard for thermal conductivity measurement B.S. 874:1988[1]. Correction factors must then be applied to find the λ-value at standard moisture content. Currently, in the U.K. these moisture factors (Table 2.2) are based on a relationship between thermal conductivity and moisture content proposed by Jakob in 1949 [2]. The Jakob

correction factors are assumed to apply to all masonry materials regardless of density. However, a study previously carried out by Stuckes, Simpson and Tinker [18,19] showed the moisture factors to be density and moisture dependent and to increase with decreasing density. In general, a moisture increase in the material increases thermal conductivity. For example,considering concrete at a density of 1250 kg/m^3, a 5 percent change approximately in λ is observed for each 1 percent change in moisture content by volume [20,21].

2.3.3 Porosity and pore characteristics

The thermal conductivity of engineering materials (at the same density and moisture content) decreases with increasing porosity. This depends upon pore size, pore shape, pore orientation, type of entrained gas and temperature.

It is known [22-30] that not only the porosity but also the pore's characteristics such as the size, shape, distribution, orientation, structure and the emissivity of the pores surfaces all have some effects on thermal conductivity. It is understood [31] for instance, that with equal density, a material with spherical air holes has twice the thermal conductivity of a material in which the solid constituents consist of spherical particles . This is because the number of contact points of the solids influence the conductivity. For the same reason the shape of solid particles, i.e. shapes of powder, grain, etc. will also have an effect on thermal conductivity.

The amount of void or pore space in a porous material plays an important role among the many factors which

influence thermal conductivity. However, no formulae are known that empirically represent with any reasonable accuracy the effect of porosity on the thermal conductivity.

The effect has been studied extensively, and numerous attempts by Euchen [22] 1932; Russell [23] 1935; Ribaud [24] 1937; Waddams [25] 1944; Francl and Kingery [26] 1954; Loeb [27] 1954; Krischer and Esdorn [28] 1956; Kingery and Klein [29] 1958 and more recently by Simpson and Stucks [11] 1986 have been made to derive simplified relationships by approximating the complex effect of pore space. As stated before, not only the porosity but also the size, shape, orientation of the pore and the emissivity in the pore have considerable effects on thermal conductivity. Consequently, even if the effects of all these factors are known separately, it would be difficult to theoretically analyse their combination because of the three-dimensional irregularity of them [30]. Eventually therefore, all the formulae on thermal conductivity influenced by porosity have had to be empirical and expressed as a function of porosity alone (Eucken[22] 1932; Russell [23] 1935; Ribaud [24] 1937; Francl and Kingery [26] 1954; Krischer and Esdorn [28] 1956) with a shortcoming of not representing satisfactorily the actual state of thermal conductivity. Notwithstanding the above, Sugawara and Yoshizawa [30] 1961 derived a reasonable formula from the results of fundamental experiments by considering pore size, pore shape and emissivity inside of the pore. They claimed that by varying the empirical exponent 'n' in their formula, the actual overall thermal conductivity can be represented more correctly than other

formula tested in their work. Their general formula is as follows:

$$\lambda = (1-A)\,\lambda_s + A\,\lambda_f \quad (W/mK) \qquad \ldots(2.2)$$

where:

$$A = \frac{2^n}{2^n - 1}\left[1 - \frac{1}{(1+P)^n}\right]$$

λ = Overall thermal conductivity of porous materials (W/mK)

λ_f, λ_s = Thermal conductivity of fluid and solid constituent respectively (W/mK)

P = Porosity (%)

n = Empirical exponent determined by mode of packing, pore size, pore shape and emissivity inside of the pore, and $n > 0$.

Unfortunately the physical significance of the parameter 'n' in terms of the structure is not known and Sugawara and Yoshizawa did not attempt to derive the empirical exponent 'n' for different kinds of materials or for composite materials like concretes but they did compare their results with Ribaud's [24] and Russell's [23] formulas and observed results of experiment at 100°C as shown in Figure 2.1. The difference between the curves can probably be attributed to the fact that all the other authors who undertook similar experimentation , except Sugawara and Yoshizawa, treated the thermal conductivity as a function of porosity alone and ignored the influence of pore size, pore shape, material structure, etc. For purposes of comparison respectively, Ribaud's [24] and Russell's [23] formulas are as follows:

$$\lambda = \lambda_a P^{1/3} + \lambda_s (1 - P^{2/3}) \qquad \ldots(2.3)$$

$$\lambda = \lambda_s \frac{P^{2/3} + Q(1 - P^{2/3})}{P^{2/3} - P + Q(1 - P^{2/3}) + P} \qquad \ldots(2.4)$$

where:

$Q = \frac{\lambda_s}{\lambda_a}$

λ_s, λ_a = Thermal conductivity of solid constituent and air respectively (W/mK)

P = Porosity (%)

Formula by other workers show similar tendencies to the above in deviating from the observed curve as shown in Figure 2.1.

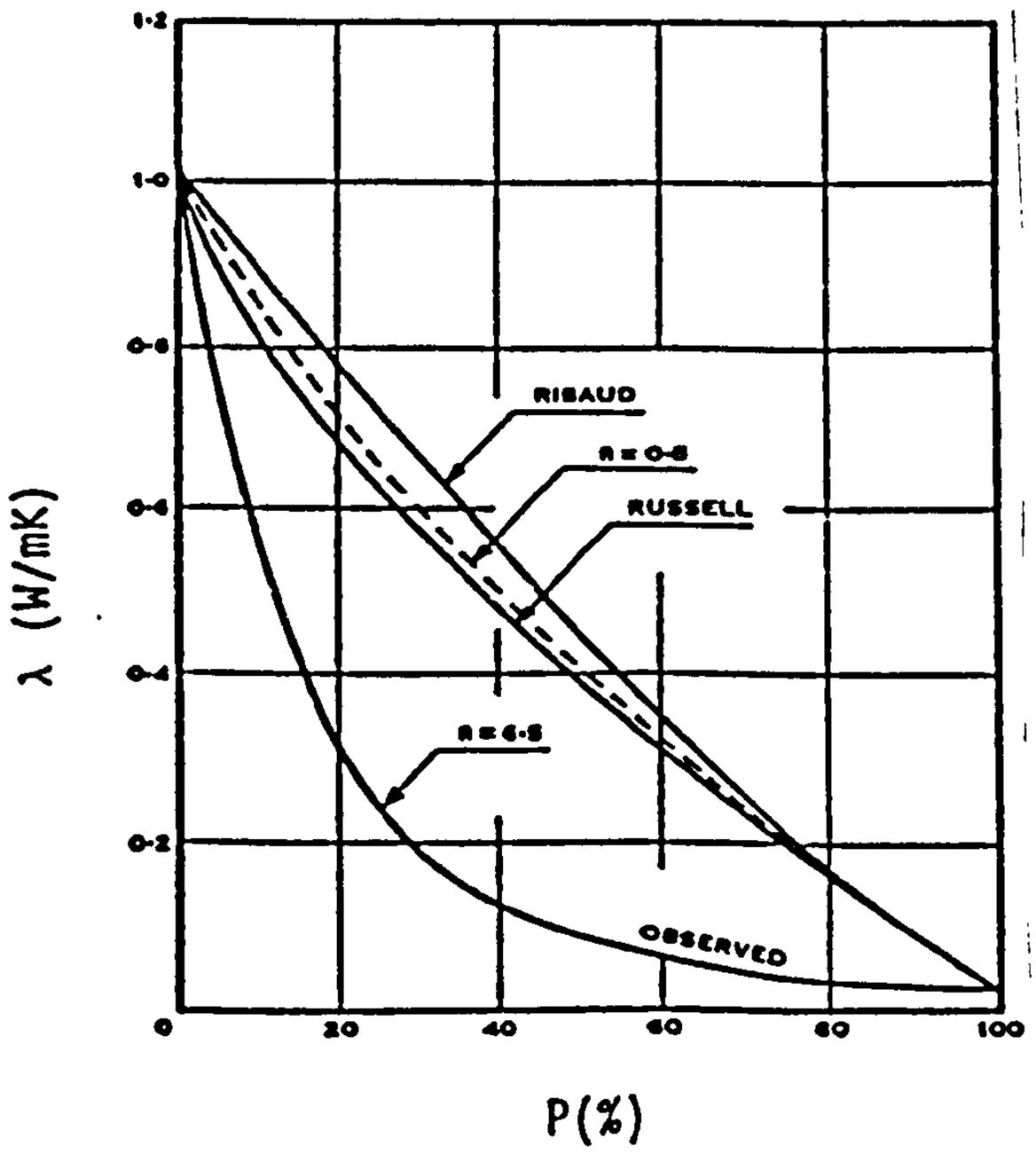

Fig.(2.1) Graph showing λ versus porosity at 100°C [30].

Sugawara and Yoshizawa claimed that if the two calculated curves of Figure 2.1 are represented by a curve

shown by the dotted line, the value of 'n' of this curve becomes 0.5. So equation 2.2 can cover any other formula on the thermal conductivity of porous material. The accuracy of the formula may be argued for different densities and moisture contents also the method used for the λ measurement could cause inaccuracies.

Due to a large number of factors, predicted, calculated and modelled values of thermal conductivity all too often show a significant spread of results. The problem is more complicated than that represented by the simple two or three-phase model that are available, since in reality individual pores may be only partially filled with water. The increase in conductivity then, is caused not only by the presence of water within the pore but also as a result of the transfer of latent heat of evaporation by the diffusion of water vapour in the air in the pore space. In this case the effective conductivity within the pore due to latent heat transfer increases rapidly with temperature due to an increase in saturated vapour pressure.

Most previous workers [32-36] have found that a linear relationship between porosity and thermal conductivity exists. The works carried out in the past by the author of this work [37], indicate that there is a linear correlation between porosity and thermal conductivity and that the relation is unique to a particular type of material.

It should be emphasized at this point, that porosity alone is not a unique specification for the state of a cellular material, since it is possible to have a large number of small cells or a few large cells, giving the same

overall porosity. In fact, porosity and the pore's characteristics must be considered as two independent variables with effective conductivity being a function of them for any given type of substance.

The importance of pore size should be emphasized here since it influences the type and combination of heat transfer mechanisms that takes place under the applied thermal gradient. Pore size can also influence the effects of individual heat transfer mechanisms in a porous material. For example, the convective heat transfer mechanism is influenced by pore size inso-much as this influences the degree of gas circulation within the pore. The convective mechanism is also influenced, to a lesser extent, by the molecular weight of the cell gas whose heat transfer characteristics are a function of its density and specific heat. Several factors influence the size of pores below which freely convecting gas is reduced to a stagnant condition. Although it is difficult to quantify this precisely, for pore sizes less then 1mm diameter, gas circulation by natural convection is stated [11,38& 39] to be virtually non-existent. With pore sizes below this level, the thermal conductivity of the higher molecular weight static pore gases will be less than that of air and thus the thermal resistance of the material will be increased. With pore sizes below about 10μm, the molecular mean-free-path effect comes into play reducing the thermal conductivity of the pore gas below its static value.

It has been shown by Loeb [27] that the relative orientation and position of pores affects the conductivity of

a material. This will be intuitively understood when it is realized that an array of pores, in a plane parallel to the direction of heat flow offers very little resistance to the heat flow since only a relatively small number of flow lines passes through the pores. When the sample is rotated through 90 degrees so that the heat flow is then perpendicular to the plane of the pores, every flow line must pass through the pore plane, so that the effect of the pores is much greater.

All engineering materials are porous, they contain voids, there are commonly filled with air. These voids are either pockets or cells more or less spherical in shape, or recesses between particles or granules of the solid. The thermal conductivity of such materials will depend upon the conductivities of the solid and of the pores, and also upon the type of pore structure and its distribution. It is understood, for instance, that materials whose microstructure is crystalline with inter-connected pores conduct more heat than those whose microstructure is vitreous with discrete pores [38].

2.3.4 Mineral composition and solid structure

The thermal conductivity of concrete is also affected by its constituent aggregates, typical values are listed in Table 2.3 [40,41].

For heavy-weight (2500-3000 kg/m^3), normal-weight (2000-2500 kg/m^3), and structural light-weight concretes (1400-1600 kg/m^3) the mineralogical characteristics of the aggregate markedly affect the conductivity of the concretes. More extensive data have been reported by Rhodes [42]. Table 2.3 confirms that the mineralogical characteristic of the

aggregate greatly affects the conductivity of the concrete made from it. In general terms, lightweight aggregates such as basalt and trachyte have a low conductivity, sandstone and limestone are in the middle range, while dolomite and quartz concrete exhibit the highest conductivity. This latter conductivity also depends on the direction of heat flow relative to the orientation of the crystals. In general the crystallinity of material increases its conductivity [43]. Jakob[2] pointed out that crystalline materials have a higher thermal conductivity than glassy substances, quoting λ-values for materials occurring in masonry. For instance, quartz crystals at 0°C have a thermal conductivity of 10W/mK normal to their axis and 19W/mK parallel to their axis, whereas quartz glass (fused silica) has a thermal conductivity of only 1.9W/mK.

The major factor affecting the conductivity of crystals is expected to be the symmetry and order of the crystalline lattice. Materials having a simple cubic lattice are expected to have a higher conductivity than more complex crystalline forms. Glassy structures, having a disordered structure, will be expected to have very low thermal conductivities [44]. Similarly, crystals having approximately the same size atomic weight components, will in general, be expected to have higher conductivities than crystals having components with a pronounced difference in atomic weight. Because of the low crystalline order in the tobermorite gel, the thermal conductivity of the cement paste is very low and comparable with that of true glasses.

Table (2.3)

Typical values of thermal conductivity of concrete[40.41]

Type of Aggregate in concretes.	Dry Density of Concrete (kg/m^3)	Thermal Conductivity (W/mK)
Barytes	2880	1.20
Dolomite	2560	3.68
Igneous	2540	1.44
Quartz	2340	2.86
Limestone	2020	1.40
Sandstone	1920	1.40
Basalt & Trachyte	480-1760	0.14-0.60

2.3.5 Temperature

The variation of thermal conductivity with temperature is known to be considerable especially for refractory materials. Consequently, the temperature at which the measurement is made, must be carefully specified and matched as closely as possible to the temperature during application. Fortunately for concretes and masonry materials, thermal conductivity is little affected by temperature within the usual ambient range. The general effect of an increase in temperature is to slightly decrease, the conductivity of ordinary concretes, but the reverse is the case with lightweight concretes [41,45]. However, at high temperatures, there is a decrease in thermal conductivity until at 800°C it is about one-half of the value at 20°C[46].

Comparison of heat conduction by the so-called amorphous or glassy and the crystalline substances is of particular interest because of their entirely opposite behaviour with increasing temperature. As Eucken [47] seems to have first stated, the thermal conductivity of amorphous bodies is small at low temperature and increases with the temperature, whereas that of crystalline substances is high and decreases with increasing temperature[2,43].

In a moist material the thermal conductivity decreases with increasing temperature. At the freezing point Jansson and Saare [48] found a discontinuity which they claim is caused by the moisture turning to ice, the ice having a higher thermal conductivity than water. Figure 2.2 shows the higher the moisture content, the greater the discontinuity.

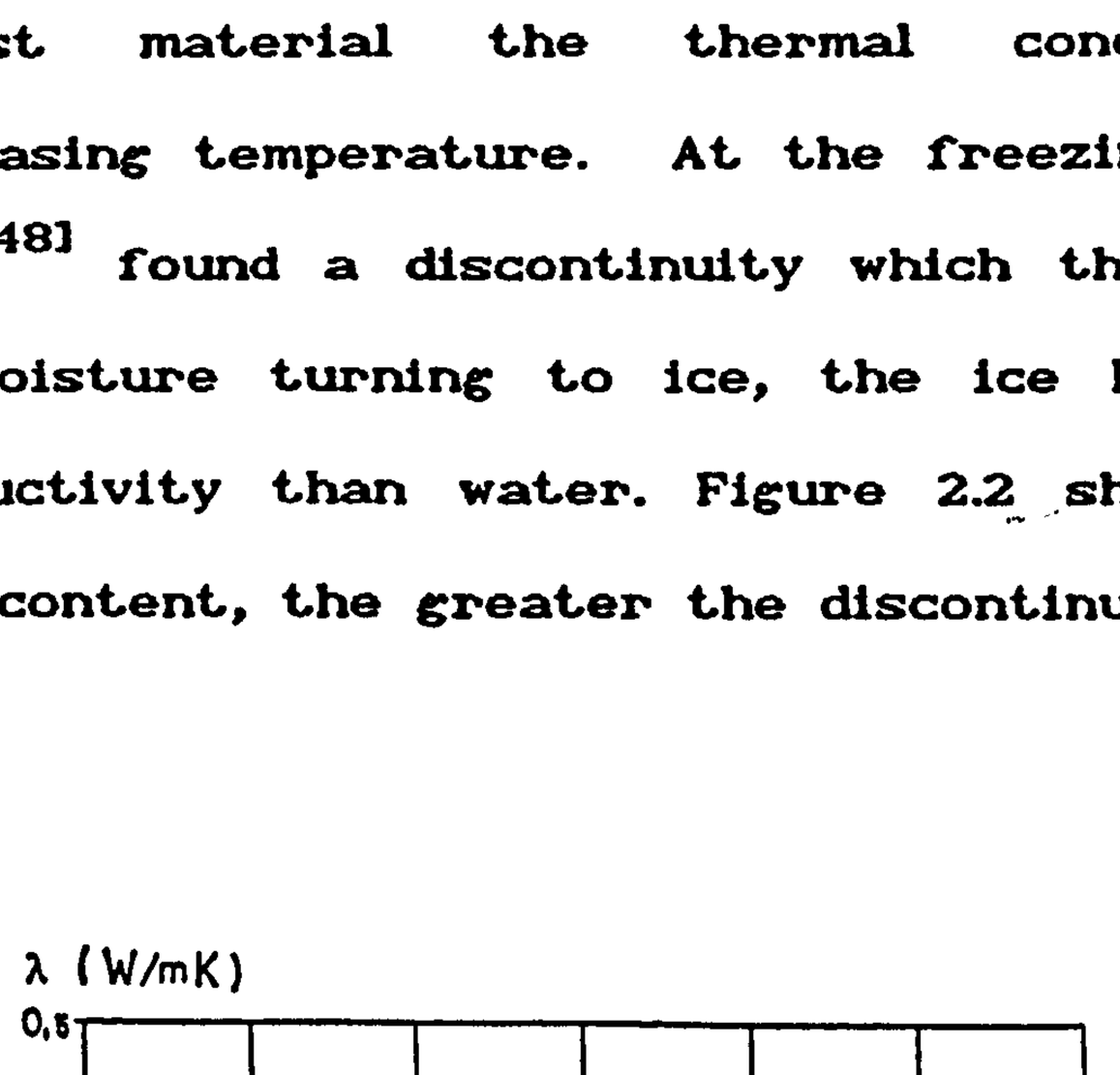

Fig.(2.2) Thermal conductivity of lightweight (530kg/m^3) concrete in relation to temperature and moisture content by weight[48]

2.4 Determination of porosity

The porosity of a porous material is the fraction of the bulk volume of the material occupied by voids. A simple method of estimating the porosity value of a concrete or mortar is by *Vacuum Saturation*. In this method after curing, the samples are sliced to make appropriate sections. The weights of water saturated samples are measured in water (W_1) and in air (W_2). The weights of dried samples are also measured (W_a). The porosity, P is calculated by the following equation:

$$\text{Porosity, } P = \frac{W_2 - W_a}{W_2 - W_1} \qquad \ldots(2.5)$$

Another approximate method of calculation developed by Cabrera [49] gives a porosity value very close to the measured value, i.e. within about ±3 percent. In this method, equations relating specific gravity and measured density are used to calculate porosity. Briefly, this method is summarised as follows:

$$P = \left(1 - \frac{Dd}{S.G._n}\right) \times 100 \qquad \ldots(2.6)$$

where:

P = Total porosity (%)

Dd = Dry density (kg/m^3)

$S.G._n$ = Specific gravity at "n" days of age.

$$S.G._n = \frac{100}{\frac{UC}{S.G._C} + \frac{HC}{S.G._{HC}} + \frac{A}{S.G._A}} \qquad \ldots(2.7)$$

where:

UC = Percent weight of Unhydrated Cement.

HC = Percent weight of Hydrated Cement.

A = Percent weight of Aggregates.

Hydration Time relations for O.P.C. is

$$r_t = 35.2 \log t \qquad \text{...(2.8)}$$

(equation valid up to 365 days)

where:

r_t = Percent hydration at time t.

t = Age in days.

2.5 Theoretical models for determining the thermal conductivity of porous materials

The thermal conductivity of a porous material basically depends on the conductivities of its component phases, the volume concentration of each and the distribution of the phases in the material. In order to model the thermal conductivity from the properties of the individual components, it is necessary to choose a model whose theoretical assumption represent the distribution and shape of the component phases within the mixture as closely as possible. However, in view of the complexdty of the structure of real materials, there are comparatively few cases where such theoretical assumptions can be applied rigorously.

Particle and pore sizes can significantly affect the heat transfer through the material. When the pores are large enough they permit convection and at high temperatures, radiation. However, the effect of convection and radiation can be neglected in this work, since the experiments were carried out at ambient temperatures on samples with reasonably small pores.

It should be acknowledged at this point, that it would be difficult to develop a theoretical model which exactly corresponds to the phase distribution of an actual material. Moreover, a model corresponding to the phase distribution of one material with a given porosity may not necessarily represent that of a second material with the same porosity.

Having indicated these difficulties, the thermal models available to predict the λ-values of porous materials, based on different phase distribution, are briefly explained below.

Many models representing multiphase media, take as a starting point the parallel and series arrangement of components. An example of a two-phase system is shown in Figure 2.3. The surfaces of each arrangement are assumed to be isothermal and perpendicular to the direction of heat flow.

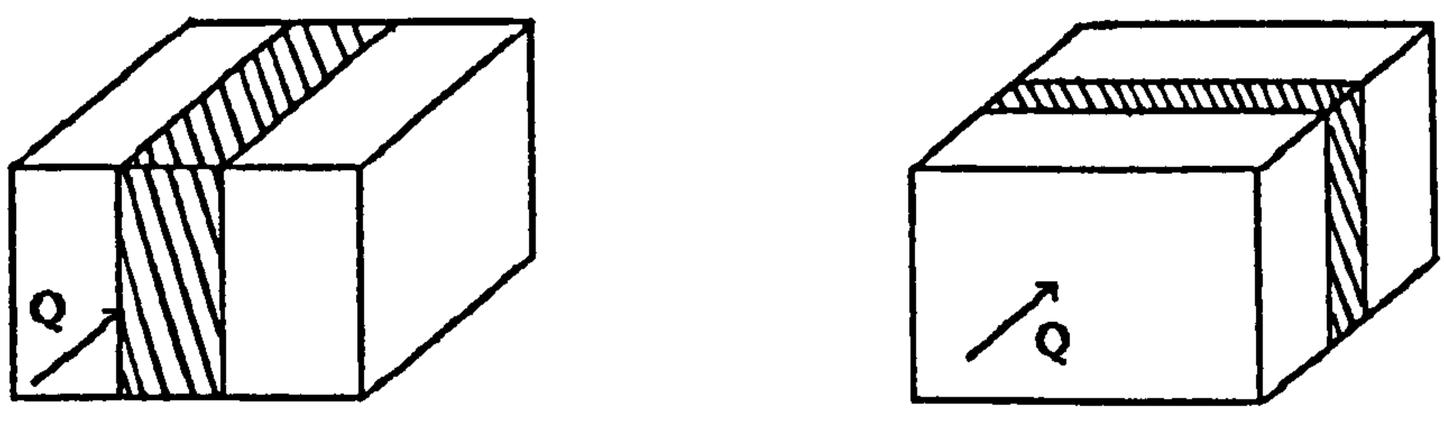

(a) (b)

Fig.(2.3) Parallel and series arrangements.

In a parallel arrangement (Figure 2.3a), the phases are assumed to be parallel with the direction of heat flow and the following equation, which predicts the maximum thermal conductivity, is derived by averaging the conductivities of phases [50,51].

$$\lambda_a = V_o\lambda_o + V_1\lambda_1 \qquad \ldots(2.9)$$

where:

λ_a = The upper effective conductivity of the porous material.

λ_o = Thermal conductivity of the solid.

λ_1 = Thermal conductivity of the gas.

V_o = Solid volume fraction.

V_1 = Gas volume fraction. i.e. (1 - Vo)

In a series arrangement, phases are assumed to be thermally in series with respect to the direction of heat flow, as shown in Figure 2.3b. Thus, thermal resistance can be calculated as the sum of the resistances of the phases and this leads to the lower limit of effective conductivity of the porous material given by [50,51]:

$$\lambda_b = \frac{1}{\frac{V_o}{\lambda_o} + \frac{V_1}{\lambda_1}} \qquad \ldots (2.10)$$

where:

λ_b = The lower effective conductivity of the porous material.

The apparent conductivity (λ) of an actual cellular material such as concrete, might be expected to lie between λ_a and λ_b, the relative position between these limitsdepending on the physical arrangement within the material. However, the ratio between λ_a and λ_b can be very great, of the order of ten to one or more, so that knowing only these limits is often of little practical help. An analysis of the problem for each particular type of geometrical arrangement of material considered is generally necessary.

In the case of fibrous materials in which the arrangement of fibres can be assumed to be approximately random. Schuhmeister [50] applied the following reasoning:

"Since the arrangement is random, the average fibre will have equal components projected on three perpendicular axes. Therefore, since two axes are perpendicular to, and one axis is parallel to, the direction of heat flow, a weighted average of the previously discussed upper and lower limits,

λ_a and λ_b, might be expected in the form

$$\lambda = \frac{1}{3}\lambda_a + \frac{2}{3}\lambda_b \qquad \text{...(2.11)}$$

Speakman and Chamberlain [52] and Baxter [53] managed to correlate some data on randomly arranged fibrous materials in this way, using numerical constants only slightly different from $\frac{1}{3}$ and $\frac{2}{3}$.

Krischer and Esdorn[28] using the combination of series and parallel models for phase distribution, derived the following equation for the thermal conductivity of a porous material. Their model assumption, based on parallel and series flow is shown in Figure 2.4 and is represented by Equation 2.12.

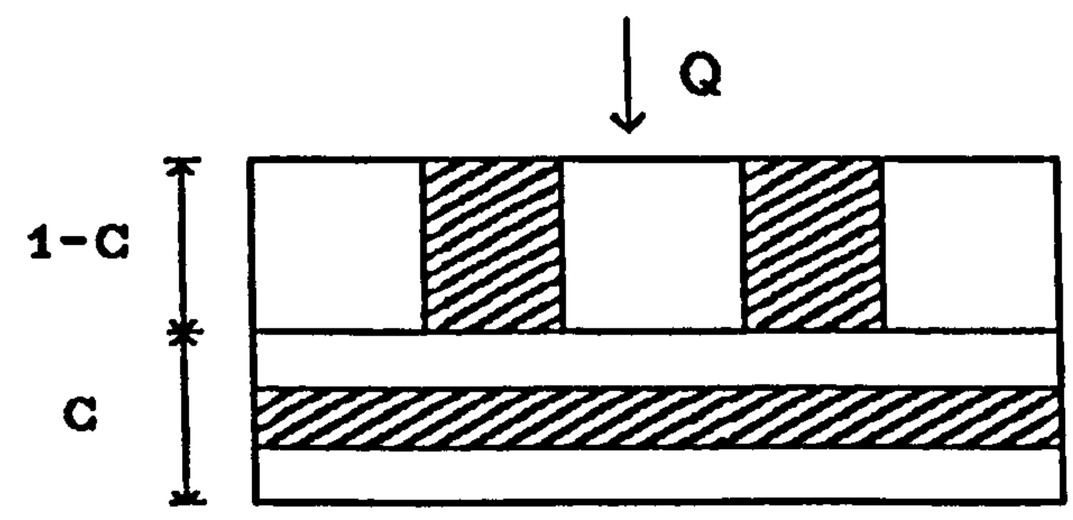

Fig.(2.4) Combination of series and parallel model [28].

$$\lambda = \frac{\lambda_a \times \lambda_b}{C \cdot \lambda_a + (1-C)\lambda_b} \qquad \text{...(2.12)}$$

where;

λ_a = thermal conductivity of parallel part.

λ_b = thermal conductivity of series part.

C = Volume fraction of series part.

Before the model can be used, an experimental thermal conductivity value is needed in order to determine the

parameter 'C' for each material. This reduces the value of the model for prediction purposes. However, the authors determined the 'C' parameter for various porous materials with densities in the range of 450-1850 kg/m^3 and its value varied between 0.048 and 0.283, a range of almost 1 : 6.

There have been several other attempts to formulate, with varying degree of success, the thermal conductivity of a two, three and eventually multi-phase system. Most of the models are based on the original work of Maxwell [54] who attempted a rigorous evaluation of the electrical permittivity of a matrix in which randomly sized spheres of one medium are randomly distributed in another. His model of thermal conductivity may be shown to be equivalent to :

$$\lambda = \frac{\lambda_o \left[1 - \left(1 - a\lambda_1\lambda_o \right) b \right]}{1 + \left(a - 1 \right) b} \qquad \ldots(2.13)$$

where:

$a = 3\,\lambda_o / 2(\lambda_o + \lambda_1)$

$b = V_1 / (V_o + V_1)$

λ = Thermal conductivity of composite.

λ_o = Thermal conductivity of the continuous phase.

λ_1 = Thermal conductivity of the randomly dispersed phase.

V_o = Volume fraction of the continuous phase.

V_1 = Volume fraction of the randomly dispersed phase.

Eucken [22] (1940) extended Maxwell's original equation to model the thermal conductivity of a matrix in which several dispersed phases are randomly distributed in one continuous phase. Eucken's model for a two-phase system

can be written as:

$$\lambda = \frac{\lambda_o V_o + 3\lambda_o \lambda_1 V_1/(2\lambda_o + \lambda_1)}{V_o + 3\lambda_o V_o/(2\lambda_o + \lambda_1)} \qquad \text{...(2.14)}$$

This expression was derived on the assumption that the spheres are far enough apart that they do not mutually interact. One of the problems which arises in the application of the Maxwell formulae to very porous solids is whether the gas or solid should be considered to be the continuous phase.

Brailsford and Major [55] (1964) extended the results of Maxwell's model by regarding a random two-phase system as having regions of both single phases in the correct proportions, embedded in a random mixture of the same two phases having a conductivity equal to the average value of the conductivity of the two-phase system, which is being calculated. From their model, thermal conductivity may be shown to be equivalent to:

$$\lambda = \frac{1}{4}\sqrt{(3V_o-1)\lambda_o+(3V_1-1)\lambda_1+\left[(3V_o-1)\lambda_o+(3V_1-1)\lambda_1\right]^2 + 8\lambda_o\lambda_1} \qquad \text{...(2.15)}$$

This model should give a good estimate of the thermal conductivity of a mixture if neither phase is continuous. Unfortunately it is limited to two phase composites which effectively reduces its application to concretes containing the solid phase and either all water or all air in the pores.

To model the simultaneous inclusion of concrete, air and water, a random three phase system was developed by Tinker [56] in which the three single phases in the correct proportions are assumed to be embedded in a random mixture of

the three phases.

Tinker's model for a three-phase system can be written as:

$$\lambda = \frac{\left[\lambda_o V_o + \frac{3\lambda_o\lambda_1 V_1}{(2\lambda_o+\lambda_1)} + \frac{3\lambda_o\lambda_2 V_2}{(2\lambda_o+\lambda_2)} + \frac{3\lambda_o\lambda_3 V_3}{(2\lambda_o+\lambda_3)}\right]}{\left[V_o + \frac{3\lambda_o V_1}{(2\lambda_o+\lambda_1)} + \frac{3\lambda_o V_2}{(2\lambda_o+\lambda_2)} + \frac{3\lambda_o V_3}{(2\lambda_o+\lambda_3)}\right]} \quad \ldots(2.16)$$

where subscripts 1, 2 and 3 refer to spherical inclusions embedded in a continuous phase 0. Since the expression is difficult to solve in the above formula, he developed a corresponding polynomial expression in λ which may be written as: $4A\lambda^3 + 2B\lambda^2 + C\lambda - AD = 0$ ...(2.17)

whose positive root lies between 0 and 1 when;

$A=(V_1 + V_2 + V_3) = 1$

$B=\left(V_1\lambda_2 + V_1\lambda_3 + V_2\lambda_1 + V_2\lambda_3 + V_3\lambda_1 + V_3\lambda_2 - 2\lambda_1V_1 - 2\lambda_2V_2 - 2\lambda_3V_3\right)$

$C=\left(V_1\lambda_2\lambda_3 + V_2\lambda_1\lambda_3 + V_3\lambda_1\lambda_2 - 2V_1\lambda_1\lambda_2 - 2V_1\lambda_1\lambda_3 - 2V_2\lambda_1\lambda_2 - 2V_2\lambda_2\lambda_3 - 2V_3\lambda_1\lambda_3 - 2V_3\lambda_2\lambda_3\right)$

$D=\lambda_1\lambda_2\lambda_3$

Reynolds and Hough [57] derived a general equation for the dielectric constant of mixtures. In this analogy voltage is equivalent to temperature, heat flux to current density, and temperature gradient to electric field. Assuming a parallel-sided slab of material having opposite faces which are each isothermal, and that heat only flows between these two faces, their equation can be written as: [54]

$$\lambda = \lambda_o + (\lambda_1 - \lambda_o) V_1 f_1 \quad \ldots(2.18)$$

or

$$\lambda = \frac{\lambda_o V_o f_o + \lambda_1 V_1 f_1}{V_o f_1 + V_1 f_1} \quad \ldots(2.19)$$

where:

$f_o = \frac{\overline{T}_o}{\overline{T}}$, $f_1 = \frac{\overline{T}_1}{\overline{T}}$ and are equivalent to field ratios. i.e. the ratio of the average temperature gradients in the two phases.

The average value of the field within a particle depends on its shape, orientation, thermal conductivity and the average thermal field and conductivity of the medium immediately outside it.

Theoretically equation 2.18 and 2.19 are equivalent but this is not so when approxdmations have to be made for the field ratios. It is suggested by Reynolds and Hough that equation 2.18 be used when inclusions of phase 1 are dispersed in a continuous phase 0 but equation 2.19 is more appropriate when the phases are of roughly equal particle size.

Simpson and Stuckes [11] extended Reynolds and Hough general equations and obtained the following equation for n + 1 phase system.

$$\lambda = \frac{\lambda_o V_o f_o + \lambda_1 V_1 f_1 + ... + \lambda_n V_n f_n}{V_o f_o + V_1 f_1 + ..., + V_n f_n} \qquad ...(2.20)$$

Since all these models (2.10 to 2.20) are based on spherical shaped pores their validity for concrete could be argued. These models are also difficult to use in practice because the thermal conductivity of the solid phase (i.e. combination of cement and aggregates) and the volume fraction of each phase must be known. However they are a useful starting point to gain a better understanding of the thermal conductivity of concrete.

UNIVERSITY LIBRARY LEEDS

2.6 Specific models for calculating the thermal conductivity of concrete

Concrete is a heterogeneous material consisting of aggregates, cement and water. A chemical hydration reaction between the cement and water causes the paste to harden and bind the aggregates into a rock-like mass (see section 7.1). The thermal conductivity of such can be estimated by using two-phase equations such as those proposed by Maxwell [58] where the continues phase may be considered as the hydrated cement and a disperse phase as the aggregate. In this case, the thermal conductivity of the concrete may be shown to be equivalent to:

$$\lambda_c = \lambda_p \left[\frac{1 + 2V_a \left(\frac{1 - \lambda_p/\lambda_a}{1 + 2\lambda_p/\lambda_a} \right)}{1 - V_a \left(\frac{1 - \lambda_p/\lambda_a}{1 + 2\lambda_p/\lambda_a} \right)} \right] \qquad \ldots(2.21)$$

where:

λ_c = Calculated thermal conductivity of concrete.

λ_p = Thermal conductivity of cement paste.

λ_a = Thermal conductivity of aggregate.

V_a = Volume fraction of aggregate.

Valore [21] evaluated the thermal conductivity of concrete using a cubic model and called it Method 2. The model (Fig.2.5) is a cube of concrete of unit volume consisting of a cube of aggregate of volume V_a encased on all sides by a layer of cement paste of uniform thickness, $(1 - V_a^{1/3})/2$. Valore considered the unit cube as a 'masonry unit', two layers of paste on opposite cube faces. Perpendicular to the direction of heat flow are 'face shells'

whose resistances are in series with that of the combination of the solid 'core' of aggregate and surrounding paste layer 'webs', parallel to heat flow.

Valore Method 2 equation can be written as:

$$\lambda_c = \lambda_p \left[\frac{V_a^{2/3}}{V_a^{2/3} - V_a + \frac{V_a}{\lambda_a / \lambda_p} + 1 - V_a^{2/3}} \right] \quad \ldots(2.22)$$

where:

λ_c = Calculated thermal conductivity of concrete.

λ_p = Thermal conductivity of cement paste.

λ_a = Thermal conductivity of aggregate.

V_a = Volume fraction of aggregate.

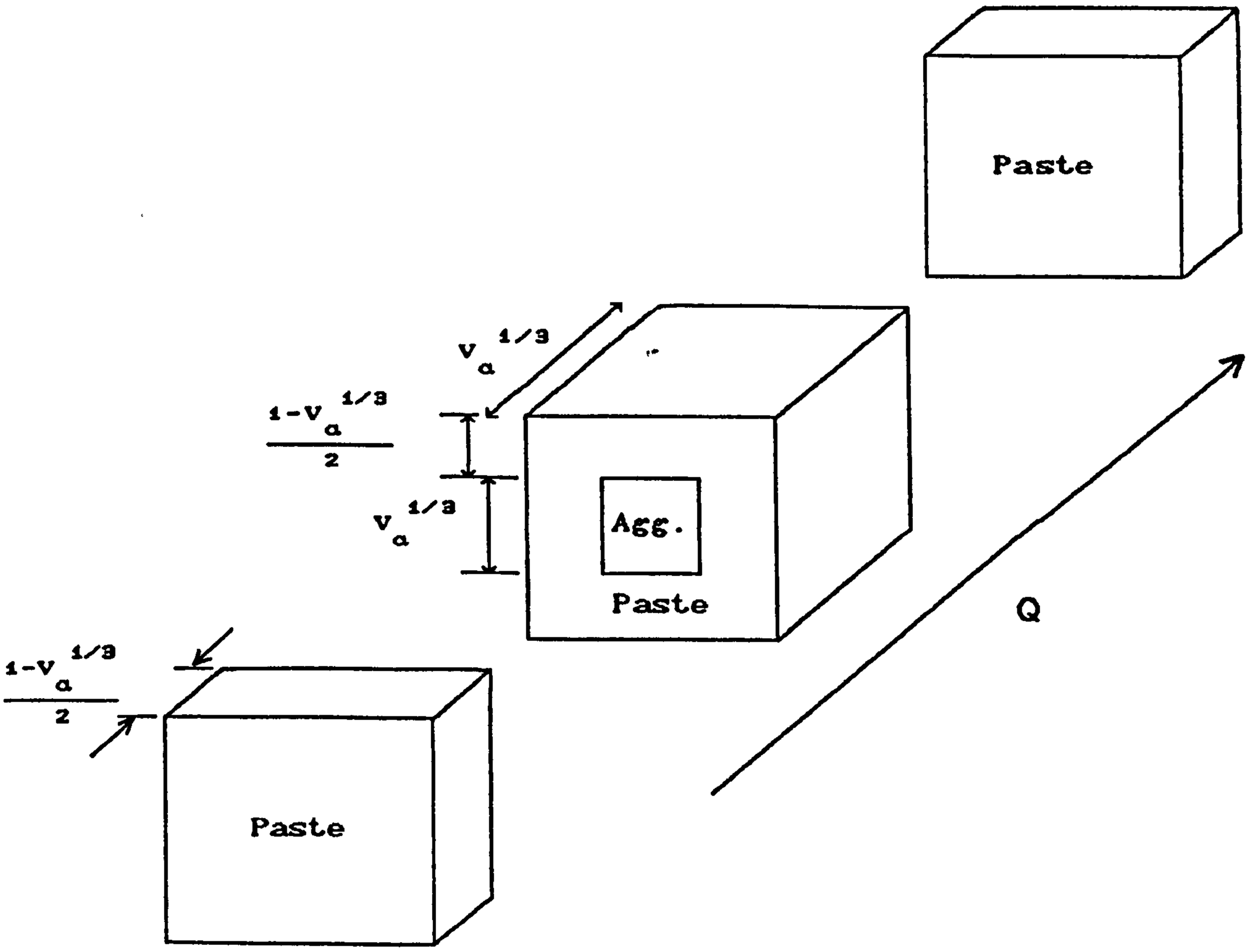

Fig.(2.5) Cubes model for calculating thermal conductivity of concrete by Method 2 [21].

If the concrete contains a fine and a coarse aggregate their λ_a values differ, it is suggested that λ_c is calculated for the paste-fine aggregate mortar first and the calculation is then repeated for the mortar-coarse aggregate combination using the appropriate V_a value in each step. Valore concluded that Method 2, (equation 2.22) appears to yield more accurate λ_c values than Maxwells equation 2.21 for normal weight concretes.

Campbell-Allen and Thorne[59] considered the structure of concrete as being a set of cubes of aggregate of uniform size arranged systematically in the mixture of cement paste. By considering the heat flow through each of the different types of path through the cube, they derived an equation for calculating the thermal conductivity of concrete as a function of the cement paste and aggregate. Their equation may be expressed as follows :

$$\lambda_c = \lambda_p(2R - R^2) + \lambda_p\lambda_a \frac{(1-R)^2}{R\lambda_a + (1-R)\lambda_p} \quad \ldots(2.23)$$

where:

$$R = 1 - \sqrt[3]{1-p}$$

p = volume of cement paste per unit volume of concrete.

λ_c = Calculated thermal conductivity of concrete.

λ_p = Thermal conductivity of cement paste.

λ_a = Thermal conductivity of aggregate.

It is difficult to use equations 2.21 - 2.23 in practice because the thermal conductivity of the cement paste and aggregate would have to be measured independently. However, the equations are useful for analyzing the effects

of different aggregates on the thermal conductivity of concrete. For example, Campbell-Allen and Thorne find that a large increase in the conductivity of the aggregate will only have a small effect on the conductivity of the concrete.

2.7 Mechanisms of moisture migration in moist specimens

Because some of the thermal conductivity measurements in this study involved moist specimens, it was considered necessary to present a brief survey on moisture movement mechanisms. Three theories have been developed to explain the physical phenomenon of moisture transfer in porous media, these are:

I) the diffusion theory.

II) the capillary flow theory.

III) the evaporation-condensation theory.

The diffusion theory is based on the assumption that the moisture flux is proportional to the gradient of moisture concentration. The capillary flow theory includes movement of water in the pores of the solid and the evaporation-condensation theory explains the movement of moisture in porous systems under the effect of temperature gradients.

During the funicular stage (liquid saturated stage), diffusion seems to be the mechanism of moisture transport. However, in the pendular stage (unsaturated liquid flow stage), experience shows [60,61] that diffusion, capillary and evaporation-condensation are the governing mechanisms in the moisture transfer process. Experimental evidences[60,61] prove that the pore size distribution of a porous medium is the important parameter affecting moisture transfer in the porous system in such a state. In the nearly dry state, all pores are empty and therefore water vapour diffusion dominates. In the high humidity region some pores are filled by capillary condensated water . In this case , these fine

pores cannot contribute to vapour diffusion any more but water migrates through them, driven by capillary forces. Because of these different mechanisms, it is not easy to predict the influence of pore size distribution and water content on moisture migration.

When a temperature gradient is applied to a porous material containing moisture, the moisture is transferred in the direction of hot to cold areas by a process of vapour diffusion. Thus, the moisture content increases at the cold side and decreases at the hot. A moisture gradient is therefore set up in the direction of cold to hot, and liquid moisture may be returned to the hot side by capillary forces. Under steady state conditions, a dynamic equilibrium exists between the two opposing processes, and moisture is no longer uniformly distributed in the material[62-64]. Thus, the measured thermal conductivity is the value over a non-uniform moisture content. The net result of this rearrangement in the initially uniform moisture distribution is that the steady state method when used with a damp material measures an apparent conductivity smaller than the 'true' value defining an isotropic specimen. It also explains the drop in the measured conductivity with increasing temperature, a result denoting the formation of a dry zone as the moisture transfers from the warmer to the colder region.

In the coarse pores of a concrete specimen, air remains present up to a considerable water content. In the moist state these pores are connected by fine, water-filled capillaries. In the air-filled pores no moisture equilibrium is obtained because of the temperature gradient. On the

warmer side of the pore the water evaporates from the separating walls of the fine capillaries and diffuses through the space of the pore towards the colder side, where it condenses. Hence it migrates through the intervening capillaries to the next cooler air-filled pores, since the capillary attraction of the balanced evaporating menisci is greater than that of the unbalanced menisci at which condensation occurs. Thus the water migrates from the warmer layers of the material to the colder.

The rate of water migration in this process is determined solely by the vapour diffusion unless the capillary forces are able to transport the water condensing in the intermediate capillaries. Generally, however, the material possesses continuous fine capillaries in addition to the large pores and the intermediate capillaries, and these continuous ones can attract from a greater distance. Thus a capillary-induced water migration is superimposed on the diffusion process and reinforces or counteracts it, depending on the moisture gradient at any given time.

2.8 Pores and porous structure of hydrated cement

The pores in hydrated cement are comprised of capillary and gel pores. The amount and distribution of porosity between capillary and gel pores changes considerably as hydration proceeds. Initially, before any hydration has taken place, all the pores are capillary pores which are created by mixing water. As hydration proceeds, the capillary spaces are filled up by the hydration products, resulting in a decrease in the capillary volume, the reverse process occurring for gel pores. With increasing hydration, the volume of these pores increases. However, since the volume of the hydrated solid is greater than the volume of the anhydrous cement, the total porosity of the system decreases. Of the total porosity of a completely hydrated specimen, 28 per cent would be due to the gel pores and the remaining would be the capillary pores[65]. The volume of capillary pores is dependent on the initial water-cement ratio. The higher the water cement ratio, the greater the volume of capillary pores. The volume of gel pores, on the other hand, is independent of the water-cement ratio. For a fixed volume of anhydrous cement, and for a given degree of hydration, the volume of gel pores will always be the same[66].

Early models of the porous structure formed by cement hydrate were based largely on water sorption isotherms. The most significant work in this field can be attributed to Powers and Brownyard[67]. Powers and Browyard also studied the structure of hardened cement by using gas adsorption techniques. They estimated the size of the gel particles and

gel pores, by basing their calculations on the assumption that there were no capillary pores present in the paste structure. The surface of the gel was determined first, and subsequently, using the concept of the hydraulic radius of particles, the size of the gel pores was determined. They estimated the diameter of gel pores to be between 20 to 40Å (.002 to .004μ).

Powers[68] visualised the gel being composed of a laminar structure, the laminae being more of less tubular and concentric, except at their outer parts, where they adapt their contours to the shape of the interstitial spaces among the bodies of the cement gel. He considers the laminae to be composed of impure colloidal (crystallite) tobermorite-like material about 30 Å thick and the spaces in between them to be pore spaces with an average width of approximately 15 Å. Fundamental to the Powers model is the acceptance of the concept that those spaces exist in the gel structure and that these account for the large measured internal surface area of the hydrated cement paste.

In the study of models for the microstructure of hydrated cement, Feldman and Sereda[69] advocated a new model based on studies of nitrogen adsorption, helium flow, differential thermal analysis and other techniques. Their model has been supported by the finding of Helmuth and Verbeck[70] on the basis of shrinkage and moisture loss tests. Feldman and Sereda[69], concluded that the gel particle or crystallite has a layered structure of irregular configuration into which water enters, not as physically adsorbed, but as a structural and chemical component that

could be designated as 'interlayer hydrate water?

The mercury intrusion technique has been used to study the hardened cement paste more extensively than gas adsorption. Work by Diamond[71], using mercury porosimetry, questions the validity of applying sorption techniques to the determination of pore size distributions, irrespective of the adsorbate. Winslow and Diamond's[72] findings agreed substantially with that of Powers and Brownyard[67], but they disagreed about the volume of pores. They found that the volume of pores smaller than 82 Å was less than that predicted by Powers and Brownyard. They concluded that the pore volume in cement paste is neither gel nor capillary, but consists of spaces left between particulate hydration products. Their conclusion substantiates the finding of Helmuth and Verbeck[70], that there is a broad and continuous pore size distribution in the gel-capillary system, instead of there being two distinct pore size ranges, one belonging to capillary and the other to gel pores.

In the study of pore structure of hardened cement paste or concrete Cusens and Cabrera[73] concluded that the total amount of voids is a function of the water/cement ratio and degree of hydration. They also concluded that " the size of the pores varies within a wide range: From the very small (<5Å) which are considered part of the structure of the C-S-H to large pores up to diameter of 100μ which occur at sites originally filled with water and that have not been filled by the reaction products generated by the hydration process ".

CHAPTER THREE

CHARACTERISTICS OF THE MATERIALS USED IN THE INVESTIGATION

The materials used for determining the thermal, engineering and microstructural properties of mortars and concretes, in this investigation are detailed as follows.

3.1 Introduction

From the onset of the project, consistency in the production of the concrete and mortar samples has been important. Careful consideration was given to the choice of each individual material and once chosen a sufficient quantity from the same batch was obtained.

Ordinary Portland Cement obtained from Ribblesdale Cement Ltd. was used throughout the test programme. The sand and coarse gravel aggregate used for the preparation of mortars and concrete was obtained from deposits in North Nottinghamshire. The limestone aggregate used was supplied by Tilcon Ltd. from their Swendon quarry and the Pellite aggregate was obtained from Teeside Slag Ltd. Tap drinking water from the county of West Yorkshire was used. To study the effect of air-entraining agent on thermal conductivity, 'Febcrete' supplied by FEB U.K. in liquid form was used.

3.2 Materials

The characteristics of materials used are detailed in the following sections.

3.2.1 Cement

The cement used in the investigation was ordinary portland cement conforming with specifications prescribed in B.S. 12: 1989[74], supplied by Ribblesdale cement Ltd. in airtight plastic containers to minimise its deterioration with time. The chemical composition of the cement as supplied by the manufacturer is shown in Table 3.1.

Table (3.1)

Properties of Ordinary Portland Cement used

Oxide composition	Per cent
CaO	64.10
SiO_2	21.06
Al_2O_3	5.09
Fe_2O_3	3.01
MgO	2.58
K_2O	0.80
Na_2O	0.33
SO_3	2.92
Mineral composition	**Per cent**
C_3S	51.8
C_2S	20.6
C_3A	8.2
C_4AF	9.1
$CaSO_4$	5.0
Specific Gravity = 3.15	

3.2.2 Coarse aggregates

Three types of coarse aggregates were used:

1) Gravel aggregate

An uncrushed quartzitic gravel delivered with a maximum size of 20mm from deposits in North Nothinghamshire with bulk specific gravity of 2.62, apparent specific gravity of 2.65 and water absorption (Per Cent of Air dry mass) of 0.50%, according to B.S. 812 : Part 2 and AMD 4615: 1984[75].

The particle shapes of the aggregate were rounded to angular with a smooth surface texture.

2) Limestone aggregate

A washed, crushed calcite aggregate, supplied by Tilcon from Swendon quarry with bulk specific gravity of 2.63, apparent specific gravity of 2.72 and water absorption (Per Cent of Air dry mass) of 1.52%, according to B.S.812 : and AMD 4615[75] was used. The particles of aggregates were irregular to angular in shape with a rough surface texture.

3) Pellite aggregate

A pelletised blast furnace slag aggregate, supplied by Teeside Slag Ltd. was used with a bulk specific gravity of 1.91, apparent specific gravity of 2.07 and water absorption (Per Cent of Air dry mass) of 7.67%, according to B.S. 3681[76]. The aggregates were irregular in shape, with a rough surface texture, internally porous and honeycombed as shown in Figure 3.1.

Pellite is a by-product of the manufacture of iron in blast-furnaces ($\simeq$ 0.2 to 0.3 Kg slag/kg iron[77]), which is used in both concrete applications, and slag cement manufacture[78,79]. The chemical composition of slag is very

often between the limits (for the main constituents) shown in Table 3.2.

Table (3.2)

Oxide composition of Pelletised blast furnace slag

Constituent	CaO	SiO_2	Al_2O_3	MgO
% by weight	40-50	25-35	10-20	2-8

3.2.3 Fine aggregate

The fine aggregate used was natural quartzitic sand, obtained from deposits in North Nottinghamshire. The sand had a water absorption coefficient of 0.09% (Per Cent of oven dry mass) with bulk and apparent specific gravity of 2.65, both determined in accordance with B.S. 812: Part 2 and AMD 4615 [75].

3.2.4 Admixture

Febcrete, supplied by FEB U.K. was used as the only air-entraining admixture in the investigation. Febcrete was a brown liquid admixture of categories A and EA with specific gravity of 1.06 and was found to conform to B.S. 5075:Part 2: 1982[80].

The maximum recommended suppliers dosage was used i.e. 0.257 litres per 100 Kg of cement. The Febcrete was dissolved in the mixing water prior to being added to concrete mix.

Fig. (3.1) Photograph of typical Pellite aggregate.

3.3 Laboratory preparation of aggregates

The aggregate size and gradation are important parameters which affect the porosity and pore size distribution of concrete. A smooth grading curve for the coarse aggregate is also important to reduce segregation[81].

The three types of coarse aggregate were air dried in a well ventilated room before a sieve analysis was carried out on representative samples of each coarse aggregate type in accordance with B.S. 812 : Part 101 : 1984 [75]. The analysis showed that all the coarse aggregates needed some modification to fall within the limits specified in B.S. 882[82]. Therefore the coarse aggregates were sieved into four fraction ranges 20-14mm, 14-10mm, 10-5mm, 5-2.36mm, and stored in separate P.V.C. drums at room temperature. The final sieve analysis on all types of coarse aggregates are given in Table 3.3.

The quartzitic sand was air dried and separated into single size fractions bysieving on 2.36mm, 1.18mm, 600μm, 300μm and 150μm sieves. The different sand fractions were combined in proportions which gave a grading near the middle range of the specified Zone M band in B.S. 882[82]. The grading of the combined fractions is shown in Table 3.4.

The graded sand was then kept dry and stored in sealed plastic barrels until required for mixing.

Table (3.3)

Sieve analysis for coarse aggregates

Sieve size	B.S.882 range for graded coarse aggregates.	Blended grade used.
	Percentage by mass passing B.S. sieves.	Percentage passing
20 mm	90 - 100	100.0
14 mm	54 - 75	74.3
10 mm	30 - 60	45.0
5 mm	0 - 10	5.0
2.36 mm		

Table (3.4)

Sieve analysis for fine aggregates

Sieve size	B.S.882 grading zone M for fine aggregates.	Blended grade used.
	Percentage by mass passing B.S. sieves.	Percentage passing
1.18 mm	45 - 100	87.5
600 μm	25 - 100	77.5
300 μm	5 - 48	26.0
150 μm	0 - 10	5.0
<150 μm		

CHAPTER FOUR

MIX DESIGN AND CHARACTERISTICS OF FRESH CONCRETE

4.1 Introduction

In this chapter , mix design method and characteristics of mixes made are detailed. In a normal mix design a specific strength is aimed for but, in this investigation, the mixes were such that they would represent a wide range of porosities and densities at a constant workability or W/C ratio.

In general, an increase in the volume of pores in a concrete results in a decrease in density. Three types of voids may exist. A mix containing water, in excess of that used in the hydration process will produce voids in the concrete. Therefore, a higher W/C ratio will result in a higher volume of voids. Relatively larger microscopic pores are produced when air-entraining agents are added to a concrete mix. The largest pores in concrete are caused by accidentally entrapped air. These are usually large enough to be seen with the unaided eye.

The quantity of pores in concrete due to excess water and entrained air can be controlled by mix design. The quantity of pores due to entrapped air is controlled by the

method of placement as well as by mix design. A concrete mix can be designed to reduce entrapped air for the particular method of placement used. The presence of any of these three types of voids decreases the density and increases the porosity of concrete.

4.2 Selection of materials

In order to investigate the effect of porosity on the conductive heat transfer of concrete it was necessary to use several coarse aggregates with different characteristics. Concrete made from quartzitic coarse aggregate was used as a reference. Limestone aggregate was chosen because it has nearly the same specific gravity and porosity as quartz but different mineral composition.

Pellite aggregate was selected because it has totally different characteristics having a porous and glassy structure with lower specific gravity.

4.3 Mix design method

The reference mix design used in this investigation followed a method suggested by Cabrera based on the concept of minimum porosity and maximum strength[83], i.e. mixes labelled "A" in Table 4.1 which have a cement : sand : coarse aggregate ratio of 1:2.33:3.5.

Changes in porosity were achieved by;

1) Changing the cement-aggregate ratio, i.e. mix proportion "B" has the same sand-cement ratio as the reference mix but increased coarse aggregate-sand ratio.

2) Changing the cement-sand ratio, i.e. mix proportion "C" has the same coarse aggregate-sand ratio as the reference mix but increased sand-cement ratio.

3) Changing the W/C ratio. A W/C ratio of 0.8 was initially used as a reference for each mix proportion and type of coarse aggregate. Subsequently this mixes were made at a constant workability of 75 ± 25mm for each mix proportion and type of coarse aggregate (see Table 4.4). This resulted in a variation in W/C ratio for each mix proportion and type of coarse aggregate. The total W/C ratios needed to achieve constant workability for respective mixes are shown in Table 4.1.

4) Using air - entraining admixture. The air-entraining admixture was used to achieve a constant workability of 75 ± 25mm for each different type of coarse aggregate for mix proportions "A" and "C". These mixes are designated by the third letter "E" in their mix code name (see Tables 4.1 or 4.4).

Using mix proportions "A", "B" and "C" and the three different types of coarse aggregate, enabled a wide range of density, porosity and different pore structures to be achieved. In total, 24 mix designes were used, their compositions are given in Table 4.1. The total porosity achieved and mean dry density of each mix are given in Table 4.2.

Table (4.1)

Composition of mixes made

Mix Code Name	Mix proportions (by mass) Cement: sand: Agg	Type of Coarse Agg	Air-entrained	Total W/C
QA /.53	1 : 2.33 : 3.5	Quartzitic	NO	0.53
QAE /.43	"	Quartzitic	YES	0.43
LA /.60	"	Limestone	NO	0.60
LAE /.50	"	Limestone	YES	0.50
PA /.90	"	Pellite	NO	0.90
PAE /.80	"	Pellite	YES	0.80
QA /.80	"	Quartzitic	NO	0.80
LA /.80	"	Limestone	NO	0.80
PA /.80	"	Pellite	NO	0.80
QB /.80	1 : 2.33 : 5.6	Quartzitic	NO	0.80
LB /.80	"	Limestone	NO	0.80
PB /.80	"	Pellite	NO	0.80
QB /.56	"	Quartzitic	NO	0.56
LB /.66	"	Limestone	NO	0.66
PB /1.05	"	Pellite	NO	1.05
QC /.90	1 : 3.73 : 5.6	Quartzitic	NO	0.90
QCE /.80	"	Quartzitic	YES	0.80
LC /.95	"	Limestone	NO	0.95
LCE /.90	"	Limestone	YES	0.90
PC /1.29	"	Pellite	NO	1.29
PCE /1.29	"	Pellite	YES	1.29
QC /.80	"	Quartzitic	NO	0.80
LC /.80	"	Limestone	NO	0.80
PC /.80	"	Pellite	NO	0.80

Notes on mix code names:

Q Stands for concretes made with Quartzitic coarse Agg.
L Stands for concretes made with Limestone coarse Agg.
P Stands for concretes made with Pellite coarse Agg.

	Cement	: Sand	: Coarse aggregate	
A	1	: 2.33	: 3.5	(Reference mix)
B	1	: 2.33	: 5.6	
C	1	: 3.73	: 5.6	

Third letter (E) Indicates Air-entrained mix (0.257 Litre/100kg of Cement).

Table (4.2)

Mean dry density and total porosity of mixes made at 'A' curing condition

Mix Code Name	Mean dry density (kg/m^3)	Total porosity by V.S. (%)
QA /.53	2282	12.9
QAE /.43	2091	14.0
LA /.60	2248	15.0
LAE /.50	2033	21.0
PA /.90	1858	21.0
PAE /.80	1557	38.5
QA /.80	2250	13.9
LA /.80	2243	15.3
PA /.80	1902	20.1
QB /.80	2291	12.6
LB /.80	2261	14.1
PB /.80	1570	23.4
QB /.56	2341	10.2
LB /.66	2291	12.1
PB /1.05	1647	25.1
QC /.90	2236	15.1
QCE /.80	2020	23.5
LC /.95	2207	17.6
LCE /.90	1988	25.5
PC /1.29	1818	25.5
PCE /1.29	1551	39.0
QC /.80	2238	12.9
LC /.80	2243	13.1
PC /.80	1745	26.1

Notes on mix code names:

Q Stands for concretes made with Quartzitic coarse Agg.
L Stands for concretes made with Limestone coarse Agg.
P Stands for concretes made with Pellite coarse Agg.

	Cement	: Sand	: Coarse aggregate
A	1	2.33	3.5 (Reference mix)
B	1	2.33	5.6
C	1	3.73	5.6

Third letter (E) Indicates Air-entrained mix (0.257 Litre/100kg of Cement).

4.4 Mixing, Curing and conditioning

The fresh concrete was mixed using a Cumflow pan mixer of 250kg capacity. Prior to mixing, the materials were spread in layers in the bottom of the pan , coarse aggregate grades first, cement and then finer grades. These were mixed dry for the first minute in order to homogenise the batched materials, water was then added and mixed for further three minutes. The workability was then checked (see section 4.4.1). The same procedure was followed for the air-entrained mixes, but the admixture was dissolved in the mixing water before being added to the batched materials. The admixture volume was deducted from the mixing water, although this quantity was minimal. Sufficient concrete was mixed to produce the samples necessary for all the specified tests.

Two 300 mm × 300 mm × 50 mm thick specimens were prepared for thermal conductivity measurements which were compacted by hand in three layers. Twenty eight 100mm cubes were cast by hand compacting in two layers. For the concretes having a very low slump, compaction was done in six layers for slabs and in three layers for cubes. After compaction the moulds were covered with wet hessian and polythene sheets to prevent water loss during the first 24 hours after casting. At the end of this period the specimens were stripped and placed in a Fog room at 20°C.

Mortar mixing (corresponding to Quartzitic and limestone concretes) was carried out in a 'Hobart AE125' bowl type mixer of 0.005 m^3 capacity. The composition of the mortar was obtained from the concrete mixes, Table 4.1. All

the ingredients were placed in the mixer and mixing lasted for two minutes at low speed, two minutes at middle speed and then a further two minutes at high speed. This mixing cycle produced homogeneous mixes which did not bleed much. For Pellite concrete mixes, mortar was sieved from concrete on a 2.36mm sieve. The mortar specimens, i.e. twelve 50mm cubes were cast by hand compaction and cured similar to the concrete mixes.

After demoulding, the specimens were cured at 20°c and 100% relative humidity for 3 days. It is known that initial curing conditions strongly affect the pore structure and composition of the hydrating phases[84], therefore the specimens were kept in a Fog room for three days to achieve good hydration. In accordance with BS874:1988[1], the concrete slabs (and 50mm mortar cubes and most of the 100mm concrete cubes) were then conditioned to constant weight in a laboratory controlled room of 65% RH and 20°c, i.e. curing regime "A" in Table 4.3 . For determination of moisture correction factors, eight mixes were selected representing various dry densities in the range 1550 to 2350 kg/m^3 and all the curing and conditioning regimes shown in Table 4.3 were carried out on them (see section 5.5.2).

Table(4.3)

Summary of curing and conditioning regimes

"A" : 3 days in Fog room + Equilibrated in 65% R.H. and 20°C

"B" : 'A' condition + Equilibrated in Fog room.

"C" : 'B' condition + Equilibrated in 65% R.H. and 20°C

"D" : 'C' condition + Equilibrated in 33% R.H.* and 24°C

"E" : 'D' condition + Equilibrated in 15% R.H.* and 40°C

"F" : 'E' condition + Oven dry at 105°C

(*) 33 per cent R.H. and 15 per cent R.H. were maintained in conditioning cabinets with saturated salt solutions of magnesium chloride and potassium hydroxide respectively.

4.5 Properties of fresh concrete

4.5.1 Workability

Workability is a property of fresh concrete which determines the ease with which it can be handled, placed and compacted thoroughly. Since workability is related to compaction, then it's importance extends to the hardened properties of concrete. The A.S.T.M.[85] defines it as "The property determining the effort required to manipulate a freshly mixed quantity of concrete with a minimum loss of homogeneity".

Three widely used tests for measuring workability are the slump, compacting factor and V-B consistometer. These are standard tests used in the U.K. and are described in detail in B.S. 1881[86]. There is no single relationship between the slump, compacting factor and V-B results for different concretes. For high workability concretes, these three methods are not sensitive enough and a flow table test (which is originally known as the German DIN 1048[87] flow table) is used. Flow table is basically a measure of the spread of a fixed quantity of concrete after jolting it in a standard manner (according to B.S. 1881[86]). In this investigation the workability of the concrete was measured by means of the slump test and for high workability mixes the flow table test was used.

The results for the workability tests are given in Table 4.4 and clearly demonstrate the changes in workability which results from changing the W/C ratio, mix proportions and the addition of air-entraining agent. As can be seen from Table 4.4 the slump was always maintained within the

range 50-100mm as recommended by Concrete Practice[88] for hand-compacted concrete. As shown in Table 4.4, some mixes had developed segregation and bleeding. Segregation is the separation of the constituents of the mix due to differences in their size and S.G. Bleeding is a particular form of segregation in which some of the components rise to the surface of the fresh concrete. Such instability in the concrete mix is caused by the matrix having insufficient strength to retain the individual aggregate particles in a homogeneous dispersion. It may be noted that entrained air reduces the danger of segregation[89]. Segregation is difficult to measure quantitively and in this investigation it was assessed on the basis of visual observation and 'feel' of the concrete, both at the time of mixing and during the measurement of slump and flow table tests.

4.5.2 Air content

Since the air content of concrete is related to its physical properties, it was considered important to determine the air content of concrete mixes with air-entraining agent according to the method specified in B.S. 1881 : Part 106[86]. The air content test basically involves measuring the reduction in volume of a known quantity of concrete resulting from an applied air pressure.

The apparatus was calibrated for the mix design used following a procedure specified in B.S. 1881 : Part 106[86]. The air pressure at which the air content of concrete should be determined was found to be 0.12 N/mm^2 and the test was carried out approximately 30 minutes after mixing, complying with the time interval specified by B.S. 5075 : Part 3[80]. The results are given in Table 4.4.

Table (4.4)

Fresh properties of mixes

Mix Code Name	Slump (mm)	Flow Table (mm)	Appearance Of Concrete	Air Content (%)
QA /.53	50	-	O.K.	-
QAE /.43	55	-	O.K.	11.0
LA /.60	60	-	O.K.	-
LAE /.50	70	-	O.K.	12.5
PA /.90	75	-	harsh	-
PAE /.80	100	-	wet	25.0
QA /.80	-	750	very wet, slight segregation	-
LA /.80	-	660	wet, slight segregation	-
PA /.80	5	-	dry, non - cohesive	-
QB /.80	-	635	slight segregation	-
LB /.80	-	545	slight segregation	-
PB /.80	5	-	harsh, slight segregation	-
QB /.56	50	-	O.K.	-
LB /.66	55	-	O.K.	-
PB /1.05	100	-	slight segregation	-
QC /.90	60	-	slight bleeding	-
QCE /.80	100	-	O.K.	12.0
LC /.95	60	-	O.K.	-
LCE /.90	100	-	O.K.	12.5
PC /1.29	50	-	shear slump	-
PCE /1.29	95	-	wet	21.0
QC /.80	5	-	slight bleeding	-
LC /.80	0	-	dry, slight bleeding	-
PC /.80	0	-	very dry, harsh	-

Notes on mix code names:

Q Stands for concretes made with Quartzitic coarse Agg.
L Stands for concretes made with Limestone coarse Agg.
P Stands for concretes made with Pellite coarse Agg.

	Cement	Sand	Coarse aggregate	
A	1	2.33	3.5	(Reference mix)
B	1	2.33	5.6	
C	1	3.73	5.6	

Third letter (E) Indicates Air-entrained mix.
(0.257 Litre/100kg of Cement.)

CHAPTER FIVE

THERMAL CONDUCTIVITY MEASUREMENT

This chapter summarises the different techniques of thermal conductivity measurement that are available. The measuring technique selected and the designed apparatus is then described in detail. In the subsequent sections, investigations into surface contact resistance and error analysis are given. In the last section of this chapter the moisture correction factors used are reviewed and a general model is derived for moisture correction over the density range studied.

5.1 INTRODUCTION

Methods of determining the thermal conductivity of concretes can be classified as either steady state or non-steady state (transient) methods.

In the steady state technique, the thermal conductivity is obtained from measurements of a temperature gradient together with the heat flux into or out of the sample in accordance with Fourier's conduction equation (Equation 2.1). Different apparatuses for steady state measurement are detailed in B.S. 874 : Part 1 and 2: 1986[5].

For the purpose of this research, the plain hot-plate method, as recommended in B.S. 874: 1973[6] was used. However, when a revised B.S. 874: was published in 1986[5], which was after the commencement of this research work, it recommended that either a guarded hot-plate method or a plain hot-plate method could be used for the testing of concretes as manufactured during this investigation.

In dynamic or non-steady state methods, the temperature distribution throughout the sample varies with time; consequently the complete differential equation of heat flow is involved and the diffusivity is measured[90]. As the measurement time is short, heat losses have a reduced influence on the measured value and moreover, they can be included in the differential heat flow equation or its boundary conditions.

Dynamic methods can be divided broadly into two categories, Periodic and Transitory, depending upon whether the thermal energy is supplied to the sample with a modulation of fixed period or as a single addition or subtraction. As a consequence the temperature changes in the sample are either periodic or transitory. In general, measurements of the power input are not required in evaluations of thermal diffusivity nor are absolute measurements of temperature, but relative changes in magnitude of temperature as a function of time and position must be recorded. The temperature detectors therefore do not need accurate calibration; all that is required is a sensitive detector whose response is linear over changes of a few degrees.

A) Periodic Methods.

The basic principle of this method, devised originally by Ångström[91], is that if one end of a sample is heated periodically, then the temperature along the sample also varies with the same period but with diminishing amplitude. Moreover, as the temperature wave travels along the sample with finite velocity there is a varying phase relationship. Measurement of the amplitude decrement and either the phase difference or velocity enables the diffusivity to be determined.

B) Transitory Methods.

Transit-state methods of conductivity measurement may conveniently be divided into two broad categories, namely those using a line source of heat and those using one or more plane sources of heat.

In both categories, the sample is initially in equilibrium with uniform temperature surrounding, then part of it is subjected to a change in thermal flux. The diffusivity is evaluated from changes in temperature which occur in measured time intervals at one or more points within the sample.

Various transient methods have been developed and refined for the rapid measurement of thermal conductivity, and it was only natural, that due to their speed these should be proposed for use with moist materials.

All the varying types of test apparatus for determining thermal conductivity have their advantages and disadvantages. Transient techniques, due to their rapid

method of measurement, minimise water migration and generally require comparatively simple equipment but it is difficult to meet the boundary conditions assumed in the mathematical solutions which are used and this limits their accuracy. Due to the latter, transient measurement techniques are generally restricted to comparative testing and quality control. Steady state methods require careful design, calibration and skilled operation of equipment to obtain accurate results and relatively long test periods present moisture migration problems.

Non-steady state methods are used chiefly in research and not at present for standard measurements; they are probably more suitable than the steady state method for investigating the influence of moisture on thermal conductivity. Their success depends upon knowing how closely the boundary conditions of temperature and heat flow are maintained throughout the experiment. For this reason they are probably less reliable than the steady-state method for routine measurement.

B.S. 874[5,6] accepts only steady-state techniques as standard methods for the determination of thermal conductivity. The plain hot-plate being most suitable for the determination of thermal conductivities of concretes at ambient temperatures. The apparatus and the method of measurement used is described in the following section.

5.1.1 Plain hot-plate apparatus

In order to deal with the range of thermal conductivities investigated, the plain hot-plate apparatus

was designed to conform with the specifications of B.S. 874: 1973 and amendments 3006 and 5173[6], and also B.S. 874: 1986[1] later in the research work. The apparatus comprised of :

A) A hot-plate to input a steady measured heat flux to the specimens.

The plate emits heat almost equally from both surfaces and consists of two flat aluminium alloy plates measuring 300 mm square, each 10 mm thick which sandwich an insulated heating element whose resistance is 2.043 ohms/m. The working surfaces have been machined flat to within 0.05mm. The heating element is made of nichrome wire, uniformly wound across the full plate as shown in Figure 5.1. The element is supplied with direct current from a Farnell TSV70 Mk.2 stabilised power unit capable of maintaining the power constant to at least $\pm$ 0.02 % over the duration of a test. The heater voltage and current are measured by two Thurlby digital multimeters with programmable computing and data logging facilities.

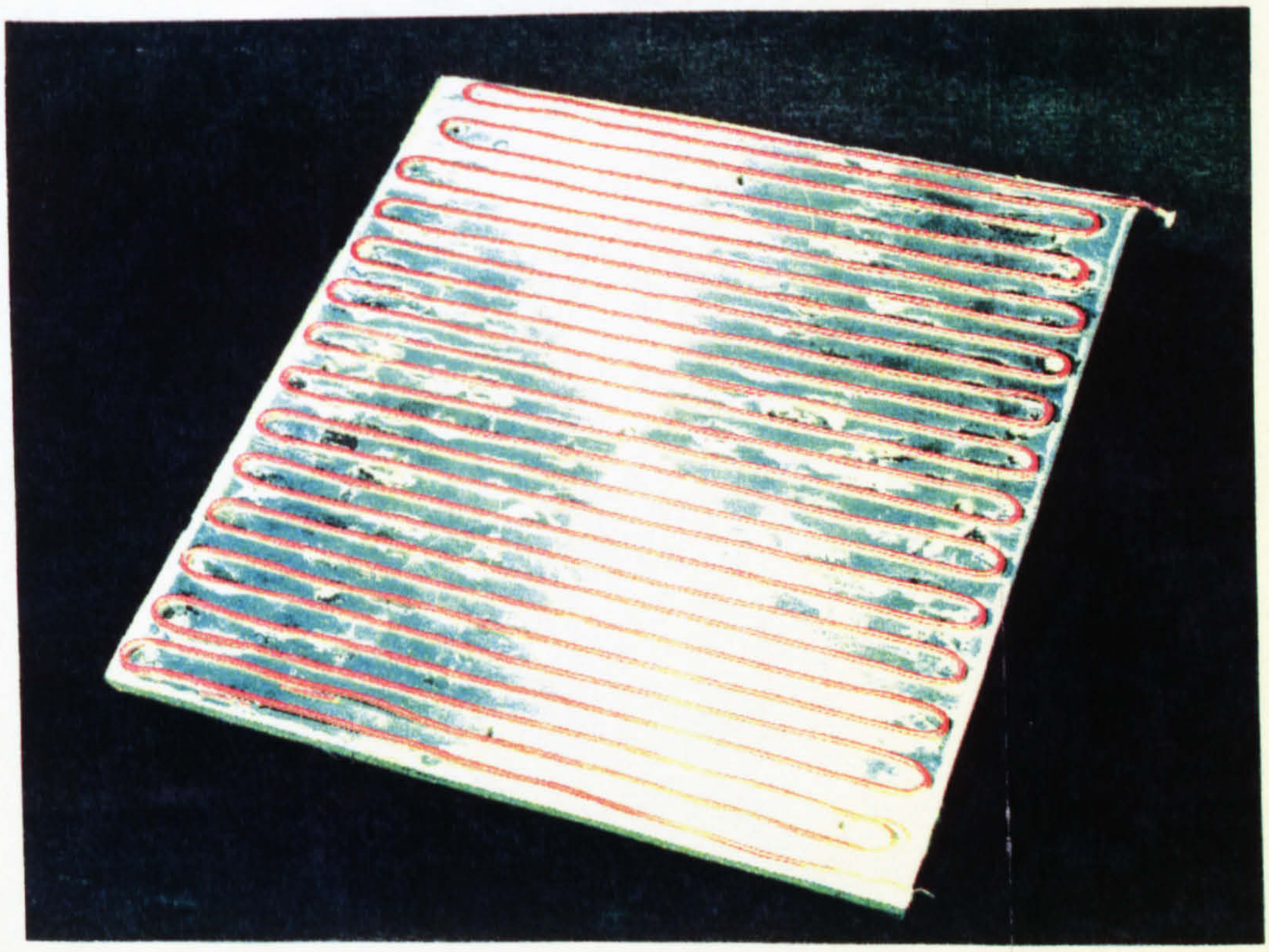

Fig.(5.1) Photograph of inside hot plate showing layout of heating element.

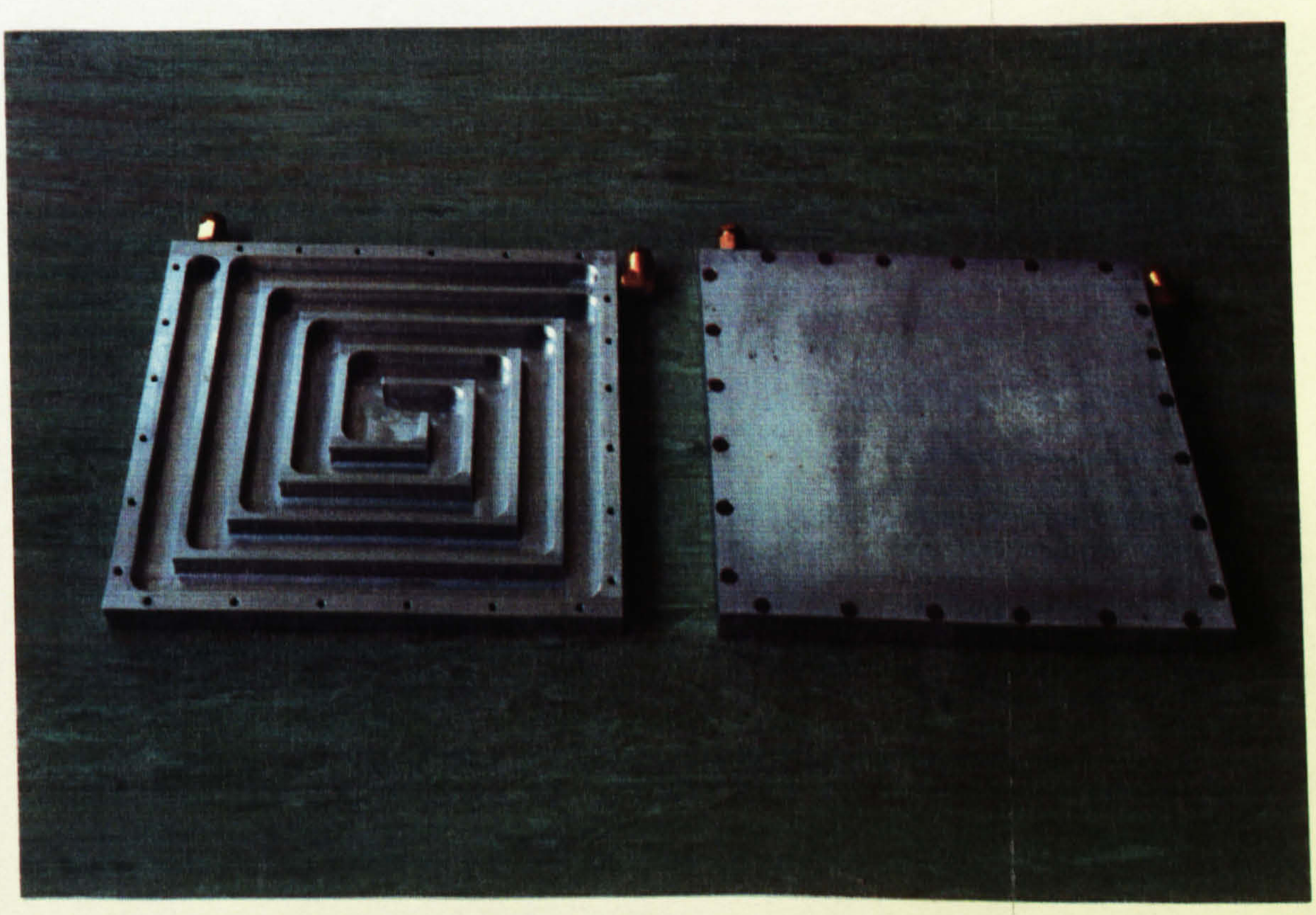

Fig.(5.2) Photograph of cold plate showing reversing spiral circulation system on the left and flat surface of completed cold plate on the right.

B) Cold-plates to remove heat after it passes through the specimens.

The cold-plates have sufficient thermal capacity to enable specimens measuring 300 mm × 300 mm × 50 mm thick, to absorb heat continuously during the test period without significant temperature rise. The cold sinks were machined from 24 mm thick aluminium alloy plates and contain a water cooled reversing spiral circulation system which is designed to minimise lateral temperature gradients and resistance to coolant flow as shown in Figure 5.2. The working surfaces have been machined flat to within 0.05mm. The coolant water, which contains a glycol antifreeze is circulated via a series of lagged plastic pipes at a rate of approximately 15 litres/min. at a temperature controlled to better than ± 0.05 °C by a Techne C-400 circulator. Heat is extracted from the coolant at a steady rate by a Techne FC-500 Flow Cooler unit which is used in series with the circulator.

C) System for measuring the temperature gradient through the specimens.

The temperature of the heated and cooled surfaces of the specimens are measured by averaging the output from four copper-constantan (Type T) thermocouples which are held in position on the samples surface by tape. All the thermocouples used were constructed by arc welding 0.2mm diameter copper-constantan wire in an argon atmosphere, rolled out flat to about 0.035mm using a purpose built miniature roller and calibrated to within ± 1 μV of each other. (The complete procedure of making, rolling and calibrating the thermocouples is detailed in Appendix III).

Single layers of 2 mm thick foamed silicone-rubber sheets are placed between the specimens and the hot-plate and the cold-plates to improve thermal contact by reducing air gaps caused by surface irregularities (Figure 5.3). Heater and cold-plates temperatures are monitored by similar thermocouples located in shallow grooves in their surfaces.

The thermocouples are connected via a copper cold-sink reference junction into the data logging system . Thermocouple outputs are recorded in microvolts by a M.F.I. 1010 and a M.F.I. 200 data logger (CIL-Electronics Ltd.) before being converted to temperature using standard conversion tables. The logger has 24 channels linked via a RS 232 communication port to an IBM XT micro-computer where data analysis is carried out.

The cold junctions of the thermocouples are electrically insulated and located at the bottom of 7 mm diameter holes drilled in a concentric circle in an 87 mm diameter copper block to half its 150 mm depth, The whole cold junction assembly is protected against sudden changes in temperature by encasing it in an insulating jacket. All the cold junctions are then assumed to be at the same temperature. The reference cold junction temperature is measured by a calibrated mercury in glass thermometer placed in a central hole in the block together with a precision platinum resistance thermometer sensor which is connected to the data logger.

The specimens are placed one on each side of the heater plate and the whole assembly is located between the cold-plates as shown schematically in Figure 5.3. To ensure

proper thermal contact, the apparatus is loaded with a mass of about 42 kg which is separated from the upper cold-plate by a slab of polystyrene insulation to prevent damage to the plate and to insulate it.

The edge heat losses are kept to a minimum by surrounding the apparatus with 100mm of insulating material. The whole hot-plate apparatus is enclosed in an insulated wooden cabinet to minimise heat losses and the effects of change in the ambient temperature (Figure 5.4). To minimise condensation, the cabinet is sealed around the edges.

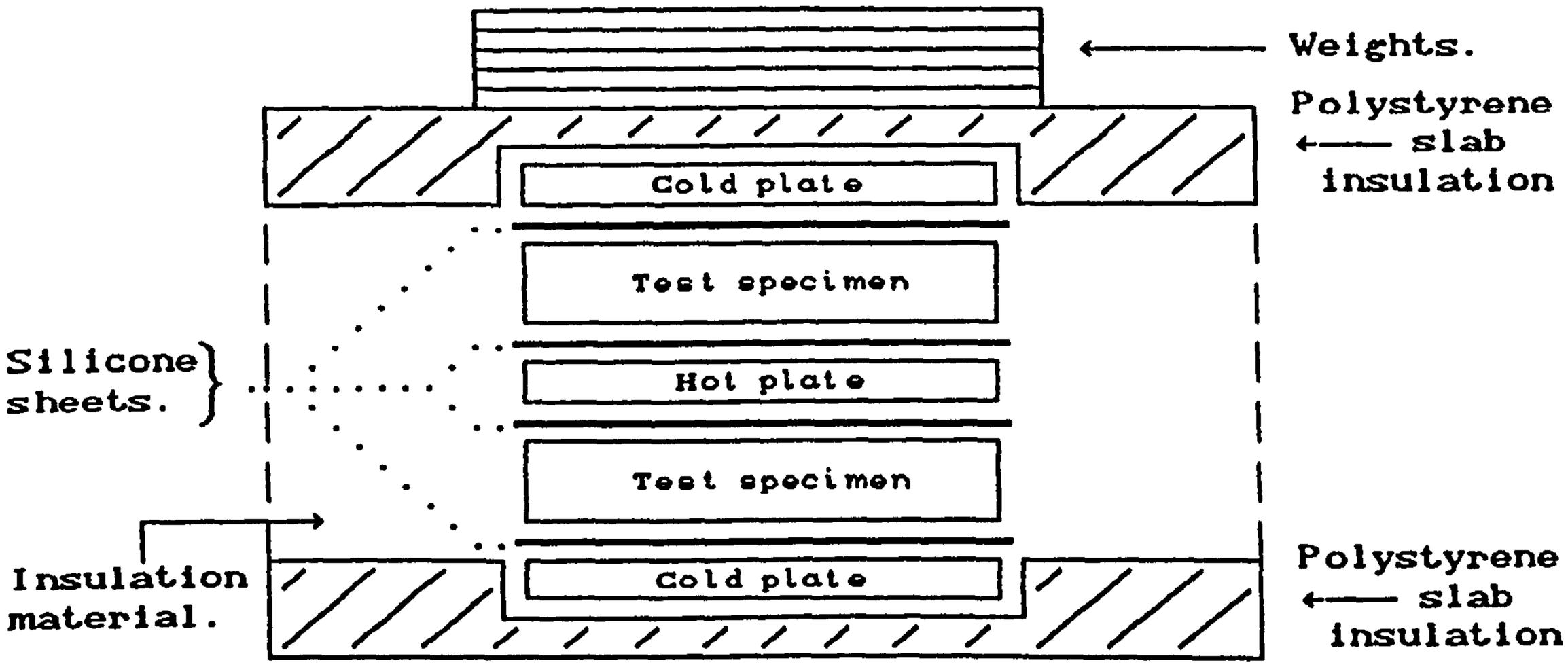

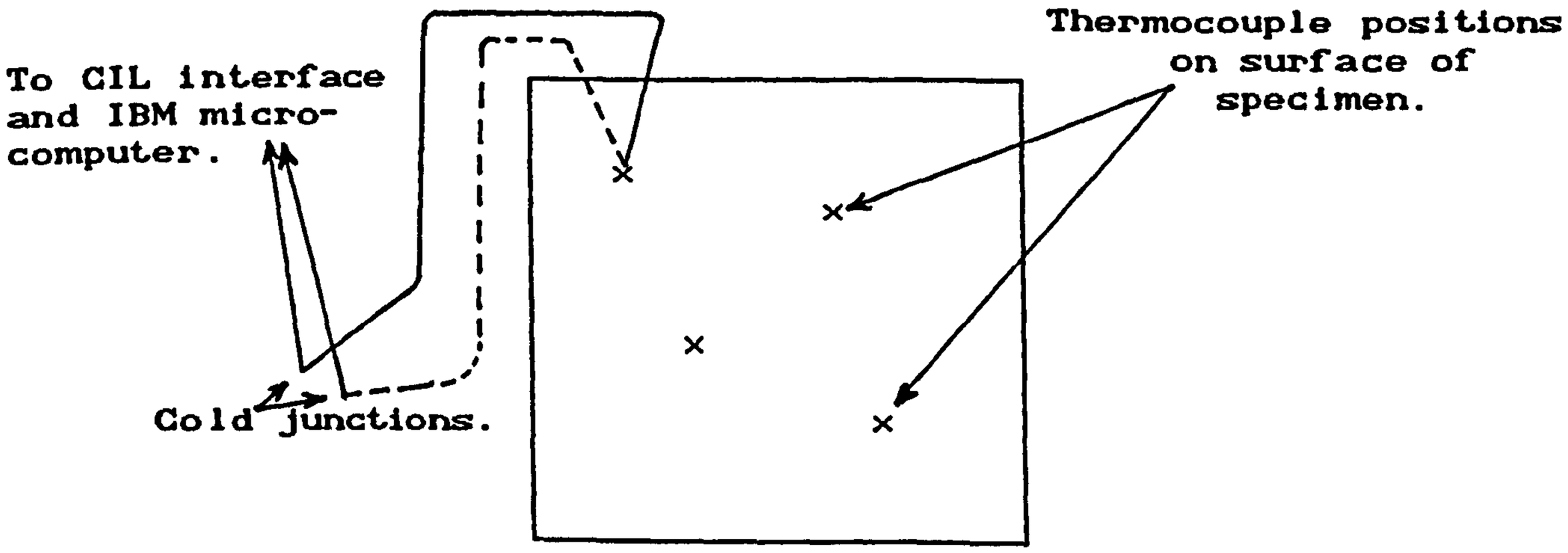

Fig.(5.3) Diagram of plain Hot-plate Apparatus and typical thermocouple arrangements on specimen surfaces.

Fig.(5.4) Photograph of opened insulating cabinet.

Fig (5.5) Photograph of the Hot-plate Apparatus and Insulating Cabinet with controlling equipment and the micro-computer.

An IBM XT micro-computer was used to collect and store the data from the apparatus and speed up the calculations of the thermal conductivity value. The print-out format presents all the information relating to each individual measurement on one sheet and is shown in Appendix III.

The complete hot-plate apparatus and insulating cabinet with controlling equipment and the micro-computer is shown in Figure 5.5.

5.1.2 Test procedure

Before placing the specimens in the apparatus they were conditioned to an equilibrium air-dry moisture content in accordance with B.S. 874: 1986[1], i.e. conditioned to constant weight in a controlled laboratory environment of 65% R.H. and 20°C. They were deemed to be in equilibrium, when three consecutive weekly weighings were the same. This ensured that any contained moisture was evenly distributed and that the moisture content was low. With the specimens assembled between hot and cold plates and the insulation in place, the heat flux was applied. Temperatures were allowed to reach steady state with hot-face temperatures at 27 $\pm$ 3°C and cold face temperature at 10 $\pm$ 3°C with a minimum difference of 15°C between them.

When steady conditions were attained, three consecutive two hourly readings of hot-plate power consumption and thermocouple output were taken to check that conditions were steady in accordance with B.S. 874[1]. The thermal conductivity measurement was taken to be the mean of the values determined for each run. At the conclusion of the test, both specimens were removed from the apparatus and

weighed, and their weights compared with the pre-test values. Any appreciable change in weight rendered the measurement invalid. i.e. if there is a variation greater than 0.2% by volume between the moisture contents before and after testing.

The thickness of the specimens was measured at eight points around the perimeter and the mean determined. A check was made to ensure that the variation in thickness across the full width of each specimen did not exceed 2% of the mean, and that the mean thickness of the two specimens did not differ by more than 2% . Length and width were also measured at three well-spaced points and the mean found. All the measurements were made using vernier callipers capable of measuring to an accuracy of 0.02 mm. The cross-sectional dimensions of the specimens were the same as the corresponding dimensions of the heater and cold plates (300 mm) and all the thickness of the specimens were all around 50mm. The flatness of slabs were measured by placing a steel straight edge across the diagonals of the faces and inserting a feeler gauge into the gap. The deviation from flatness of all the specimens were less than 0.05 mm over their full length and width.

To determine the average moisture content and dry density of the specimens, the slabs were oven dried at 105 °C for 48 hours. Drying at this temperature for 48 hours reduced the slabs to a constant mass after which the dry density could be determined. Specimens were cooled to ambient temperature in a desiccator to prevent moisture regain. The moisture content of the specimens during test was determined in accordance with B.S.2972 'Methods of test for thermal insulating materials'[92].

5.2 Calibration of plain hot-plate apparatus

To determine thermal conductivity accurately by the plain hot-plate method, the edge heat loss from the sides of the specimens has to be taken in to account. This was achieved by comparing the thermal conductivities of a pair of glass fibre slabs, obtained in the plain hot-plate apparatus with those obtained on the same sample in a guarded hot plate. The sample were provided, by a British Calibration Service accredited laboratory at Salford University.

The edge loss q_l thus equals:

$$q_l = q_p - q_g = (\lambda_p - \lambda_g) \frac{A\Delta t}{L} \qquad \ldots(4.1)$$

where:

q_l = Rate of heat loss (W)

q_p = Rate of heat flow through plane hot-plate (W)

q_g = Rate of heat flow through guarded hot-plate (W)

λ_p = Thermal conductivity from plane hot-plate (W/mK)

λ_g = Thermal conductivity from guarded hot-plate(W/mK)

A = Area of slab (m^2)

Δt = Temperature difference across the hot and cold faces (K)

$\Delta\theta$ = Mean sample temperature ($^\circ$C)

L = Thickness of slab (m)

Therefore the heat loss, q_l at various mean sample temperatures were determined and the graph of q_l against $\Delta\theta$ was plotted as shown in Figure 5.6. The data were statistically correlated by regression analysis and the following equation was found to be the best fit.

$$q_l = -0.291 + 0.065\ \Delta\theta \qquad \text{with } r=0.999$$

This edge loss correction equation was incorporated in to the thermal conductivity calculation program to correct the λ-values obtained for any edge loss error.

Great care was taken in the packing arrangement of the quilt insulation inside the cabinet to be identical each time the rig was assembled so that the edge loss factor would not be altered. Should a change in the insulation layout within the plain hot-plate apparatus take place, then the edge loss process would have to be repeated.

Having determined the heat loss corrections, the rig was calibrated by measuring the thermal conductivity of a pair of Siporex samples and comparing the results obtained with those provided by an accredited test house on the same slabs. The Siporex slabs were also used for checking the long term stability, accuracy and repeatability of the apparatus, at regular intervals throughout the duration of the research programme.

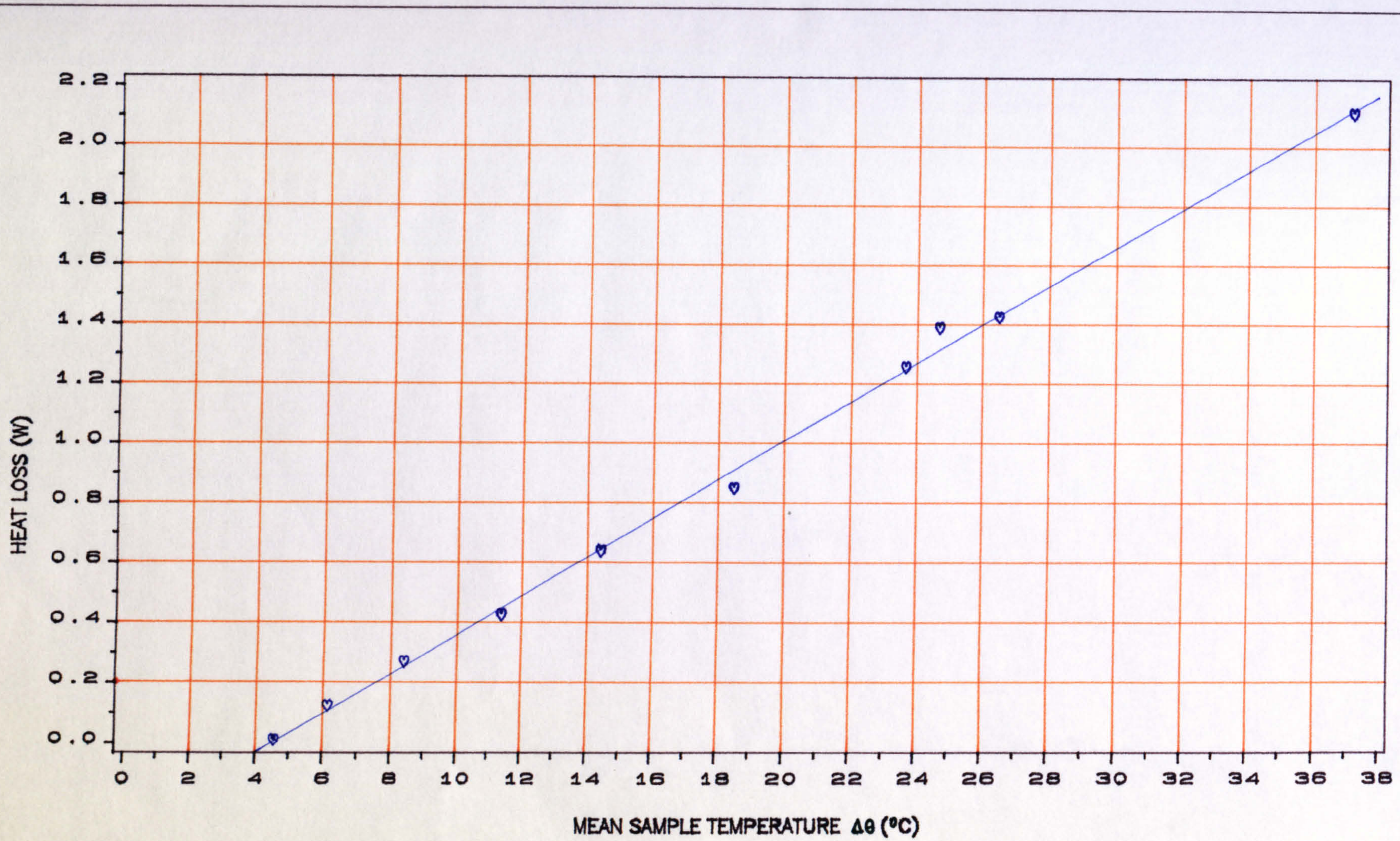

FIGURE (5.6): Heat Loss Vs. Mean Sample Temperature For Rig Calibration Using Glass Fibre Slabs

5.3 Preliminary investigations and results

The test apparatus used at the commencement of the research programme had been designed for low density concretes hence it was necessary to check the capability of the equipment for normal density use.

One pair of dense concrete slabs (ρ = 2275 kg/m^3) were selected for trial runs. After the initial tests, it was found that the output of the power unit must be increased to almost twice the original capacity in order to achieve a temperature difference of 15 °C across the specimen to meet the requirements of B.S. 874 [6]. After making this improvement it was found that the heat exchange unit (Techne FC200 Flow Cooler) had insufficient cooling power to remove all the heat flux through the slabs so it was replaced by a larger cooler (Techne FC500).

With this heat exchange unit and original circulator, a repeat measurement was made and it was found that the temperatures of the hot and cold surfaces of the specimen and also the temperature difference across them could be maintained at the desirable temperature recommended by B.S.874[6]. Hence this equipment set up was adopted for the research programme.

5.3.1 Investigation into surface contact problems

Many investigators [93,94] have recognized that the precise method of measuring surface temperatures' with thermocouples can significantly alter the measured thermal conductivity. Hence before commencing the full scale thermal conductivity measurements, it was essential to investigate how one can ensure a good thermal contact between the

thermocouple's hot-junction and the faces of the specimens. For this investigation different methods of fixing thermocouples were examined. At the begining Tinker's method[95] of fixing the thermocouple's hot-junction to the faces of the foamed silicone-rubber sheets, by applying a thin layer of silicone rubber, was adopted. This method is fast, reproducible and easy (see method 1 below) compared to fixing the thermocouple's hot-junction directly to the faces of the specimens with adhesive tape as B.S.874[1,6] recommends.

To investigate the surface contact problem further, twelve different techniques of fixing the thermocouple to the concrete slabs were developed and compared with each other. All the fixing techniques were carried out with 0.2 mm diameter Type T (copper-constantan) thermocouples, on the same dense concrete samples (ρ = 2275 kg/m^3). The apparatus was initially loaded with a mass of about 32.3 kg.

Method 1 The thermocouples were fixed onto their respective sides of the foamed sheets with a thin layer of silicone rubber adhesive. Care was taken to ensure that the beads formed were all of the same thickness as possible (between 0.4 mm to 1.4 mm in thickness) so that any existing air gaps on the surfaces would be similar.

Method 2 The beads were flattened with a 'G-clamp' and care was taken to ensure that they were all approximately the same thickness (between 0.2 mm to 0.4 mm). The thermocouple's hot-junctions were again fixed to the faces of the foamed silicone-rubber sheets and care was taken to ensure intimate contact with the specimen.

Method 3 The flattened thermocouples were fixed to the faces of the foamed silicone-rubber sheets and a smear of zinc oxide contact paste (heat sink compound) applied between the bead head and the surface of the concrete specimen.

Method 4 Same technique as method 3 was used except that heat sink compound was also smeared round the thermocouple's bead head.

Method 5 A small piece of aluminium foil, about 40mm x 50mm was stuck on to the foamed silicone sheet and the thermocouple's hot-junction was fixed on top of the aluminium foil by applying a thin layer of silicone rubber. Heat sink compound paste was applied between the bead head and the surface of the concrete specimen.

Method 6 Same technique as previous method was used except that heat sink compound paste was smeared round the thermocouple's bead head.

Method 7 Method 2 was repeated with 270 per cent increase in clamping force. i.e. a load of 90.4kg was applied instead of 32.3kg.

Method 8 Method 3 was repeated with 270 per cent increase in clamping force.

Method 9 Thermocouples held in position on the sample's surface by tape, with the end of the thermocouple flattened and a smear of heat sink compound paste between the bead head and the surface of the concrete specimen (recommended British Standard method).

Method 10 The 0.2mm diameter thermocouple's wires were joined by arc welding, then rolled out flat to 0.1mm, 0.075mm, 0.05mm and eventually to 0.035mm using a miniature hardened steel roller. These foiled thermocouples were then held in position on the sample's surface by tape with a smear of heat sink compound paste between the foil and the surface of the concrete specimens.

Method 11 Method 9 was repeated with 270 per cent increase in clamping force.

Method 12 Method 10 was repeated with 270 per cent increase in clamping force.

A different thermocouple fixing method is recommended in B.S. 874 for materials having λ-values greater than 0.5 (W/mK) [1,6]. That is to cement the thermocouples into grooves made in the specimen's face. Several attempts were made at trying to cement thermocouples into preformed grooves in the faces of the samples but, due to the number of slabs to be tested, this method proved to be extremely impractical. Another major problem was the inaccuracy in measuring the distance between the two thermocouples across the thickness of the slabs.

5.3.2 Results and trends

The results of the investigation in to surface contact problems are summarised in Table 5.1.

TABLE (5.1)

Summary results of surface contact methods

Method No.	Av.Temp. Diff.(K)	Av.sample Temp.(K)	Av.mc.% by vol.	Measured λ (W/mK)	λ @ 3% m.c. (W/mK)
1 — Beads not flattened.	16.3	17.6	3.73	2.04	1.98
2 — Beads flattened.	16.4	17.1	2.28	2.01	2.14
3 — Flattened & ZnO pasted.	15.9	17.7	2.37	2.14	2.27
4 — Flattened & ZnO pasted round the bead head.	16.3	17.9	2.34	2.03	2.16
5 — Flattened, AL. foiled & ZnO pasted.	16.2	19.4	2.35	2.22	2.36
6 — Flattened, Al & ZnO pasted round the bead head.	16.3	19.1	2.24	2.21	2.38
7 — Flattened & 270% inc.wt.	16.1	16.4	2.28	2.04	2.19
8 — Flattened, ZnO pasted & 270% inc.wt.	15.9	16.2	2.37	2.15	2.29
9 — Flattened, taped & ZnO pasted.	16.0	18.8	2.44	2.26	2.39
10 — Rolled,taped & ZnO pasted	14.2	19.8	2.73	2.98	3.06
11 — Flattened, taped, Zno pasted, & 270% inc.wt.	15.6	17.4	2.44	2.32	2.45
12 — Rolled,taped Zno pasted & 270% inc.wt.	14.2	19.8	2.73	2.98	3.06

For the tests above and considering the heat conduction equation given previously, $Q = \lambda \frac{A\Delta t}{L}$, the heat flux Q, the thermal conductivity of the specimens, its area and thickness were the same for each test. The only variable differing from one test method to another was Δt, the temperature difference across the sample. This is measured

and its value attributed to the contact temperature measured on the hot and cold faces of the specimen.

When a better contact was made between the thermocouple's measuring junction and surface of the specimen, the value of Δt for the same power input, was lower. This is shown by the λ values given in Table 5.1.

By rearranging the heat conduction equation it can be readily seen that by reducing Δt an increased λ-value results. Consequently, all other parameters remaining the same, an increased λ-value in any test indicates better surface contact between thermocouple's hot-junction and the face of the specimen.

From the results of tests carried out, (Table 5.1), the following points can be concluded:

I) By decreasing the thickness of the thermocouple's bead, the surface contact between measuring junction and the face of the specimen is improved. This is due to the fact that by flattening or rolling the thermocouple's bead, the contact area with the surface of the specimen is increased and any air gap that exists is reduced. For lower density materials, such as Siporex (625 kg/m^3) and glass fibre (100 kg/m^3), any increase in thermal conductivity was found to be insignificant under the same thermocouple positioning regimes. The contact resistance problem was found to be more profound on high conductive materials and hence the choice of an appropriate testing method was important when testing dense concretes.

II) The thermal conductivity values measured by carrying out the twelve different fixing methods were

compared with the standard curve proposed by Arnold [13] (See section 2.3.2 and Table 2.1) to ensure that the thermal conductivity of laboratory prepared concretes agreed with that of concretes produced by external sources. As can be seen from Table 2.1, which is based on 'best fit' of a wide variety of materials, for a dry density of 2275 kg/m^3 a λ-value of about 1.60 W/mK is obtained. This can be favourably compared with more explicit λ-values particular to gravel aggregates also published by Arnold. At a density of 2275 kg/m^3 a λ-value of about 1.73 W/mK is obtained from Arnold's data on gravel aggregates. concerningly, results obtained from the twelve methods outlined above, shows a significantly higher values of thermal conductivity for a similar density.

To ensure that this significant difference in λ-value was not a result of measurement error, the pair of concrete slabs used in the experiment were sent to a B.S. accredited test house for confirmatory measurement. Repeat tests, under specified thermocouple fixing methods, confirmed the thermal conductivity values obtained at Leeds. Although the sources of Arnold's data are not known (but thought to have come mainly from Jakob's published data) they are presumably based on the results of measurements made over forty years ago. Hence the apparently low thermal conductivity values of Arnold's high density materials might be due to the non-standardisation of the measurement method and the low accuracy of the measuring equipment available at that time.

III) Heat sink compound paste reduces surface contact resistance since it provides a more efficient transfer of

heat to the thermocouples. For the same reason, the conductivity increases when paste is applied all over the thermocouple's hot-junction rather than applying it only to the bead head (compare method 3 with method 4).

IV) Aluminium foil was used to stop the thermocouple's bead head sinking into the foamed silicone sheet. Unfortunately the results proved to be unreliable since the aluminium foil might have affected the e.m.f. generating across the thermocouple wires.

V) Increasing the weight acting on the samples has no significant effect on surface contact. Increasing the weight by 270 per cent, increases the λ-value by less than 3 per cent (compare method 2 with 7, method 3 with 8, method 9 with 11 and method 10 with 12) and this is within the measurement error.

VI) Method 10 is extremely time consuming, nevertheless it was the chosen technique for all the thermal conductivity measurements. It produces the best surface contact result over all ranges of density and is also the method recommended by B.S.874: 1986: part 2[1]. An apparatus loading of 42 kg was adopted to ensure proper thermal contact and to comply with B.S. 874.

5.4 Tolerance of apparatus and experimental error

From the onset of the research, strict control was imposed an all manufacturing tolerances for the individual components of the hot-plate apparatus. For purpose of comparison with the requirement of B.S. 874, the tolerances actually achieved by the individual components of the apparatus is shown in Table 5.2.

Table (5.2)

Comparison between B.S.874:1988[1] and achieved tolerances.

Component	B.S. 874 requirements	Actually achieved
-Ambient air temp. fluctuation.	< ± 2°C	< ± 0.3°C
-Heater plate flatness.	< 0.1 mm	< 0.05 mm
-Uncertainly in power measurement.	< ± 0.25%	< ± 0.1 %
-Cold plate flatness.	< 0.1 mm	< 0.05 mm
-Surface temp. fluctuation of the cold plates for duration of the test.	< ± 0.1°C	< ± 0.05°C
-Rolled thermocouple thickness.	< 0.05 mm	< 0.04 mm
-Apparatus insulation.	> 100 mm	*100mm+50mm
-Difference in mean thickness between the two specimens.	< 2 %	< 1.4 %
-Accuracy of the instruments used to measure thickness.	< ± 0.025mm	± 0.02
-Deviation from flatness of the specimen faces.	< 0.2 mm	< 0.05 mm
-Difference in mean bulk density of the two specimens.	< ± 5 %	< ± 1.9 %
-Difference in three successive set of readings of face temperatures.	< 0.05°C	< 0.05°C

(*) 100mm is the insulating thickness around the specimens and 50mm is the insulation inside the walls of the cabinet.

B.S. 874[5] requires that three consecutive conductivity values have a maximum spread of 2% . With the

apparatus used, a maximum spread of less than 0.5% was achieved. The standard also requires that all temperature readings on an individual hot and cold specimen surface should lie within $\pm$ 0.5°C of the average temperature of that face. This was always achieved with the apparatus on lower density concrete but with denser specimens, the variation in temperature on any face occasionally was as much as $\pm$ 0.8°C. This was considered when analysing the experimental uncertainty of the apparatus.

To verify compliance with the critical requirements of B.S.874, a pair of concrete specimens (ρ = 2275 kg/m^3) and a pair of Siporex specimens ($\rho \simeq$ 625 kg/m^3) were sent to a B.S. accredited test house at Salford University for measurement of thermal conductivity. The results obtained confirmed values obtained from the Leeds apparatus. Moreover, a thermal conductivity measurement carried out on a pair of BCS (British Calibration Service) audit specimens ($\rho \simeq$ 1150 kg/m^3, i.e. the densest specimens that could be obtained from them) confirmed the accuracy of the plain hot-plate apparatus to be within 1% of the BCS value for that particular pair of specimens.

An analyses of random and systematic uncertainties associated with the measurement was undertaken which revealed an overall random error of $\pm$ 1.76% . The largest individual error of $\pm$ 1.32% was in measurement of temperature difference across the specimen (for highest density specimen). An attempt was made to identify any systematic errors and to reduced them as much as possible. This proved difficult and an allowance was made for the indefinable accuracy in

flatness of the specimens and associated thermal contact problems. To allow for this latter two, a total error of ± 3% was thought to be realistic.

The plain-hot plate apparatus was therefore deemed capable of measuring the thermal conductivity of high density, homogeneous, isotropic materials with an accuracy of better than ± 3% and a repeatability of better than ± 3% . However for lower density materials the accuracy and repeatability is thought to be much better.

The long term performance of the apparatus was monitored by repeat measurement of the thermal conductivity of a pair of Siporex specimens. Measurements were made approximately every six months. The long term stability and repeatability achieved is shown in Table 5.3.

Table (5.3)

Long term stability of plain-hot plate apparatus using Siporex specimens.

Date	λ @ 3% m.c. (W/mK)
15/1 /88	0.205
17/5 /88	0.201
22/11/88	0.201
1 /2 /89	0.205
18/8 /89	0.204

Note:

- λ corrected by Jakob moisture factors
- $\rho \simeq 625$ kg/m^3

5.5 Moisture correction factors

5.5.1 Introduction

In general increasing moisture content increases thermal conductivity of materials as mentioned earlier. Since building elements often contain moisture, the effect of moisture becomes important in calculating different thermal properties of building materials. Conductivity measurements are rarely made at moisture contents that are found in the built form so 'moisture correction' factors are used to adjust the measured values to the moisture contents found in practice. An initial decision has to be made on what is a 'Standard' moisture content to be assumed in the calculations. This is a practical judgement since moisture levels in masonry walls are likely to vary considerably depending for example on factors such as indoor and outdoor climate, type of masonry, process within the building etc. Since it is not feasible to take all such factors into account at the design stage it has been found convenient to assign a specific moisture content to a leaf of a wall depending upon its degree of protection and its construction material. For example in Britain it is assumed that protected and unprotected leaves of concrete masonry walls contain 3 and 5per cent moisture by volume respectively whereas brick masonry walls are only assumed to contain 1 percent moisture by volume if they are protected. These values are based on experimental evidence from a number of buildings [13].

In practice, the λ-value of a hygroscopic material cannot be measured at a specific moisture content of 3 or 5

per cent moisture content by volume. Instead, in accordance with BS874:1988[1] it is normally determined at its equilibrium 'air-dry' value, this is usually between 1 to 5 per cent moisture content by volume. Once the λ-value at its equilibrium moisture content has been determined then moisture correction factors must be applied to determine the λ-value at the specific moisture content required.

The moisture correction factors used in the U.K. are commonly referred to as the 'Jakob' factors. They have been used since they first appeared in his book on 'Heat Transfer' [2] in 1949 (they give the ratio of the thermal conductivity at a given moisture content by volume λ_v to that of a dry material, λ_o). The factors are quoted at various moisture contents in Table A3.23 of the CIBSE Guide, 1986[7] and are applied to all masonry materials regardless of density or matrix composition. They represent an approximate 11% change in λ for each 1% change in moisture content by volume.

In France, the moisture correction factors that are used are specified in CSTB, REEF 58[96] and are the same as those used in the U.K. German moisture correction factors are given in DIN 52612 part 2[97] and differ from U.K. and French values, they represent a 6% change in λ for each 1% change in moisture content by volume. The Italian moisture factors are given in UN1-CT1 7357[98] and represent a linear change in λ of about 5% for each 1% change in moisture content by volume. The latter two countries values are more or less the same and are about one half the correction values applied in the U.K. and France.

Comparison and analysis of moisture factors used in EEC countries have been reported in a joint publication by the author[99].

In the USA a very different set of moisture factors have been proposed for use. On the basis of data, published by Valore[21], a relationship based on moisture content by weight rather than by volume is used. The corrections are based on a change in λ of about 6% for each 1% in moisture content by weight. Hence, at density of 1000 kg/m^3, the USA, Italian and German corrections are about the same, but at a density of 2000 kg/m^3, the USA correction is double the correction used in the two other previously comparable countries and more in agreement with factors used in U.K. and France. Therefore it is apparent that density should be one of the variables in the moisture factor equation.

In recent years it has become apparent that the correction factors used in Britain are inaccurate[19,100]. Hence a study has been carried out to establish a more precise relationship between the thermal conductivity of concretes in the density range 1550 to 2350 kg/m^3 and moisture content and a relationship for the standardisation of measured λ-values is proposed. The authors of the above referenced papers have presented the results of studies undertaken on aerated concretes and lightweight aggregates concretes in the density range of 400-900 kg/m^3 and 1100-1500 kg/m^3 respectively.

5.5.2 Experimental procedure for moisture factor determination

Eight pairs of specimen slabs of different densities and different mix composition, containing limestone, quartzitic or Pellite aggregates were selected (so that they were representative of all mixes in the study) and tested in accordance with BS874:1988[1], their mix properties are given in Table 5.4.

TABLE (5.4)

Mix composition and bulk dry density of slab specimens selected

Mix Code Name	Type Of Coarse Agg.	Dry Density (kg/m^3)	W/C Ratio	Cement:Sand:Agg. Ratio	Air - entrained
PCE /1.29	Pellite	1551	1.29	1:3.73:5.6	Yes
PC /1.29	"	1818	1.29	"	No
LCE /0.90	Lime_stone	1988	0.90	"	Yes
LC /0.95	"	2207	0.95	"	No
QAE /0.43	Quartz	2091	0.43	1:2.33:3.5	Yes
QC /0.90	"	2236	0.90	1:3.73:5.6	No
QA /0.53	"	2282	0.53	1:2.33:3.5	No
QB /0.56	"	2341	0.56	1:2.33:5.6	No

Notes on mix code names:

Q Stands for concretes made with Quartzitic coarse Agg.
L Stands for concretes made with Limestone coarse Agg.
P Stands for concretes made with Pellite coarse Agg.

	Cement	: Sand	: Coarse aggregate	
A	1	: 2.33	: 3.5	(Reference mix)
B	1	: 2.33	: 5.6	
C	1	: 3.73	: 5.6	

Third letter (E) Indicates Air-entrained mix (0.257 Litre/100kg of Cement).

After casting, the specimens were stored in a Fog room (100% relative humidity and 20°C) for 3 days before they were conditioned to constant weight at 65% relative humidity and

20°C for several weeks (i.e. "A" curing condition). The thermal conductivity of the slabs was then measured at their equilibrium air-dry moisture content. To increase the moisture content of the specimens, they were placed in the Fog room and left until a constant weight was reached ("B" curing condition). At this condition the thermal conductivity of the specimens was measured and the moisture content recorded. The moisture content of the specimens was then reduced by storing them at 65% relative humidity and 20°C again ("C" curing condition). When constant weights were reached, the specimens were tested for thermal conductivity at slightly higher moisture content than first 'air-dry' condition. After completion of the thermal conductivity measurements, the specimens were placed in an environmental cabinet of 33% relative humidity and 24°C for several weeks to reach constant weight ("D" curing condition) and then thermal conductivity values were determined for each pair of specimens. The specimens were then placed in another environmental cabinet of 15% relative humidity and 40°C and tested when constant weight was reached (i.e. at "E" curing condition). This procedure was adopted rather than wetting and drying since it gives a more uniform moisture distribution throughout the specimens.

To determine the average moisture content and oven dry density of the specimens, the slabs were oven dried at 105°C for 48 hours after all the thermal conductivity measurements were carried out. Drying at this temperature for 48 hours reduced the slabs to a constant mass after which the dry density could be determined. Specimens were cooled to

ambient temperature in a desiccator to prevent moisture regain. The specimens were then wrapped in thin impermeable plastic film to prevent moisture regain and a measurement of the thermal conductivity of the 'dry' specimens (λ_o) was attempted. Unavoidably, all the specimens had a small gain in weight during the test and this prevented measurement below about 0.04 per cent moisture content by volume.

5.5.3 Results and trends of moisture factors

The measured thermal conductivity values which were obtained for all the specimens are given in Table 5.5 together with their moisture content by volume during test. Because the four pairs of Pellite and Limestone specimens gave unacceptably large increments in their moisture content between their respective 'A' and 'B' curing conditions, they were additionally conditioned to constant weight at 80% R.H. and 20°C for several weeks (by using a saturated salt solution of ammonium sulphate in a conditioning cabinet). The slabs were then tested for thermal conductivity at their respective moisture content. The results of these additional tests are also included in Table 5.5.

Table (5.5)

Thermal conductivity results.

Mix Code Name	Dry Density (kg/m^3)	Moisture Content (% vol)	λ (W/mK)	Mix Code Name	Dry Density (kg/m^3)	Moisture Content (% vol)	λ (W/mK)
	1551	0.10	0.533		2091	0.06	2.084
	"	0.75	0.587		"	1.84	2.227
	"	0.81	0.571		"	4.04	2.240
PCE/1.29	"	1.09	0.579	QAE/.43	"	4.23	2.241
	"	1.86	0.593		"	5.52	2.385
	"	9.18	0.845		"	8.62	2.731
	"	14.38	0.939				
	1818	0.09	0.705		2236	0.08	2.187
	"	0.98	0.756		"	1.11	2.340
	"	1.42	0.778		"	2.20	2.542
PC /1.29	"	1.75	0.774	QC/.90	"	2.69	2.523
	"	3.55	0.810		"	3.86	2.567
	"	6.93	0.960		"	11.17	3.290
	"	15.49	1.179				
					2282	0.04	2.702
	1988	0.11	1.243		"	* 0.05	2.800
	"	1.12	1.330		"	* 1.37	2.964
	"	1.59	1.372		"	2.64	3.005
LCE/0.90	"	1.84	1.379	QA/.53	"	5.04	2.942
	"	2.70	1.424		"	5.71	2.967
	"	6.69	1.694		"	6.73	2.952
	"	10.65	1.879		"	9.97	3.203
	2207	0.10	1.564		2341	0.06	2.834
	"	1.20	1.683		"	2.68	3.187
	"	2.75	1.798		"	4.46	2.993
LC /0.95	"	2.97	1.770	QB/.56	"	4.80	3.207
	"	4.71	1.827		"	5.63	3.226
	"	8.49	2.137		"	8.83	3.551
	"	13.13	2.289				

(*) Repeated measurements at 65% RH, 20 °C and oven dried conditions taken at the end of the curing conditions.

Whenever high moisture content specimens (in excess of about 7%) were measured extra care was taken to determine the λ value within the first 60 hours of installing the specimens in the rig. This is because the apparent λ-value decreases with time during the measurement at high moisture content because of condensation on the cold face of the specimens[15]. The data given in Table 5.5 are plotted in

Figure 5.7. Results clearly show that, as expected, λ increases with increasing moisture content for all densities.

Regression analysis on the data produced a 'best-fit' equation for each density. The regressed data is shown in Table 5.6 and is represented by the solid lines given in Figure 5.7. The equations were of a linear form $\lambda = \lambda_o + Amc$, where A is a constant and 'mc' is per cent moisture content by volume.

Table (5.6)

Regression equation relating λ to mc per cent by volume.

Density (kg/m^3)	Regression equation	Correlation Coefficient 'r'
1551	$\lambda = 0.547 + 0.027$ mc	0.997
1818	$\lambda = 0.719 + 0.030$ mc	0.998
1988	$\lambda = 1.263 + 0.058$ mc	0.996
2207	$\lambda = 1.604 + 0.053$ mc	0.991
2091	$\lambda = 2.031 + 0.071$ mc	0.938
2236	$\lambda = 2.242 + 0.095$ mc	0.990
2282	$\lambda = 2.806 + 0.034$ mc	0.900
2341	$\lambda = 2.840 + 0.074$ mc	0.910

On the basis of data given in Table 5.5 and using regression analysis, a general expression to predict thermal conductivity λ was obtained as a function of both the moisture content 'mc' and the dry density 'ρ' of the sample such that:

$$\lambda = 2.021 \times 10^{-2} \times e^{2.097 \times 10^{-3} \rho + 2.904 mc} \quad (r=0.961) \quad \ldots(5.1)$$

for $1550 \leq \rho \leq 2340$ kg/m^3 and $0 \leq mc \leq 16\%$ (by Vol.).

From equations in Table 5.6 the thermal conductivity at zero moisture content (λ_o) was obtained by extrapolation for each density. This enabled the thermal conductivity at a finite moisture content to be expressed in terms of the dry

value in order to obtain moisture factors F given by:

$$F = \frac{\lambda}{\lambda_o} \qquad \ldots(5.2)$$

Moisture factors obtained from their respective regression equations enabled a relationship between moisture factors and density to be obtained at selected values of moisture content. These are plotted in Figure 5.8 which shows that, generally, the moisture factors decrease with increasing density. This is in agreement with work published on concretes having lower densities[19,100]. This behavior is to be expected since the relative effect of additional heat transfer due to moisture will tend to decrease as the thermal conductivity of the solid matrix increases.

On the basis of the interpolated points shown in Figure 5.8 and using further regression analysis, a general expression to predict the moisture factor F was obtained as a function of both the moisture content 'mc' and the dry density 'ρ' of the sample such that:

$$F = 1.174 - 8.449\times10^{-5}\rho + 35.688\times10^{-3}\ mc \quad (r=0.912) \ldots(5.3)$$

where

$$1550 \leq \rho \leq 2340\ kg/m^3 \text{ and } 0 \leq mc \leq 5\% \text{ (by vol.)}$$

The solid lines in Figure 5.8 are derived from equation 5.3 and represent the lines of best fit. They can be seen to be in very good agreement with the experimental data particularly at values of lower moisture content.

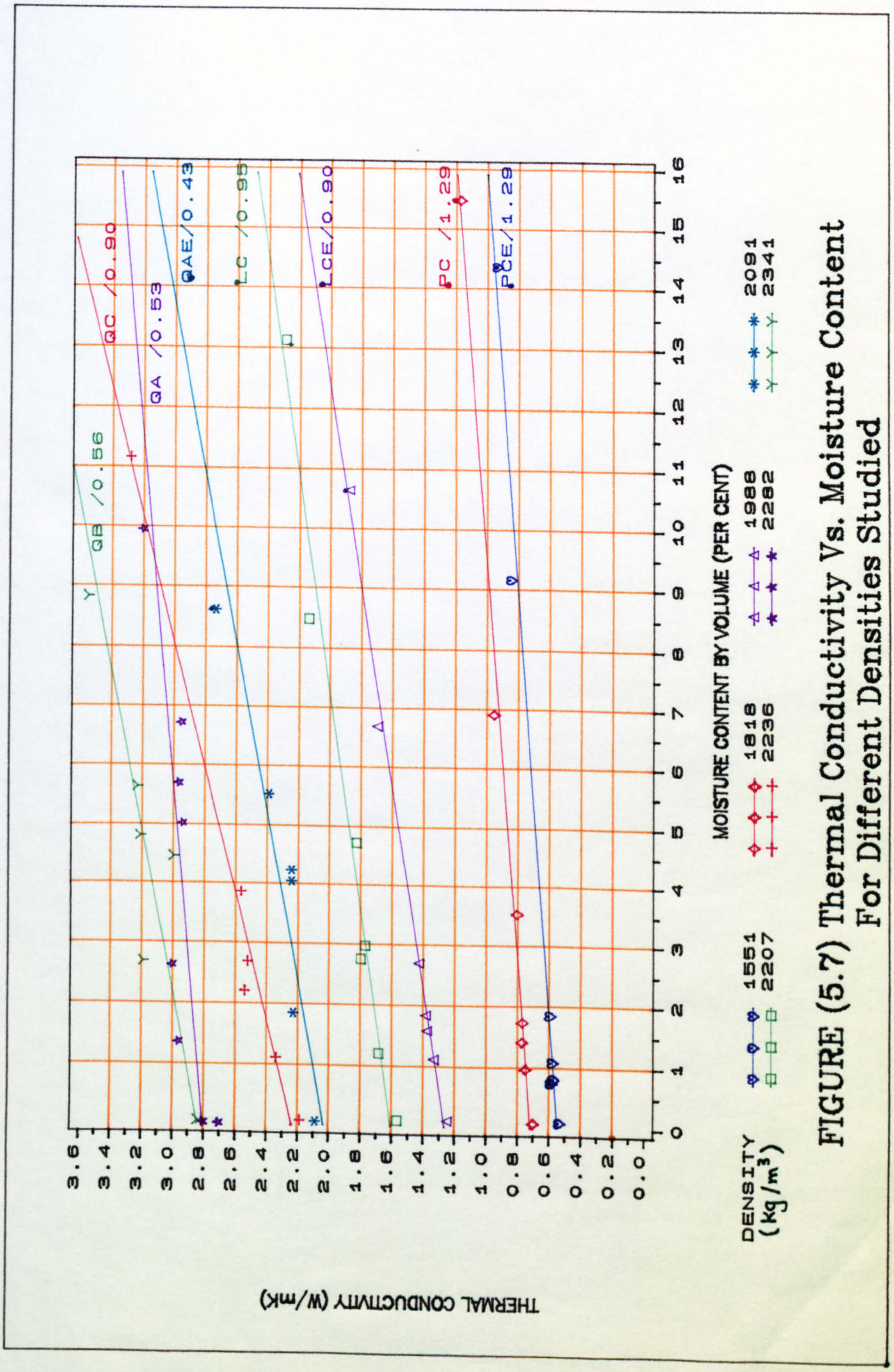

FIGURE (5.7) Thermal Conductivity Vs. Moisture Content For Different Densities Studied

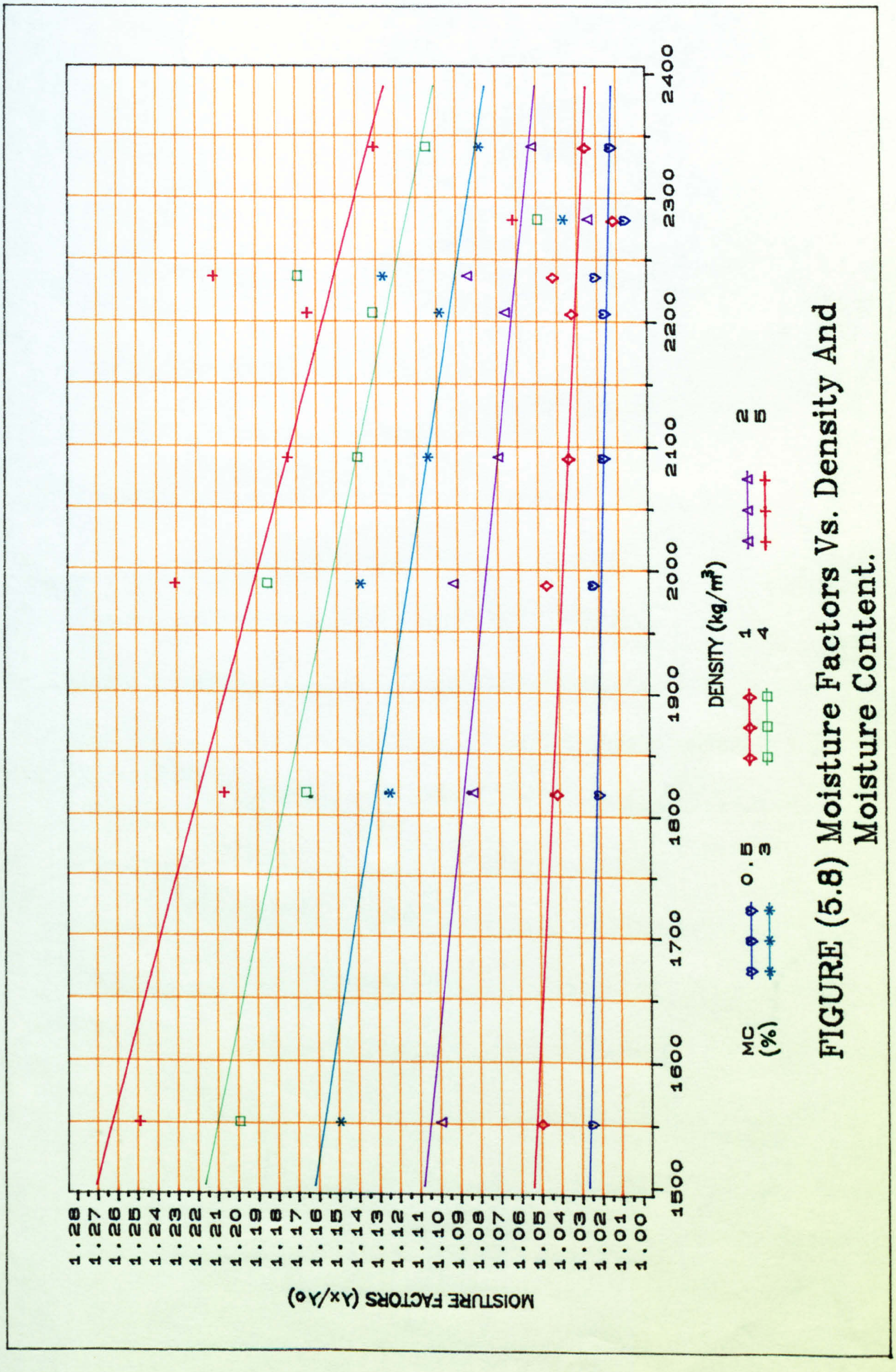

FIGURE (5.8) Moisture Factors Vs. Density And Moisture Content.

The thermal conductivity λ_s at some required moisture content (s) can be obtained in terms of the thermal conductivity λ_x measured at a moisture content (x) such that:

$$\lambda_s = \frac{F_s}{F_x} \lambda_x \qquad \ldots(5.4)$$

where F_s and F_x are the moisture factors appropriate to the moisture contents (s) and (x) respectively and obtained from equation 5.3.

In order to examine the accuracy of the general expression (i.e. equation 5.3) derived to predict moisture factors, the thermal conductivity at a standard moisture content of 3% by volume, was determined for selected concretes (i.e. specimens which have the widest range of moisture content for each type of concrete) from the data given in Table 5.5 and compared against the expected values from Figure 5.7. For comparison purposes the data is presented in Table 5.7.

The same data sets were also normalised to 3% moisture content by volume using the Jakob correction factors as presented in Table A3.23 of the CIBSE guide. Results are presented in the right hand columns of Table 5.7.

By comparing λ-values corrected to 3% moisture content by the derived moisture factor equation with experimental value it can be seen that the differences between the two are less than 4 per cent and the total mean percentage difference being 1.73 per cent. This is in accord with percentage errors normally associated with hot-plate measurements of thermal conductivity in the high density range investigated.

The difference between the mean corrected value and experimental is about 0.2 per cent but the difference between Jakob's mean corrected value and the experimental is between about 0.5 to 6 per cent.

Table (5.7)

Comparison of thermal conductivity values corrected to 3% moisture content (by vol.).

Aggregate (Mix Code Name)	Dry Density (kg/m^3)	Moisture Content (% vol.)	Thermal Conductivity At 3 % M.C.(Vol.)				
			Experimental λ (W/mK)	Corrected Using Eqn.5.3		Corrected Using Jakob	
				λ (W/mK)	% Diff.	λ (W/mK)	% Diff.
Pellite (PC/1.29)	1818	0.09	0.801	0.777	- 3.0	—	—
	"	0.98		0.807	+ 0.7	0.934	+16.6
	"	1.42		0.819	+ 2.2	0.900	+12.4
	"	1.75		0.806	+ 0.6	0.860	+ 7.4
	"	3.55		0.797	- 0.5	0.791	- 1.2
	"	6.93		—	—	0.815	+ 1.7
	"	15.49		—	—	0.796	- 0.6
			Mean	0.801		0.849	
Limestone (LC/0.95)	2207	0.10	1.767	1.727	-2.3	—	—
	"	1.20		1.788	+1.2	2.010	+13.8
	"	2.75		1.812	+2.5	1.826	+ 3.3
	"	2.97		1.772	+0.3	1.774	+ 0.4
	"	4.71		1.730	-2.1	1.692	- 4.2
	"	8.49		—	—	1.730	- 2.1
	"	13.13		—	—	1.623	- 8.1
			Mean	1.766		1.776	
Quartz (QC/0.90)	2236	0.08	2.517	2.418	-3.9	—	—
	"	1.11		2.494	-0.9	2.833	+12.6
	"	2.20		2.610	+3.7	2.697	+ 7.2
	"	2.69		2.549	+1.3	2.572	+ 2.2
	"	3.86		2.497	-0.8	2.474	- 1.7
	"	11.17		—	—	2.438	- 3.2
			Mean	2.514		2.603	

It can also be seen from the table that the Jakob factors tend to inflate the conductivity when correcting from a lower value upwards to 3% and deflate the value when

correcting from a higher value downward. The magnitude of such error on the samples tested was in some instances in excess of 16 per cent.

The experimental value and the mean λ-values corrected to 3 per cent moisture content for each density (from their results up to 5 per cent moisture content) together with the ranges of the percentage difference between them are given in Table 5.8. From the table it can be seen that the mean difference between the corrected and experimental value is, in all cases, less than 3.6 per cent and on average is 2.2 per cent. The maximum percentage difference value can be seen to be 6 per cent which is considered to be appropriate for the high density range being investigated.

The mean λ-values corrected to 3 per cent moisture content by the Jakob factors, together with the mean percentage difference and the ranges of percentage difference between the experimental value and corrected values are given in the right hand columns of Table 5.8. It can be seen that the difference between the corrected and experimental values is, in all cases, much greater than that achieved using equation 5.3. Moreover, the mean difference between the experimental and the corrected value ranges from 5 to 12 per cent. In each case this is considerably higher than the difference obtained using equation 5.3.

Table (5.8)

Summary of thermal conductivity data corrected to 3% moisture content by volume

Mix Code Name	Dry Density (kg/m^3)	λ At 3% M.C. By Vol. (W/mK)						
		Experi-mental λ_3	Equation 5.3			Jakob		
			Mean λ_3	Mean % Diff	Range of % Diff.	Mean λ_3	Mean % Diff	Range Of % Diff.
PCE/1.29	1551	0.620	0.612	2.1	0.8-5.5	0.694	12.0	4.5-23.9
PC /1.29	1818	0.801	0.801	1.4	0.5-3.0	0.849	6.7	0.6-16.6
LCE/0.90	1988	1.430	1.422	1.5	0.5-3.7	1.495	5.1	0.1-12.4
LC /0.95	2207	1.767	1.766	1.7	0.3-2.5	1.776	5.3	0.4-13.8
QAE/0.43	2091	2.236	2.235	2.9	1.3-3.6	2.206	5.2	2.5- 9.6
QC /0.90	2236	2.517	2.514	2.1	0.8-3.9	2.603	5.4	1.7-12.6
QA /0.53	2282	2.931	3.017	3.0	2.1-3.8	2.673	10.1	5.3-16.3
QB /0.56	2341	3.063	3.060	3.6	1.2-6.0	2.941	6.4	3.4- 8.4

Since a 5 per cent moisture content by volume is assigned to the outer leaf of a concrete masonry wall, the data corrected to 5% moisture content was also analysed. The mean value for the thermal conductivity corrected to 5% moisture content from each set of data on different densities up to 5.5% moisture content using both equation 5.3 and Jakob Factors is given in Table 5.9 where it is compared with the experimental value. The mean corrected values are summarised in the same Table together with the mean and the range of difference between the corrected and experimental values. It can be seen that the mean difference between the experimental value and that corrected using equation 5.3 is less than 5.6 per cent and on average is 3.2 per cent. On the other hand if Jakob is used for the correction, the mean difference varies from 4 to 12 per cent, considerably higher than that obtained

using equation 5.3. Moreover, the range of the difference has a maximum value of about 23.5 per cent.

Table (5.9)

Summary of thermal conductivity data corrected to 5% moisture content by volume

Mix Code Name	Dry Density (kg/m^3)	λ At 5% M.C. By Vol. (W/mK)						
		Experi-mental	Equation 5.3			Jakob		
			Mean	Mean	Range	Mean	Mean	Range
		λ_5	λ_5	% Diff	of % Diff.	λ_5	% Diff	Of % Diff.
PCE/1.29	1551	0.680	0.650	4.4	1.3-8.5	0.76	11.7	4.3-23.5
PC /1.29	1818	0.863	0.852	1.7	0.6-4.3	0.929	7.6	0.3-18.4
LCE/0.90	1988	1.543	1.513	2.0	0-5.6	1.635	6.0	0.1-13.9
LC /0.95	2207	1.873	1.881	1.8	0.8-3.0	1.942	5.8	1.0-17.4
QAE/0.43	2091	2.396	2.379	3.3	2.3-4.3	2.413	4.0	0.4-11.8
QC /0.90	2236	2.703	2.678	2.3	0.4-4.7	2.847	5.9	0.1-14.7
QA /0.53	2282	2.983	3.122	5.6	1.5-8.5	2.932	6.8	1.5-12.7
QB /0.56	2341	3.220	3.262	4.1	0.2-6.6	3.217	4.5	0.5-10.4

The results and analysis given in this section, on the effect of moisture on the thermal conductivity of lightweight and normal-weight concretes, have been reported in a joint publication by the author[101].

CHAPTER SIX

ENGINEERING AND MICROSTRUCTURAL TESTS OF MORTAR AND CONCRETE

6.1 Introduction

This chapter describes the engineering and microstructural tests carried out on the mortar and concrete specimens during this investigation. Cube compressive strength of all mixes was determined following B.S. specification [86].

Vacuum saturation and mercury porosimetry techniques are explained and methods of preparation of specimens and the experimental procedure for the determination of porosity by vacuum saturation and for determination of pore size distribution by MIP are explained in detail.

6.2 Cube compressive strength

The cube compressive strength is used in civil engineering, as specified by British Standard[102,103], to judge concrete quality. However, recent developments in concrete technology indicate the importance and relevance of other parameters such as permeability, porosity and pore size distribution when the performance and durability of concrete is to be assessed. Nevertheless, strength is commonly accepted as means of determining the compliance of hardened concrete with specification.

The strength of concrete is affected by many factors. The most important factors are the concrete constituents, methods of preparation, curing and test conditions. In practice, at a certain age and curing conditions, water cement ratio and degree of compaction which reflect porosity and pore size are assumed to be the most important factors on the strength of concrete.

In this study compressive strength determination of 100 mm cubes for all mixes cured in Fog room and three days in Fog room + curing at 20°C and 65% RH conditions were tested at age of 3, 7, 28, and 91 days in accordance with B.S. 1881 : Part 116 [86], using a digital automatic compressive cube crushing machine (Tonipact 3000).

6.3 Measurement of total porosity

The porosity of a material is the fraction of its bulk volume occupied by voids. The porosity of a material, such as concrete or mortar can be determined by measuring any two of the three quantities; bulk volume, pore volume or solid volume. In this investigation the porosity of concrete was determined by vacuum saturation and the porosity of mortar was determined by mercury intrusion porosimetry.

6.3.1 Vacuum saturation

There are a number of methods to determine the total porosity of a material such as concrete. Among them water penetration is the simplest of the methods when compared with gas absorption or mercury intrusion. Water absorption can be determined by immersing the sample in water for prolonged periods, or by boiling the sample in water for some hours. In the petroleum industry it is usual to immerse the sample in water under vacuum, in order to find its total porosity[104]. However, cement paste, mortar and concrete, when compared to rocks, are more complicated due to the presence of large number of very fine pores[105]. Moreover, some of these pores have bottle necks. It is therefore, doubtful that total saturation or maximum total absorption is reached by any method.

In order to fill all accessible pores in the sample with water, it is necessary to empty these pores first from air and water before allowing water to penetrate them. Keulen[106] proposed a test based on this principle, and more recently RILEM[107] recommended a similar test for full water

saturation. Briefly, these tests are based on evacuating the pre-dried sample first, and then letting water fill the pores, while the sample is still under vacuum. After a specific period, the pressure is brought back to atmospheric while the sample is still in water until it reaches constant weight.

Although the vacuum saturation of concrete is not widely used, evidence shows that it is gaining acceptance and this method provides a closer approach to total or full saturation of samples in a relatively short time[107,108]. This is, however dependent on factors such as the size of the sample, amount of vacuum and the time of evacuation. RILEM[107] recommends that no inner part of a sample should be more than 100mm deep and the amount of vacuum should be less than 0.750 - 1.875 mmHg. Keulen[106] recommends a vacuum of 0.8 mmHg and de-aired water to be used to facilitate fast entry Of water to the pores without air blockage.

In this investigation samples used were 75mm in diameter which were cored from 100mm concrete cubes. A vacuum pressure of about 0.9 bar was used.

6.3.1.1 Apparatus

The apparatus that was used is shown in Figure 6.1 and was developed by Cabrera and Lynsdale [109] at the University of Leeds. It is based on the principle of vacuum saturation discussed earlier. The schematic arrangement of the apparatus is shown in Figure 6.2 and it consists of the following components as shown in the Figure.

1. Vacuum desiccator

2. A 10 - litre pyrex bottle with tap
3. Vacuum pump
4. Three-way valve, to be connected to the desiccator, vacuum pump and water tank
5. Flask with side opening, to work as a trap
6. Vacuum gauge, reading up to 1 bar of vacuum
7. Tubing

6.3.1.2 Experimental procedure

The cylindrical concrete samples were dried to constant weight in an oven of 105°C. Distilled water brought to boiling for about 5 minutes was poured into the pyrex storage bottle and left to cool overnight.

The oven dried samples were weighed and placed in the vacuum desiccator. At this stage valves W and A (Figure 6.2) were closed, and valve V, which leads to the vacuum pump, opened. The vacuum pump was started and evacuation took place for 3 hours. At the end of 3 hours,valve V was closed and W opened to let water fill the desiccator and the samples to about 3cm above the samples level. Then valve W was closed and V opened to let the pump continue evacuation for another 6 hours. At the end of this time valve V was closed and the vacuum pump stopped. At this stage valve A was opened, to let air to enter the desiccator and the pressure be raised to atmospheric. This provided additional force which pushes water into pores of the samples. The samples were then left over night in water to reach constant weight, before being weighted in water and in air.

The porosity was calculated by the following equation:

$$P = \frac{W_{sat} - W_{dry}}{W_{sat} - W_{water}} \times 100 \qquad \ldots(6.1)$$

where;

P = Total porosity open to water (%)

W_{sat} = Saturated samples weight in air

W_{water} = Saturated sample weight in water

W_{dry} = Oven dried sample weight

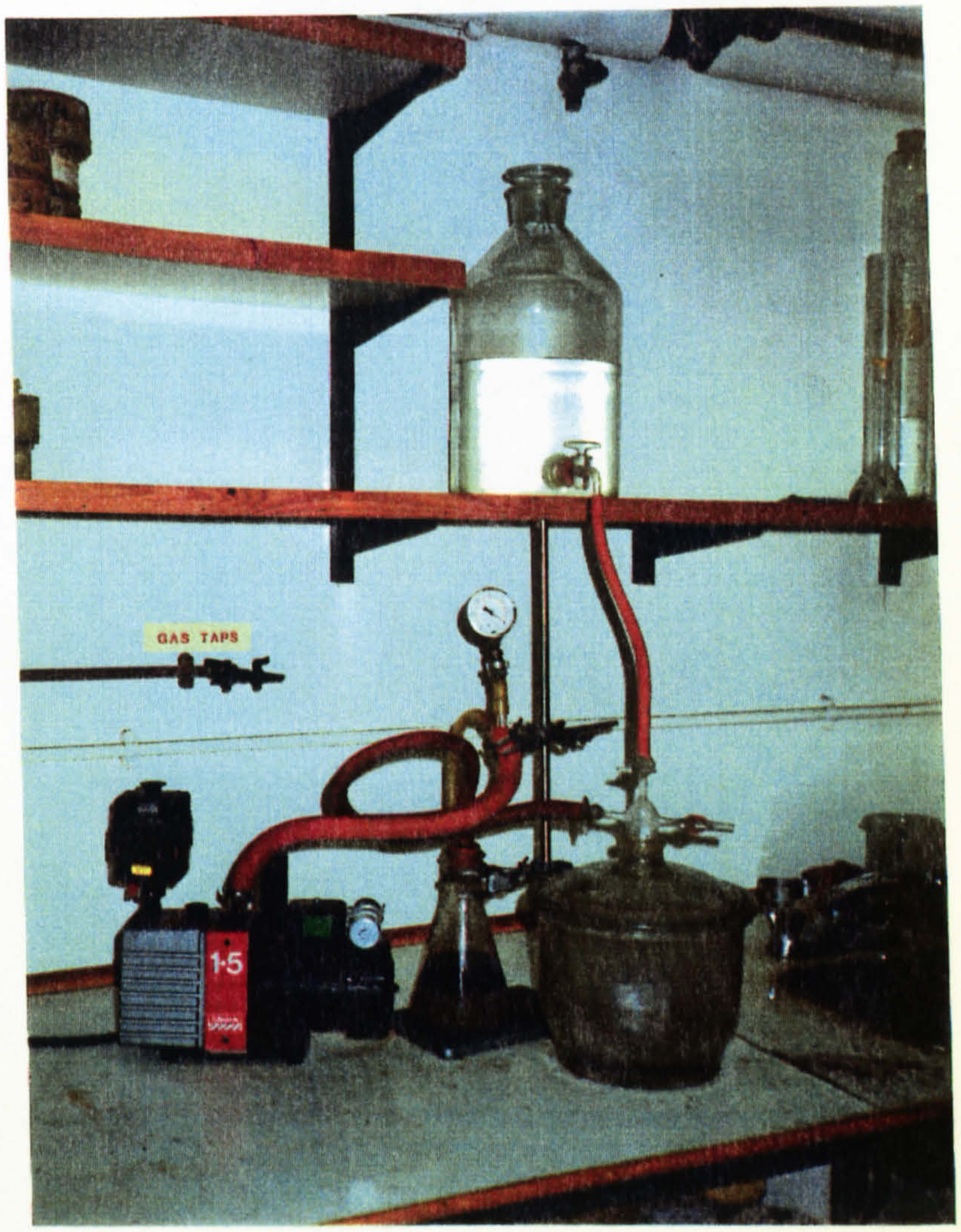

Fig.(6.1) Photograph of vacuum saturation apparatus

1.vacuum desiccator
2.pyrex water container
3.vacuum pump
4.three-way valves
5.trap
6.vacuum gauge

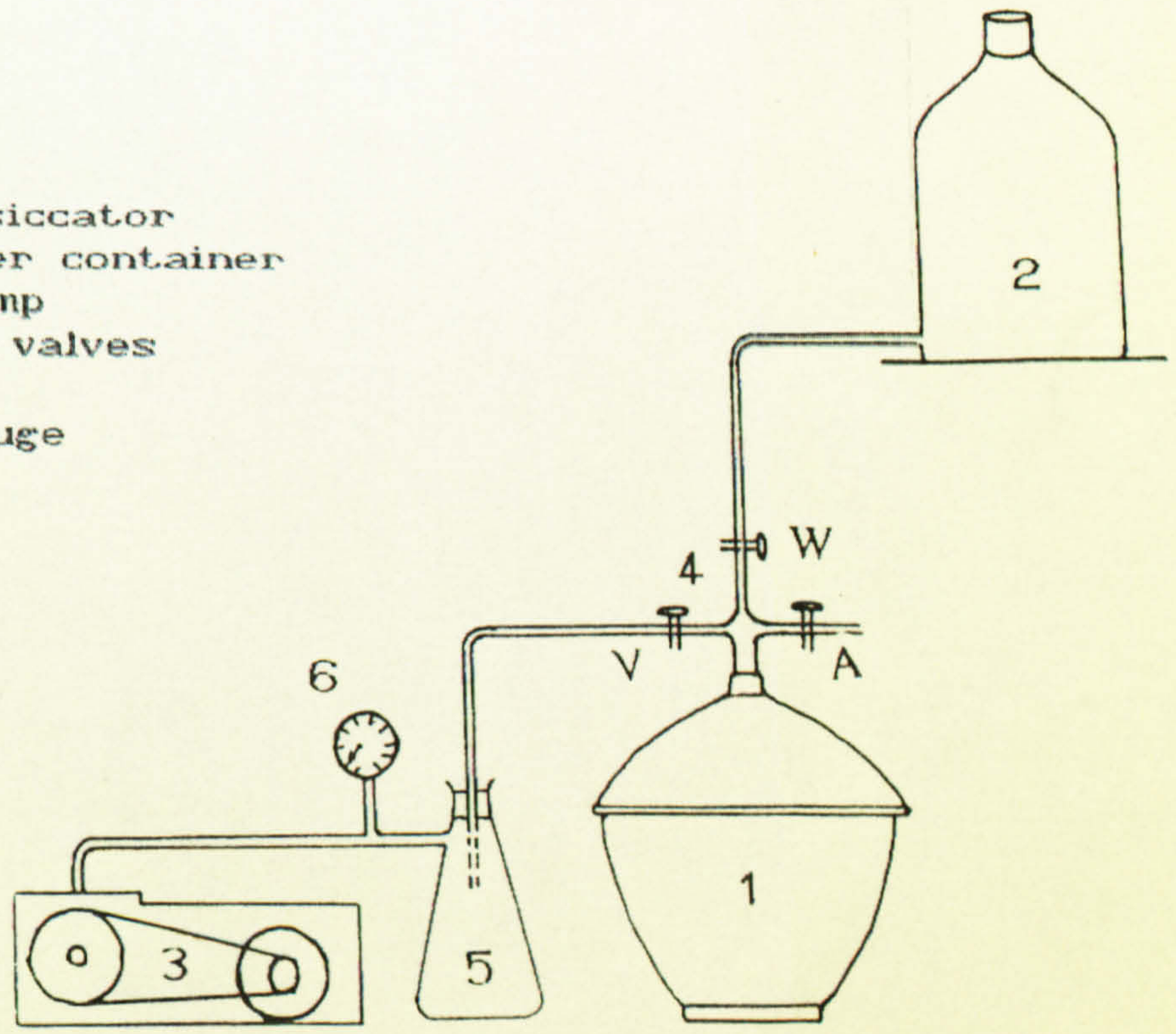

Fig.(6.2) Schematic diagram of vacuum saturation apparatus[109]

6.4 Pore size distribution measurement

Pore characteristics of building materials cannot be solely described by total porosity but they should include pore size, shape and structure. These parameters are related directly to the performance and engineering properties of concrete[105].

The pore size distribution can be determined using different techniques, however each has its limitations and requires certain arbitrary assumptions to be made. Some of these techniques are: low temperature gas adsorption - desorption, microscopy, flow and diffusion of gases through porous media, so-called suction curves, fluid evaporation velocity, X-ray small angle scattering, and mercury porosimetry[110,111]. The main limitation of these techniques is the range of pore sizes they are capable of detecting. Mercury porosimetry, however, provides an advantage over other techniques in this regard, since it can operate over a large range of pore sizes, and most often its range overlaps at least partly with that of other techniques[72,111]. Other advantages of mercury porosimetry are:

(a) It is known for its good reproducibility of results, and is most suited for comparative studies such as looking at the effect of age, curing, W/C ratio and admixtures on the pore size distribution of cement paste or mortars.

(b) Mercury porosimetry provides additional information besides the pore size distribution,such as: total porosity, specific gravity, pore surface area, average and median pore diameters, and pore shape (by using the hysteresis data

resulting from the extrusion of mercury by reduction of pressure).

(c) It is a well established technique, and there are a number of commercially available porosimeters on the market.

(d) It is a rapid and simple technique to conduct, usually taking two hours to provide a 'fingerprint' for a particular sample.

6.4.1 Mercury porosimetry method

The mercury porosimetry method has been reviewed in detail by many investigators[71,72,110-112]. It involves evacuating the gases from the pores and then forcing mercury into the sample by systematically increasing the pressure on mercury. Both the volume of mercury intruded and the pressure to achieve the intrusion are measured. From these data the cumulative pore volume against pore diameter or a pore size distribution curve is plotted. Winslow and Diamond[72] applied this technique for the study of porosity in cement systems in 1970, and since then it has been used world-wide.

The principle of this technique is based on penetrating a non-wetting liquid, such as mercury, into the pores of a porous medium. Since the liquid is non-wetting, i.e. its contact angle with the pore walls is greater than 90°, then pressure is needed to force it to penetrate into the pores. The pressure required, to force the mercury into the pores, increases as the pore diameter decreases. Therefore, forcing mercury in step-wise increments of pressure, and at the same time monitoring the volume of mercury penetrating the sample

after each pressure increment, will yield a volume-pressure curve, which can then be converted to volume-pore size curve using the Washburn equation. This equation is based on the assumption that the pores are right angle cylinders:

$$d = - \frac{4 \delta \, Cos \, \theta}{p} \qquad \ldots(6.2)$$

where:

d = pore diameter filled at pressure p

δ = surface tension of mercury

θ = contact angle between mercury and the sample

p = applied pressure

Mercury has a high surface tension and is non-wetting to all materials (with the exception of a few noble metals). It also provides additional benefits in the design of porosimeters, since it is a conductor[113].

6.4.2 Mercury porosimetry apparatus

A number of porosimeters have been constructed over the years[110]. The main difference amongst them are : the minimum low pressure they can obtain, the maximum high pressure they can reach and the technique by which mercury penetration is monitored. The latter includes varied designs for monitoring the mercury penetration ranging from mechanical movement, eyesight (through a sight hole even at elevated pressure), electrical (through changes in resistance or capacitance), a combination of electrical and mechanical changes, and the use of γ-radiation[111].

The instrument used in this investigation was Micromeritics Autopore 9200 Mercury Penetration Porosimeter[113] shown in Figure 6.3, capable of exerting 414

Mpa (60000 Psi) pressure. It produces pore volume and pore size distribution measurements of porous materials for pore sizes nominally from 360 μ to 0.003 μ (30 Å) diameter, with intrusion volumes up to 1.8cc. It is a fully automated instrument controlled by a microprocessor, for both the low and high pressure cycles. The complete pressurisation of the sample is done in two stages; a low pressure run from 3.45-172.4 KPa and high pressure run from 0.172-414 MPa. These two pressurisation stages are carried out in two different types of chambers. The low pressure chambers can run up to four samples simultaneously, whilst the high pressure chambers can run up to two samples[113].

An air pump is used to apply pressure in the low pressure run. Pressure measurement is accomplished with a 0-0.207 MPa semiconductor, strain gauge type pressure transducer. High pressure is generated by a gear pump in the high run. The pump is integral with a hydraulic fluid reservoir, and its output is indicated by a pressure gauge. High pressure are measured by means of three pressure transducers in ranges of 0.207-2.07 MPa, 0-27.6 MPa and 0-414 MPa.

The progress of mercury penetration into the sample is monitored by detecting changes in the electrical capacitance of the penetrometer. The stem of the glass penetrometer is coated with a metallic coating, when mercury is filled in the penetrometer a capacitance is formed, the value of which keeps changing as mercury is pressurised into the sample. These changes in the capacitance are detected using a capacitance transducer. The instrument uses six capacitance

transducers to measure the capacitance change caused by the reduction in height of the mercury column in the penetrometer capillary. Four of these are used in low pressure chamber with a detachable cable. The remaining two are mounted in high pressure chambers and make electrical contact to the penetrometer through a high pressure insulator. The changes in capacitance are then converted into changes in volume of mercury through the use of penetrometer calibration constant pre-stored in the memory by the user. The penetrometer calibration constant is a ratio of volume to capacitance. Mercury volume changes of well below one microlitre with accuracies to better than 1 per cent of the full scale volume of the penetrometer are achieved[113]. It is reported[113] that the straight line relationship between the volume and capacitance for a particular penetrometer and its constant holds as long as the percentage capillary of mercury used in penetrating the sample is between 25 and 90 per cent.

The brief sequence of general operations of the porosimeter are as follows:

(1) Evacuation, or de-gassing, of the samples in the low pressure chambers.

(2) Filling of mercury into the penetrometer (in the low pressure chambers).

(3) Pressurisation of mercury up to 0.172 MPa, i.e. low pressure run (in the low pressure chambers).

(4) Loading the penetrometers in the high pressure chambers and commencing the high pressure run up to 414 MPa.

(5) De-pressurisation of mercury back to atmospheric pressure.

(6) Analysis and printing of the data.

The data is produced in a report which consists of 6-7 pages of tabulated and plotted data. Due to the large volume of tabulated data involved which needed further processing and analysis the data files were sent to Amdahl 580 through systime 8780 to be used with statistical and plotting package programs available in Amdahl i.e. 'Statistical Analysis System' (SAS).

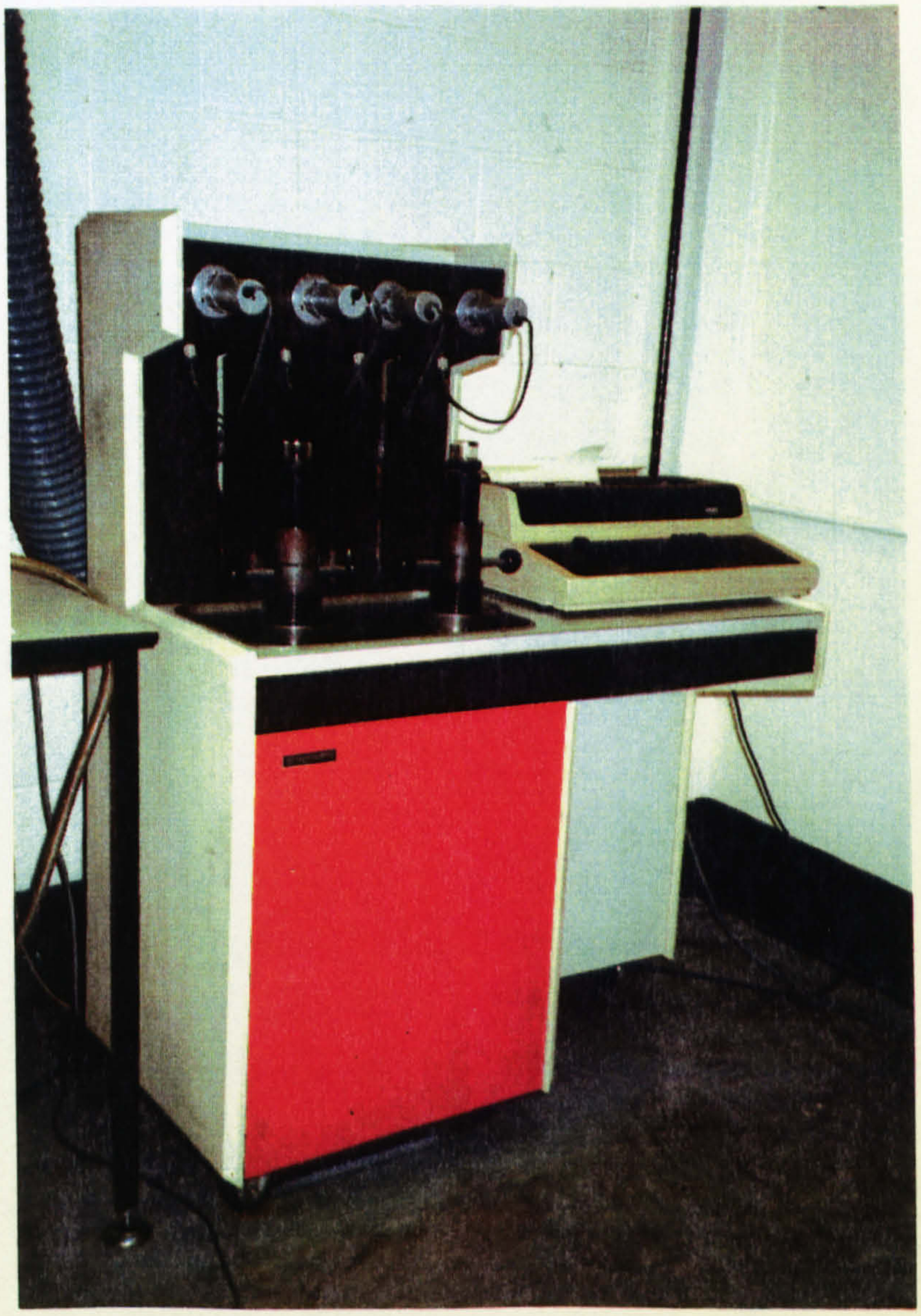

Fig.(6.3) Photograph of mercury porosimeter apparatus.

6.4.3 Sources of error in mercury porosimetry

In the following section some important sources of error are explained.

A) Type of pores

Ritter and Drake [114], pointed out that the assumption of cylindrical pore geometry is an important source of error. They reported that the extrusion curve does not coincide with the intrusion curve. This was attributed to mercury being trapped in the ink-bottle pores of the samples. This type of pore has an entry radius smaller than that of the pore itself and will not be intruded until the pressure is high enough to force mercury to pass through the narrow neck. The total volume of mercury intruded through these kind of pores is attributed to the radius of the neck which is smaller than the true radius of pore. This will shift the pore size distribution curve to the finer pores which does not represent the true curve. However, the model of cylindrical pores is well accepted and used exclusively in the published works on mercury porosimetry.

There are some pores which have an entry smaller than the minimum pore diameter which can be measured, or they are completely isolated. Such pores cannot be measured by mercury intrusion porosimetry.

B) Surface tension of mercury

The value of the surface tension of mercury is usually taken to be 484 or 485 dyne/cm. However, values ranging from 410-515 dyne/cm are quoted[111]. The cleanliness of mercury affects its surface tension; it was found that impurities can

change the surface tension by as much as 30 per cent [111]. Therefore, the mercury used for this investigation was always distilled mercury. It is, however, reported[110] that the error produced from the use of an incorrect surface tension is not great. The value for the surface tension of mercury used in this study was 484 dyne/cm.

C) Contact angle of mercury

Contact angles of mercury with pore walls often quoted are in the range of 112 to 142°, and the most commonly used are 130° or 140° [110-114]. In most of the published work on mercury porosimetry, the contact angle used was assumed rather than measured. However, attempts have been made to measure the contact angle of mercury with hardened cement paste. Winslow and Diamond[72] measured the contact angle at two different drying conditions. They found a contact angle of 117° and the mercury surface tension of 484 dyne/cm for oven-dried specimens. They found that the contact angle will vary according to drying conditions. It is interesting that it is generally considered that the contact angle may vary with the applied pressure but recently it has been shown[115] that for relatively hard materials such as porous alumina this is not the case. The results also showed no evidence of sample damage at high pressure which gave validity to the mercury intrusion technique.

The value for the contact angle used in this study was 130°, this being the most frequently used value by research workers in the field.

6.4.4 Sample preparation and test procedure

Sample preparation is one of the important factors which influences the results of mercury porosimetry and its reproducibility. In some investigations it is customary to use fragments of a cube of cement paste, mortar or concrete, after crushing it for strength. This practice is not recommended, because of the possibility of micro-cracks which may distort the pore size distribution[108,110]. Better reproducibility of results can be obtained when porosimetry is conducted on mortar samples cored from a larger sample. For this investigation cylindrical cores 25mm in diameter were drilled and cut from 50mm mortar cubes using a diamond saw. The samples were kept wet throughout the cutting process, by dripping water from a reservoir onto the specimen. The specimens were then cut such that the excess was removed from the cast ends where density variation is most likely to occur. The remaining pieces were then cut into appropriate sizes to be used in the test. The samples were dried in an oven at 105°C for 24 hours to achieve constant weight. The samples should be free of volatile materials such as adsorbed water or other compounds with high vapour pressure. These materials evaporate during the vacuum procedure and prolong the time required to achieve the desired vacuum reading before mercury intrusion.

The most appropriate penetrometers were selected based on a general knowledge of the appropriate size and the approximate porosity of the samples. Dry samples were weighed and loaded into the penetrometers. Penetrometers

were sealed and weighed again. Four penetrometers could be prepared and inserted into low pressure ports. Appropriate informations relating to weights, contact angle, surface tension, table of pressure and equilibrium time were then entered by the keyboard for each of the penetrometers, and the analysis was started. The same pressure table was used for all the specimens and equilibrium time of 30 seconds was used for both low and high pressures.

The machine automatically evacuates the samples, fills them with mercury and pressurises them up to 172.4 KPa in the low pressure ports, as designated by the pressure points in the table used by the computer. The low pressure run takes about 40 minutes to be completed. After that penetrometers were weighed again and two of them were transferred into high pressure vessels. Appropriate information was entered again and the high pressure analysis started. The machine automatically increases the pressure to the designated pressures in the table selected and pressurised the samples up to 414 MPa. The pressure can be checked in high pressure chambers through the terminal. After completion of the high-pressure analysis, the samples are automatically depressurised and returned to ambient pressure. The data from the low-pressure file are combined with high-pressure data, and the report is printed on the terminal. These data were then transferred to a mainframe computer for further analysis.

6.5 Microscopic observation

The Scanning Electron Microscope (SEM) was used for the study of the micromorphology and analysis of fracture surface of mortars and aggregates particles. The micromorphology of cement hydration products has been studied by many research workers[116-121]. Most researchers have concentrated their efforts on examining the C_3S and C_2S component of cement. This approach is largely justified since C_3S and C_2S together constitute about 75 per cent of portland cement. Moreover, a number of investigators, such as Ciach and Swenson[122] have shown that the hydrated structure of cement paste vary much like its two principal constituents.

6.5.1 Specimen preparation

The most common method of specimen preparation in scanning electron microscopy is to coat the fractured surface with various materials such as carbon or gold.

In this study the aggregate particles and specimens of selected mortar mixes were oven dried and mounted on alloy plattens. A reasonably flat fracture surface was chosen for SEM analysis. The specimens were gold coated using Emscope SC500 Sputter coater and the alloy plattens were loaded to a 'Camscan series 3' scanning electron microscope for analysis.

This study was directed primarily towards investigating how the microstructure of mortar mixes changes under different conditions of curing and mix compositions and in corporation of air entraining agent.

CHAPTER SEVEN

DEGREE OF HYDRATION AND CARBONATION

7.1 Hydration of Cement

Cement is a system composed of numerous minerals which react with water at different rates, give hydration products of different composition and crystallinity, and influence the engineering properties (such as thermal conductivity) of the final product in different ways. According to Powers[65], as hydration proceeds, the reaction products (cement gel) are deposited in surrounding water filled space. The cement gel consists of pores, which are called gel pores, and constitutes about 28% of the gel volume. The remaining water filled space, amongst the cement gel, creates capillary pores or cavities after drying. Therefore, converting capillary pores to gel pores, as a function of hydration, results in reducing the size of pores, since gel pores are smaller than capillary pores. The pores in the capillary pore system gradually become smaller and smaller until the connection between the capillary pores is blocked by cement gel. This, in effect, is related to the behaviour of the material in terms of its engineering properties.

The hydration of cement has been investigated by numerous workers and the process is now established

[66,123,124]. The main components of Portland cement i.e. tricalcium silicate (C_3S), dicalcium silicate (C_2S), tricalcium aluminate (C_3A) and tetracalcium aluminoferrite (C_4AF) react with water to produce complex hydrates. The main events that take place during the setting process of a normal cement paste are visualized as proceeding through four stages[66,125,126].

The first stage lasts for only several minutes after the water has come into contact with the cement grains. Hydration commences quickly on the C_3S phase with both lime and silica passing into solution, initially in the same molar ratio (3:1) as in the anhydrous compound. The immediate product formed in pastes on mixing has a CaO: SiO_2 ratio near to 3. This forms as a coating on the C_3S surfaces and retards the reaction which results in a dormant period of little activity (stage 2). The unstable primary products have a large excess of lime in their structure and , after a few hours, dissolution or splitting off of this initial product results in an acceleration of the hydration as water diffuses through the surface coating (stage 3). This leads to the formation of a second product of C-S-H(I) gel of lower $CaO:SiO_2$ ratio (1.5 or less)[127]. This is then quickly followed by the formation of a third stable product. C-S-H(II) gel, which has a lime: silica ratio of 1.5 - 2.0. During this third stage, the rate of heat evolution increases reaching a peak between 6 and 11 hours after mixing and is assigned to the reaction on the alite phase. As the activity of this third stage subsides, the fourth stage or period of

hardening begins. The completely hydrates silicate has a lime: silica ratio of about 1.4 - 1.6[127].

In the presence of a limited amount of water the reaction of C_3S and C_2S (which together make up 75 to 80% of the cement) with water can be represented typically as[128]:

$$2\ C_3S + 6\ H \longrightarrow C_3S_2H_3 + 3\ CH \qquad \ldots(7.1)$$

tricalcium silicate (Alite) — water — gel — Calcium hydroxide

$$2\ C_2S + 4\ H \longrightarrow C_3S_2H_3 + CH \qquad \ldots(7.2)$$

(Blite)

The principal cement hydration product is a calcium silicate hydrate. The formula $C_3S_2H_3$ is only approximate because the composition of this hydrate is actually variable over quite a wide range. Studies on the microstructure of cement indicate that calcium silicate hydrates exist in a variety of forms: fibrous particles, flattened particles, a reticular network and some other form. Since the time that Diamond (1976)[116] proposed a classification of the C-S-H gel particles as seen in the SEM, much work has been produced using better and more sophisticated instruments[73]. The original morphological types proposed by Diamond are still used by many investigators. These are: type I acicular, type II reticulated or honeycomb, type III small discs or spheres and type IV dense 'inner products'. Calcium hydroxide which is released when C_3S and C_2S react with water, can be identified as hexagonal crystals.

In Portland cement the hydration of C_3A involves a reaction with sulphate ions which are supplied by the dissolution of gypsum. The primary initial reaction of C_3A is[128]:

$$C_3A + 3\ CSH_2 + 26\ H \longrightarrow C_6AS_3H_{32} \qquad \ldots(7.3)$$

tricalcium aluminate — gypsum — water — ettringite

Ettringite is a stable hydration product only while there is an ample supply of sulphate available. If the sulphate is all consumed before the C_3A has completely hydrated, then ettringite transforms to another calcium sulfoaluminate hydrate containing less sulphate, vis.

$$2\ C_3A + C_6S_3H_{32} + 4\ H \longrightarrow 3\ C_4ASH_{12} \qquad \ldots(7.4)$$

this second product is called monosulphoaluminate.

7.2 Thermal analysis methods

There are various methods of determining the progress of hydration[73], such as the determination of : (a) the amount of calcium hydroxide in the paste; (b) the amount of non-evaporable water; (c) the specific gravity of the paste; (d) the amount of unhydrated cement (using X-ray quantitative analysis); (e) the heat evolved by hydration and (f) indirectly from the strength of the hydrated paste[105]. In methods (a), (b), (c) and (f), the values of calcium hydroxide content, non-evaporable water, specific gravity and strength are determined at different ages and compared with corresponding values obtained for fully hydrated cement for the degree of hydration determination.

Thermal analysis methods such as differential thermal analysis (DTA) and thermogravimetry (TG) have been widely used in determining the amount of calcium hydroxide in different cement paste systems. Midgley[129] made a comparative study using DTA, TG, Quantitative X-ray, glycol extraction and alcohol-glycerol and concluded that thermal analysis techniques give the most reliable result if the total calcium hydroxide content of a set Portland cement is required.

Thermogravimetry is a well established technique [130-132]. In this technique a sample is heated at a controlled rate and the weight loss is recorded at various temperatures or times. When hardened cement paste is heated gradually it will lose weight due to dehydration, dehydroxylation or decomposition of its components. Since the above mentioned processes can occur at certain

temperature intervals they can be easily identified by comparison with standard peaks.

7.2.1 A quantitative determination of calcium hydroxide content from TG results

Water is released, during the dehydration of calcium hydroxide at a temperature between about 420°C and 534°C, according to the following equation [130,133]:

$$Ca(OH)_2 \longrightarrow CaO + H_2O \uparrow \qquad \ldots(7.5)$$

This equation indicates that the weight loss corresponding to one gramme-molecule of water (18g) is due to the dehydroxylation of one gramme-molecule of calcium hydroxide (74g). However, small amounts of calcium hydroxide might carbonate in the presence of carbon dioxides:

$$CO_2 + Ca(OH)_2 \longrightarrow CaCO_3 + H_2O \qquad \ldots(7.6)$$

this must be calculated and added to find the original calcium hydroxide content.

Calcium carbonate decomposes at a temperature between about 600°C and 780°C as:

$$CaCO_3 \longrightarrow CaO + CO_2 \uparrow \qquad \ldots(7.7)$$

This equation indicates that one gramme - molecule of CO_2 (44g) is due to decomposition of one gramme-molecule of $CaCO_3$ (100g). But, this weight of $CaCO_3$ is originally generated from the carbonation of one gramme-molecule of $Ca(OH)_2$ i.e. 74g. Therefore, the weight loss of one gramme-molecule of CO_2 (44g) corresponds to one gramme-molecule of $Ca(OH)_2$ (74g) in the original sample. The total amount of calcium

hydroxide can therefore, be determined from the TG trace shown in Figure 7.1, using the following equation [133]:

$$W_{Ca(OH)_2} = M_1 \times \frac{74}{18} + M_2 \times \frac{74}{44} \qquad \ldots(7.8)$$

where:

$W_{Ca(OH)_2}$ = Percentage of total amount of Calcium hydroxide in the sample.

M_1 = Percentage of mass lost between 420 to 534°C as shown in Figure 7.1.

M_2 = Percentage of mass lost between 600 to 780°C as shown in Figure 7.1.

7.2.2 Determination of non-evaporable water

By measuring the non-evaporable water present in cement paste, the progress of hydration can be monitored [66,130,134,135]. It has to be noted that although this method is frequently used to determine degree of hydration, it is not an absolute measure of the degree of hydration, because neither the composition of the major hydration product (C-S-H), nor the stoichiometry of the reaction is well defined[134]. The results may also be affected by the method of drying the sample to remove the evaporable water, since some of chemically bound water may be released as well.

The non-evaporable water is defined as the loss in weight when cement paste is ignited to 1000°C after having been equilibrated at 100°C. In this method the percentage of non-evaporable water is expressed as the ratio of the weight loss to the ignited weight. However, some of this weight

loss is due to the decomposition of $CaCO_3$ at a temperature between 600 to 780°C, as mentioned earlier, therefore the total weight loss should be corrected taking this into account[130].

In this investigation, it was found reasonable to ignite the sample at 1000°C and calculate the non-evaporable water as [136]:

$$W_{NE} = \frac{M_3}{100 - (M_3 + M_2 + M_1)} \times 100 \qquad \ldots(7.9)$$

where:

W_{NE} = Percentage of total non-evaporable water in the sample.

M_1 = Percentage of mass lost between 420 to 534°C as shown in Figure 7.1.

M_2 = Percentage of mass lost between 600 to 780°C as shown in Figure 7.1.

M_3 = Percentage of mass lost between 100 to 420°C as shown in Figure 7.1.

Powers and Brownyard[67] have shown that for cement paste made from type I and II Portland cements, the non-evaporable water accounts for 21.8% of the total weight at complete hydration. In this investigation however, a value of 21.4% [136] of the total weight at complete hydration is taken for the non-evaporable water.

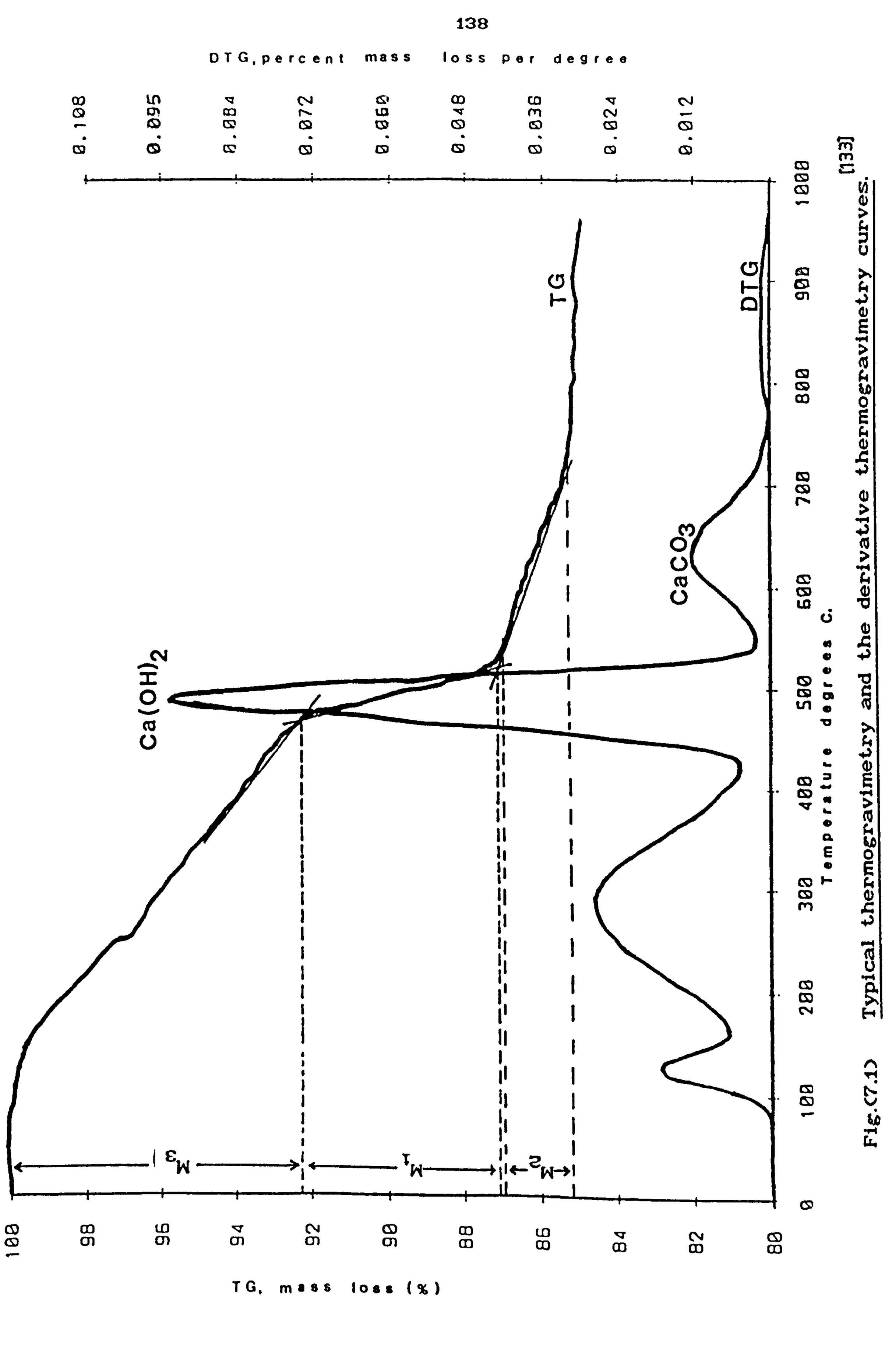

Typical thermogravimetry and the derivative thermogravimetry curves. [133]

Fig.(7.1)

7.3 Apparatus and procedure

The apparatus used in this study was a Stanton Redcroft model TG-750[137] in which the gravimetric balance was modified by Cabrera and Clease[138] so as to give a computerised output like the one shown in Figure 7.1. The apparatus consists mainly of an electro-microbalance, a furnace, and operation programmer unit and the data acquisition unit (see Figure 7.2). The temperature scale of the apparatus was calibrated with materials of known temperature changes (i.e. Kaolinite and Calcium oxalate monohydrate) by Lynsdale[108].

In order to determine the calcium hydroxide content and also combined water of mortars[133], samples were cut from a cube of mortar (cured similar to thermal conductivity and porosity samples) and placed in an oven of 105°C. When constant weight was reached (usually after 24 hours) the samples were taken out of the oven and ground using an electrical high speed grinder. The samples were taken from the middle part of the cubes to minimise carbonation effects. The powdered samples were passed through a 75μm sieve (in order to improve the uniformity of the sample) and kept in a sealed bottle under nitrogen atmosphere. Great care was taken between these operations, and the samples were kept in sealed polythene bags and kept in a desiccator containing silica gel and nitrogen atmosphere, in order to minimise partial carbonation.

The platinum crucible was filled with powdered samples and the furnace was closed. The furnace was kept in an atmosphere of nitrogen gas flowing at the rate of 15 ml/min.

The samples were heated to 1000°C at a constant rate of 30°C per minute and the weight losses were continuously monitored.

The furnace was cooled by water, to achieve fast cooling rate (i.e. cooling from 1000 to 100°C in ten minutes). The test was fast, and it usually required 40 minutes to obtain thermogram for a sample.

Typical thermogravimetry (TG) and the derivative thermogravimetry (DTG) curves of the samples are shown in Figure 7.1. The TG curves are obtained by plotting the cumulative mass loss against temperature while the DTG curves are obtained from the TG curves by plotting the percentage mass loss per degree of temperature.

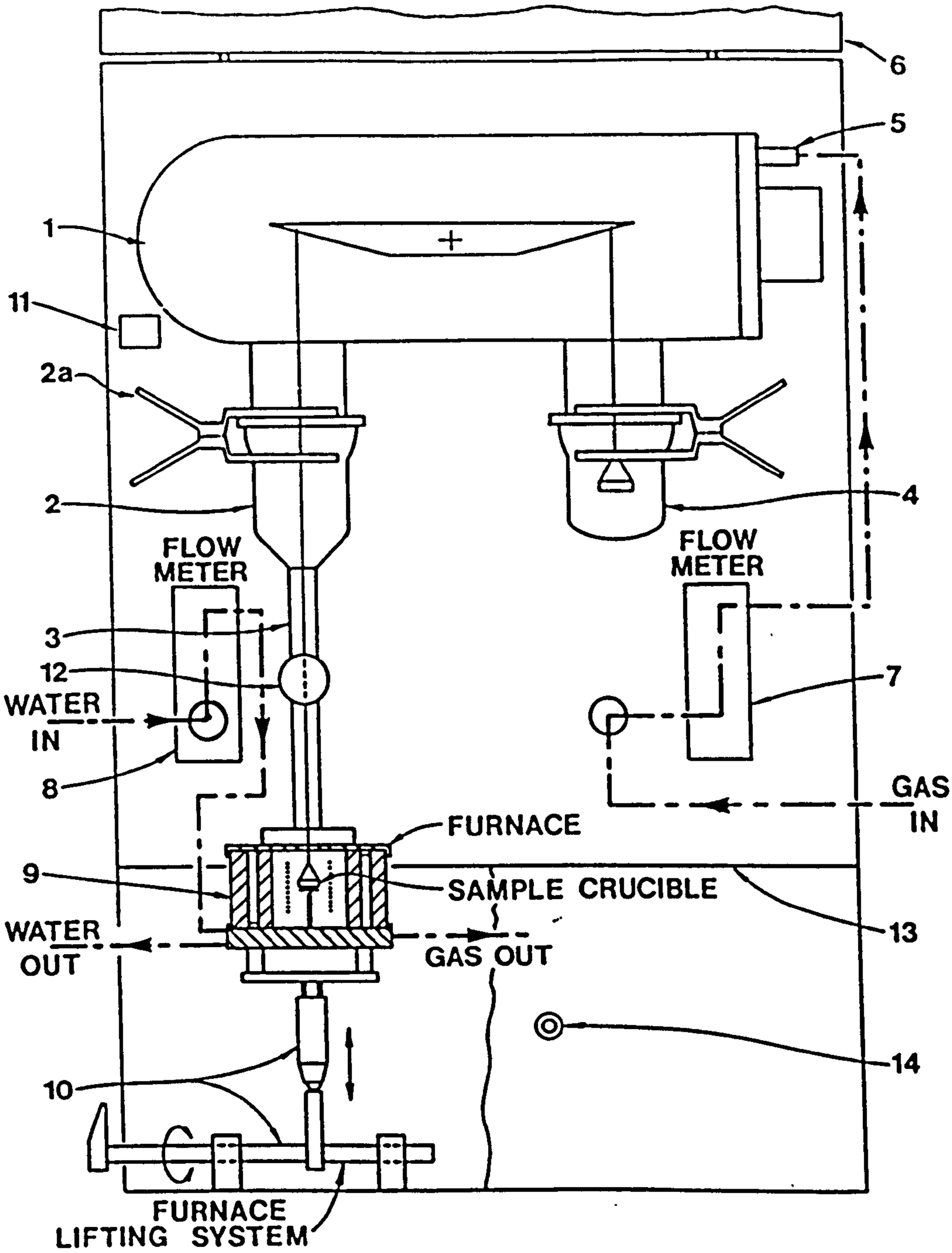

1 the electronic microbalance and glass vacuum assembly
2 glass ball and socket joint
2a spring clip
3 glass hangdown tube
4 glass cap to cover poise pan
5 vacuum connectors
6 metal front cover to protect balance from extraneous light
7 gas-flow meter
8 water-flow meter
9 furnace assembly
10 furnace lifting mechanism
11 level indicator
12 hangdown tube retaining bracket
13 top of furnace assembly console
14 alarm reset button

Fig.(7.2) Schematic diagram of TG-750 showing the components[137].

7.4 Carbonation

It is known that carbonation changes the microstructure of cement paste and affects the engineering properties of concrete[66,105,139-143]. There is agreement to the fact that carbonation reduces the total porosity of concrete and alters its pore size distribution so that as an overall effect carbonation tends to marginally increase the thermal conductivity. In the literature, data on the change of thermal conductivity of concrete due to carbonation is non-existent so this can not be confirmed from published data.

The process of carbonation which take place when carbon dioxide from the environment diffuses through moist concrete can be expressed in a simplified form as equation 7.6 $\left[\text{i.e.,}\quad CO_2 + Ca(OH)_2 \longrightarrow CaCO_3 + H_2O\right]$ and as:

$$C\text{-}S\text{-}H + CO_2 + H_2O \longrightarrow CaCO_3 + SiO_2(gel) + H_2O \quad \ldots(7.10)$$

Carbonation is a fairly slow process and the rate at which carbon dioxide penetrates concrete and reacts to form calcium carbonate depends, among the other factors[142], on the permeability of the concrete to carbon dioxide which in turn depends mostly on micromorphology of the cement paste and concrete. The relative humidity that prevails also strongly influences the rate of carbonation[142,143]. Therefore concrete mix parameters, curing and condition of exposure of concrete affect the rate of carbonation of concrete.

Contradictions exist on the range of pore sizes which are affected by carbonation. Houst et al[144] have concluded

that pores with a diameter between 100 Å (0.01 μm) and 1000 Å (0.1 μm) are largely reduced by carbonation whereas pores bigger than 2000 Å (0.2μm) are hardly affected. It has also been reported that carbonation reduces the volume of pores with diameters between 0.1 Å ($10^{-5}\mu$m) and 100Å (0.01μm) by a factor of 2 [145]. Cabrera et al[142] carried out studies on carbonation of mortars containing cement, PFA, silica fume and trass and concluded that carbonation tend to fill pores mainly in the range of 100 to 10^4 Å (0.01 to 1 μm), reduces the total porosity and the mean pore diameter. Pihlajavaara[146] on the other hand presented limited data and concluded that pores less than 125 Å in diameter are hardly affected by carbonation and the influence of carbonation on the pores between 200 Å (0.02 μm) and 1000 Å (0.1 μm) was found to be greater than the smaller pores.

7.4.1 Experimental methods to monitor carbonation

Two methods were used to monitor the extent of carbonation in all the mixes.

1) <u>Depth of carbonation</u>

Assessment of the carbonation depth was carried out by spraying the surface of a freshly broken 100mm concrete cube with a pH indicator (2 per cent solution of phenolphthalein in ethyl - alcohol). In a non - carbonated part a purple-red colouration is obtained since concrete is still highly alkaline and in a carbonated part no colouration is occurred.

The depths of carbonation measured perpendicularly to three faces of the broken concrete cube are averaged for mean

value (D) of the carbonation depth as shown in Figure 7.3. The depth of carbonation of the trowelled face is ignored because trowelling results in a noticeably small depth of penetration. Two cubes were used for each tests.

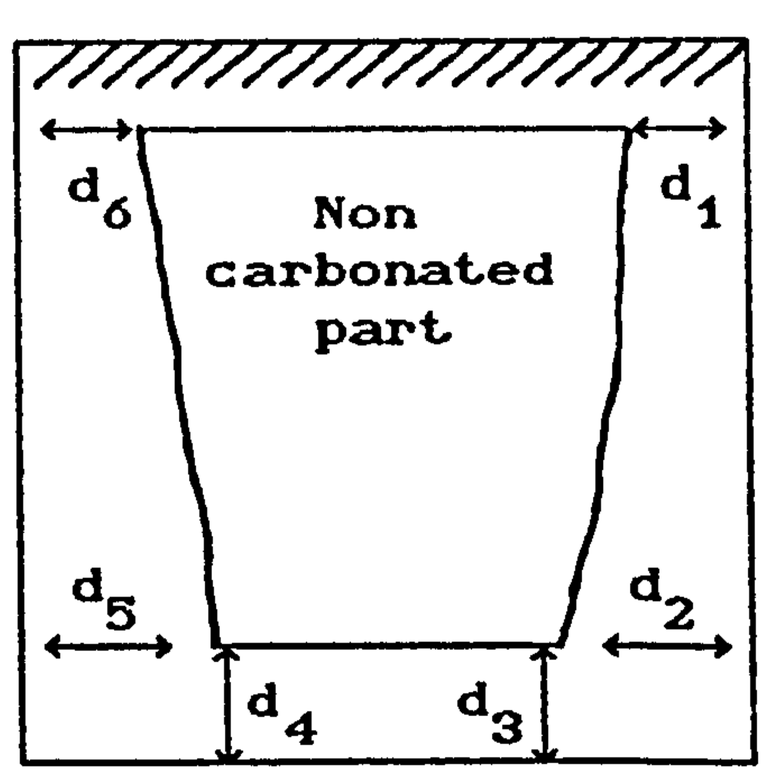

$$D = \frac{d_1 + d_2 + \ldots + d_6}{6}$$

Fig.(7.3) Depth of carbonation on a cross section of a concrete cube after carbonation.

2) Quantitative evaluation of carbonation

The amount of calcium carbonate formed due to carbonation was determined by thermogravimetry as described in section 7.2.1.

CHAPTER EIGHT

PRESENTATION OF RESULTS

8.1 Introduction

The experimental results of the tests described in previous chapters are presented in the following order:

1. Thermal conductivity (for 'A' curing condition)
2. Mercury porosimetry
3. Vacuum saturation
4. Thermogravimetry
5. Carbonation depth
6. Scanning electron microscope
7. Compressive strength

8.2 Thermal conductivity results for 'A' curing condition

λ-values at 3 per cent moisture content by volume (adjusted using the derived moisture correction factor in section 5.5.3) for the 24 pairs of concrete specimens are given in Table 8.1, together with the free W/C ratio of the concrete mixes i.e. after taking the water absorption of the coarse aggregate in to account. The measurement were made after the 'A' curing condition and according to BS 874: 1988[1]. A typical measurement print-out of the results is given in Appendix III.

Table (8.1)

Thermal conductivity of concrete specimens at 3% m.c. (by vol.)

Mix No.	Concrete Code Name	λ @ 3% m.c. (W/mK)	Mean Dry Density (kg/m^3)	Free W/C Ratio
1	QA /0.53	2.76	2282	0.51
2	QAE /0.43	2.17	2091	0.42
3	LA /0.60	1.75	2248	0.55
4	LAE /0.50	1.50	2033	0.45
5	PA /0.90	0.91	1858	0.63
6	PAE /0.80	0.65	1557	0.53
7	QA /0.80	2.56	2250	0.78
8	LA /0.80	1.81	2243	0.75
9	PA /0.80	0.99	1902	0.53
10	QB /0.80	2.52	2291	0.77
11	LB /0.80	1.73	2261	0.71
12	PB /0.80	0.65	1570	0.37
13	QB /0.56	2.86	2341	0.53
14	LB /0.66	1.89	2291	0.57
15	PB /1.05	0.69	1647	0.62
16	QC /0.90	2.61	2236	0.87
17	QCE /0.80	1.99	2020	0.77
18	LC /0.95	1.81	2207	0.86
19	LCE /0.90	1.44	1988	0.82
20	PC /1.29	0.82	1818	0.86
21	PCE /1.29	0.63	1551	0.87
22	QC /0.80	2.70	2238	0.77
23	LC /0.80	1.96	2243	0.71
24	PC /0.80	0.85	1745	0.37

Notes on mix Code names:

Q Stands for concretes made with Quartzitic coarse Agg.
L Stands for concretes made with Limestone coarse Agg.
P Stands for concretes made with Pellite coarse Agg.

	Cement	Sand	Coarse aggregate	
A	1	2.33	3.5	(Reference mix)
B	1	2.33	5.6	
C	1	3.73	5.6	

Third letter (E) indicates Air-entrained mix.
(0.257 Litre/100kg of Cement.)
Numbers indicate the total W/C ratios.

8.3 Pore size distribution and total porosity results using Mercury Intrusion Porosimetry (MIP)

8.3.1 Repeatability of data

Mercury porosimetry is a reliable and reproducible technique [72,110-111], however, the reproducibility can be affected by many factors such as the cleanliness of mercury, the sample's dimension and other factors, some of which were mentioned in section 6.4.3.

In this investigation, the uniformity of mortar preparation was assessed by measuring the pore size distribution of a number of mortar samples prepared at different times with the same composition, and cured under the same condition. As shown in Figures 8.1 and 8.2, the results are consistent and repeatable. The standard deviation of total porosity of the mortar samples was 0.30 and the standard deviation of median pore diameter was 0.02. The results reported are the mean of two test in identical samples.

8.3.2 MIP results

The mercury intrusion porosimetry test was carried out on samples of mortars for the 24 mixes and at various curing conditions. The results are presented in Table 8.2. Information obtained using MIP measurements of the 24 samples studied are presented as cumulative pore volume of mercury intruded against the logarithm of pore diameter in Figures 8.3 - 8.5, 8.7, 8.9, ... 8.21. This graphical presentation shows readily the total porosity, the threshold diameter and the limiting pore size. Figures 8.6, 8.8, 8.10, ... 8.20 present the incremental pore size distribution curves. These graphs show the actual pore volume for each pore diameter.

They also show peaks of pore volume in a particular distribution.

Figures 8.22 - 8.27 shows the pore size distribution results for different type of coarse aggregates used in the concrete mixes.

A summary of results for the mortar and coarse aggregate samples obtained from the MIP data including their calculated total porosity (using equation 2.6) are presented in Table 8.2.

Table (8.2)

Summary of MIP results for mortars and coarse aggregates

Mix No.*	Mortar Code Name #	Dry Density (g/cc)	Apparent Density (g/cc)	Total Intrusion Volume (cc/g)	Calculated Total Porosity (%)	Median Pore Diameter (μm)
1A		2.0492	2.4552	0.0807	16.5	0.0936
1B		2.0179	2.4268	0.0835	16.8	0.0950
1C	A /0.53	2.0545	2.4512	0.0789	16.2	0.0996
1D		2.0381	2.4282	0.0788	16.1	0.0889
1E		2.0346	2.4271	0.0794	16.2	0.0918
2A		1.9357	2.4468	0.1079	20.9	0.3759
2B		1.9364	2.4007	0.0998	19.3	0.2924
2C	AE/0.43	1.9172	2.4445	0.1132	21.6	0.2579
2D		1.9143	2.4347	0.1117	21.4	0.2382
2E		1.9202	2.4501	0.1125	21.6	0.3975
3	A /0.6	2.0288	2.4473	0.0843	17.1	0.1367
4	AE/0.5	1.8696	2.4218	0.1219	22.8	0.2581
5	PA /0.9	1.9093	2.4698	0.1189	22.7	0.2790
6	PAE/0.8	1.8293	2.4038	0.1307	23.9	0.2823
7,8	A /0.8	2.0238	2.4698	0.0892	18.1	0.1348
9	PA /0.8	2.0052	2.4018	0.0827	16.5	0.1367
10,11	B /0.8	1.9504	2.4272	0.1006	19.6	0.1649
12	PB /0.8	2.0545	2.4512	0.0789	16.2	0.1175
13A		2.0457	2.4580	0.0820	16.8	0.0917
13B		2.0379	2.4405	0.0808	16.5	0.0798
13C	B /0.56	2.0458	2.4368	0.0782	16.0	0.0760
13D		2.0317	2.4303	0.0807	16.4	0.0782
13E		2.0306	2.4342	0.0818	16.6	0.0908
14	B /0.66	2.0147	2.4408	0.0868	17.5	0.1693
15	PB /1.05	1.9001	2.4005	0.1093	20.8	0.3394
16A		1.9593	2.4881	0.1088	21.3	0.3233
16B		1.9965	2.4431	0.0915	18.3	0.1689
16C	C /0.9	1.9552	2.4588	0.1048	20.5	0.2819
16D		1.9875	2.4642	0.0969	19.3	0.2253
16E		2.0239	2.4771	0.0904	18.3	0.1629
17	CE/0.8	1.8459	2.4240	0.1290	23.8	1.0057

(*) letters after mix numbers indicate the curing conditions.

(#) First letter (P) indicates mortar's been sieved from Pellite concrete. Letters (A) and (B) indicate Cement-sand ratio of 1:2.33 and (C) indicates Cement-sand ratio of 1:3.73. Letter (E) indicates Air-entrained mix.

Table (8.2) (continued)

Mix No.*	Mortar Code Name #	Dry Density (g/cc)	Apparent Density (g/cc)	Total Intrusion Volume (cc/g)	Calculated Total Porosity (%)	Median Pore Diameter (μm)
18A		1.9071	2.4601	0.1213	22.5	0.3752
18B		1.9613	2.4619	0.1037	20.3	0.2353
18C	C /0.95	1.9401	2.4644	0.1097	21.3	0.3567
18D		1.9459	2.4437	0.1053	20.5	0.2671
18E		1.9160	2.4664	0.1165	22.3	0.3705
19A		1.8509	2.5068	0.1418	26.2	1.8138
19B		1.8067	2.4233	0.1408	25.4	1.7829
19C	CE/0.9	1.7878	2.4334	0.1484	26.5	1.8321
19D		1.7929	2.3887	0.1391	24.9	1.8023
19E		1.7984	2.4324	0.1449	26.1	1.8105
20A		2.0144	2.5168	0.0995	20.0	0.2917
20B		2.0215	2.4632	0.0886	17.9	0.1932
20C	PC /1.29	1.9158	2.4704	0.1168	22.4	0.6908
20D		1.9734	2.5109	0.1085	21.4	0.3921
20E		1.9126	2.4415	0.1133	21.7	0.4567
21A		1.8940	2.4552	0.1208	22.9	1.2760
21B		1.9221	2.4656	0.1144	22.0	0.5539
21C	PCE/1.29	1.9091	2.4752	0.1198	22.9	0.9189
21D		1.9239	2.4822	0.1169	22.5	0.7048
21E		1.9561	2.4591	0.1046	20.5	0.4562
22,23	C /0.8	1.9966	2.4588	0.0944	18.8	0.3003
24	PC /0.8	2.0492	2.4552	0.0807	16.5	0.0938
Coarse Aggregates						
Quartz	5 -10 mm	2.5020	2.6585	0.0236	5.9	0.8060
Quartz	10-14 mm	2.6345	2.7079	0.0104	2.7	0.3756
Quartz	14-20 mm	2.5981	2.6549	0.0080	2.1	0.5312
Limestone	5 -10 mm	2.4803	2.6721	0.0289	7.2	0.3719
Limestone	10-14 mm	2.5297	2.6709	0.0209	5.3	0.1919
Limestone	14-20 mm	2.6218	2.6842	0.0087	2.3	0.2107
Pellite	5 -10 mm	1.9445	2.5913	0.1288	25.0	1.0312
Pellite	10-14 mm	1.7402	2.3478	0.1486	25.9	1.5308
pellite	14-20 mm	2.0859	2.7709	0.1182	24.7	1.7066

(*) letters after mix numbers indicate the curing conditions.
(#) First letter (P) indicates mortar's been sieved from Pellite concrete.Letters (A) and (B) indicate Cement-sand ratio of 1:2.33 and (C) indicates Cement-sand ratio of 1:3.73. Letter (E) indicates Air-entrained mix.

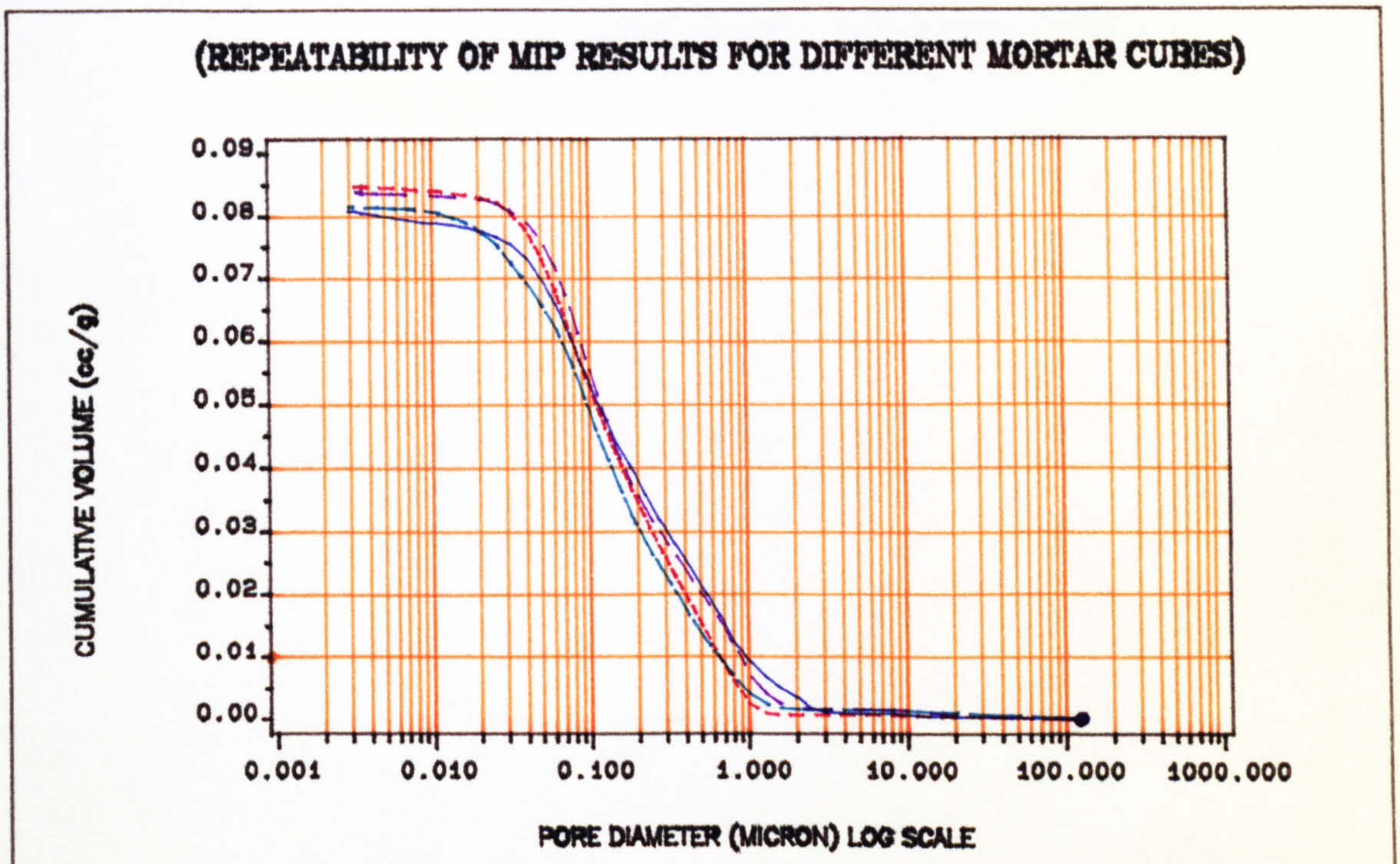

FIGURE (8.1) Cumulative volume vs. pore diameter for mortar : mix A , W/C=0.8

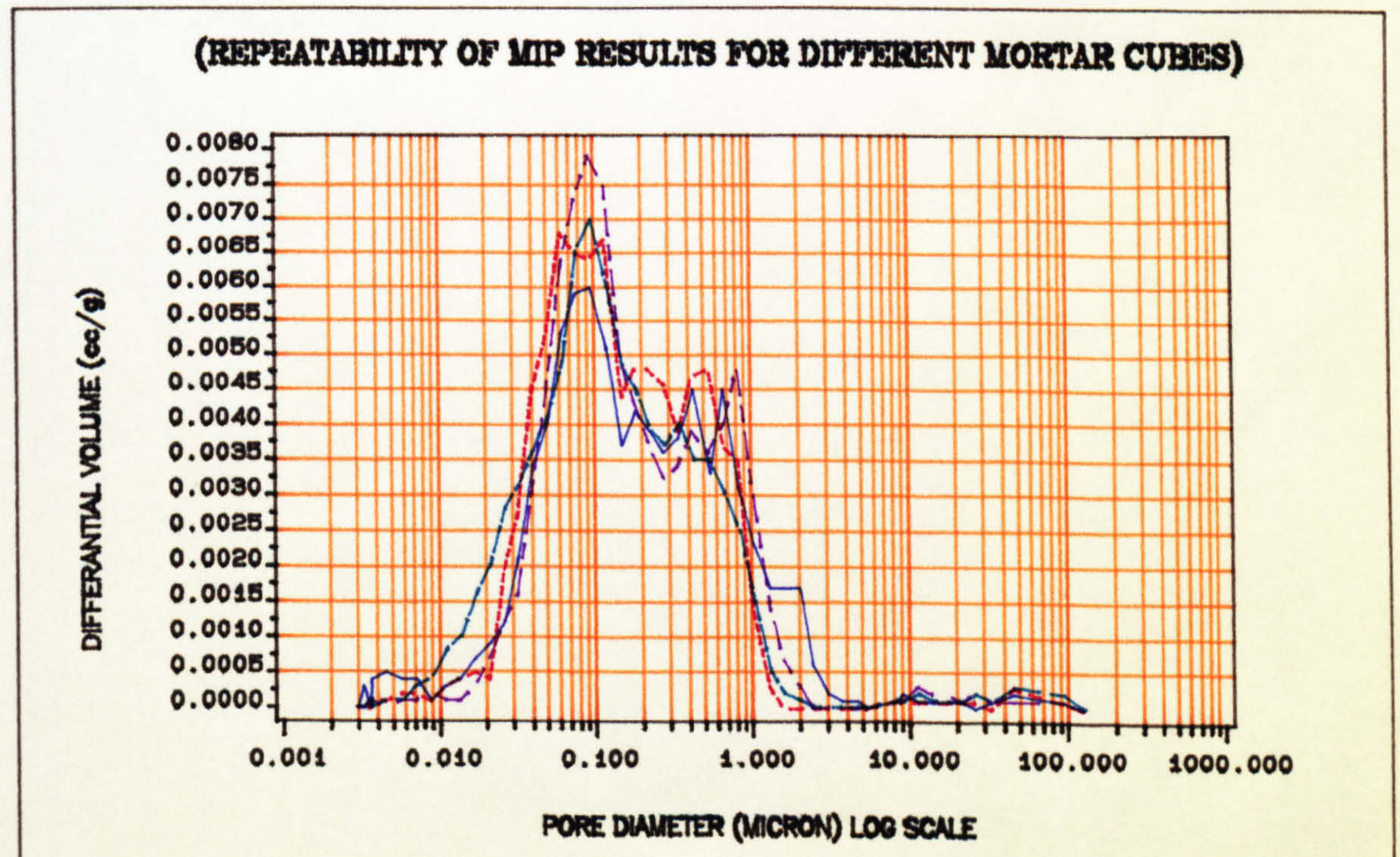

FIGURE (8.2) Incremental pore volume vs. pore diameter for mortar : mix A , W/C=0.8

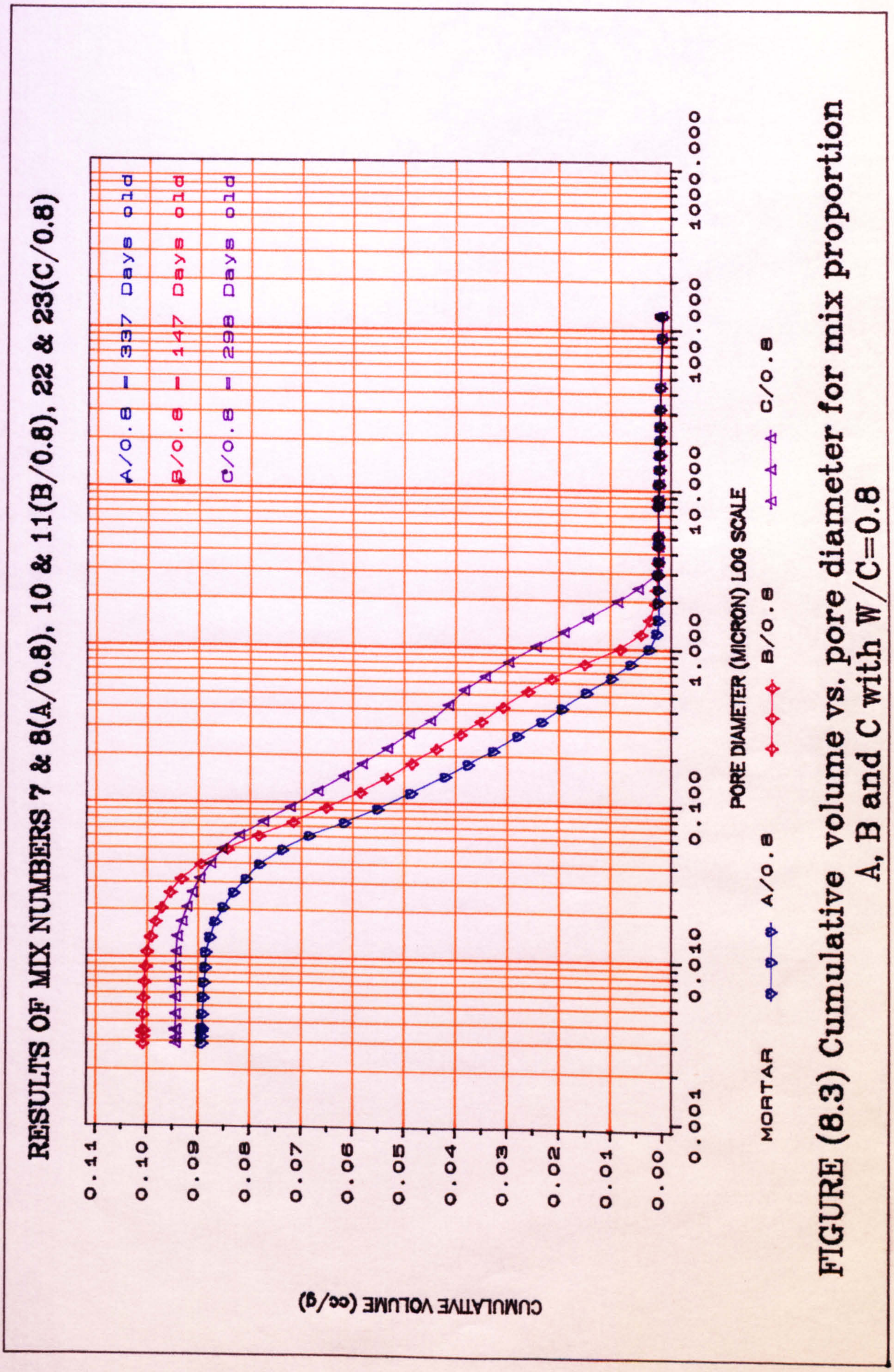
RESULTS OF MIX NUMBERS 7 & 8(A/0.8), 10 & 11(B/0.8), 22 & 23(C/0.8)
A/0.8 = 337 Days old
B/0.8 = 147 Days old
C/0.8 = 298 Days old
Cumulative volume vs. pore diameter for mix proportion A, B and C with W/C=0.8
A/0.8
B/0.8
C/0.8
CUMULATIVE VOLUME (cc/g)
PORE DIAMETER (MICRON) LOG SCALE
MORTAR

FIGURE (8.3) C

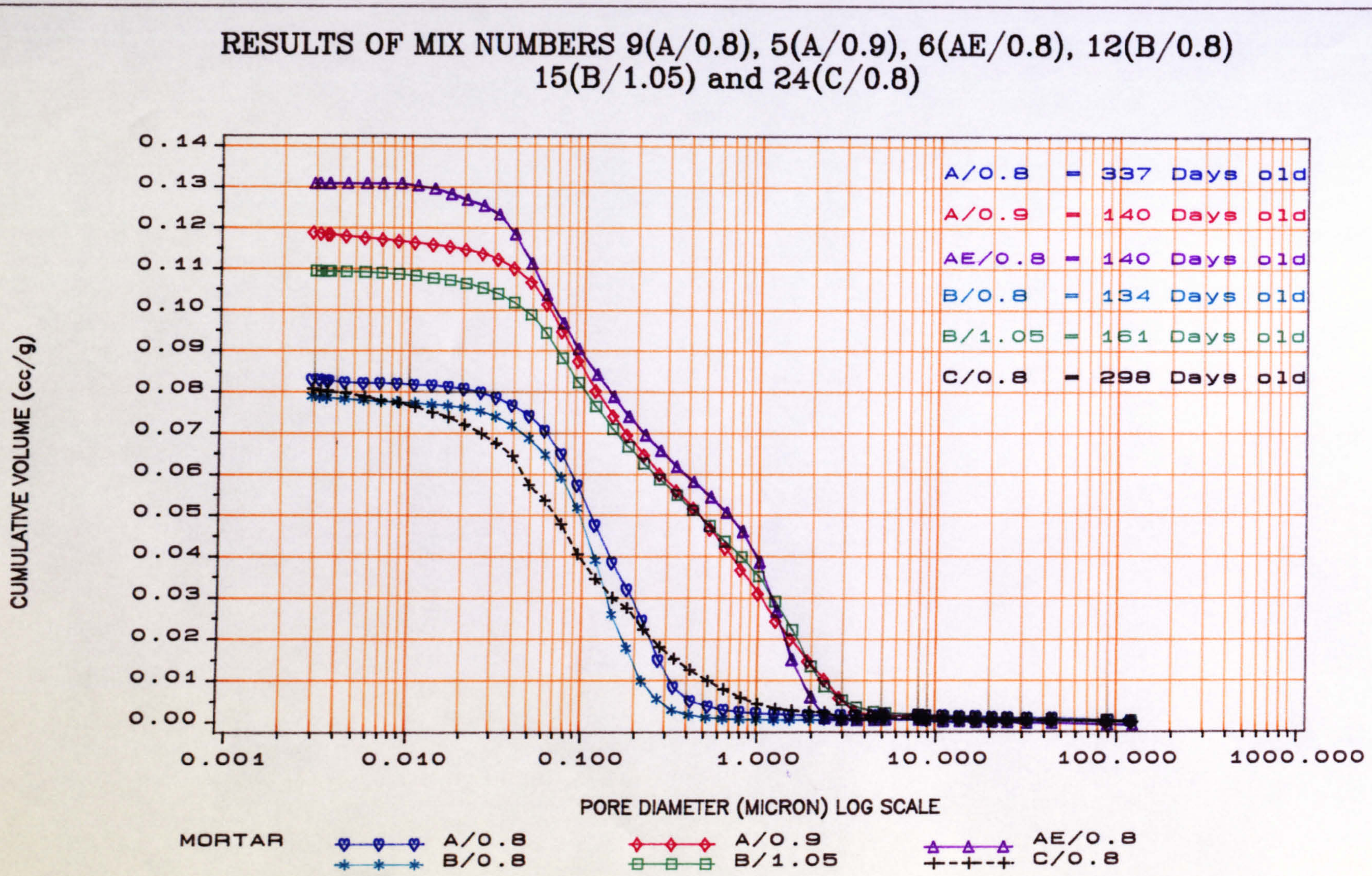

FIGURE (8.4) Cumulative volume vs. pore diameter for mortars sieved from Pellite concretes on 2.36mm sieve

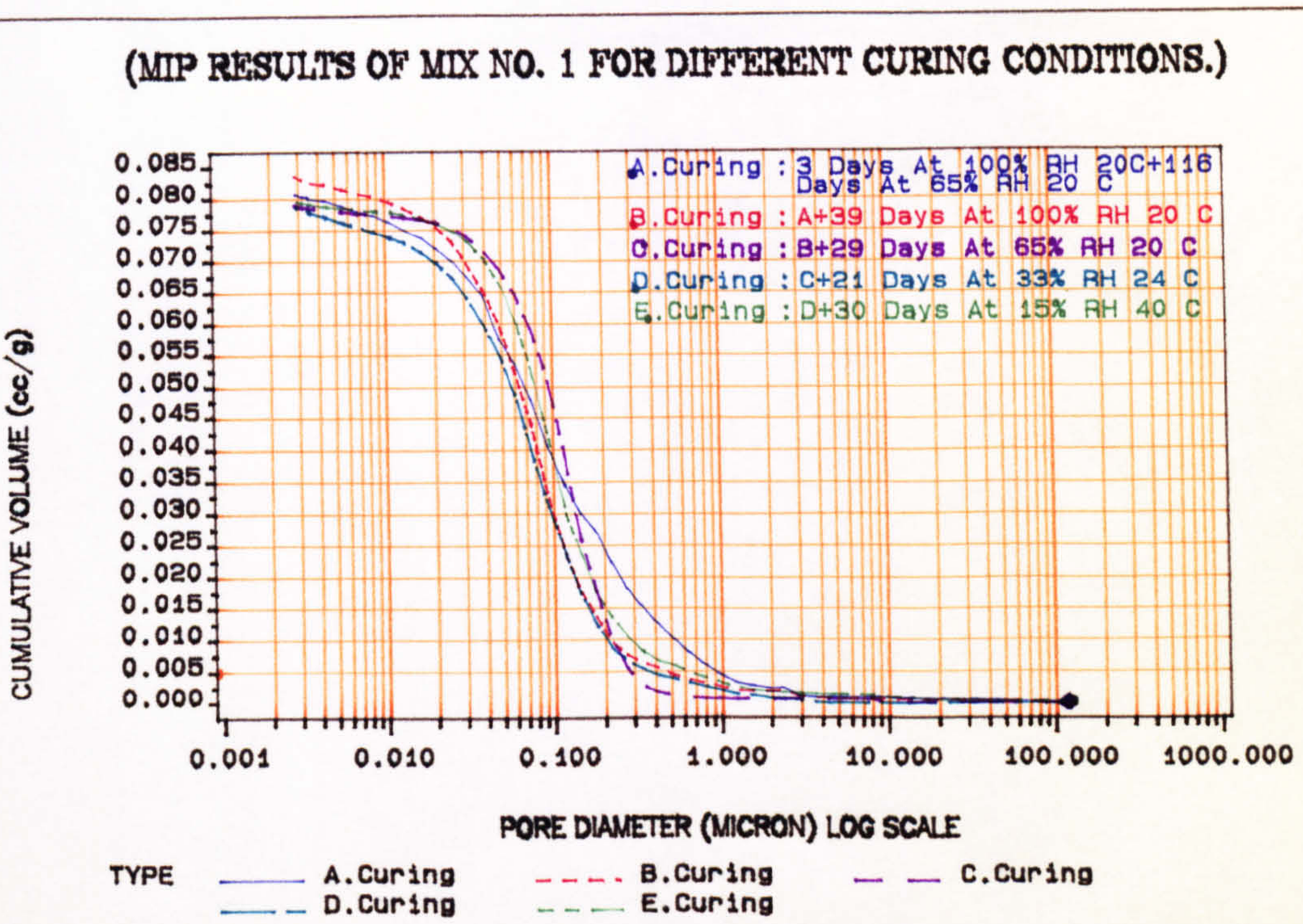

FIGURE (8.5) Cumulative volume vs. pore diameter for mortar : mix A , W/C=0.53.

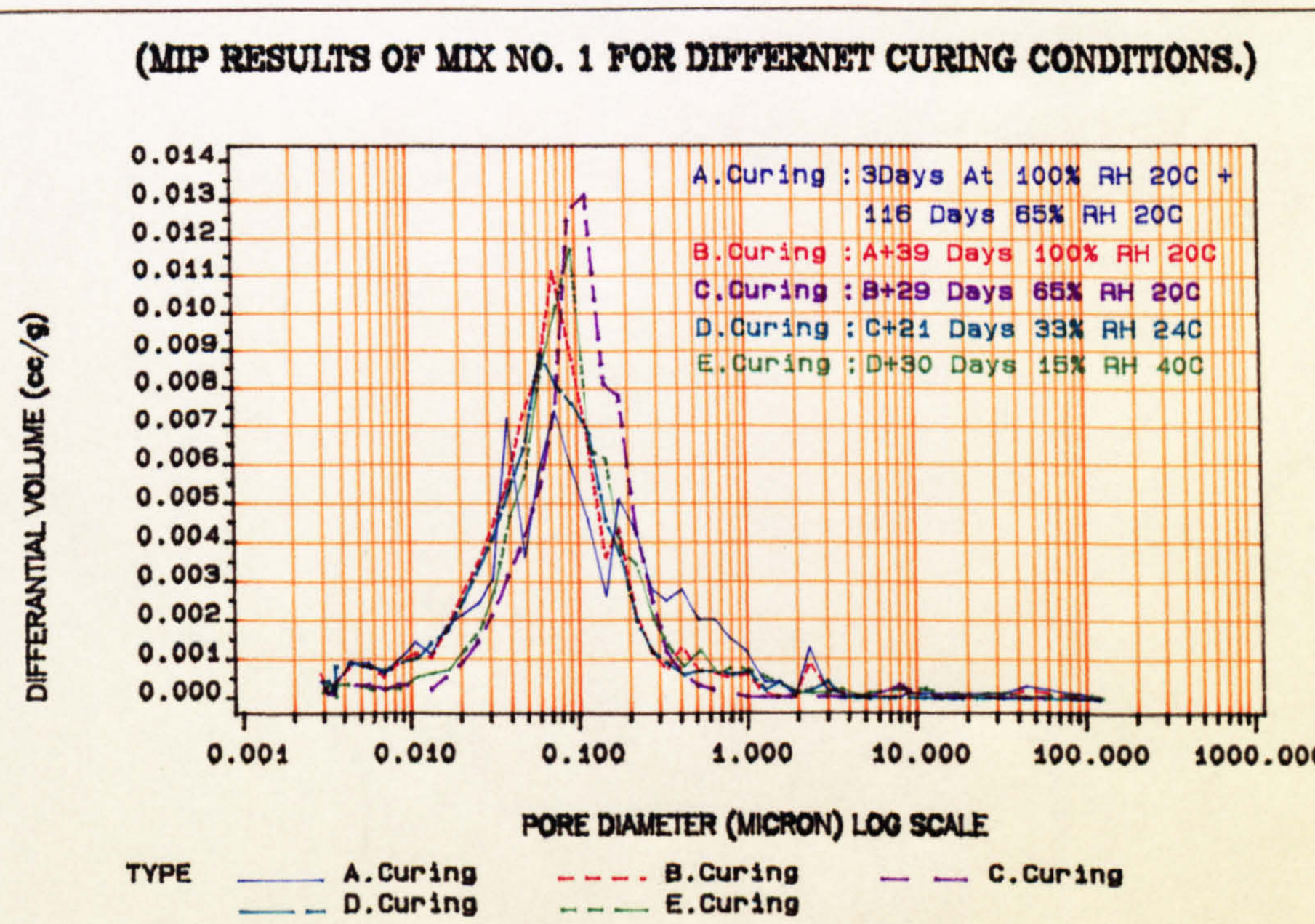

FIGURE (8.6) Incremental pore volume vs. pore diameter for mortar : mix A , W/C=0.53.

(MIP RESULTS OF MIX NO. 2 FOR DIFFERENT CURING CONDITIONS.)

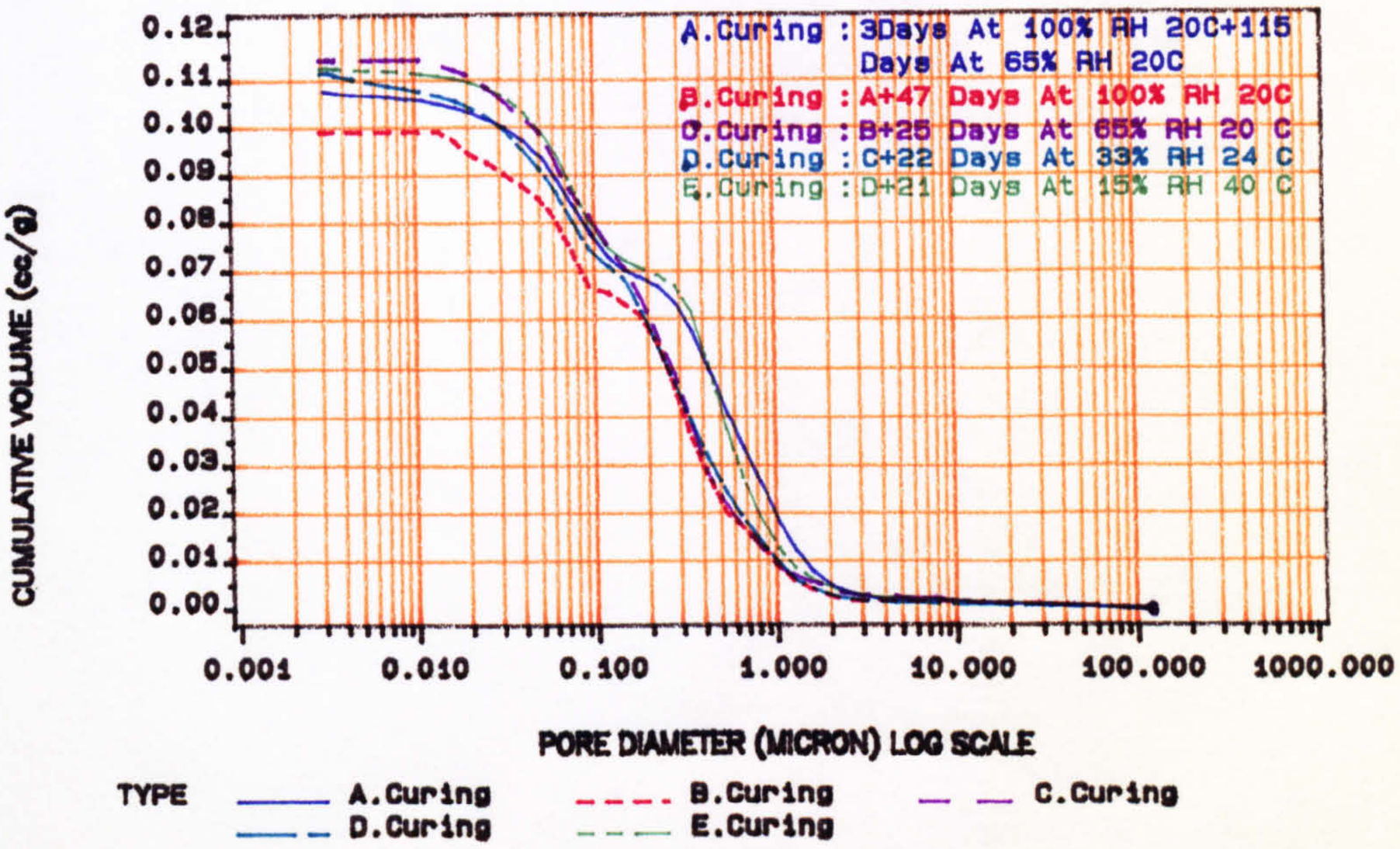

FIGURE (8.7) Cumulative volume vs. pore diameter for air entrained mortar : mix A , W/C=0.43.

(MIP RESULTS OF MIX NO. 2 FOR DIFFERNET CURING CONDITIONS.)

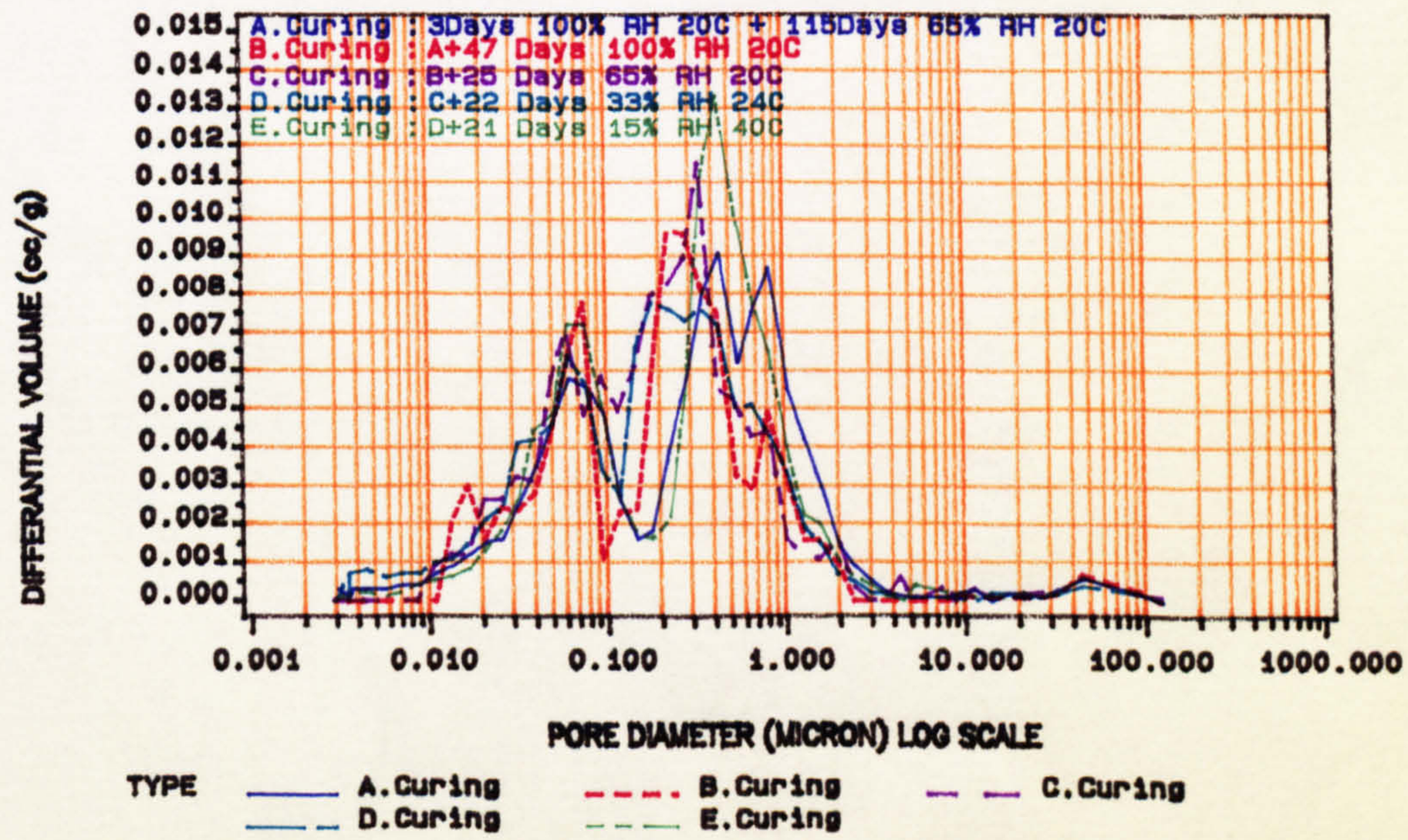

FIGURE (8.8) Incremental pore volume vs. pore diameter for air entrained mortar : mix A , W/C=0.43.

(MIP RESULTS OF MIX NO. 13 FOR DIFFERENT CURING CONDITIONS.)

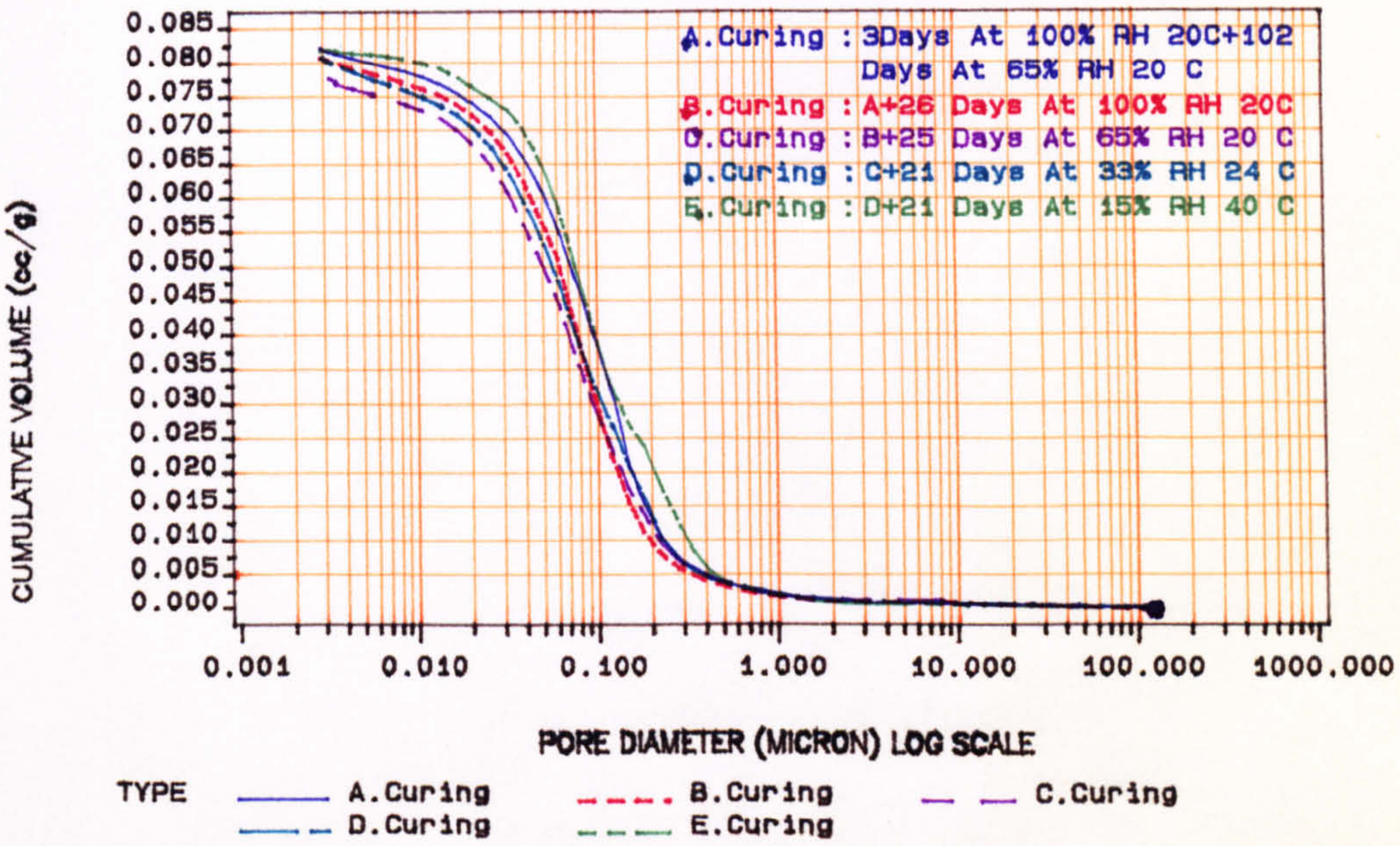

FIGURE (8.9) Cumulative volume vs. pore diameter for mortar : mix B , W/C=0.56.

(MIP RESULTS OF MIX NO. 13 FOR DIFFERNET CURING CONDITIONS.)

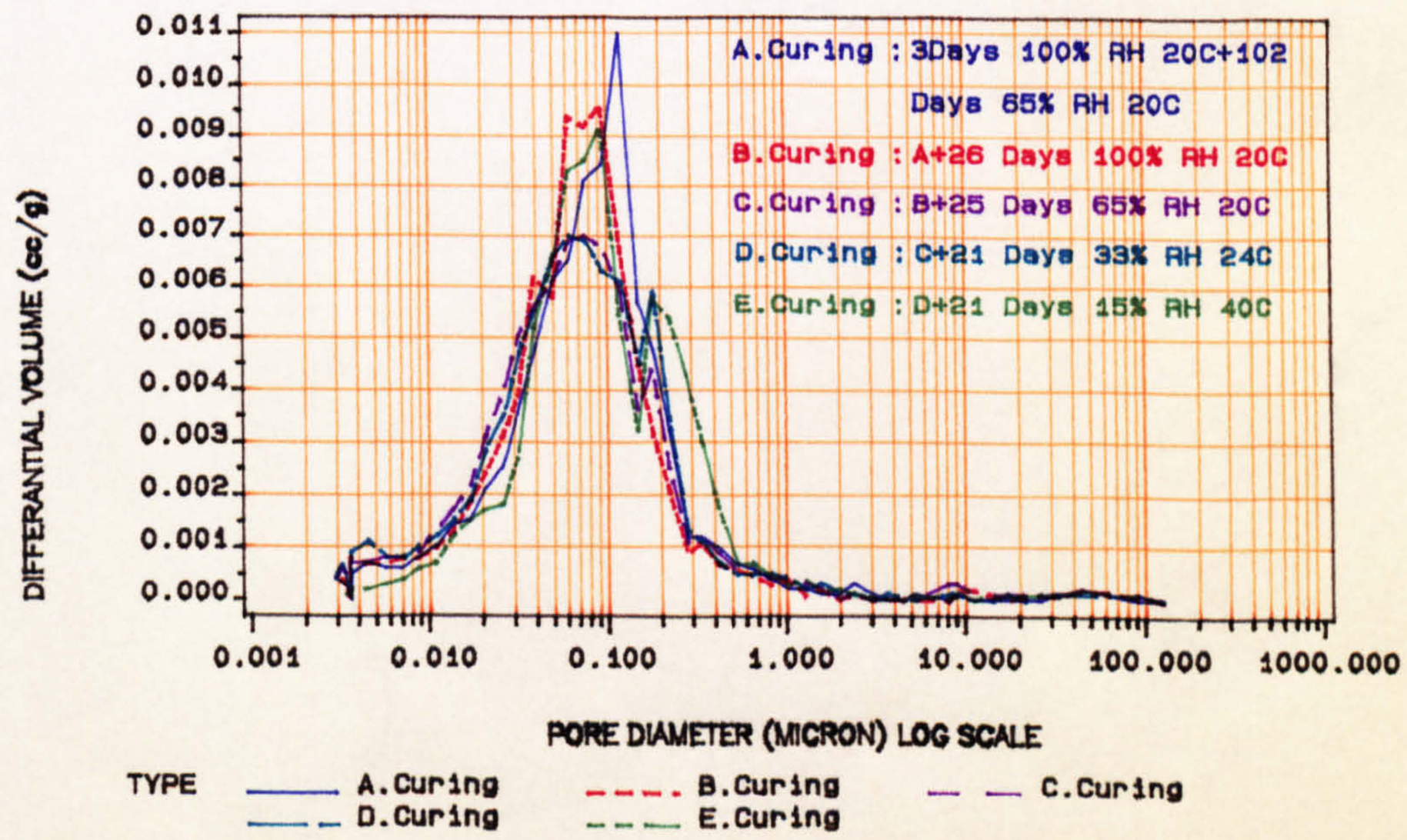

FIGURE (8.10) Incremental pore volume vs. pore diameter for mortar : mix B , W/C=0.56.

(MIP RESULTS OF MIX NO. 16 FOR DIFFERENT CURING CONDITIONS.)

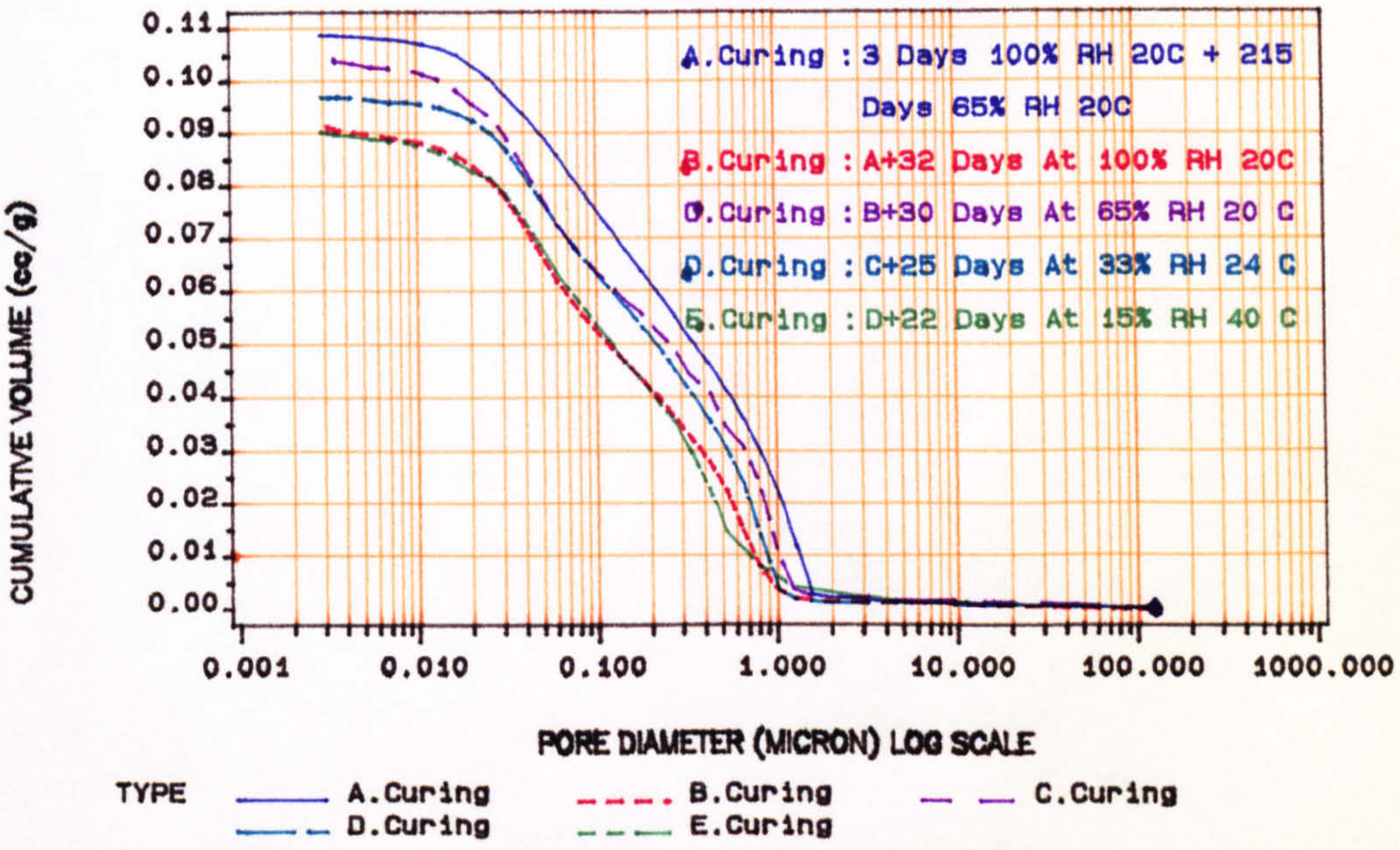

FIGURE (8.11) Cumulative volume vs. pore diameter for mortar : mix C , W/C=0.90.

(MIP RESULTS OF MIX NO. 16 FOR DIFFERNET CURING CONDITIONS.)

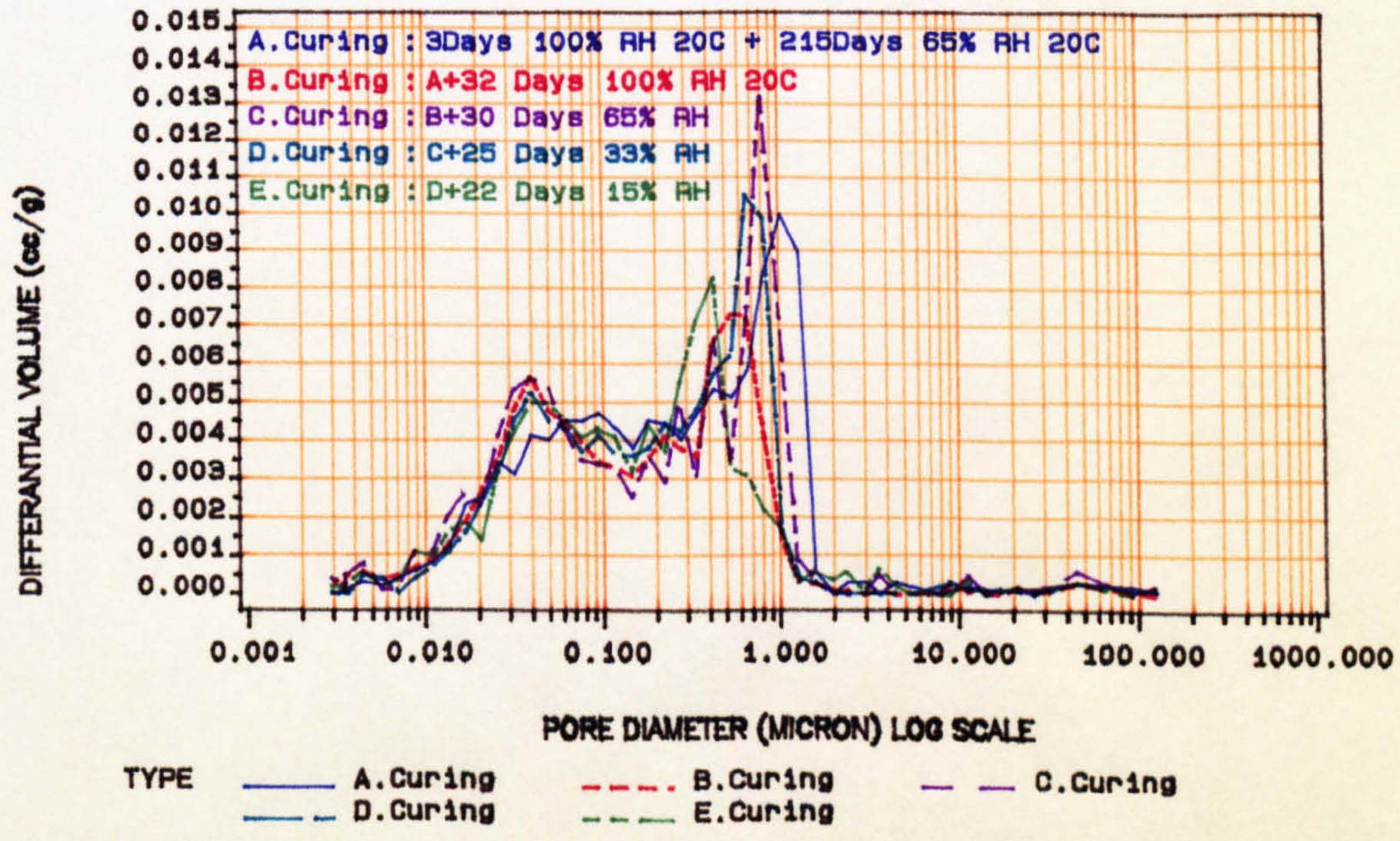

FIGURE (8.12) Incremental pore volume vs. pore diameter for mortar : mix C , W/C=0.90.

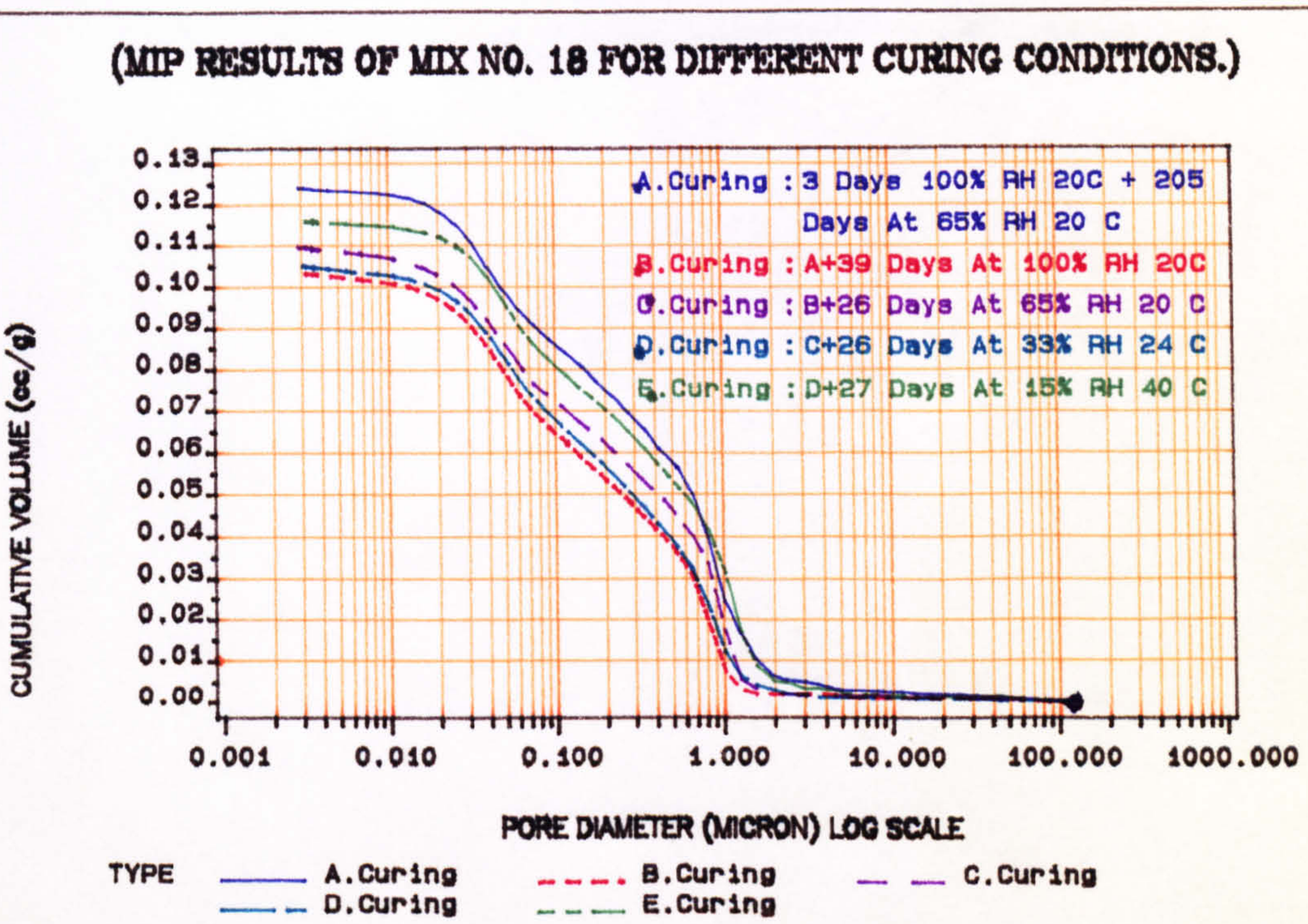

FIGURE (8.13) Cumulative volume vs. pore diameter for mortar : mix C , W/C=0.95.

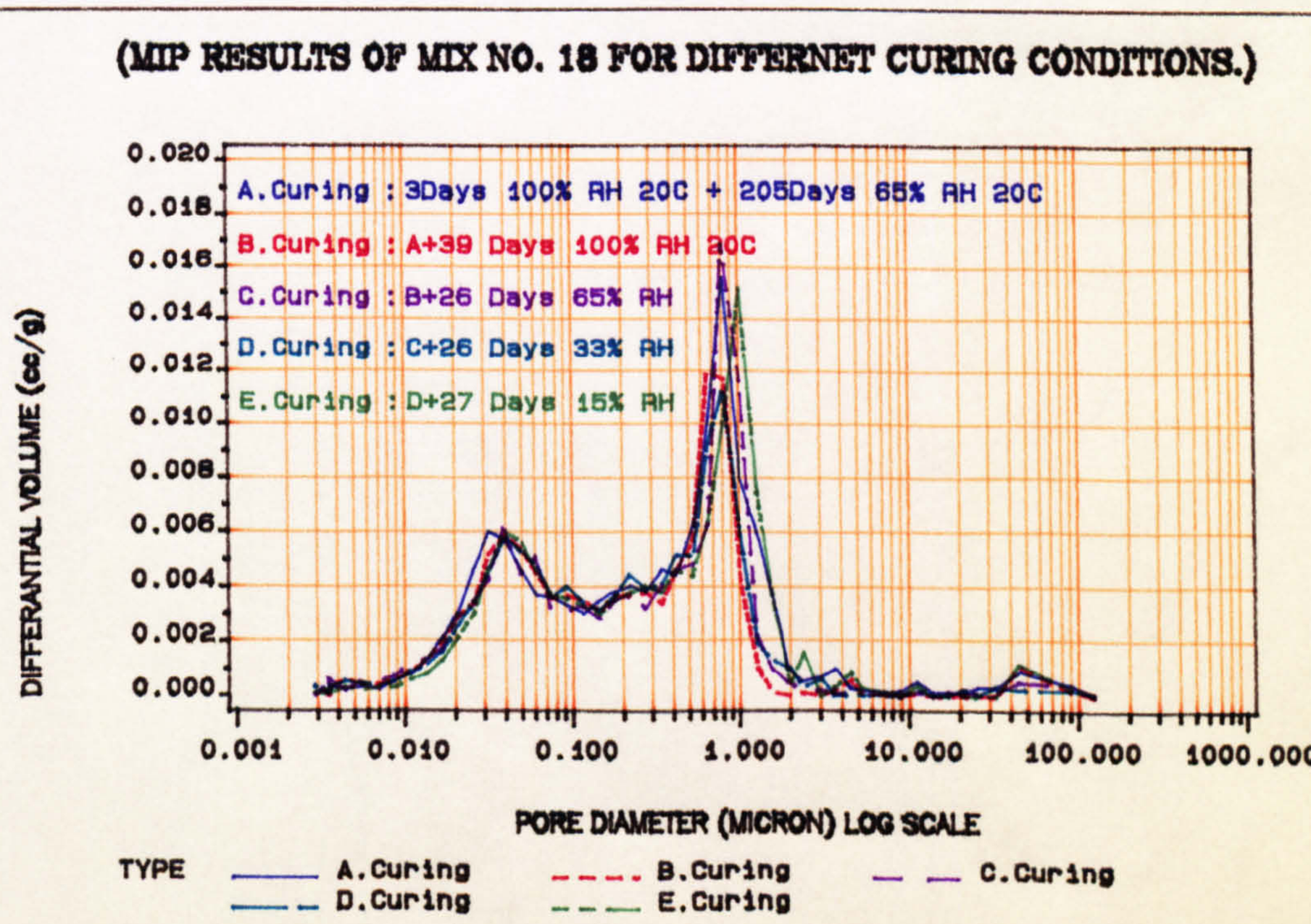

FIGURE (8.14) Incremental pore volume vs. pore diameter for mortar : mix C , W/C=0.95.

(MIP RESULTS OF MIX NO. 19 FOR DIFFERENT CURING CONDITIONS.)

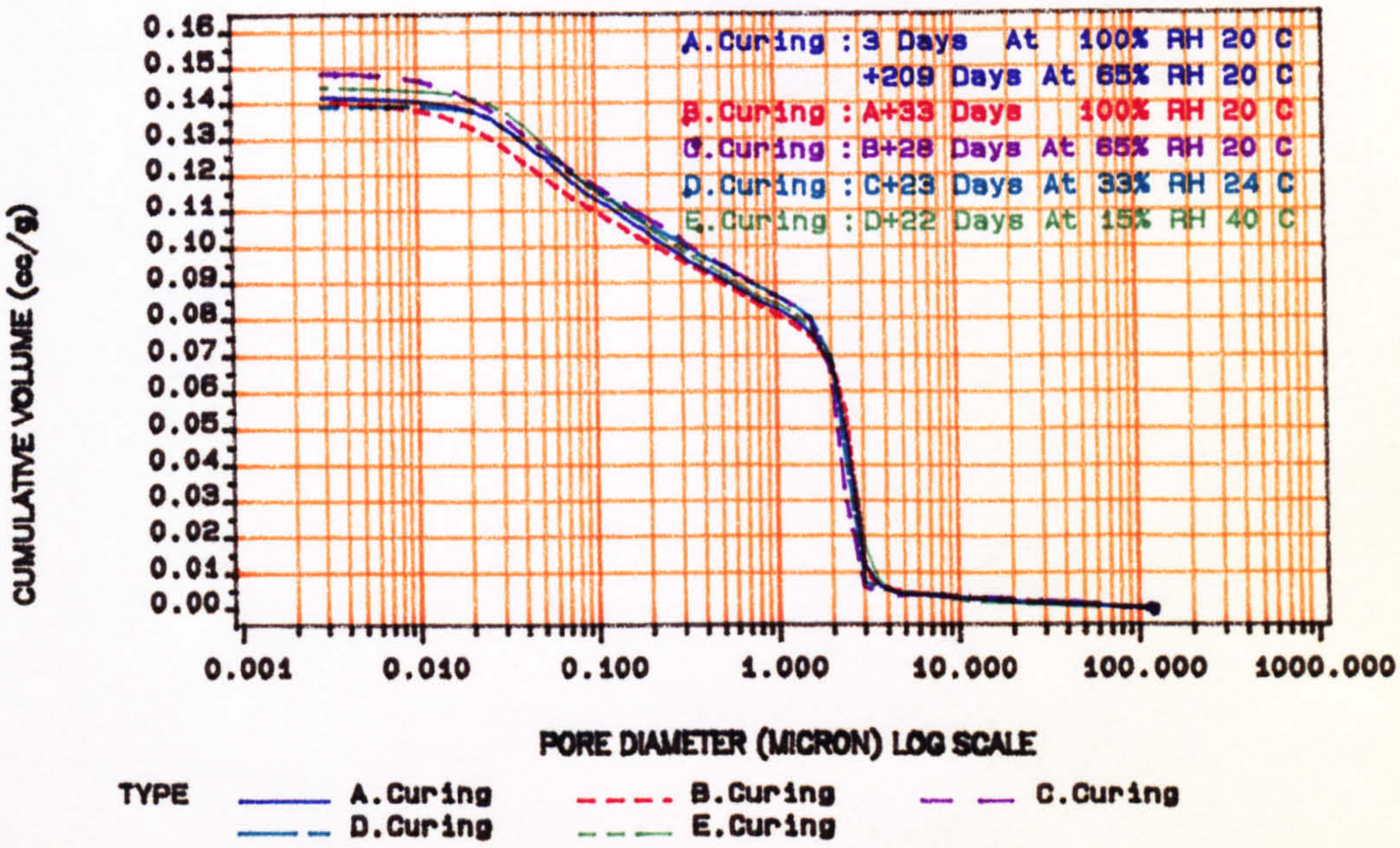

FIGURE (8.15) Cumulative volume vs. pore diameter for air entrained mortar : mix C , W/C=0.90.

(MIP RESULTS OF MIX NO. 19 FOR DIFFERNET CURING CONDITIONS.)

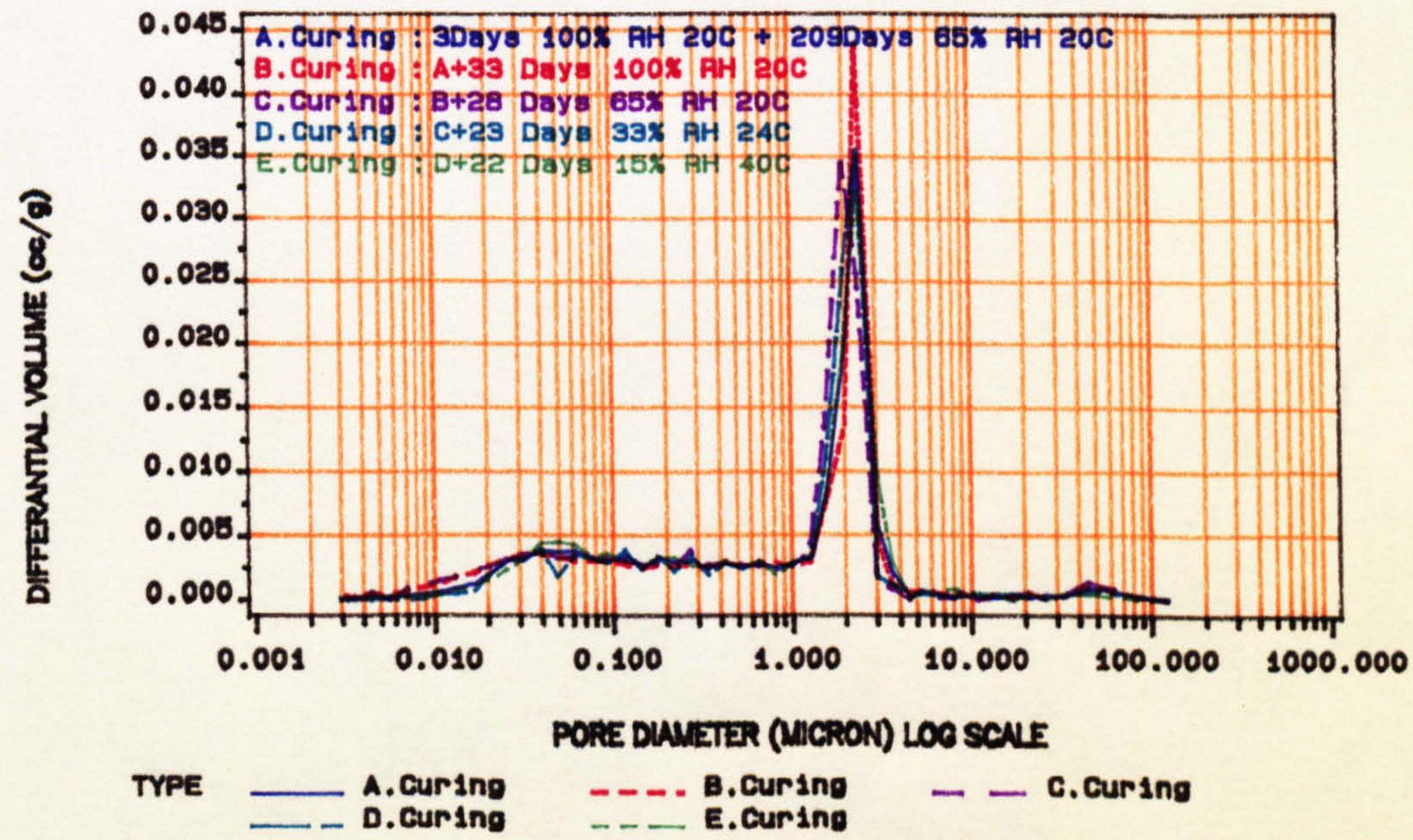

FIGURE (8.16) Incremental pore volume vs. pore diameter for air entrained mortar : mix C , W/C=0.90.

(MIP RESULTS OF MIX NO. 20 FOR DIFFERENT CURING CONDITIONS.)

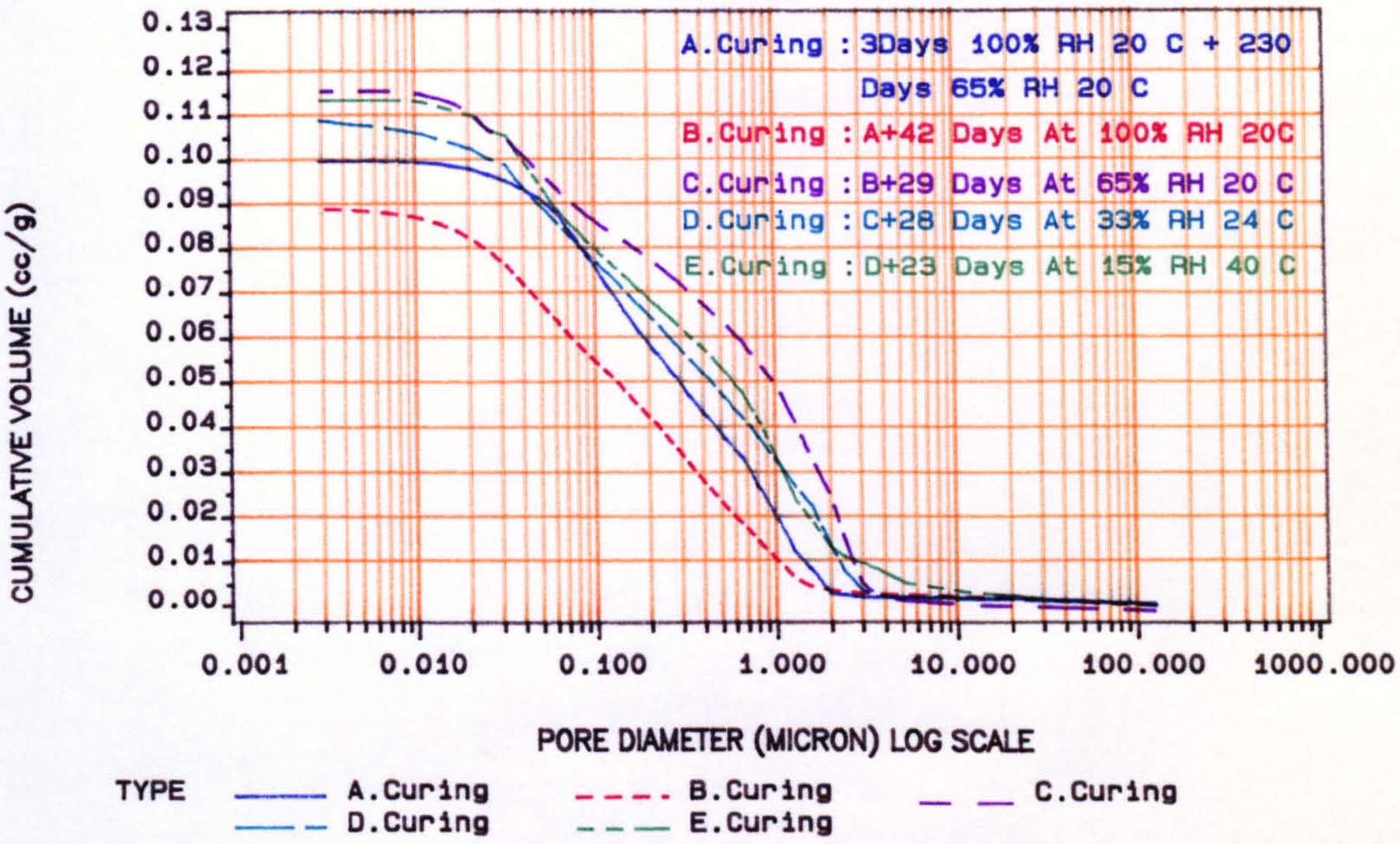

FIGURE (8.17) Cumulative volume vs. pore diameter for sieved mortar : mix C , W/C=1.29.

(MIP RESULTS OF MIX NO. 20 FOR DIFFERNET CURING CONDITIONS.)

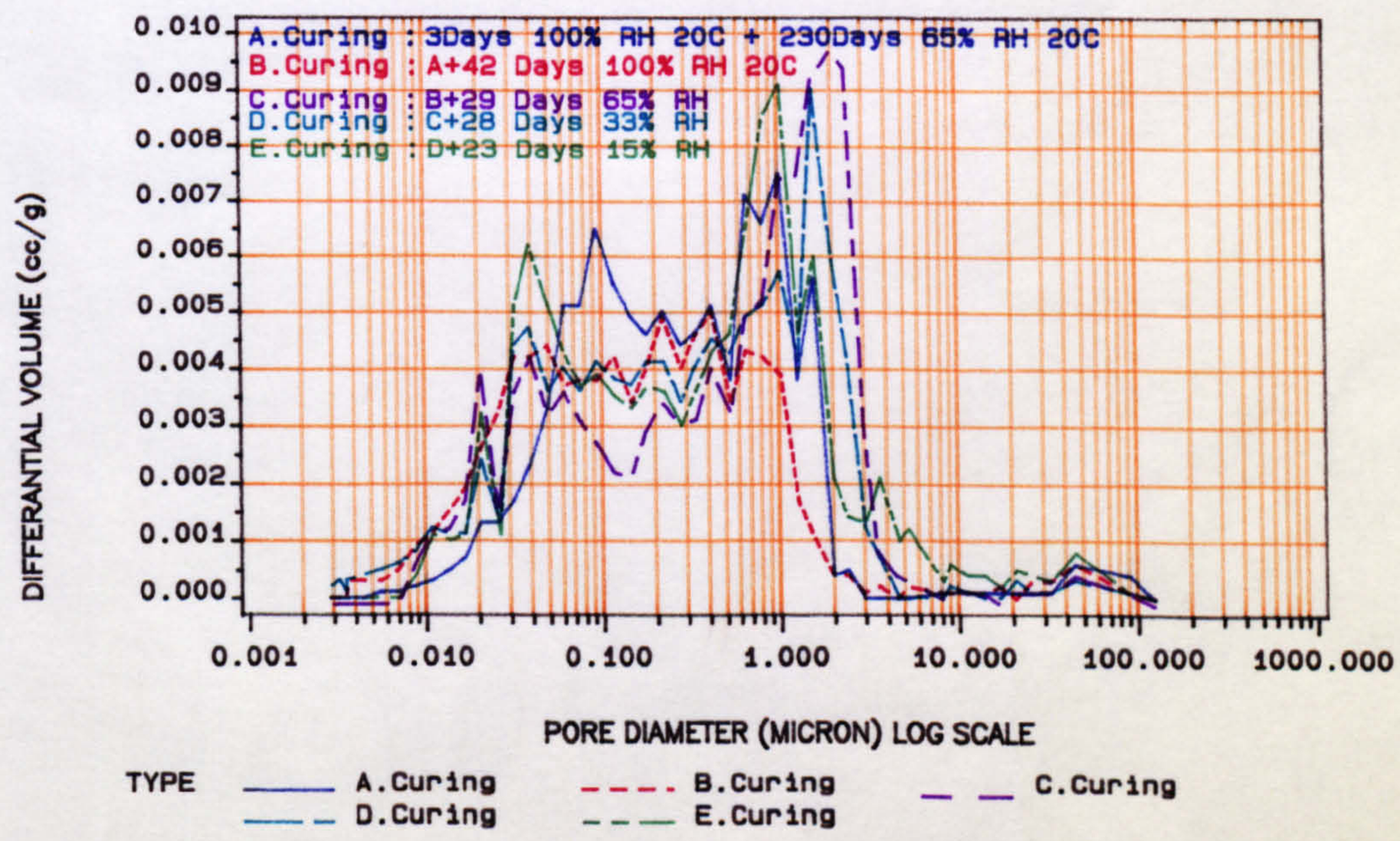

FIGURE (8.18) Incremental pore volume vs. pore diameter for seived mortar : mix C , W/C=1.29.

(MIP RESULTS OF MIX NO. 21 FOR DIFFERENT CURING CONDITIONS.)

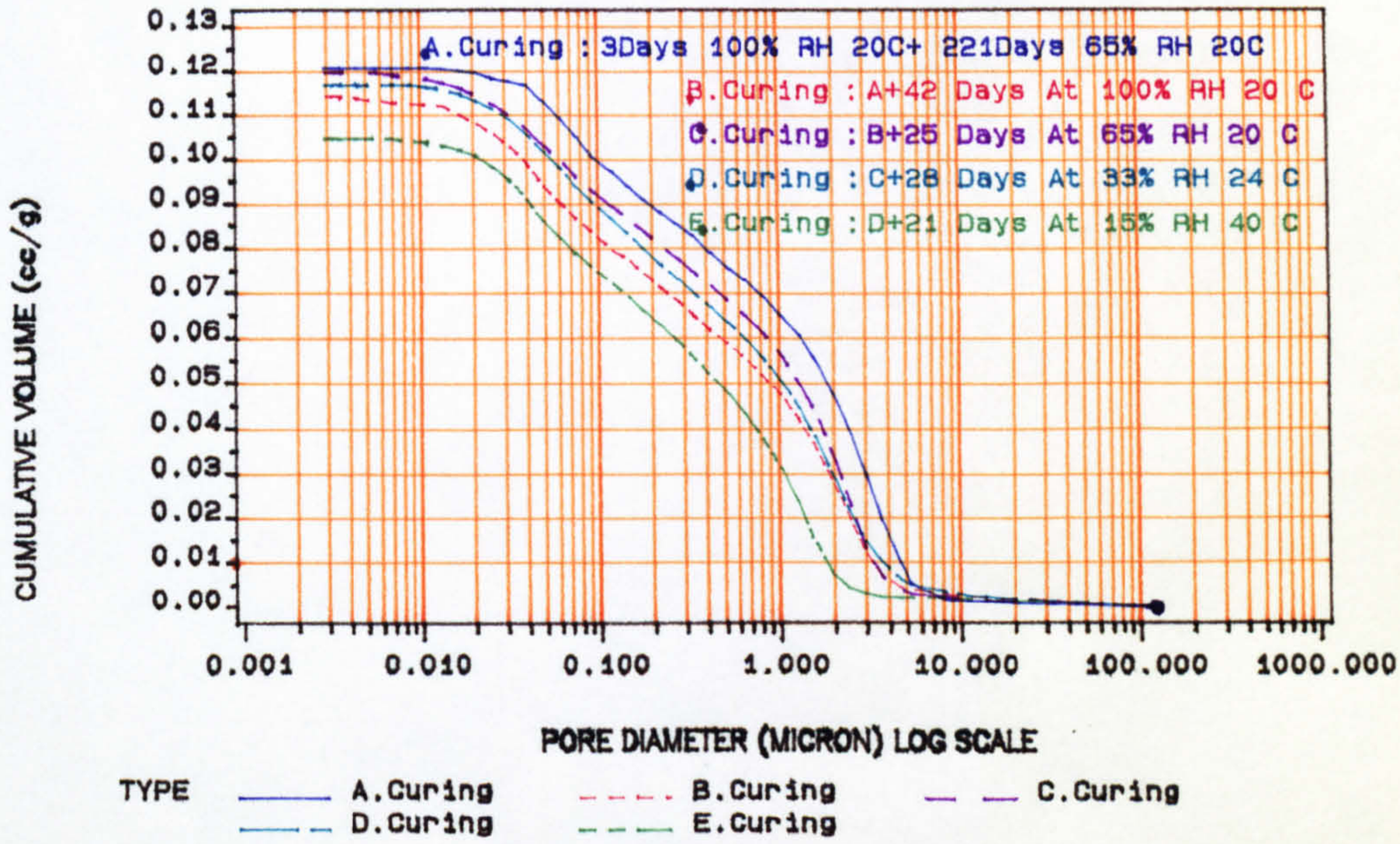

FIGURE (8.19) Cumulative volume vs. pore diameter for air entrained sieved mortar : mix C , W/C=1.29.

(MIP RESULTS OF MIX NO. 21 FOR DIFFERNET CURING CONDITIONS.)

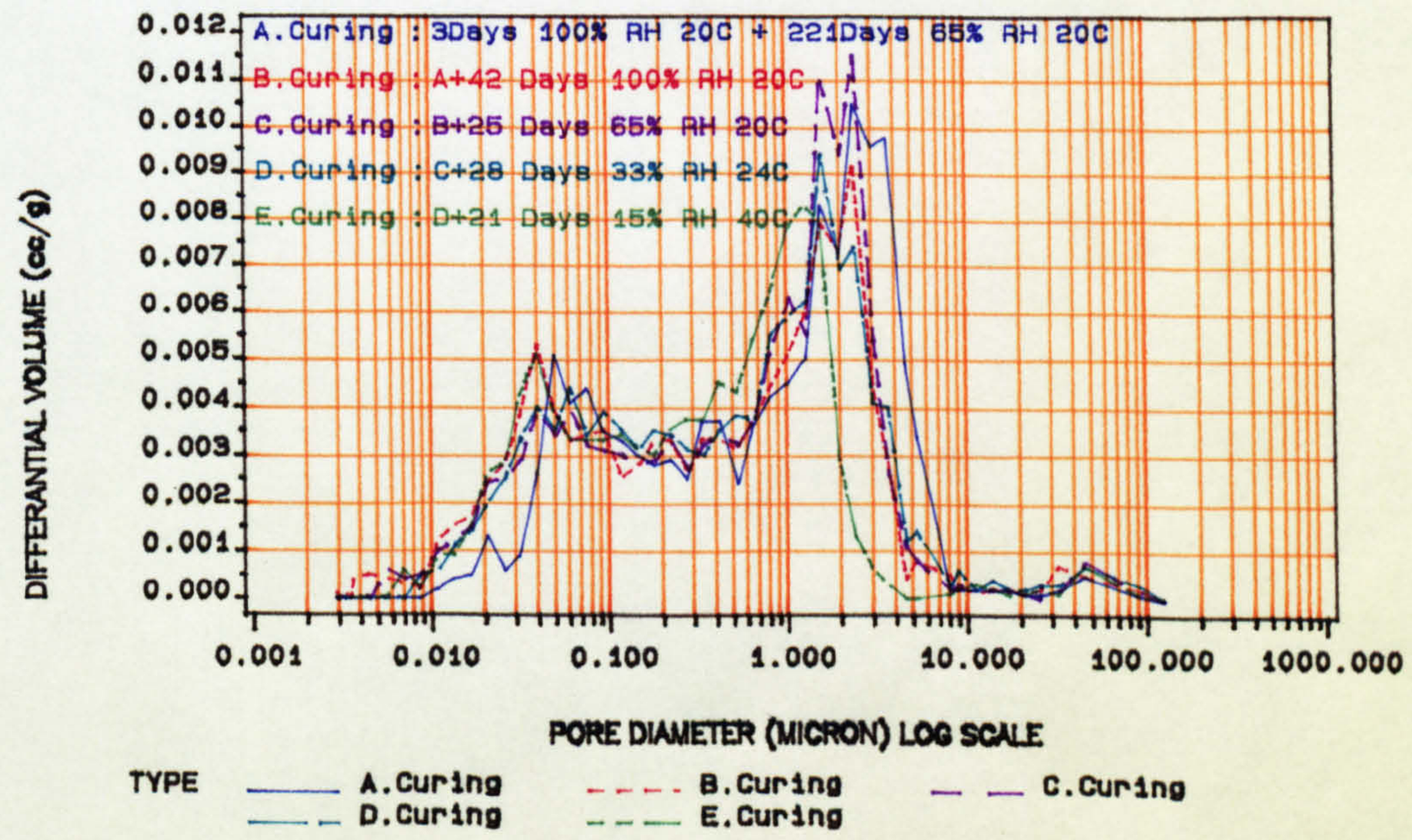

FIGURE (8.20) Incremental pore volume vs. pore diameter for air entrained sieved mortar : mix C , W/C=1.29.

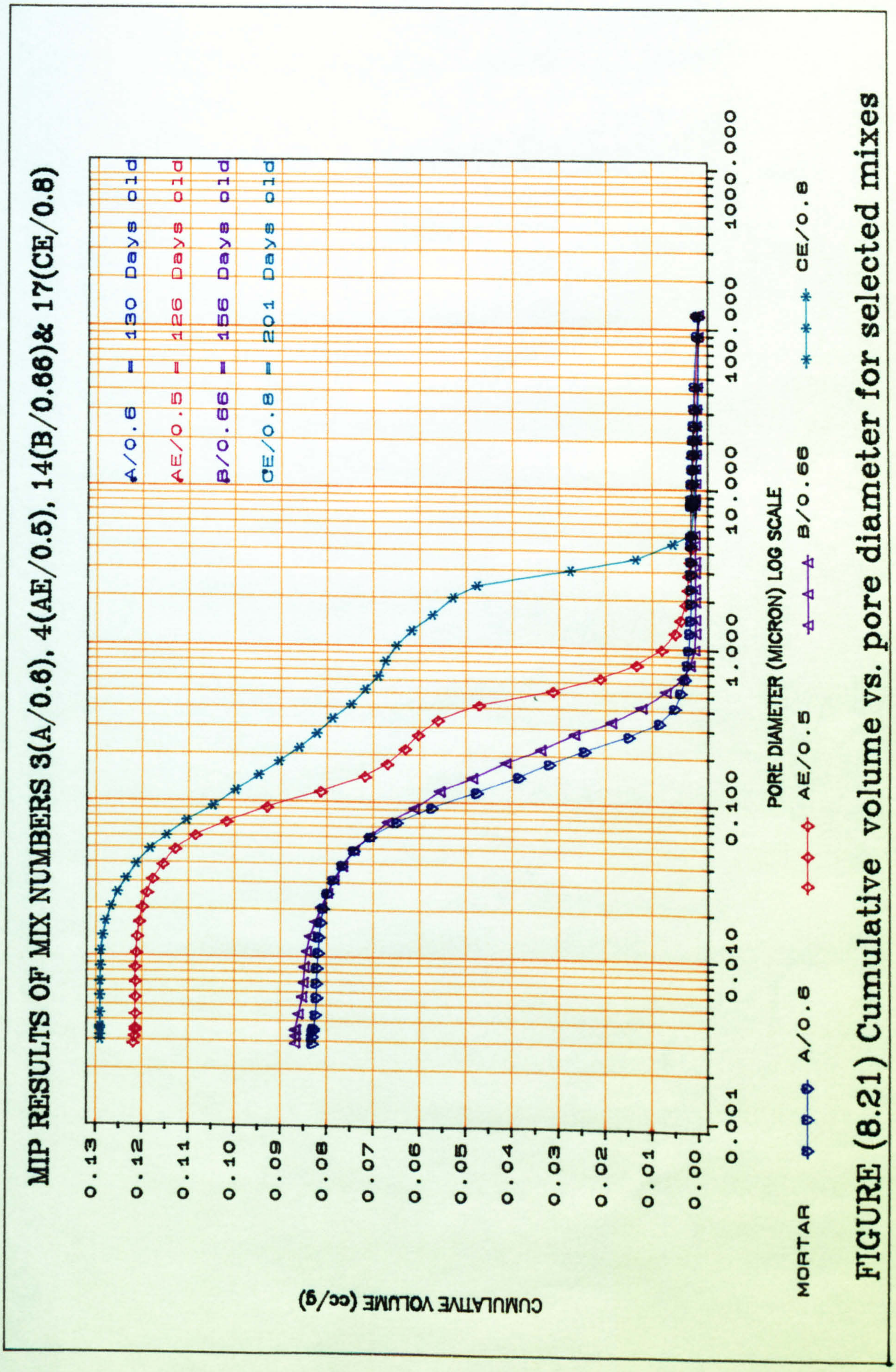

FIGURE (8.21) Cumulative volume vs. pore diameter for selected mixes

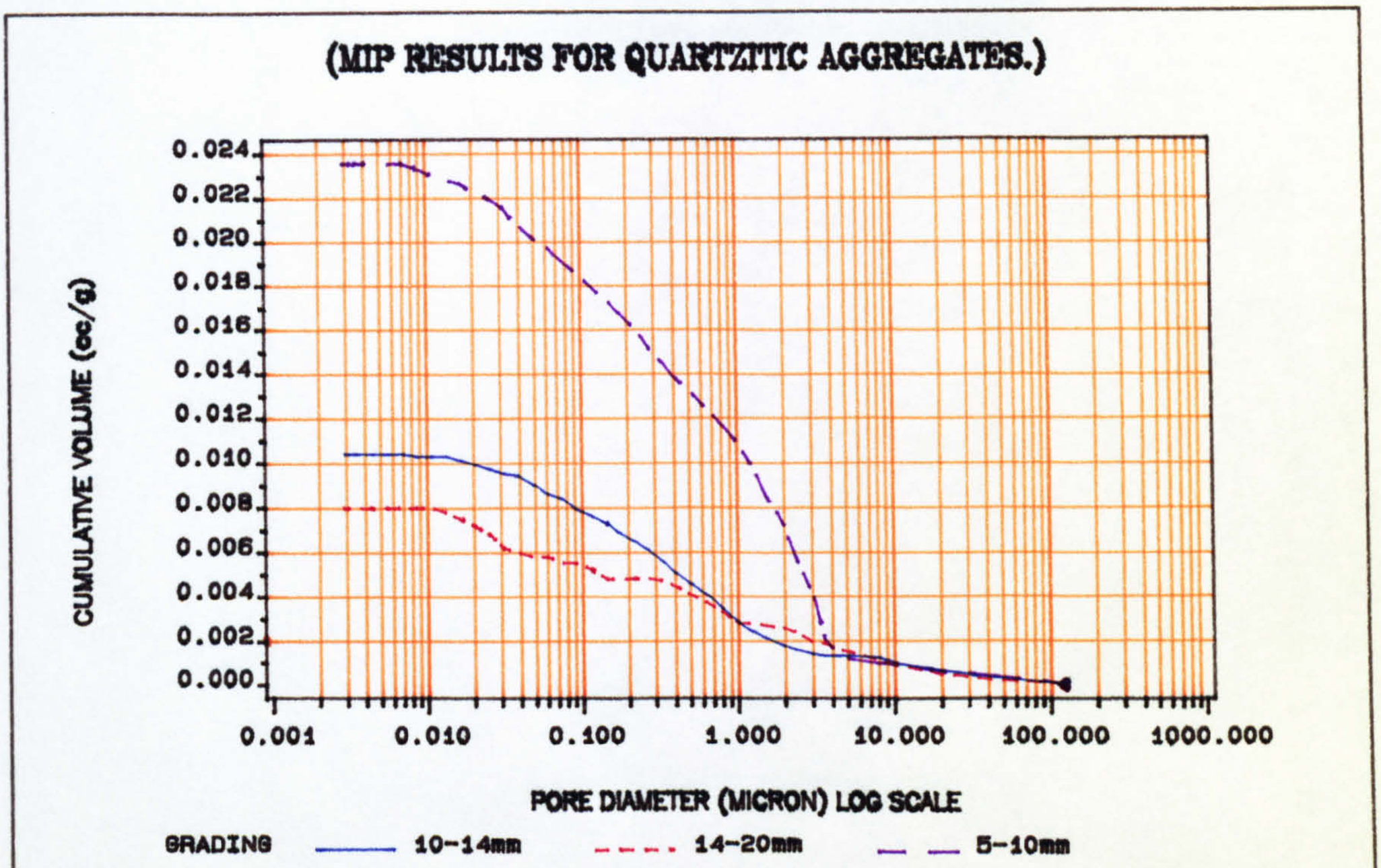

FIGURE (8.22) Cumulative volume vs. pore diameter for quartzitic aggregates of different sizes.

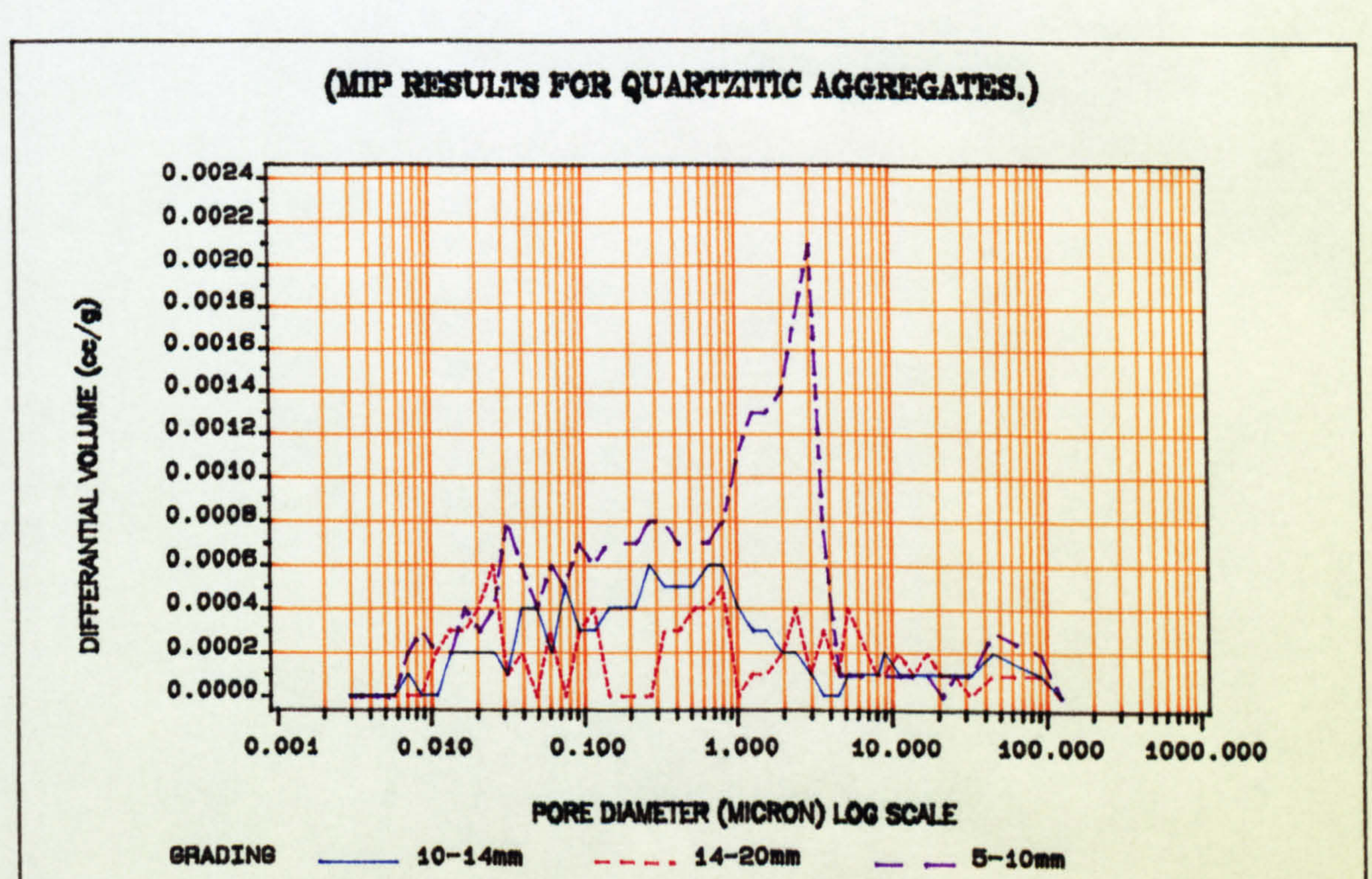

FIGURE (8.23) Incremental pore volume vs. pore diameter for quartzitic aggregates of differnt sizes.

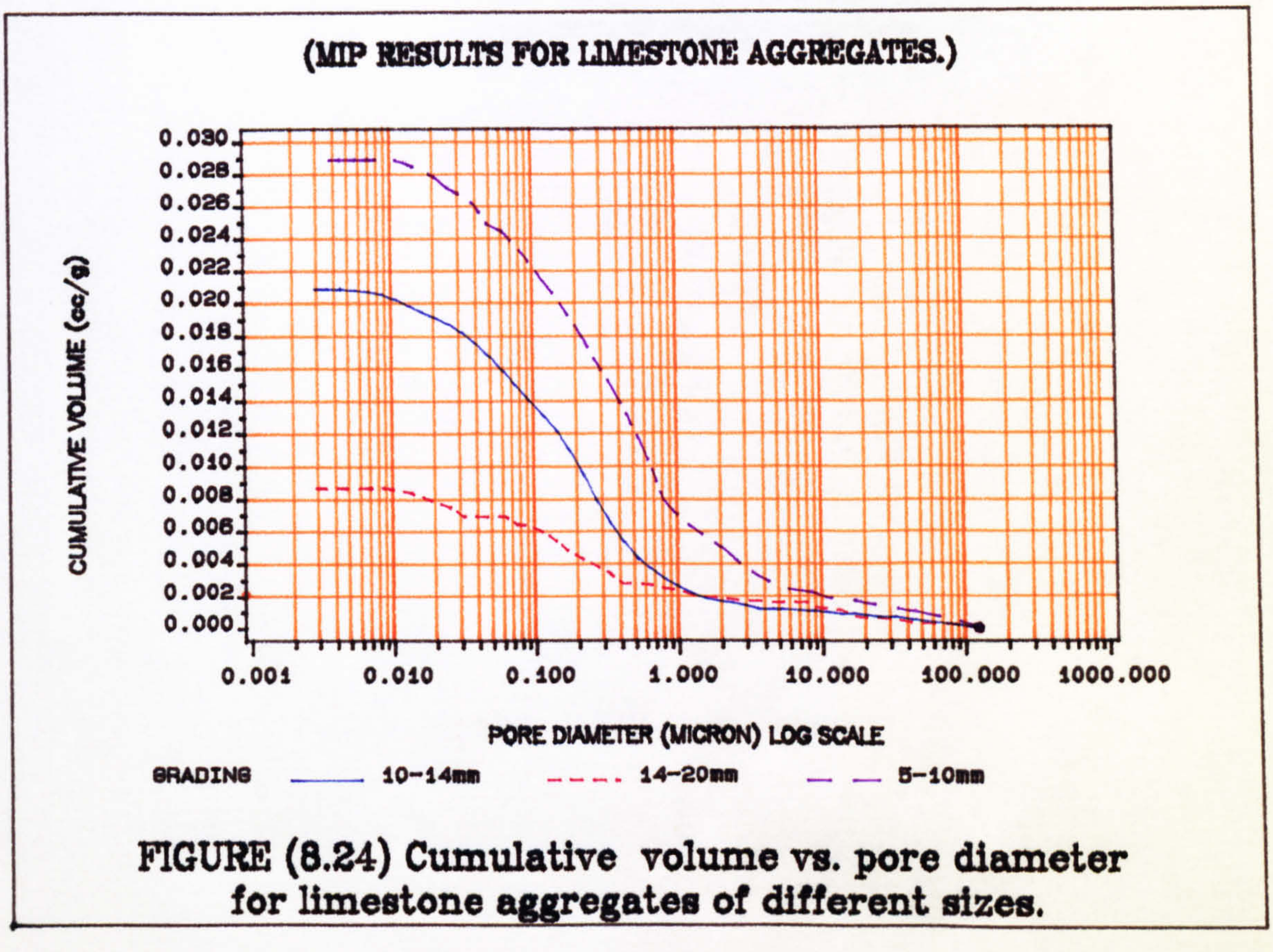

FIGURE (8.24) Cumulative volume vs. pore diameter for limestone aggregates of different sizes.

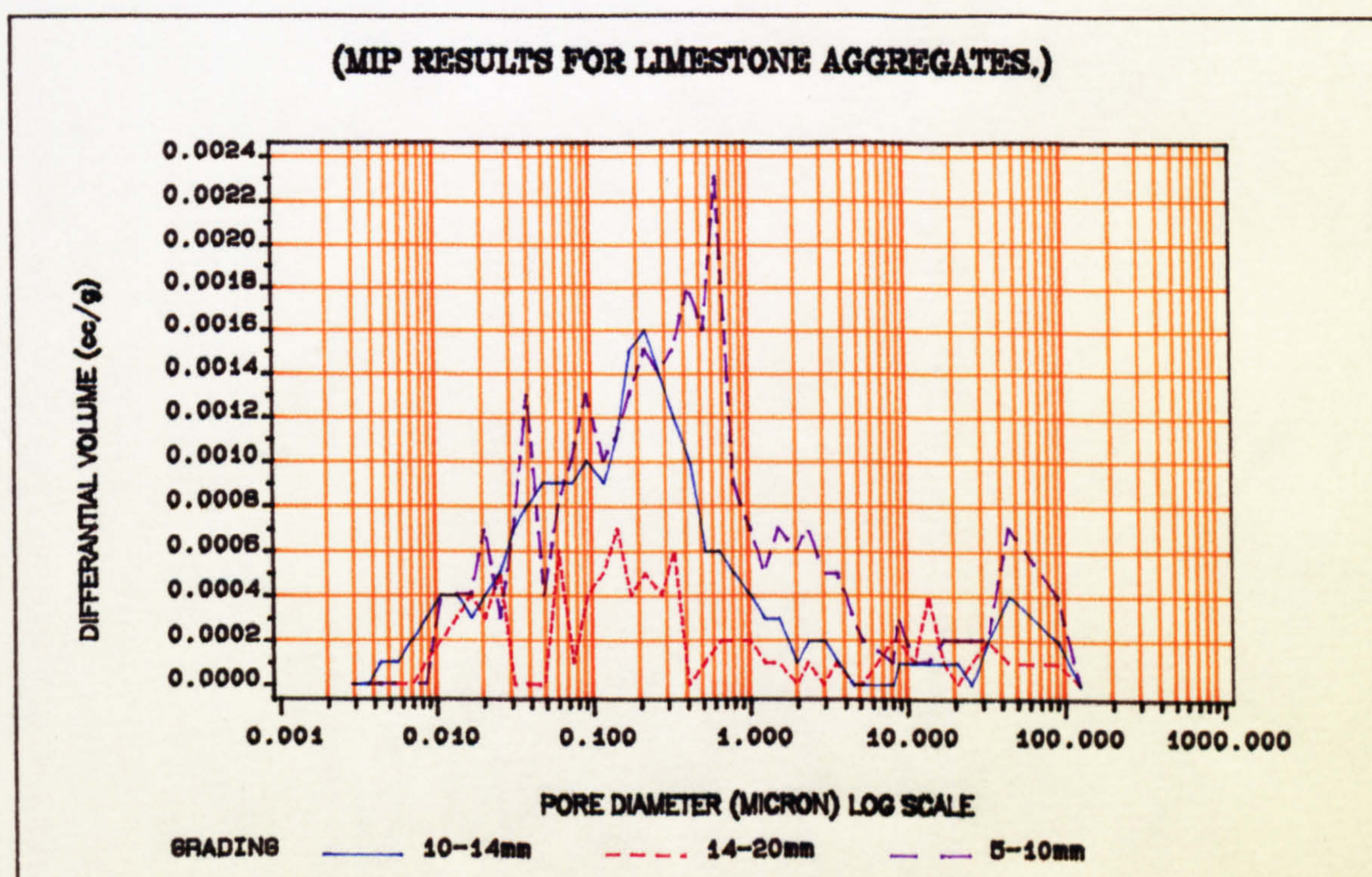

FIGURE (8.25) Incremental pore volume vs. pore diameter for limestone aggregates of differnt sizes.

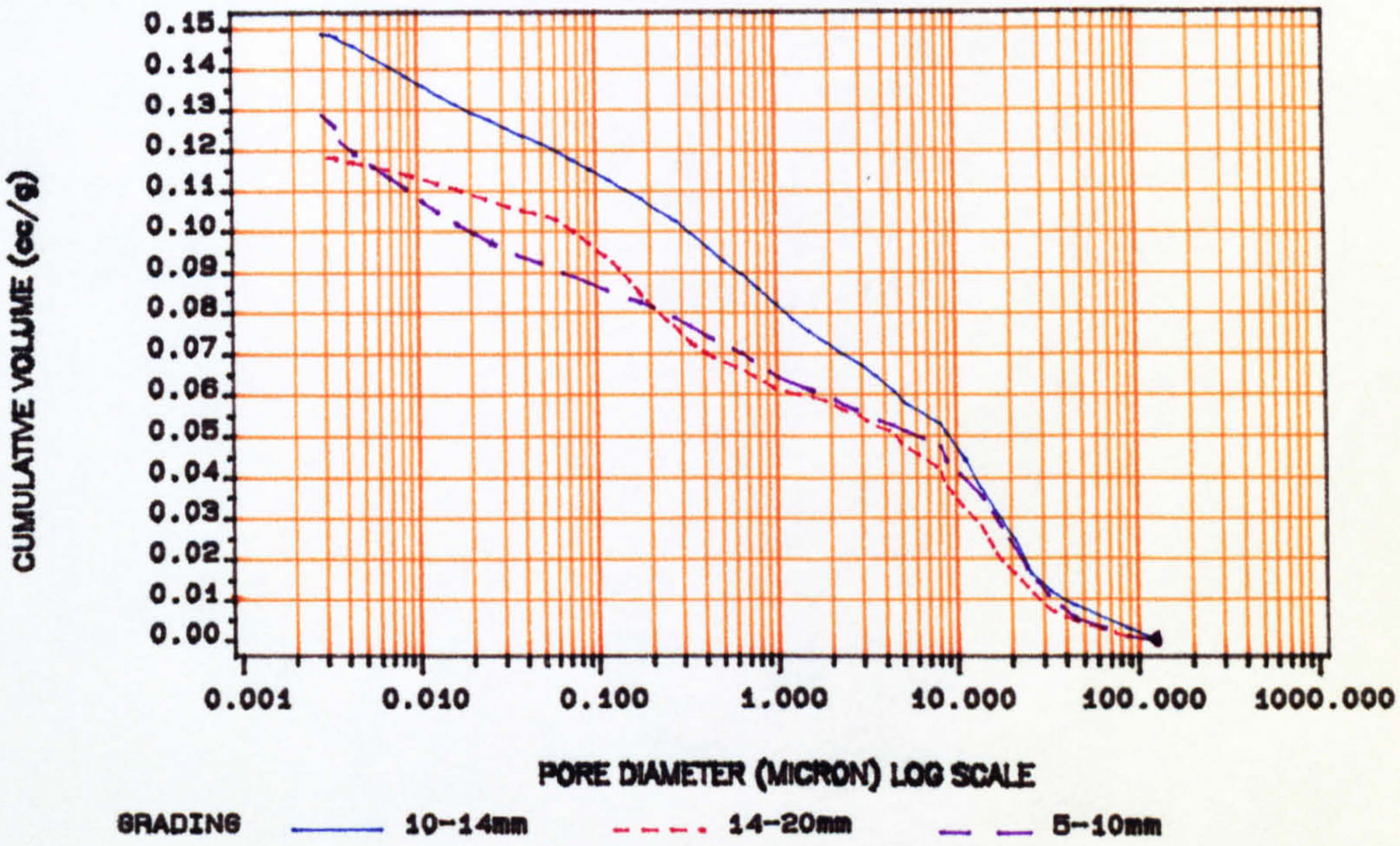

FIGURE (8.26) Cumulative volume vs. pore diameter for Pellite aggregates of different sizes.

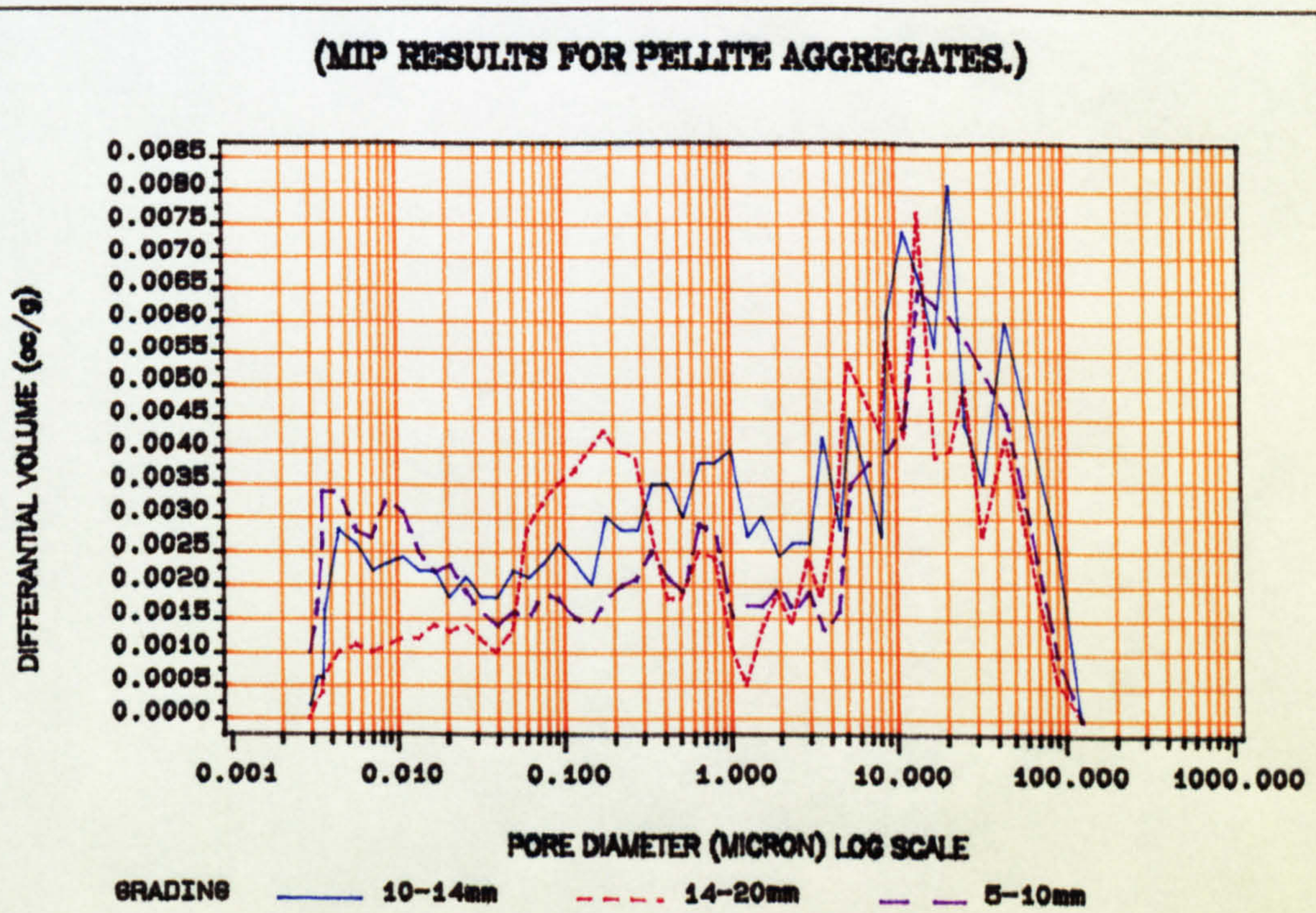

FIGURE (8.27) Incremental pore volume vs. pore diameter for Pellite aggregates of differnt sizes.

8.4 Vacuum saturation results

The results obtained for the total porosity of concretes by vacuum saturation are presented in Table 8.3. Two samples were tested for each mix and the total porosities were calculated using equation 6.1.

Table (8.3)

Results of vacuum saturation tests

Mix No.*	Mix Code Name	W_{dry} (g)	W_{sat} (g)	W_{water} (g)	Total Porosity (%)	Mean Total Porosity (%)	Age (days)
1A	QA /0.53	851.8	901.9	519.0	13.08	12.9	121
1A		858.2	907.0	525.3	12.78		
1B		874.0	918.2	534.5	11.52	11.7	160
1B		871.8	917.1	533.3	11.80		
1C		866.3	911.5	529.2	11.82	11.7	192
1C		876.1	920.6	537.3	11.61		
1D		864.1	910.9	527.3	12.20	12.2	213
1D		868.4	915.1	532.3	12.20		
1E		872.1	918.1	534.4	11.99	12.0	244
1E		867.6	913.6	530.3	12.00		
2A	QAE/0.43	804.8	858.0	474.9	13.89	14.0	120
2A		813.9	867.9	485.0	14.10		
2B		797.8	851.3	469.6	14.02	14.5	167
2B		803.9	861.2	477.3	14.93		
2C		803.1	855.7	472.6	13.73	13.5	196
2C		800.6	851.3	468.3	13.23		
2D		798.2	848.1	473.5	13.32	13.5	218
2D		781.1	833.5	452.7	13.76		
2E		824.8	875.3	490.2	13.11	13.1	240
2E		821.1	871.3	489.0	13.13		
3	LA /0.60	869.0	925.3	539.9	14.61	15.0	130
		856.3	915.2	530.9	15.33		
4	LAE/0.50	775.2	855.3	472.3	20.91	21.0	126
		770.9	851.8	469.5	21.16		
5	PA /0.90	732.1	814.5	430.1	21.44	21.0	140
		738.4	817.6	433.7	20.63		
6	PAE/0.80	565.4	711.7	337.1	39.06	38.5	140
		582.8	725.2	349.5	37.90		

(*) letters after mix numbers indicate the curing conditions.

Table (8.3) (continued)

Mix No.*	Mix Code Name	W_{dry} (g)	W_{sat} (g)	W_{water} (g)	Total Porosity (%)	Mean Total Porosity (%)	Age (days)
7	QA /0.80	885.9 893.0	939.4 945.6	559.6 561.3	14.09 13.69	13.9	337
8	LA /0.80	864.4 858.9	923.1 917.6	540.3 534.4	15.33 15.32	15.3	337
9	PA /0.80	733.9 729.7	811.0 806.5	427.8 423.3	20.12 20.04	20.1	337
10	QB /0.80	880.4 883.9	929.7 931.5	545.8 548.6	12.84 12.43	12.6	143
11	LB /0.80	880.2 875.6	933.3 930.4	550.3 547.4	13.86 14.31	14.1	147
12	PB /0.80	639.1 627.6	720.6 707.2	372.5 366.0	23.42 23.33	23.4	134
13A	QB /0.56	907.2	945.5	561.6	9.98	10.2	108
13A		898.9	939.0	555.8	10.46		
13B		911.2	948.3	563.5	9.64	9.4	134
13B		908.3	943.8	559.0	9.23		
13C		904.9	940.3	558.5	9.27	9.4	163
13C		897.9	934.3	549.1	9.44		
13D		904.4	944.2	558.4	10.32	10.1	184
13D		903.6	941.7	558.6	9.95		
13E		912.0	947.9	563.9	9.35	9.6	206
13E		893.7	930.9	553.4	9.85		
14	LB /0.66	883.8 889.4	928.7 936.6	549.6 553.4	11.84 12.32	12.1	156
15	PB /1.05	681.0 618.9	774.7 703.4	401.4 366.1	25.10 25.05	25.1	161
16A	QC /0.90	855.4	914.6	529.8	15.38	15.1	219
16A		860.7	918.0	533.8	14.91		
16B		842.3	901.4	521.6	15.56	15.7	251
16B		834.1	894.7	513.2	15.88		
16C		845.9	903.3	521.5	15.03	14.8	284
16C		851.2	906.5	524.7	14.48		
16D		860.0	912.4	530.5	13.72	14.1	309
16D		854.9	910.4	528.0	14.51		
16E		854.4	911.0	523.7	14.61	14.6	332
16E		850.9	907.5	519.7	14.60		

(*) letters after mix numbers indicate the curing conditions.

Table (8.3) (continued)

Mix No.*	Mix Code Name	W_{dry} (g)	W_{sat} (g)	W_{water} (g)	Total Porosity (%)	Mean Total Porosity (%)	Age (days)
17	QCE/0.80	766.2 775.2	857.6 862.8	476.4 481.4	23.98 22.97	23.5	201
18A		838.3	906.3	521.4	17.67	17.6	211
18A		854.0	912.4	528.7	17.57		
18B		835.8	901.3	517.1	17.05	16.9	250
18B		831.2	895.8	511.6	16.81		
18C	LC /0.95	847.6	905.9	522.6	15.21	15.6	280
18C		839.3	900.5	517.6	15.98		
18D		852.8	911.7	525.5	15.25	15.3	306
18D		845.9	904.9	518.7	15.28		
18E		845.0	903.2	521.0	15.23	15.2	334
18E		839.9	900.8	500.6	15.22		
19A		749.6	847.0	470.0	25.84	25.5	214
19A		757.8	852.3	475.2	25.06		
19B		764.8	860.5	478.5	25.25	25.3	247
19B		757.6	854.1	472.2	25.27		
19C	LCE/0.90	737.8	838.6	459.4	26.58	25.9	280
19C		758.1	854.3	472.8	25.22		
19D		751.4	844.8	465.9	24.65	24.3	303
19D		762.4	853.5	474.4	24.03		
19E		768.9	861.4	479.5	24.22	23.7	327
19E		777.3	866.4	482.8	23.23		
20A		691.7	788.1	411.1	25.57	25.5	241
20A		683.4	779.2	402.9	25.46		
20B		678.7	773.6	399.8	25.39	25.3	283
20B		673.9	768.5	394.4	25.29		
20C	PC /1.29	693.3	785.7	408.7	24.51	24.6	316
20C		687.7	781.1	403.1	24.71		
20D		678.1	772.4	398.1	25.19	25.0	344
20D		674.5	767.4	393.1	24.82		
20E		713.7	801.0	425.2	23.23	23.0	368
20E		708.5	794.8	416.6	22.82		

(*) letters after mix numbers indicate the curing conditions.

Table 8.3 (continued)

Mix No.*	Mix Code Name	W_{dry} (g)	W_{sat} (g)	W_{water} (g)	Total Porosity (%)	Mean Total Porosity (%)	Age (days)
21A	PCE/1.29	569.0	715.0	341.0	39.04	39.0	223
21A		566.4	715.3	334.0	39.05		
21B		574.4	710.9	339.1	36.71	36.7	265
21B		570.0	706.3	334.8	36.69		
21C		575.7	708.2	335.6	35.56	35.8	294
21C		571.2	705.7	333.1	36.10		
21D		566.1	702.5	332.9	36.90	36.8	322
21D		568.3	703.9	334.6	36.72		
21E		599.1	728.7	352.5	34.45	34.7	345
21E		713.6	871.6	419.6	34.96		
22	QC /0.80	704.8	746.4	428.6	13.09	12.9	298
		699.2	738.9	427.1	12.73		
23	LC /0.80	733.4	773.6	451.8	12.49	13.1	298
		709.0	752.5	435.4	13.72		
24	PC /0.80	659.5	754.7	386.5	25.86	26.1	298
		682.5	781.8	403.4	26.24		

(*) letters after mix numbers indicate the curing conditions.

8.5 Thermogravimetry results

The results for the degree of hydration and carbonation are presented in Table 8.4. Some selected TG and DTG curves of the mortars are presented in Appendix IV.

Table (8.4)

The degree of hydration and carbonation results for mortar mixes

Mix no.*	Mortar code name #	Calcium hydroxide content (degree of hydration) in (%)	Non-evaporable water content (degree of hydration) in (%)	Carbo-nation (%)	Age (days)
1A		41.1 (83.4)	4.3 (66.1)	8.0	121
1B		38.9 (78.9)	4.2 (65.3)	8.2	160
1C	A /0.53	40.9 (83.0)	4.3 (66.1)	8.3	192
1D		49.0 (99.4)	5.3 (81.9)	8.2	213
1E		42.2 (85.6)	4.5 (69.3)	8.5	244
2A		44.3 (89.6)	5.3 (82.6)	8.8	120
2B		33.3 (67.5)	3.7 (57.6)	8.8	167
2C	AE/0.43	36.8 (74.6)	4.0 (61.6)	8.9	196
2D		34.9 (70.8)	3.9 (60.9)	8.9	218
2E		37.1 (75.3)	3.9 (60.2)	8.7	240
3	A /0.60	36.1 (73.2)	4.1 (63.0)	8.3	130
4	AE/0.50	31.9 (64.7)	3.7 (57.7)	8.9	126
5	PA /0.90	37.1 (75.3)	4.7 (73.7)	9.1	140
6	PAE/0.80	38.6 (78.3)	4.9 (76.2)	9.0	140
7,8	A /0.80	32.7 (66.3)	4.2 (64.6)	8.4	337
7,8		33.2 (67.3)	4.2 (64.6)	8.6	337
7,8		33.6 (68.2)	4.3 (67.2)	8.4	337
7,8		34.4 (69.8)	4.4 (68.6)	8.3	337
9	PA /0.80	32.0 (64.9)	4.4 (68.3)	9.2	337
10,11	B /0.80	32.9 (66.7)	3.8 (58.4)	7.6	147
10,11		34.3 (69.6)	4.0 (62.5)	7.6	147
10,11		32.9 (66.7)	3.7 (57.2)	7.4	147
12	PB /0.80	26.0 (52.7)	3.2 (50.4)	8.9	134
13A	B /0.56	37.5 (76.1)	3.8 (59.4)	7.8	108
13B		42.0 (85.2)	4.4 (68.5)	8.0	134
13C		49.3 (100)	5.1 (79.5)	7.8	163
13D		31.6 (64.1)	3.8 (58.6)	7.9	184
13E		39.7 (80.5)	4.3 (67.5)	7.8	206

(*) letters after mix numbers indicate the curing conditions.

(#) First letter (P) indicates mortar's been sieved from Pellite concrete, Letters (A) and (B) indicate Cement-sand ratio of 1:2.33 and (C) indicates Cement-sand ratio of 1:3.73. Letter (E) indicates Air-entrained mix.

Table 8.4 (continued)

Mix no.*	Mortar code name #	Calcium hydroxide content (degree of hydration) in (%)	Non-evaporable water content (degree of hydration) in (%)	Carbo-nation (%)	Age (days)
14	B /0.66	41.8 (84.8)	4.5 (70.1)	8.1	156
15	PB /1.05	31.8 (64.5)	4.1 (63.8)	9.2	161
16A		33.4 (67.7)	3.0 (66.3)	7.9	219
16B		31.2 (63.3)	2.8 (61.9)	8.0	251
16C	C /0.90	36.0 (73.0)	3.2 (70.7)	7.8	284
16D		30.0 (60.9)	2.6 (57.5)	8.1	309
16E		38.1 (77.3)	3.3 (72.9)	7.9	332
17	CE/0.80	30.1 (61.1)	2.6 (57.5)	9.2	201
18A		34.8 (70.6)	3.0 (66.3)	8.1	211
18B		38.8 (78.7)	3.4 (75.1)	8.0	250
18C	C /0.95	31.6 (64.1)	2.7 (59.7)	8.2	280
18D		29.1 (59.0)	2.6 (57.5)	8.3	306
18E		49.3 (100)	4.1 (90.6)	8.0	334
19A		32.6 (66.1)	2.9 (64.1)	7.8	214
19B		27.4 (55.6)	2.4 (53.0)	8.0	247
19C	CE/0.90	27.7 (56.2)	2.4 (53.0)	8.1	280
19D		30.8 (62.5)	2.7 (59.7)	8.0	303
19E		28.9 (58.6)	2.5 (55.3)	8.1	327
20A		29.8 (60.4)	2.6 (57.5)	8.0	241
20B		23.4 (47.5)	2.1 (46.4)	8.2	283
20C	PC /1.29	23.7 (48.1)	2.0 (44.2)	8.1	316
20D		23.9 (48.5)	2.1 (46.4)	8.1	344
20E		26.5 (53.8)	2.3 (50.8)	8.3	368
21A		26.6 (54.0)	2.3 (50.8)	9.1	223
21B	PCE/1.29	23.7 (48.1)	2.1 (46.4)	9.2	265
21C		37.4 (75.9)	2.9 (64.1)	9.1	294
21D		30.9 (62.7)	2.6 (57.5)	9.0	345
22,23	C /0.80	36.8 (74.6)	3.0 (66.3)	8.4	298
24	PC /0.80	30.2 (61.3)	2.6 (57.5)	8.6	298

(*) letters after mix numbers indicate the curing conditions.

(#) First letter (P) indicates mortar's been sieved from Pellite concrete.Letters (A) and (B) indicate Cement-sand ratio of 1:2.33 and (C) indicates Cement-sand ratio of 1:3.73. Letter (E) indicates Air-entrained mix.

8.6 Depth of carbonation results

Results of the depth of carbonation for concrete at various curing conditions are presented in Table 8.5. These results are averages of two and sometimes three concrete cubes.

Table (8.5)

Results of the depth of carbonation for concretes.

Mix No.*	Concrete code name	Depth of Carbonation (mm)	Age (days)
1A		0	121
1B		0.5	160
1C	QA /0.53	0.5	192
1D		0.5	213
1E		1	244
2A		0	120
2B		0.5	167
2C	QAE/0.43	1	196
2D		1	218
2E		1	240
3	LA /0.60	0	130
4	LAE/0.50	0	126
5	PA /0.90	0	140
6	PAE/0.80	0	140
7	QA /0.80	0	337
8	LA /0.80	2	337
9	PA /0.80	4	337
10	QB /0.80	0	147
11	LB /0.80	2	147
12	PB /0.80	0	134
13A		0	108
13B		0	134
13C	QB /0.56	0.5	163
13D		0.5	184
13E		0.5	206
14	LB /0.66	0	156
15	PB /1.05	0	161
16A		2	219
16B		5	251
16C	QC /0.90	6	284
16D		6	309
16E		6	332
17	QCE/0.80	1	201
18A		0	211
18B		4	250
18C	LC /0.95	3	280
18D		5	306
18E		6	334
19A		3	214
19B		4	247
19C	LCE/0.90	10	280
19D		10	303
19E		12	327
20A		0	241
20B		3	283
20C	PC /1.29	8	316
20D		10	344
20E		10	368
21A		0	223
21B		6	265
21C	PCE/1.29	16	294
21D		17	322
21E		19	345
22	QC /0.80	3.5	298
23	LC /0.80	4	298
24	PC /0.80	5	298

(*) letters after mix numbers indicate the curing conditions.

8.7 SEM results

SEM observation was carried out on fresh fractured surface of mortar mixes, numbers: 7, 8 (A/0.8), 22, 23 (C/0.8), 20 (PC/1.29 at A, B and E curing conditions), 21 (PCE/1.29 at A, B and E curing conditions), 13 (A&B/0.56, A to D curing conditions) and different types of coarse aggregates at different magnifications. Selected SEM photographs are given in chapter 9 section 9.7 , where the appropriate discussion is presented.

8.8 Compressive strength results

The results of the cube compressive strength tests on concrete mixes are given in Table V.1 in Appendix V and the mean values of these results are tabulated in Table 8.6. These results are average of two and sometimes three tests. Whenever the difference between two test results were more than 3% then a third cube was tested.

Table (8.6)

Summary of cube compressive strength results for concretes

Mix no.	Concrete code name	Compressive strength (N/mm^2)						
		Fog room curing				3 days fog room + creep room curing		
		Age (days):				Age (days):		
		3	7	28	91	7	28	91
1	QA /0.53	34.5	42.7	52.2	56.2	46.4	54.2	57.0
2	QAE/0.43	23.0	24.3	27.9	31.2	29.7	33.1	36.6
3	LA /0.60	34.2	43.2	51.5	55.1	45.8	52.3	55.6
4	LAE/0.50	19.7	23.1	27.2	29.4	24.2	28.6	31.7
5	PA /0.90	15.7	22.6	37.0	37.7	24.6	27.3	32.1
6	PAE/0.80	3.8	6.8	9.1	10.4	8.5	9.2	9.5
7	QA /0.80	20.1	26.1	41.2	44.3	30.8	41.7	44.9
8	LA /0.80	22.6	28.5	37.1	43.9	30.6	37.9	44.0
9	PA /0.80	19.2	26.3	32.8	34.4	24.2	29.5	32.2
10	QB /0.80	18.5	24.4	33.0	35.1	24.1	33.9	35.2
11	LB /0.80	22.8	29.0	36.4	39.9	32.8	36.6	40.0
12	PB /0.80	9.9	11.8	13.6	16.2	11.9	14.3	17.0
13	QB /0.56	35.3	46.1	52.3	57.9	45.4	55.5	59.6
14	LB /0.66	35.7	43.0	46.3	48.7	45.5	50.6	53.8
15	PB /1.05	9.2	10.0	10.3	12.0	10.1	13.5	15.7
16	QC /0.90	15.5	19.5	23.9	26.1	20.3	25.3	26.1
17	QCE/0.80	7.7	10.7	14.9	15.6	11.7	14.9	15.9
18	LC /0.95	18.4	22.5	28.5	29.4	22.5	30.5	29.5
19	LCE/0.90	6.9	9.7	11.8	11.9	10.1	12.7	13.8
20	PC /1.29	9.6	12.1	12.1	17.8	12.1	14.3	20.7
21	PCE/1.29	2.4	3.0	4.1	4.3	3.8	4.4	4.4
22	QC /0.80	19.4	23.0	29.5	31.2	23.3	29.5	31.1
23	LC /0.80	21.7	26.9	33.6	38.3	29.2	34.0	38.1
24	PC /0.80	10.8	11.5	13.4	20.4	12.2	14.4	22.2

CHAPTER NINE

DISCUSSION AND ANALYSIS OF RESULTS

9.1 Thermal conductivity

As mentioned in section 2.3, the main factors effecting the thermal conductivity of concretes at ambient temperature are density, moisture content and pore characteristics. Because all the λ-values have been adjusted to 3 per cent moisture content by volume using the expression derived in section 5.5.3, the effects of moisture has been eliminated. The relationships between thermal conductivity and the main parameters of density, total porosity and pore size distribution are discussed in section 9.8. In this section only the effects of using different type of aggregates, course aggregate/sand and water/cement ratios are discussed.

From Table 8.1 it can be seen, by comparing mix numbers 7-9, 10-12 and 22-24 which have the same individual group mix proportions and W/C ratios, that the type of aggregate affects the λ-value of the concrete immensely, this is primarily as a direct result of changes in aggregate density, total porosity, median pore diameter and mineral composition of aggregates. In Figure 9.1, λ-values of these mixes are shown as a bar chart. As it can be seen from this figure, Pellite concretes which have the lowest density have consequently the lowest conductivity of the three aggregates.

This is due to its relatively low specific gravity, high porosity and vitreous internal pore structure of the aggregate. Limestone concretes exhibit a higher conductivity (about 80 to 160 per cent higher than Pellite concretes). Quartz concretes have the highest density and hence conductivity of the three aggregates used with a conductivity about 40 to 50 per cent higher than the limestone concretes. Comparison of mixes with about the same free W/C ratios i.e. mixes 16, 18, 20 and 1, 3, 9 (see Figure 9.2) shows the same trend and the same percentage increase in thermal conductivity as when the total W/C ratios are equal.

From Table 8.1 it can also be seen that with the three aggregates used, alterations to the mix proportions change the resultant density, total porosity and median pore diameter (see also Table 9.4) of the concrete and this affected the λ-value. Mix proportions 'A' and 'C' have a sand to coarse aggregate ratio of about 1:1.5. Mix proportion 'B' has a sand to coarse aggregate ratio of about 1:2.4. Therefore, by comparing concretes made with a 1:1.5 ratio ('A' mix proportion) and concrete made with 1:2.4 ratio ('B' mix proportion), the effect of decreasing the sand/coarse aggregate ratio on main parameters and hence on the thermal conductivity is found since both mix proportions have the same sand/cement ratio. For example comparing mixes 7-9 with 10-12 (see Figure 9.3) shows that decreasing sand to coarse aggregate ratio decreases the λ-values (between 2 to 52 per cent for the mixes studied). This is due to introducing more pores in the mix since there are not enough sand particles to fill the gaps between coarse aggregates in

the mix 'B' matrix. This in turn affects the main parameters mentioned before, i.e. density, total porosity and median pore diameter, and causes the λ-value to be reduced. The reason for the noticeable reduction of λ-value with decreasing sand/coarse aggregate ratio in Pellite concrete can be due to the large difference between the thermal conductivity values of sand (mortar) and Pellite aggregates (Pellite aggregates having much lower λ-value than the mortar). Since the volume of the Pellite aggregate increases when a lower sand/coarse aggregate ratio is used, the λ-value will reduce substantially.

The effect of changing the cement/sand ratio on thermal conductivity depends on the changes it causes to the main parameters. Decreasing the cement/sand ratio from 1:2.33 ('A' mix proportions) to 1:3.73 ('C' mix proportions) in some cases (Pellite concretes) increases the porosity and reduces the density (compare mix 9 with 24) such that the λ-value decreases and in some other cases (limestone and quartz concretes) reduces the porosity and doesn't cause any changes in the density, (compare mixes 8 with 23 and 7 with 22) such that λ-value increases (see Table 9.4).

Increasing the W/C ratio increases the number of larger pores in the mortar matrix which reduces density, increases porosity and hence reduces the conductivity. This effect can be seen by comparing mixes 1 with 7, 13 with 10, 14 with 11, 23 with 18 and 24 with 20 in Figure 9.4.

When an air entraining agent added to a mix it increased the size and number of larger pores and hence the

total porosity which in turn reduced the density. This reduced the thermal conductivity of the concretes as expected. Comparing mixes 9 with 6, 20 with 21 and 22 with 17 shows between about a 10 to 18 per cent reduction in density and corresponding 30 to 50 per cent reduction in λ-values (see Figure 9.5).

- SUMMARY -

- Because the main parameters, i.e. density, total porosity and median pore diameter, are more dependent upon type of aggregate than W/C ratio or mix proportions, then the λ-values are also more dependent upon type of coarse aggregate than W/C ratio or mix proportion of concretes.

- Quartzitic aggregate concretes give the highest conductivity and the Pellite concretes the lowest due to the effects these aggregates have on the main parameters.

- Air entraining agent reduces the thermal conductivity of concrete by as much as 50 per cent in some cases.

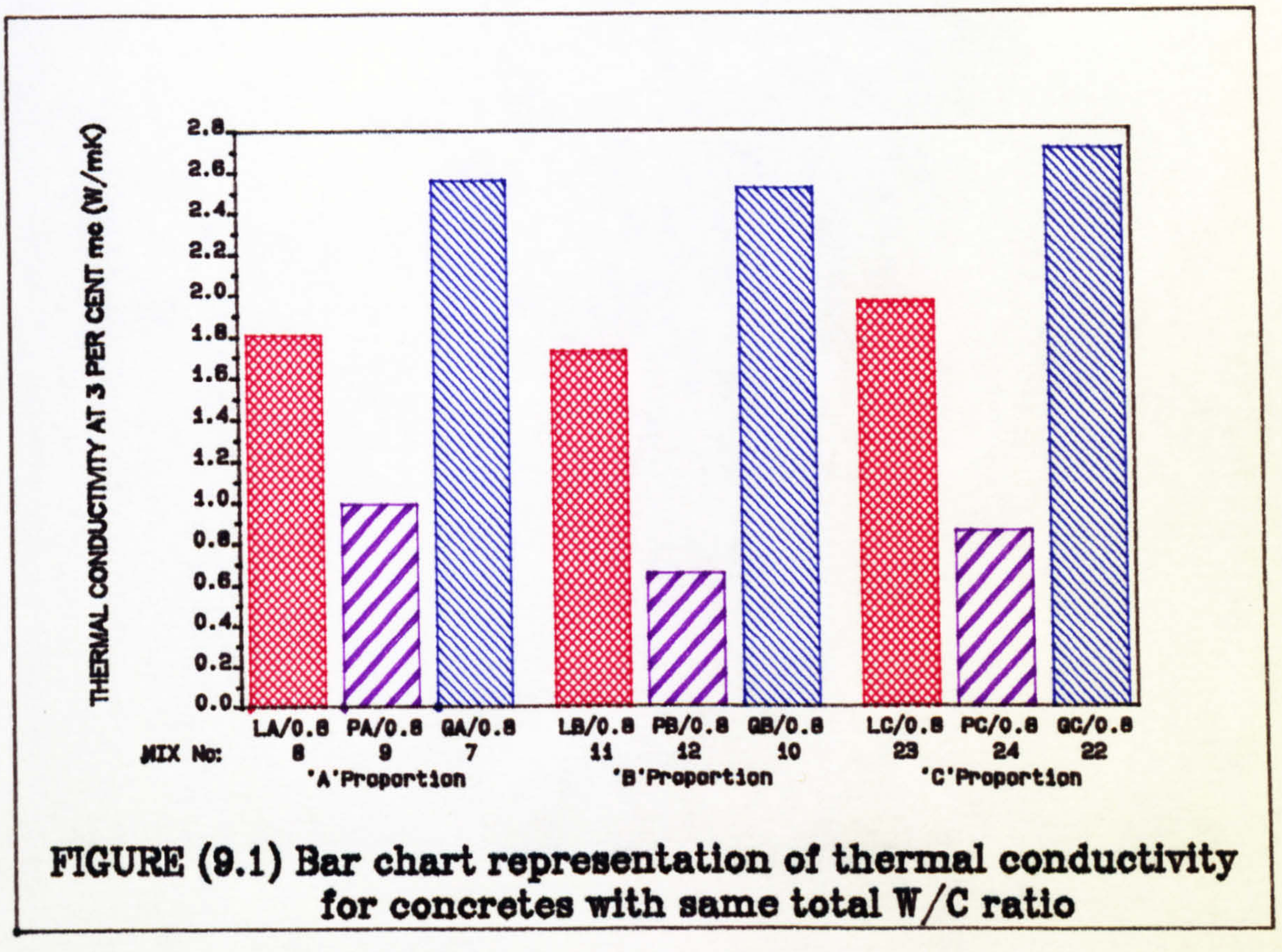

FIGURE (9.1) Bar chart representation of thermal conductivity for concretes with same total W/C ratio

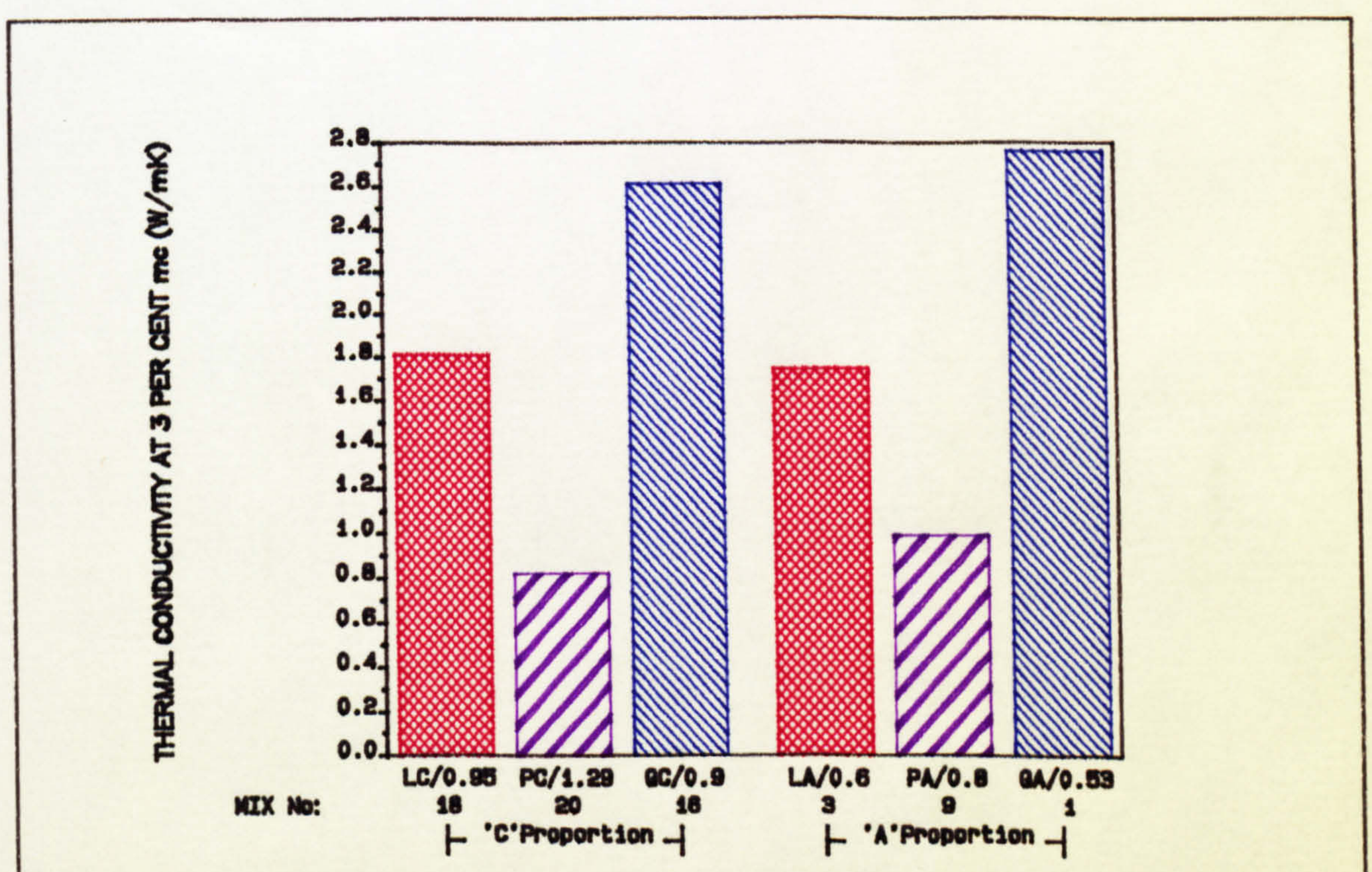

FIGURE (9.2) Bar chart representation of thermal conductivity for concretes with same free W/C ratio

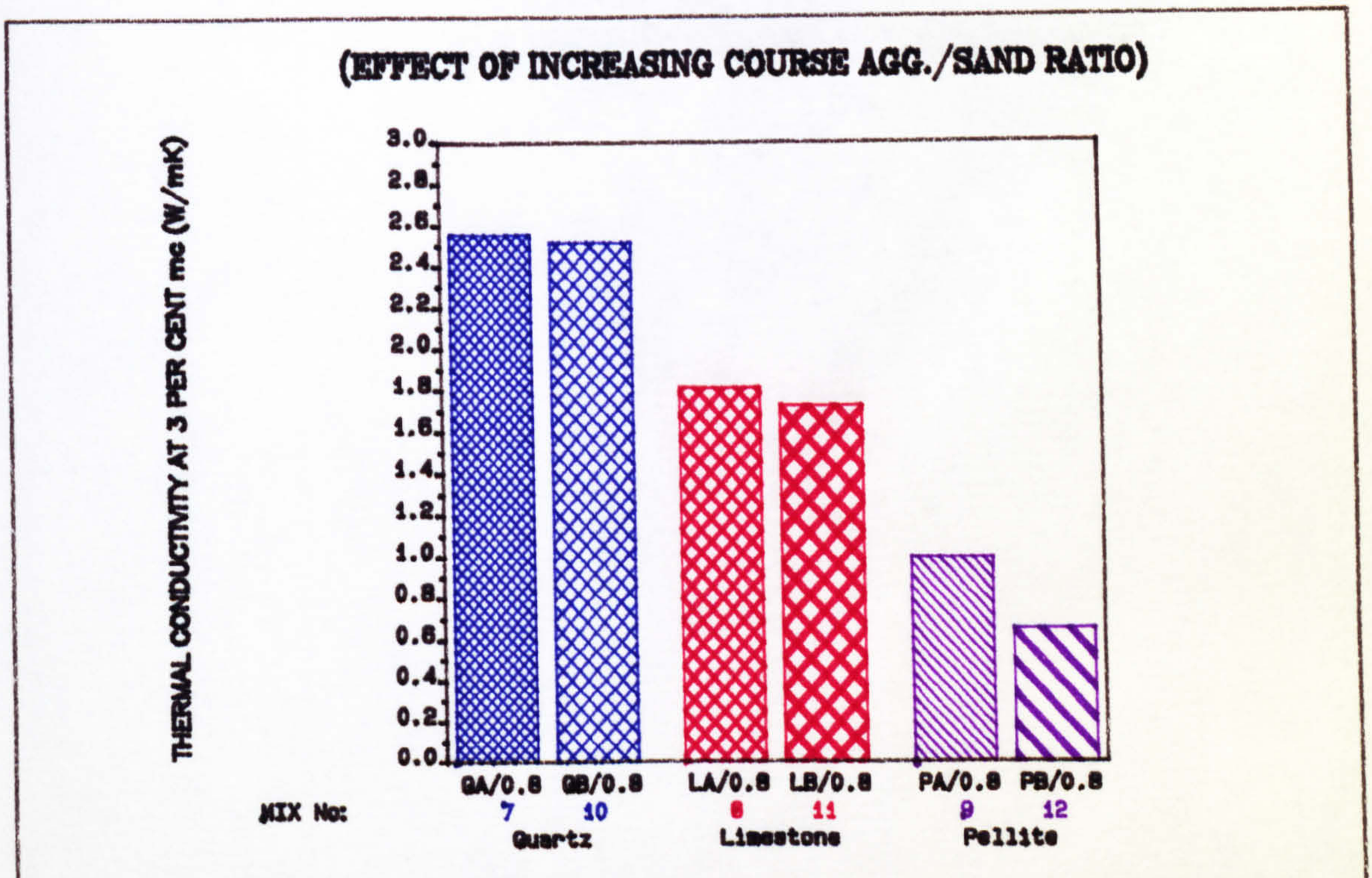

FIGURE (9.3) Bar chart representation of thermal conductivity for A & B proportion concretes with same total W/C ratio

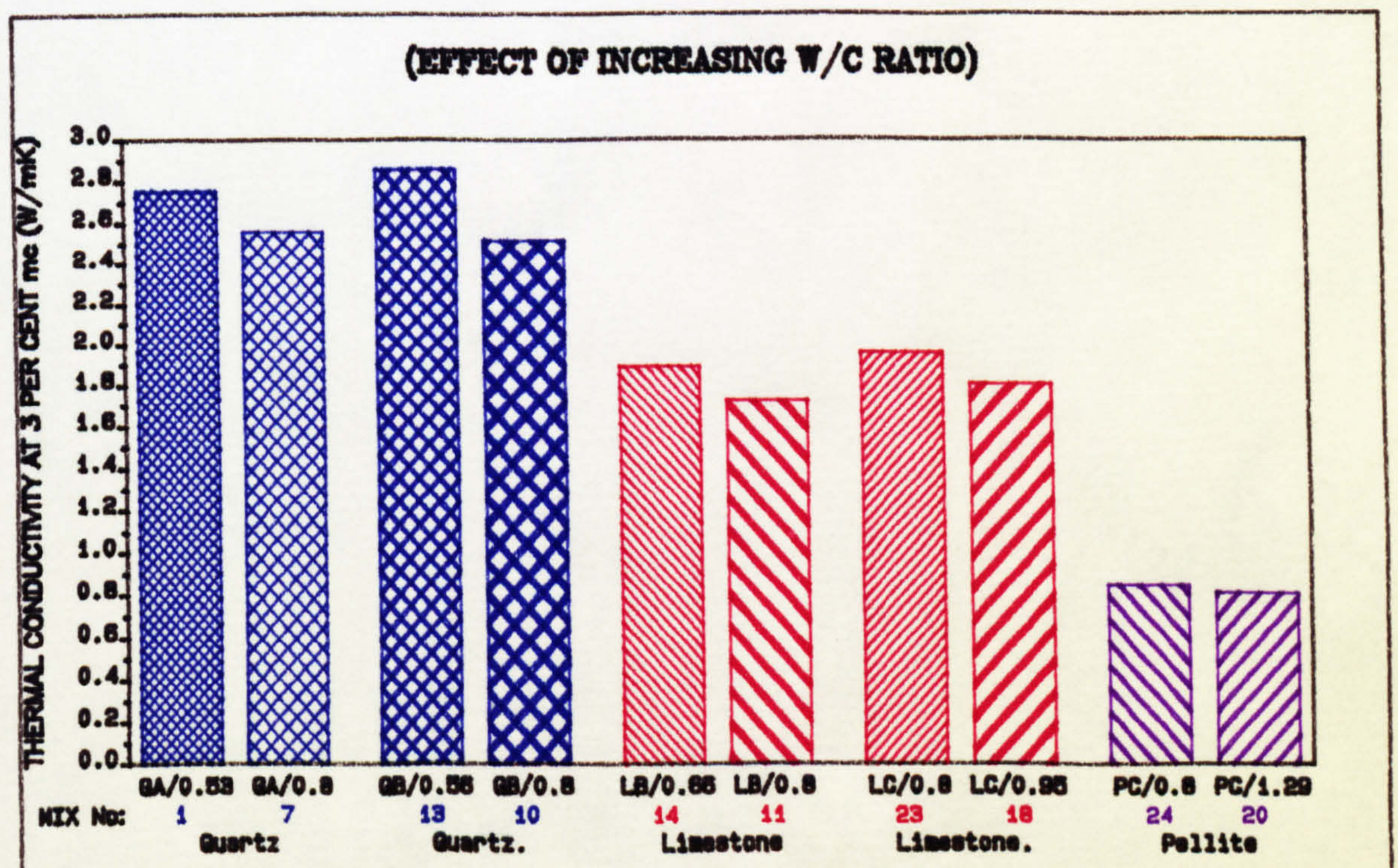

FIGURE (9.4) Bar chart representation of thermal conductivity for selected concretes

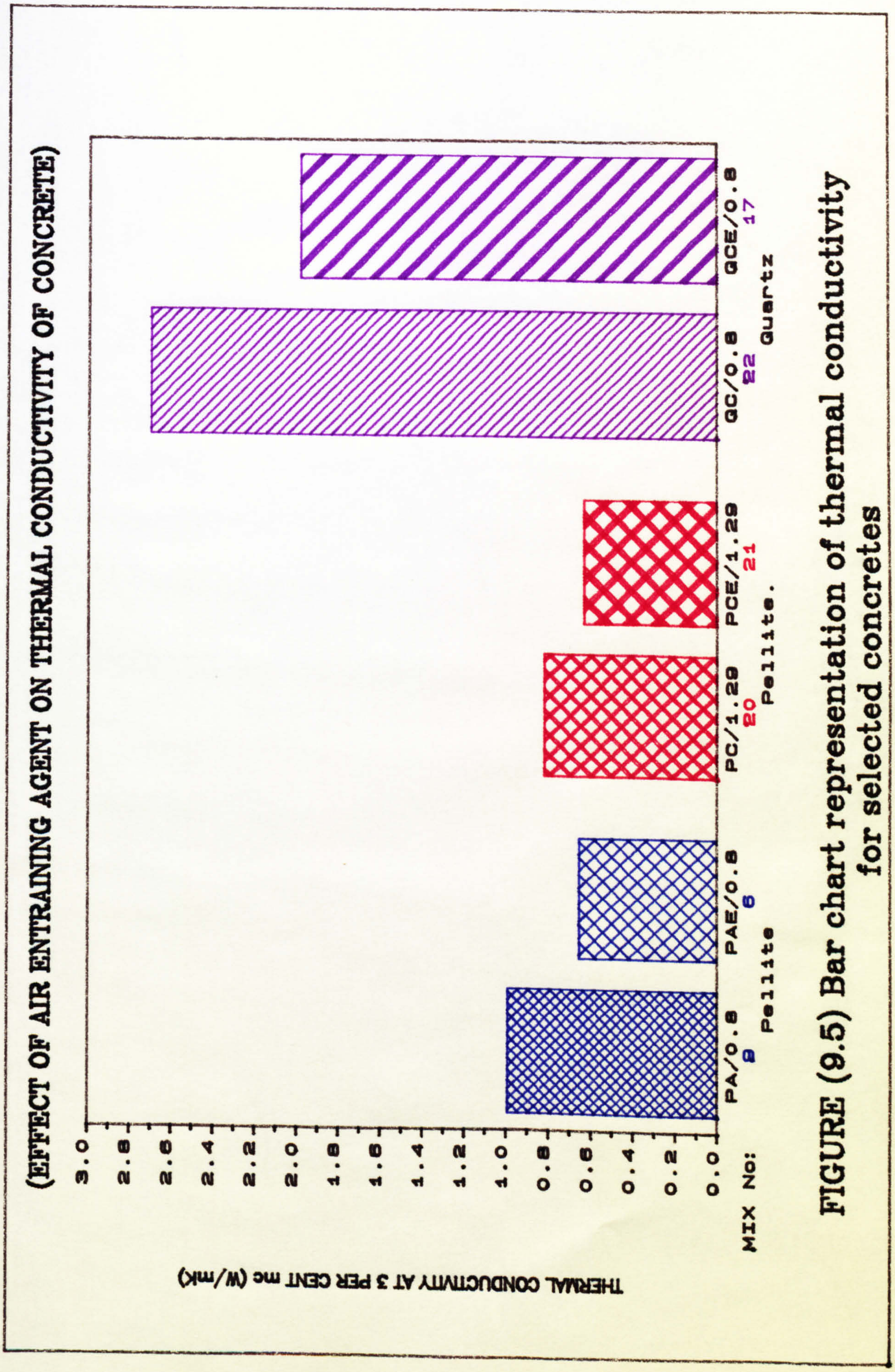

FIGURE (9.5) Bar chart representation of thermal conductivity for selected concretes

9.2 Mercury porosimetry

The effects of composition, and curing regimes on the pore size distribution and porosity of mortars are discussed in this section. The data has been presented in Figures 8.3 to 8.21 and Table 8.2. The analysis is made using typical results of some of the mixes and curing regimes.

a) Effect of age and successive curing

It is generally believed [147,148] that due to conversions of large pores into smaller pores as a function of hydration and the production of new hydration products with age the pore size distribution and total porosity is reduced. The pore size distribution function for mortar mixes A/0.8 and B/0.8 (A and B mortar ratios have exactly the same mix proportion) are shown in Figure 8.3. It can be seen from these distributions that the total porosity reduces with age. It can also be seen that the distributions is shifted towards smaller pores with increased age. Although both mixes are old but hydration process is believed to continue slowly up to one year. Carbonation can also help this phenomenon [142,147]

The cumulative and incremental pore size distributions for the eight mortar mixes which were cured successively in various curing conditions are shown in Figures 8.5 to 8.20. A common feature of these distributions is the very small variation of the parameters which characterize the pore structure, i.e. total porosity and median pore diameter (see Table 8.2). The standard deviations for the eight mortar mixes are shown in Table 9.1.

These variations are close to the repeatability of the MIP tests and thus the effect of curing regime is practically nil. However the effect of age is manifested in a reduction of total porosity and median pore diameter. The effect of curing has artificially being masked because the mortars had already reached their laboratory maximum hydration potential (see section 9.4).

Table (9.1)

Standard deviation of total porosity and median pore diameter for the eight mortar mixes which were cured successively in 'A' to 'E' curing conditions

Mix no.	S.D. of porosity	S.D. of median pore diameter
1	0.29	0.004
2	0.97	0.071
13	0.30	0.007
16	1.34	0.070
18	1.01	0.065
19	0.65	0.018
20	1.78	0.188
21	1.00	0.326

The cumulative and incremental pore size distributions of these eight mortars also show that the pore sizes are mainly between 0.01 to 10 micron in diameter. Figures 9.6 to 9.13 present the distribution of the eight mortars in the bar chart form by dividing the pore diameters into four designated ranges [149] as follows:

Pore size range (microns)	Range designated name	
< 0.01	gel pores	
0.01 - 0.1	micro pores	capillary pores
0.1 - 1	meso pores	capillary pores
1 - 100	macro pores	

The volume for each range is the summation of the pore volume for the pores within that range. It can be seen from these bar charts that the average differences in pore volume in each range are also not significant for different curing conditions.

b) Effect of water-cement ratio

Comparison of the results in Table 8.2 shows that porosity increases by increasing W/C ratio. This is because when W/C ratio is higher than about 0.38[150,151], all the cement can hydrate and the excess water from the mix causes capillary pores to be made. Figures 9.14 to 9.21 show the cumulative and incremental pore size distributions of mixes with different W/C ratios. Comparison has been made for mixes which have nearly the same age in these figures. In Figures 9.14 and 9.15 all mixes compared have same sand-cement ratio (mix proportion A or B) and their W/C ratio ranges between 0.53 to 0.8. Their total porosity values changes from 16.5% to 19.6% . This corresponds to an increase of about 1.2% in porosity for an increase of 0.1 in W/C ratio. Figures 9.16 and 9.17 show the distributions for mix proportion 'C' with W/C ratio varying between 0.8 to 0.95 and total porosity increasing about 2.5% for each 0.1 increase in W/C ratio. Figure 9.18 and 9.19 show the effect of increasing W/C ratio for mortars sieved from pellite concretes for mix proportion 'B' and 'C'. These figures clearly show that total porosity increases as the W/C ratio increases. This is about 1.8% for mix proportion B and 0.7% for mix proportion C for each 0.1 increase in W/C ratio. It is interesting to note that the increase in total porosity

results mainly from the increase of the capillary and macro pores which in turn increase the median pore diameter. Figures 9.20 and 9.21 show the effect of W/C ratio on air entrained mortars. These figures show that the increase in total porosity is again brought about by the increase of capillary and macro pores as a result of increasing W/C ratio (by comparing mix number 2 with 4 and mix number 17 with 19). The increase in total porosity for air entrained mix proportion A or B and air entrained mix proportion C are about 2.7% and 2.4% respectively for each 0.1 increase in W/C ratio in these mixes.

c) Effect of air entraining

The effect of air entraining on the porosity and pore size distribution of mortars is shown in Figures 9.22 and 9.23. As expected a higher porosity is observed in air entrained mortars than in the admixture-free mortars. The total intrusion volume is increased by about 27, 24 and 18 per -cent (and the total porosity by about 21, 19 and 13 per cent) respectively for mortars with 0.8, 0.9 and 1.29 W/C ratio. The effect of air entraining agent is more pronounced for lower W/C ratios than higher W/C ratios. For air entrained mixes the pore volume peaks occur in macro pore size range and the pore sizes are shifted from meso pores to macro pores which in turn increase the median pore diameter and total porosity. Further evidence of this can be clearly seen by comparing the bar chart of mix number 16 with 19 (Figure 9.9 with 9.11) and mix number 20 with 21 (Figure 9.12 with 9.13).

d) Effect of mix proportion

The effect of increasing sand/cement ratio can be studied in Figure 8.3. By comparing the cumulative pore size distribution of mix numbers 7 & 8 (A/0.8) with 22 & 23 (C/0.8) it can be seen that total porosity is increased with increased sand/cement ratio. This increase in total porosity is found to be about 3.7% (from Table 8.2).

9.2.1 Coarse aggregates

The cumulative and incremental pore size distributions of the three types of coarse aggregates used for three grades of 5-10 mm, 10-14 mm and 14-20 mm are shown in Figures 8.22 to 8.27. It can be seen from these distributions that pellite aggregates have the highest total porosity and that pore volume peaks are in the large pore range (10-100 microns in diameter). The three different grades of pellite aggregates tested show very similar pore size distributions and total porosities.

Limestone aggregate has slightly higher total porosity than quartz and this higher total porosity is the result of general increase in micro pore sizes. The smaller grade sizes of quartzitic and limestone aggregates give higher total porosity. During the preparation of these aggregates the crushing process probably results in the micro-cracking of aggregate fragments. These 'cracks' then increase the volume of capillary pores.

- SUMMARY -

- Although the effect of age results are very limited, MIP results confirm the known trend that as a paste hydrates the total pore volume reduces and a reduction in pore sizes takes place.

- The successive curing used for establishment of moisture correction factors does not affect the total porosity or pore size distributions of mortars.

- Increase in the total porosity is brought about by the increase of the capillary and macro pores as a result of increasing W/C ratio.

- The air entraining agent used increases total porosity by about 18 per cent and shifts the pore sizes to the macro pore range which in turn increase the median pore diameter.

- The effect of air entrainment is more pronounced for lower W/C ratios (within the W/C ratio range used in this investigation).

- Mix proportions slightly effects the pore size distribution of mortars. Increasing the sand - cement ratio (within the ratio studied in this investigation) increases the total porosity.

- Pellite aggregate has larger pore diameters than quartz and limestone and has very high total porosity (about 25%). Limestone aggregates have slightly higher total porosity than quartz (total porosity of limestone aggregate is between about 2 to 7%).

(MIP RESULTS FOR MIX NO.1 AT DIFFERENT CURING CONDITIONS.)

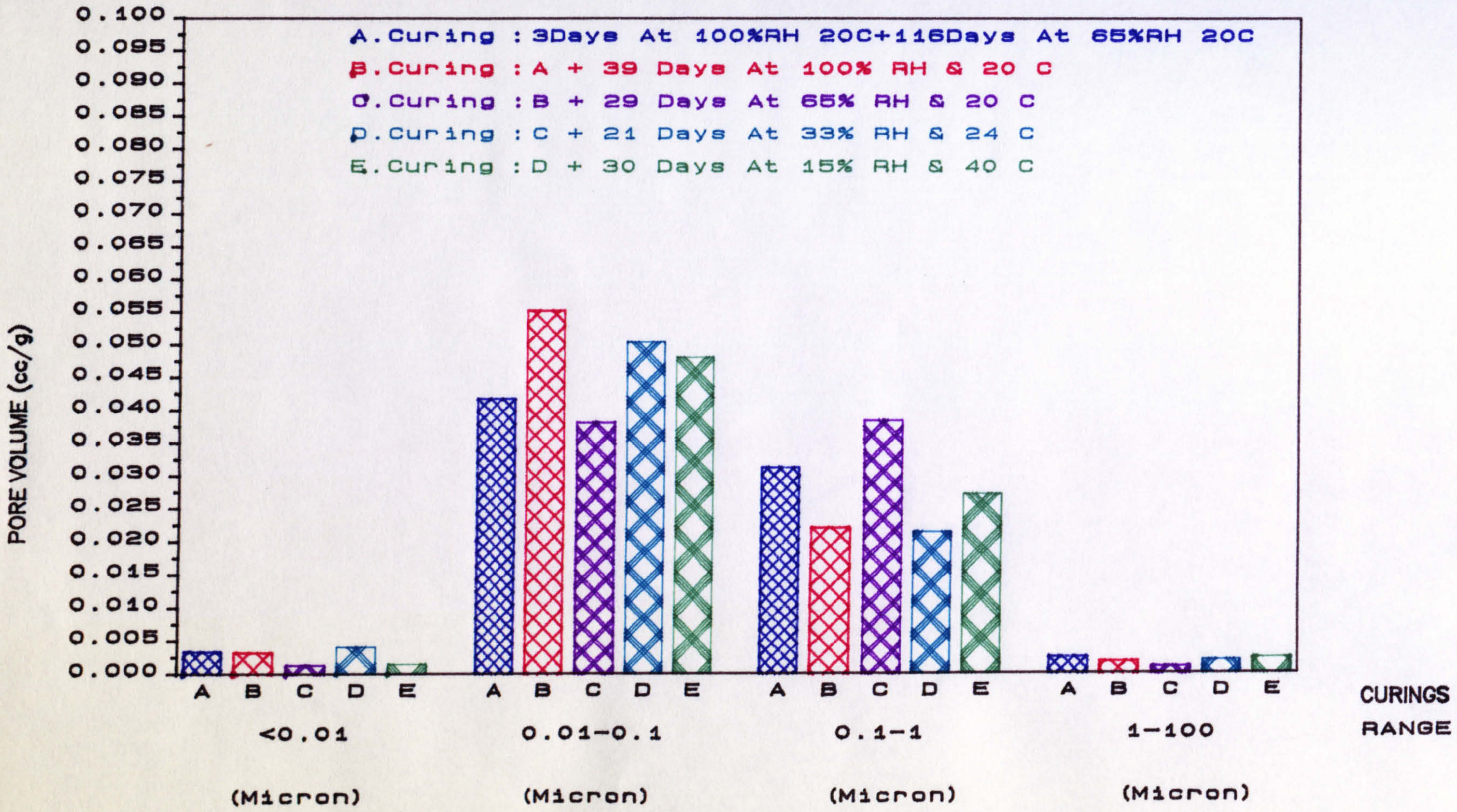

FIGURE (9.6) Bar chart representation of pore volume for mortar : mix A , W/C = 0.53

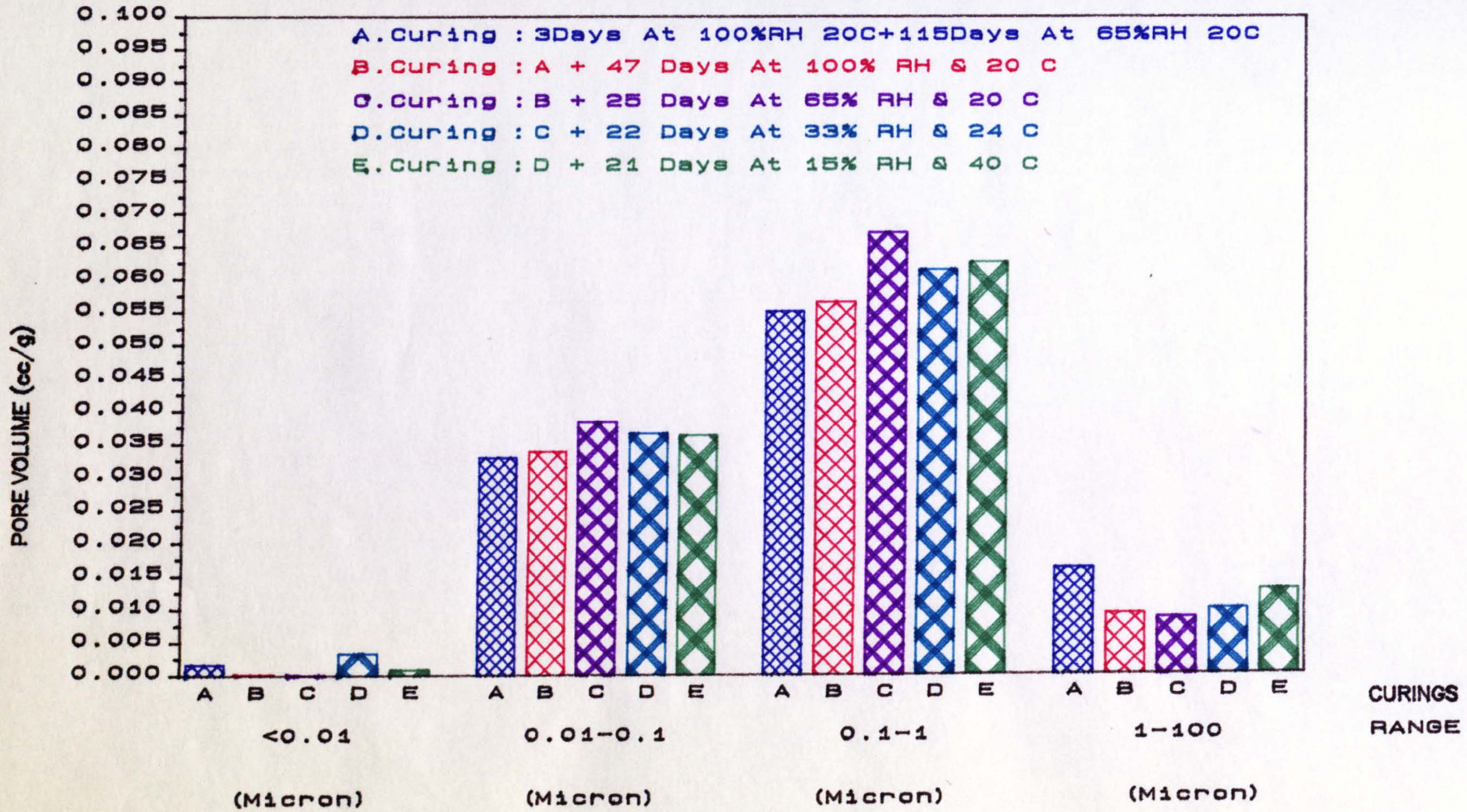

FIGURE (9.7) Bar chart representation of pore volume for air entrained mortar : mix A , W/C = 0.43

(MIP RESULTS FOR MIX NO.13 AT DIFFERENT CURING CONDITIONS.)

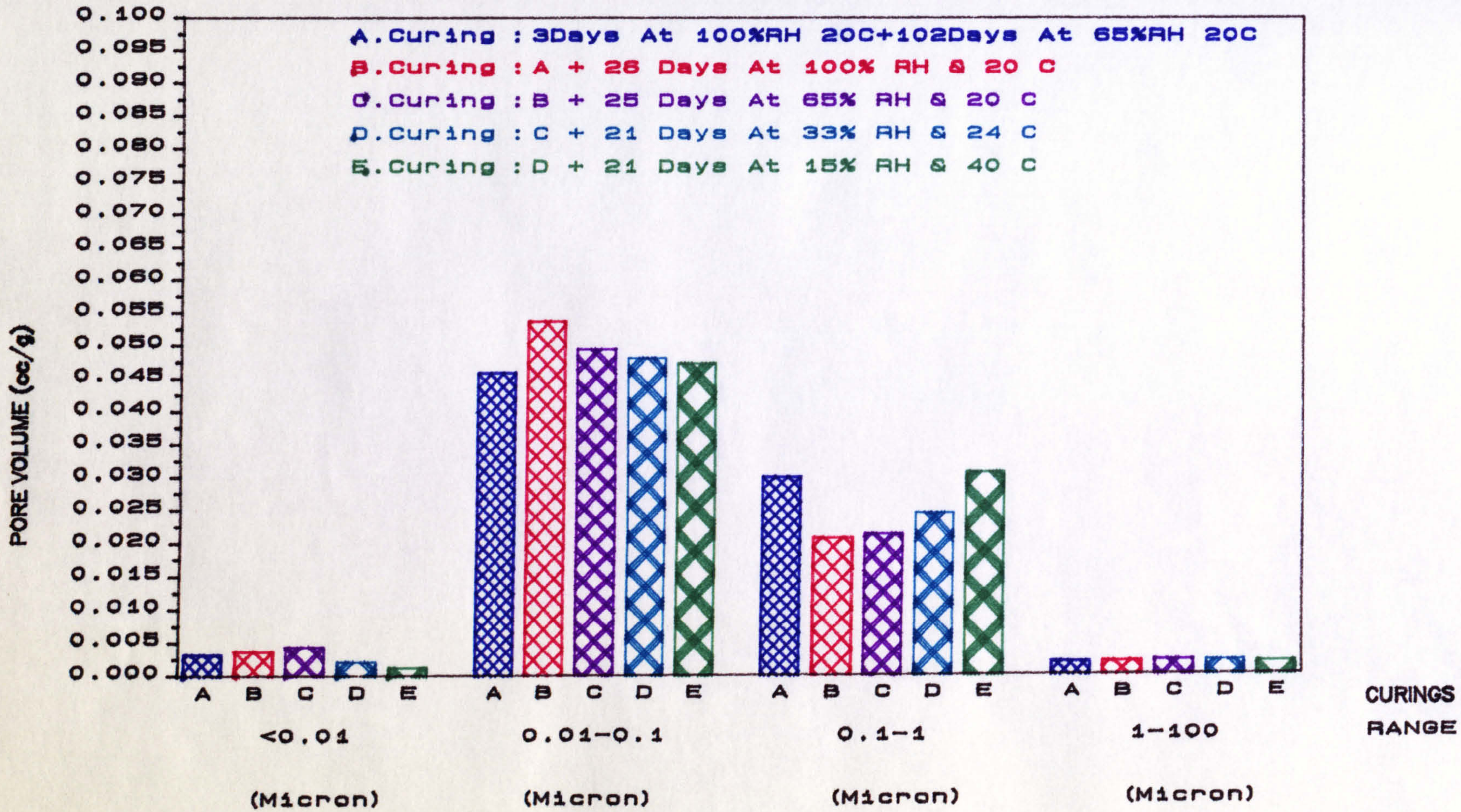

FIGURE (9.8) Bar chart representation of pore volume for mortar : mix B , W/C = 0.56

(MIP RESULTS FOR MIX NO.16 AT DIFFERENT CURING CONDITIONS.)

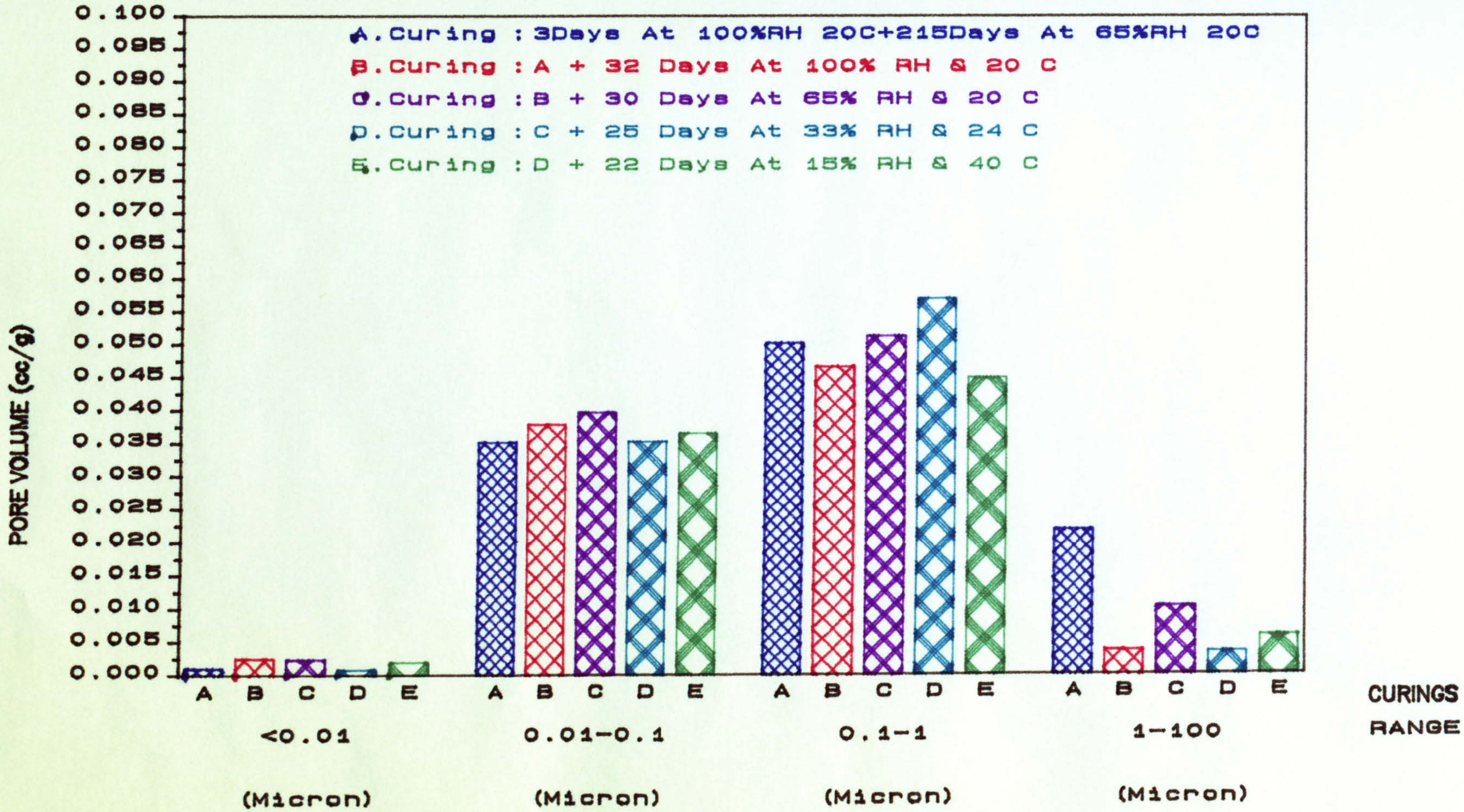

FIGURE (9.9) Bar chart representation of pore volume for mortar : mix C , W/C = 0.90

(MIP RESULTS FOR MIX NO.18 AT DIFFERENT CURING CONDITIONS.)

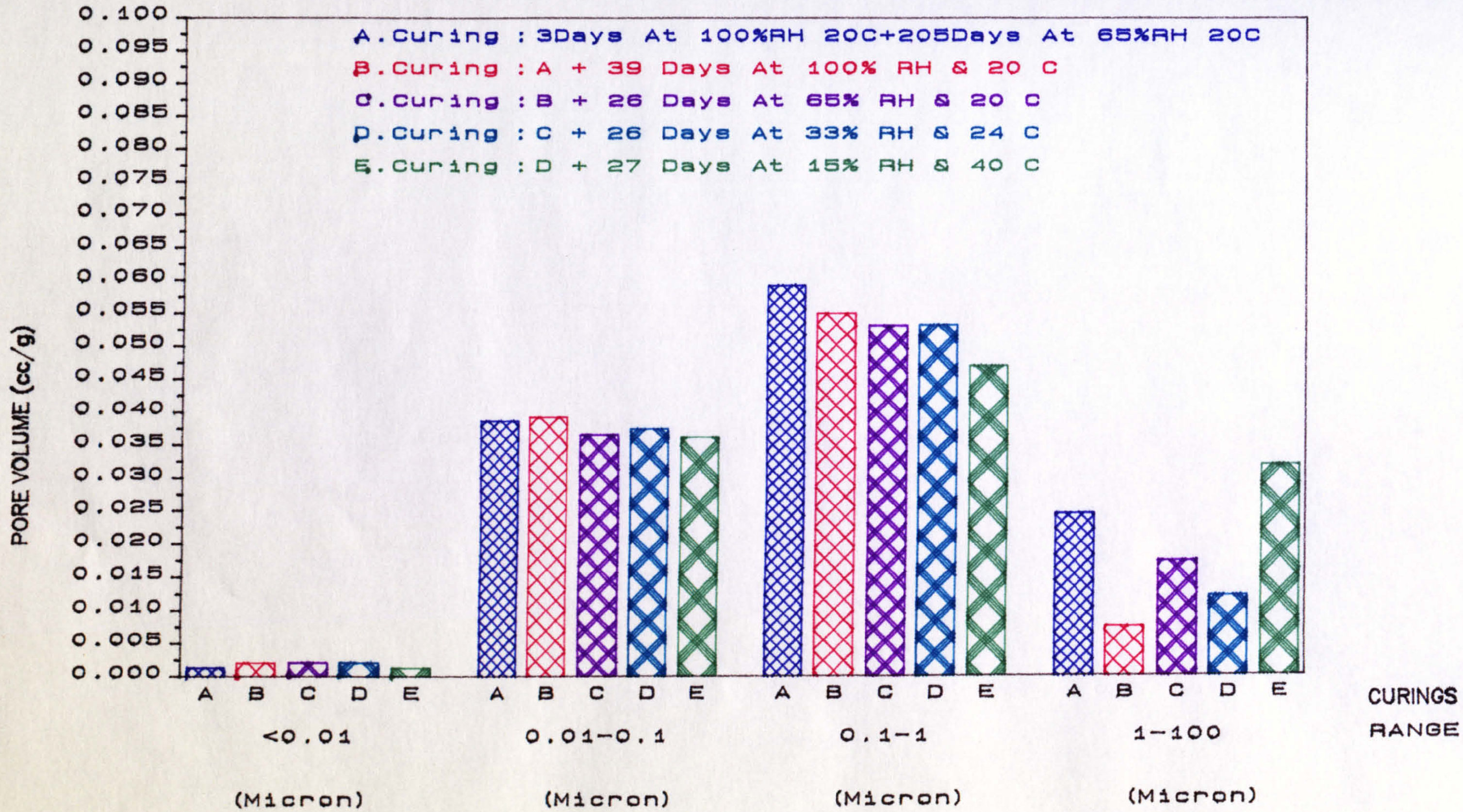

FIGURE (9.10) Bar chart representation of pore volume for mortar : mix C , W/C = 0.95

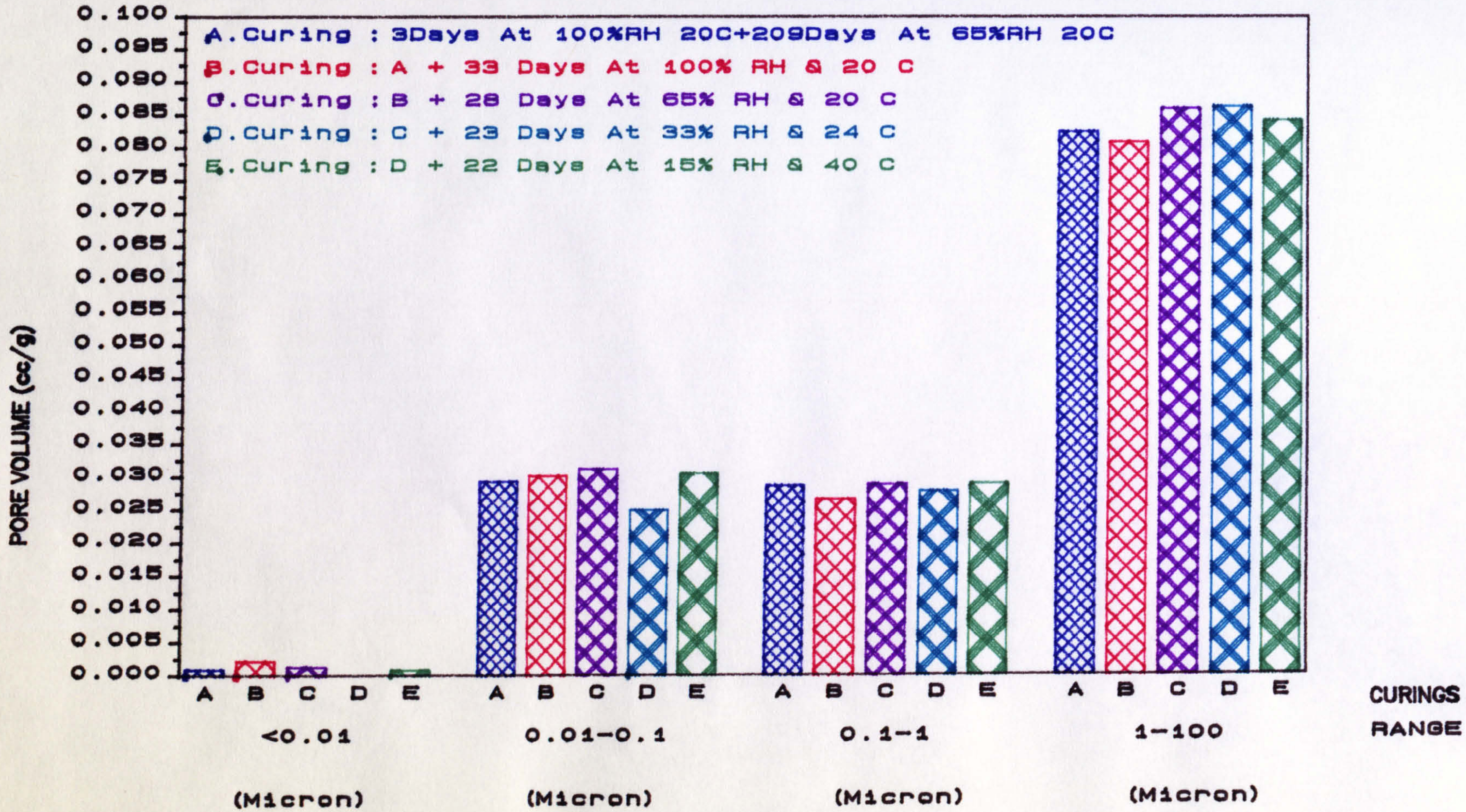

FIGURE (9.11) Bar chart representation of pore volume for air entrained mortar : mix C , W/C = 0.90

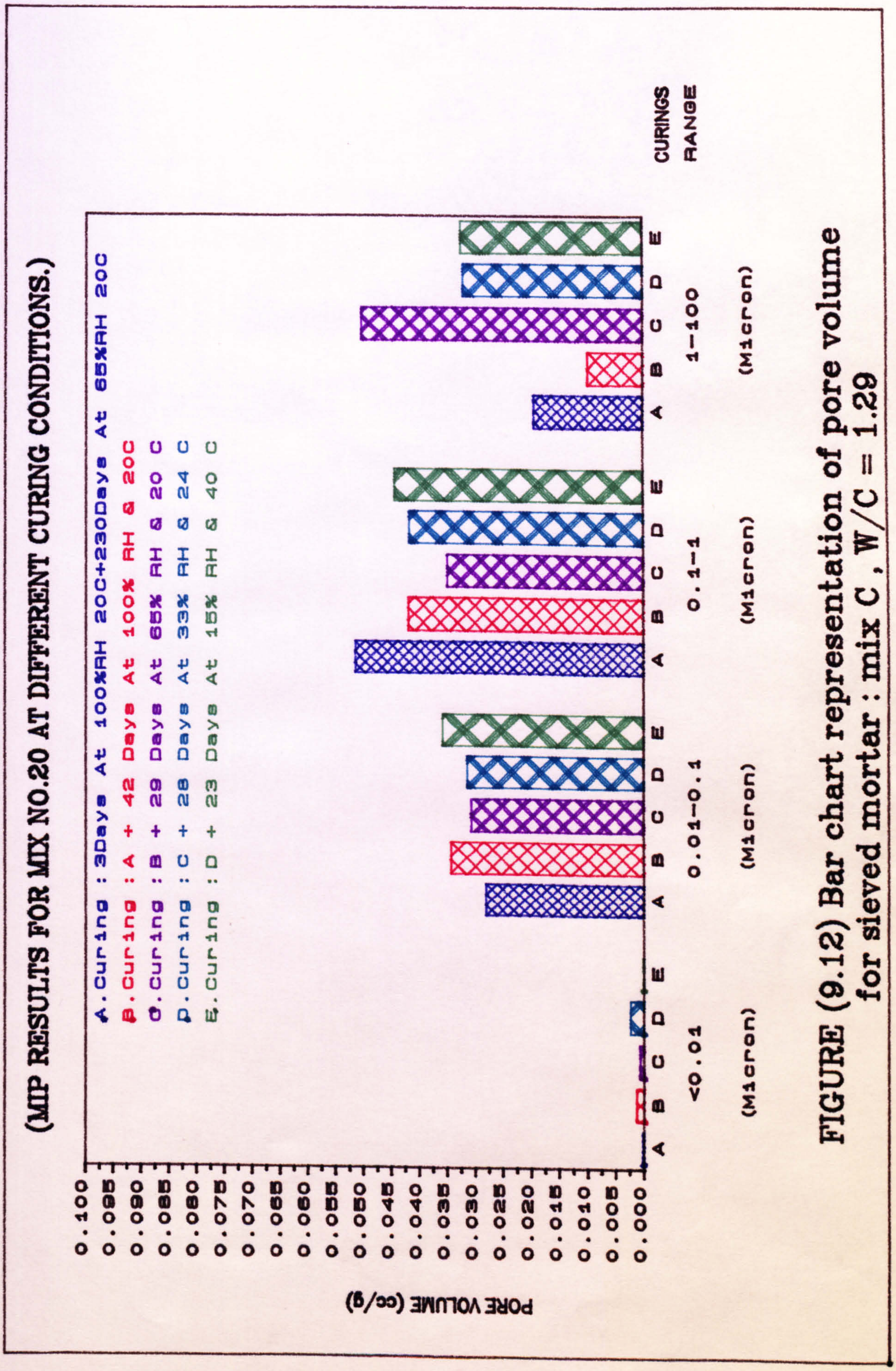

FIGURE (9.12) Bar chart representation of pore volume for sieved mortar : mix C , W/C = 1.29

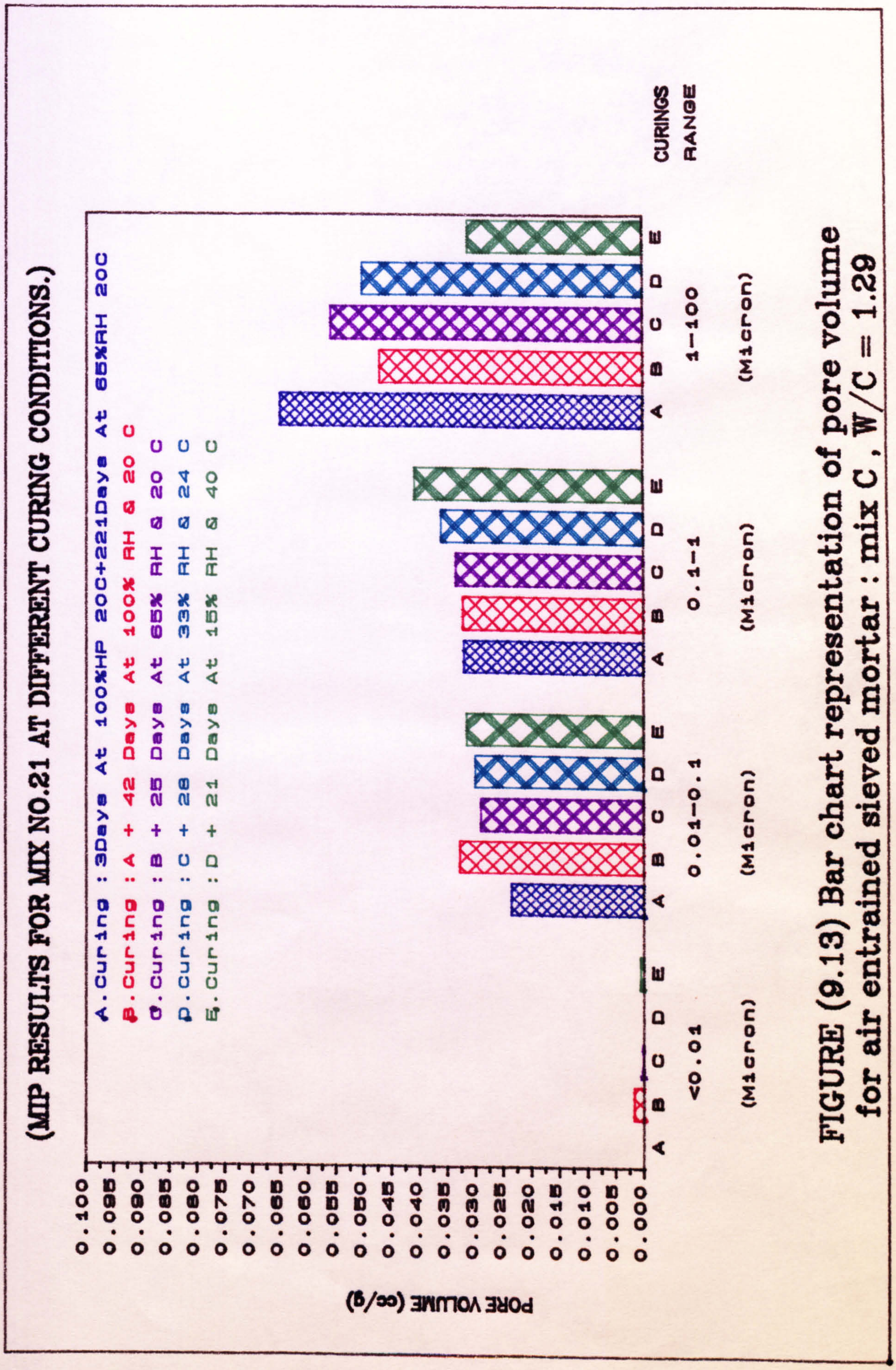

FIGURE (9.13) Bar chart representation of pore volume for air entrained sieved mortar : mix C, W/C = 1.29

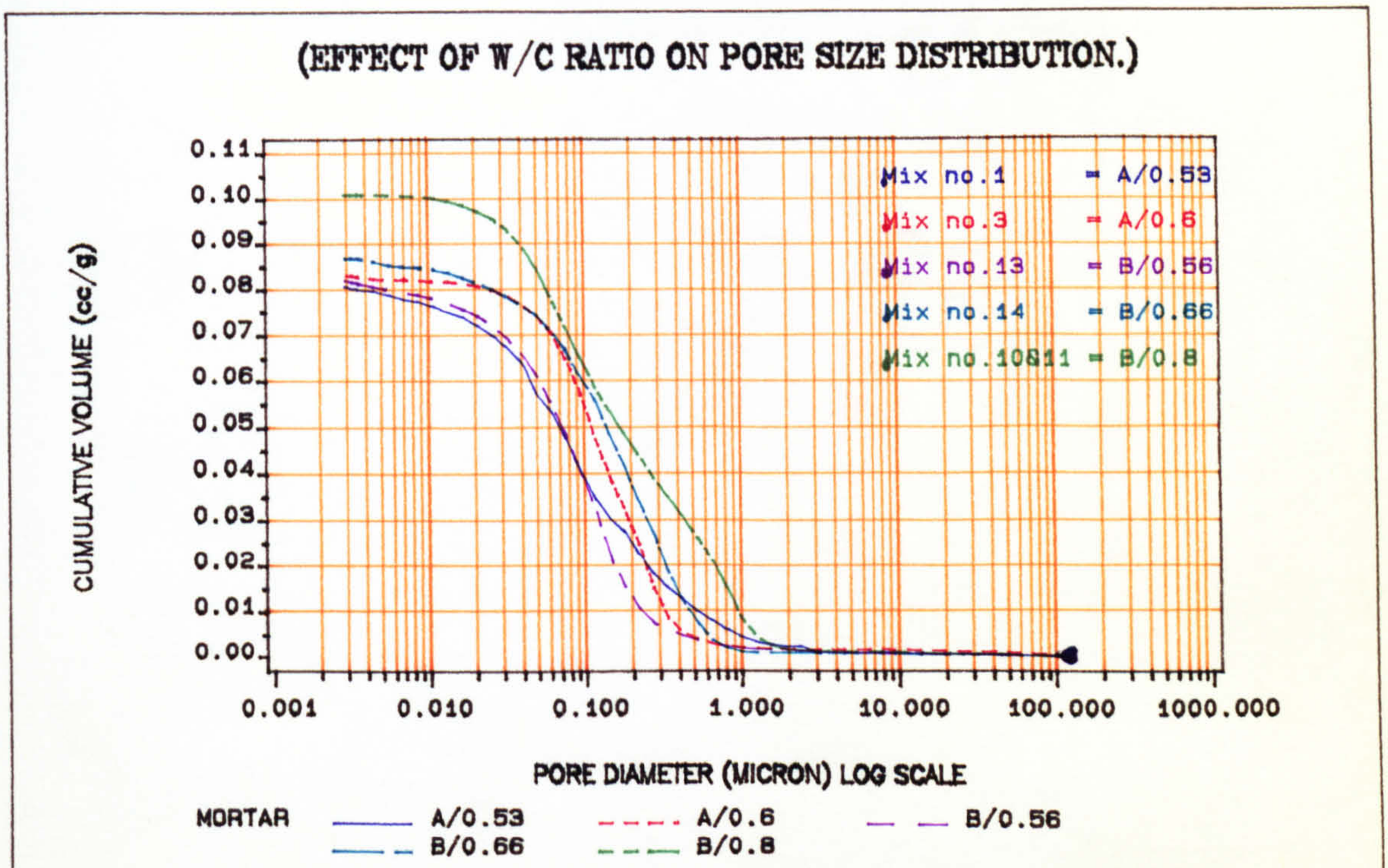

FIGURE (9.14) Cumulative volume vs. pore diameter for mortar mix proportions A and B (which are the same).

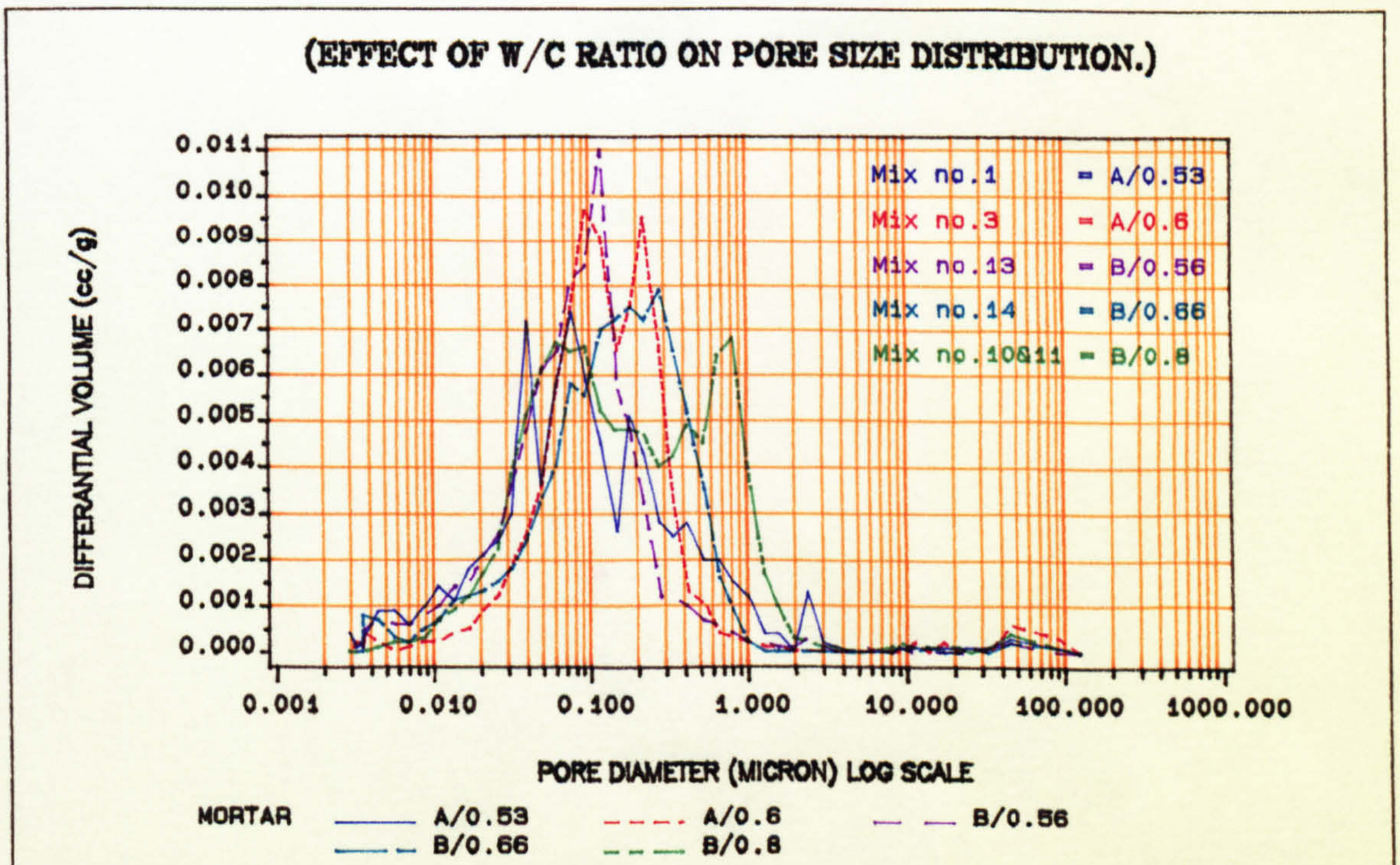

FIGURE (9.15) Incremental pore volume vs. pore diameter for mortar mix proportions A and B.

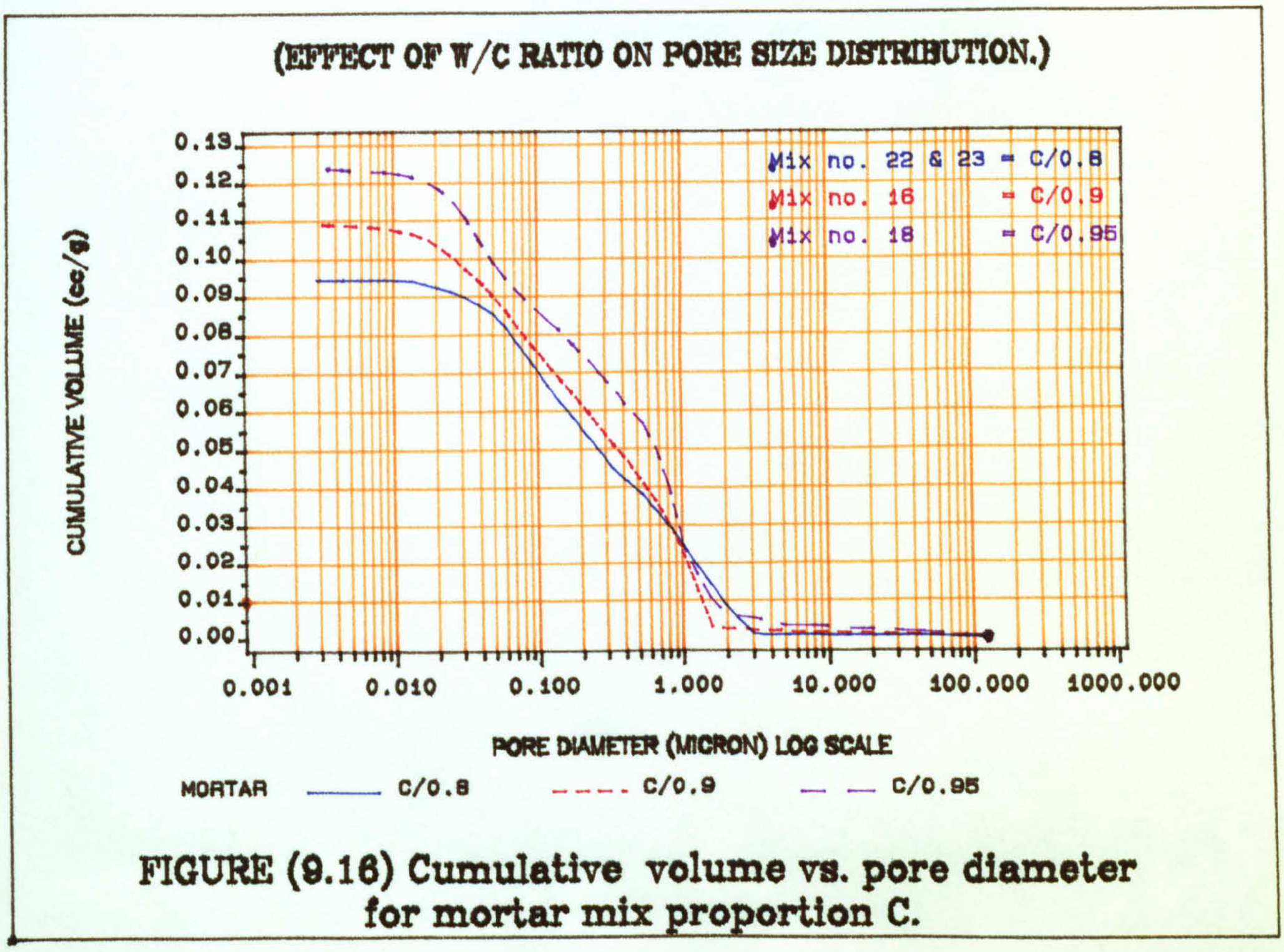

FIGURE (9.16) Cumulative volume vs. pore diameter for mortar mix proportion C.

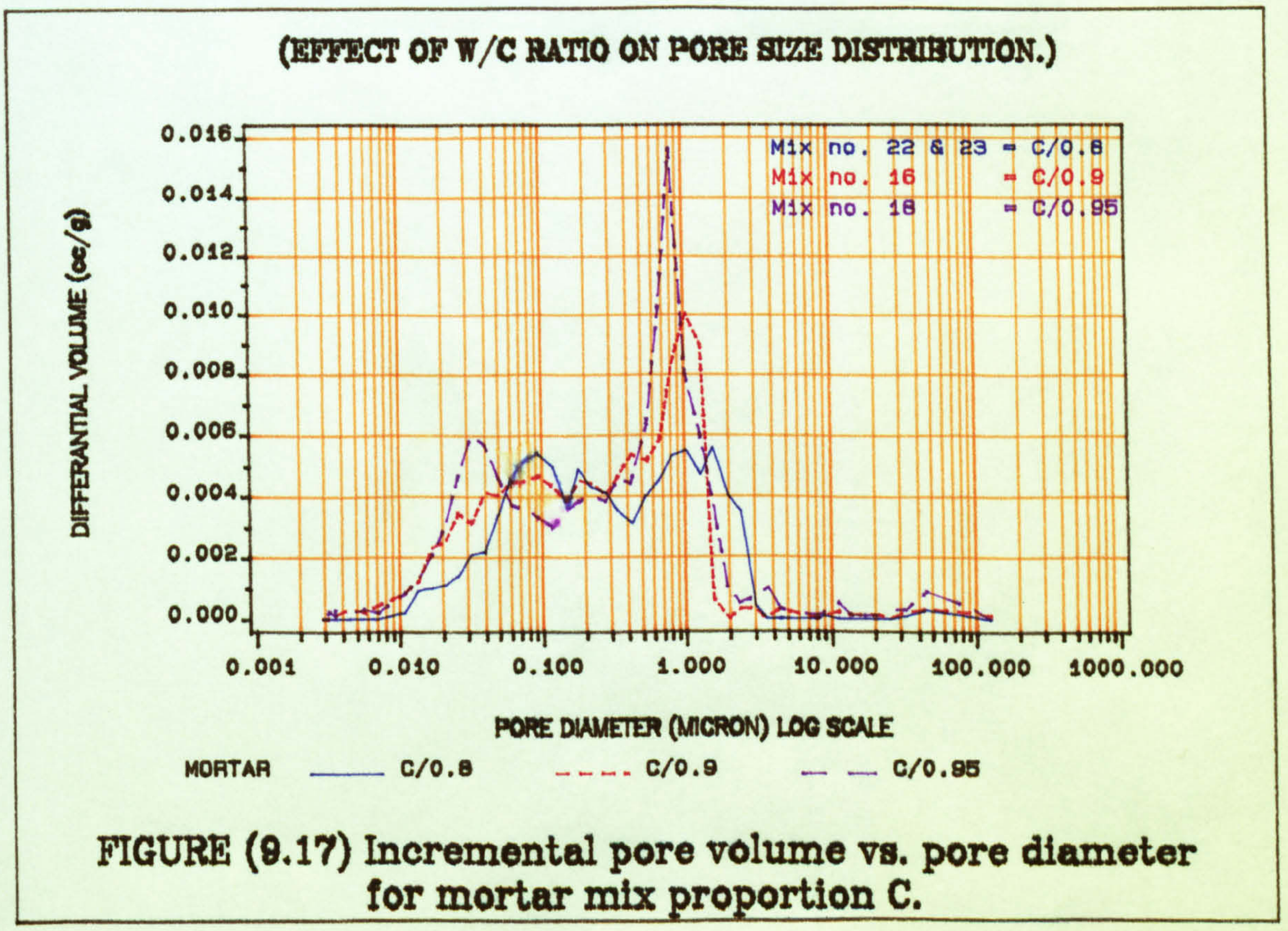

FIGURE (9.17) Incremental pore volume vs. pore diameter for mortar mix proportion C.

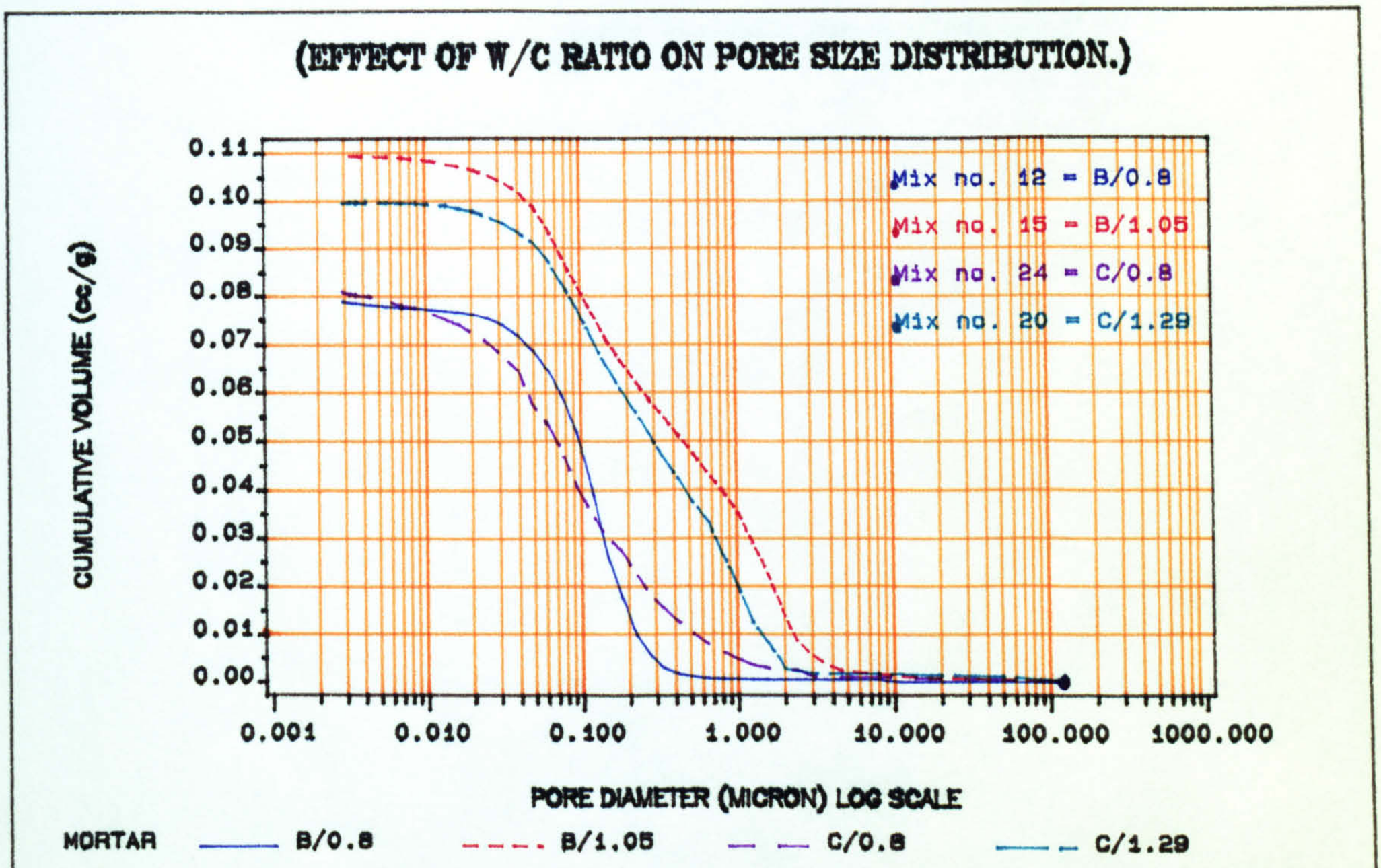

FIGURE (9.18) Cumulative volume vs. pore diameter for mortars sieved from Pellite concretes.

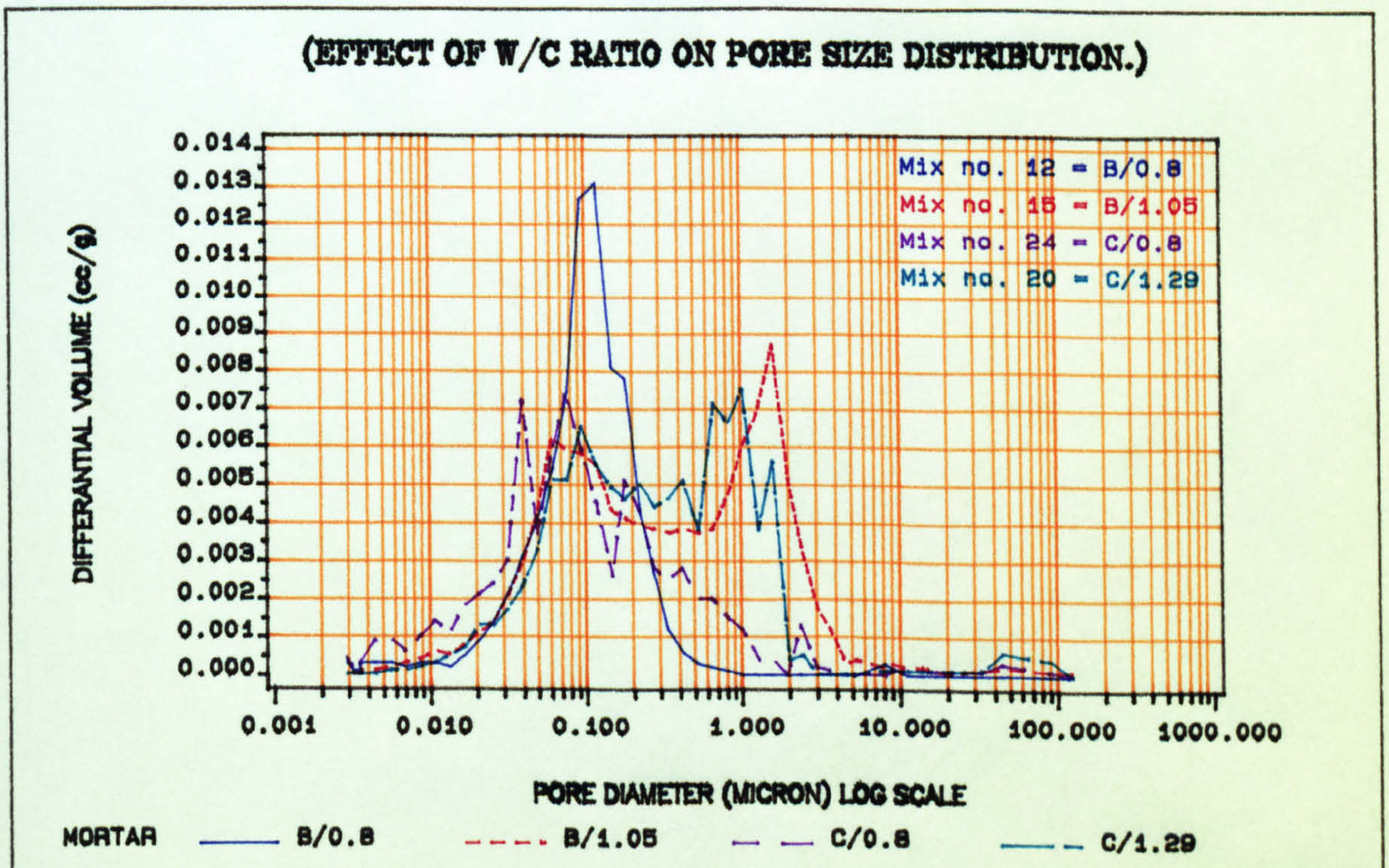

FIGURE (9.19) Incremental pore volume vs. pore diameter for mortars sieved from Pellite concretes.

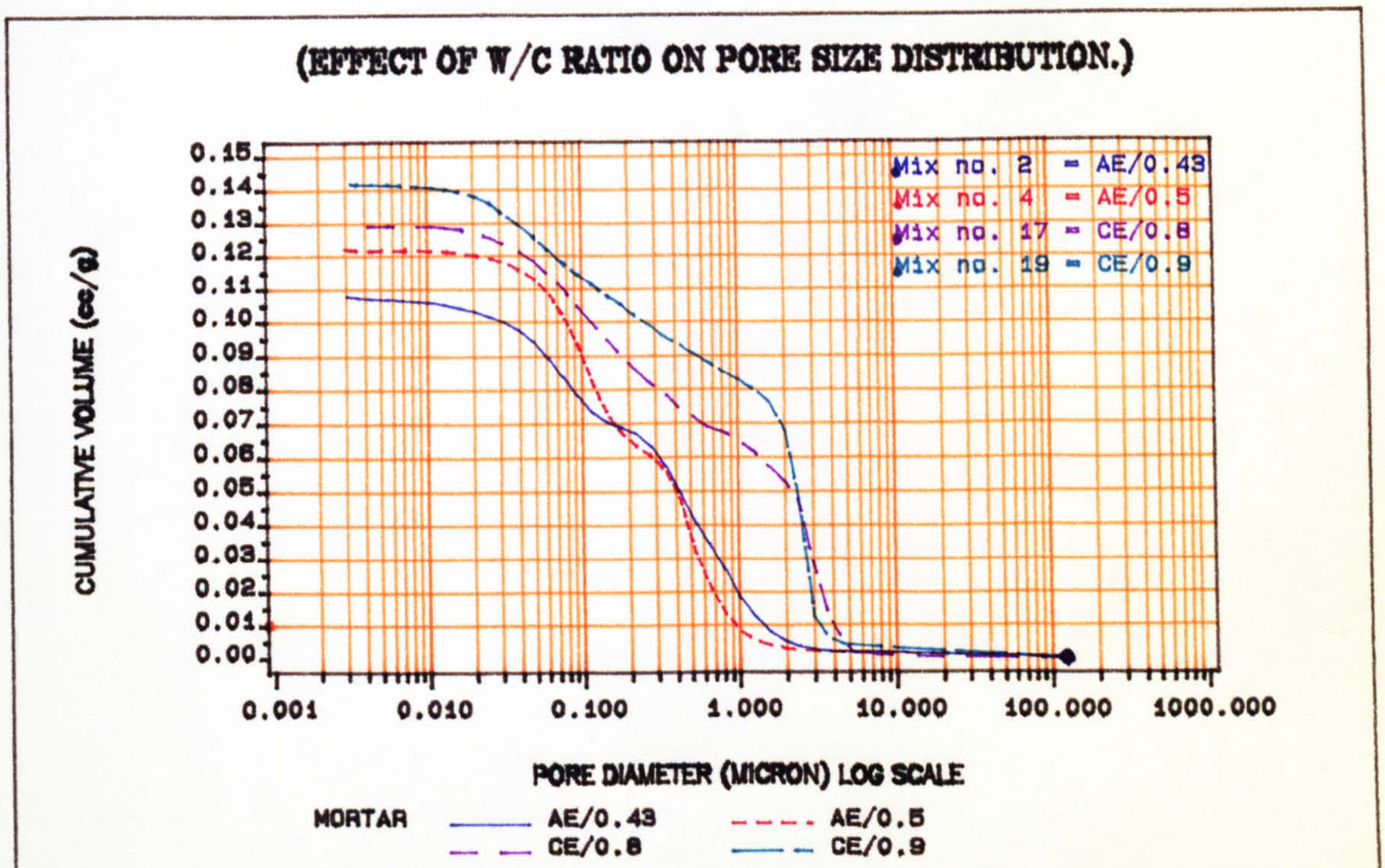

FIGURE (9.20) Cumulative volume vs. pore diameter for air entrained mortars.

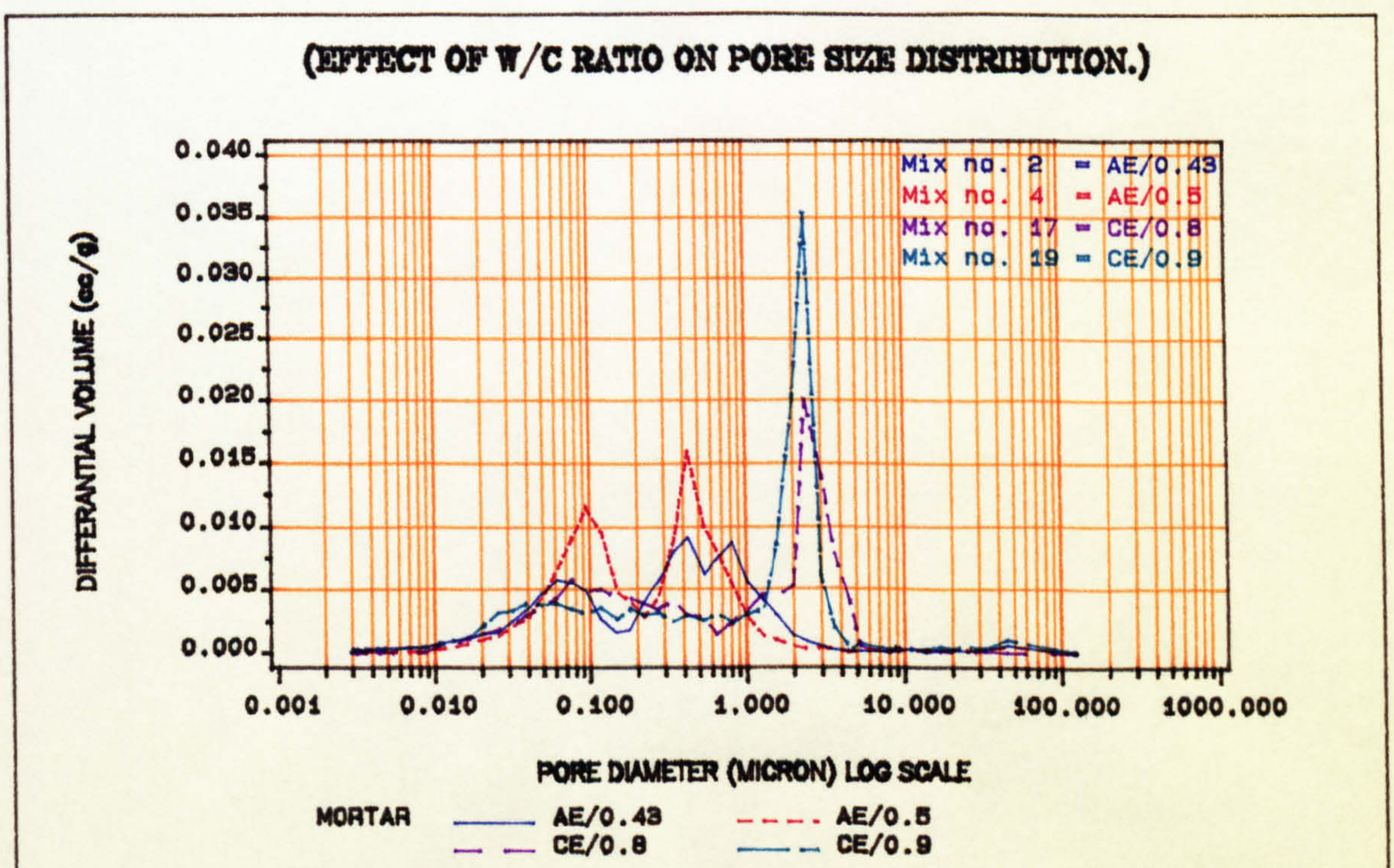

FIGURE (9.21) Incremental pore volume vs. pore diameter for air entrained mortars.

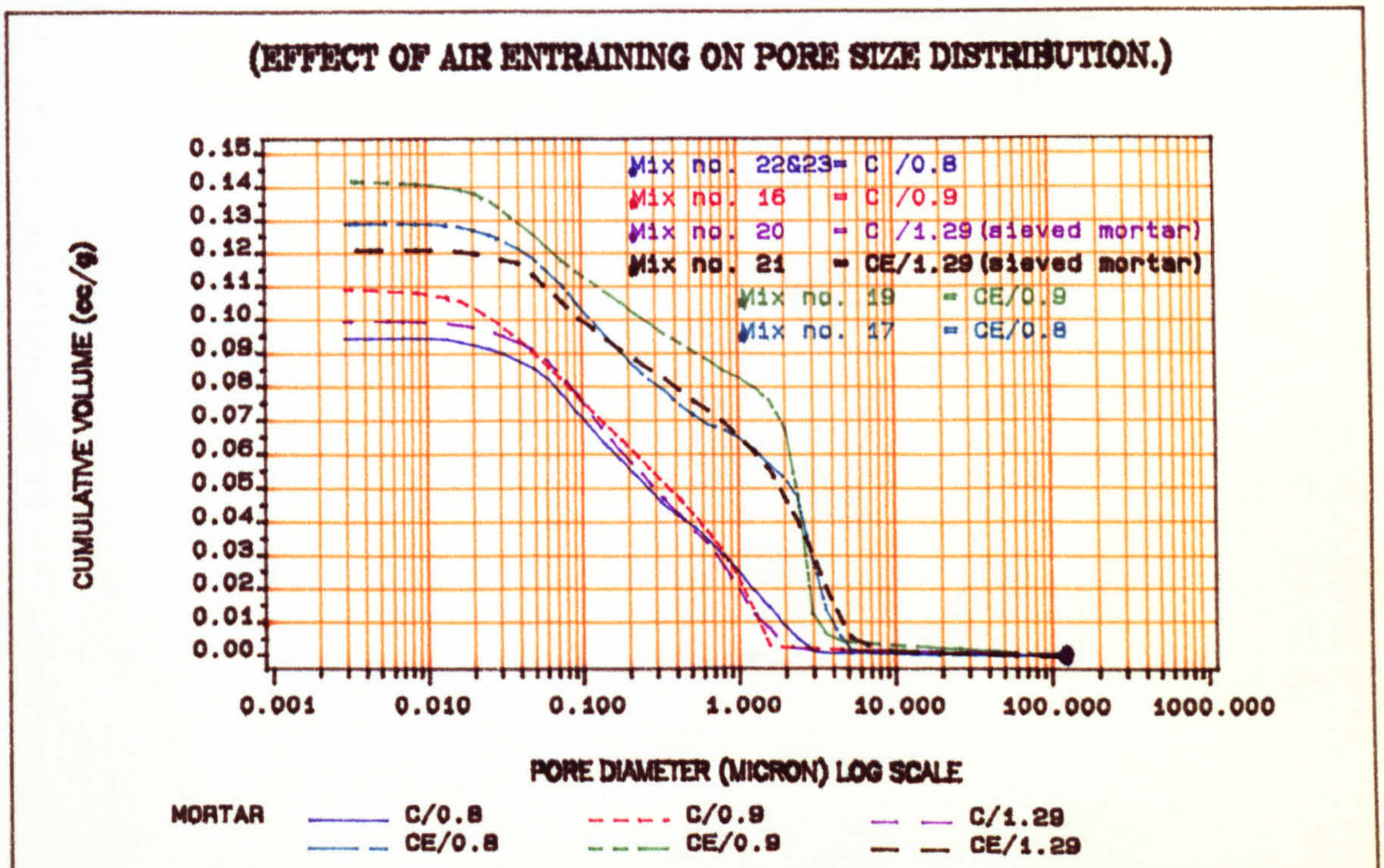

FIGURE (9.22) Cumulative volume vs. pore diameter for selected mortars.

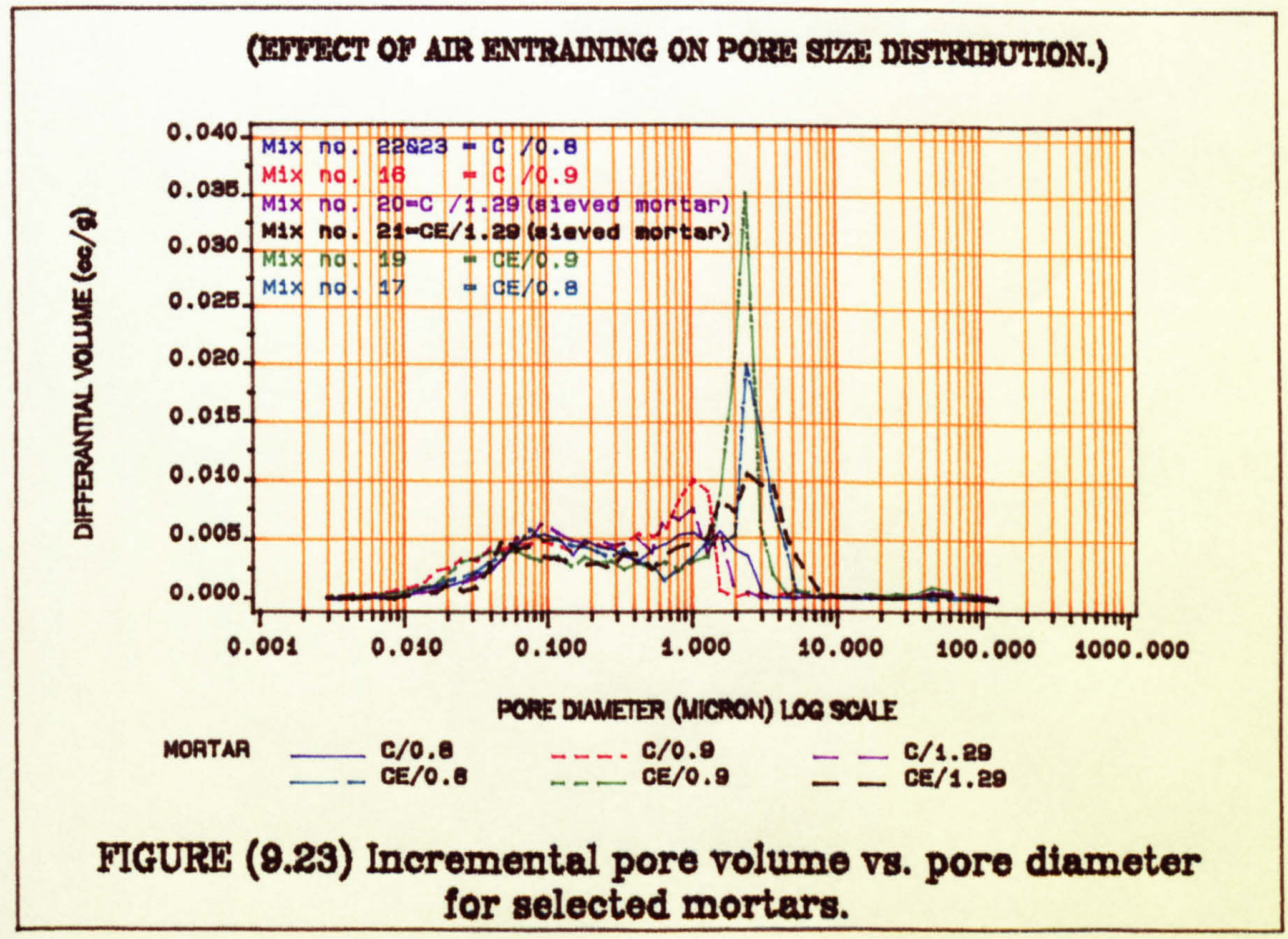

FIGURE (9.23) Incremental pore volume vs. pore diameter for selected mortars.

9.3 Vacuum saturation

The total porosity results of concretes obtained by vacuum saturation are given in Table 8.3. The porosity values reported are average of two results per test. The variation was within 1% of the mean (few instances reached 3%). This confirms the repeatability of the test procedure used.

The effect of different variables on the total porosity of concretes can be studied from Table 8.3 and are shown below:

a) Effect of successive curing and age

Comparison of total porosity values for the eight concrete mixes which were cured successively in various curing conditions do not show a general trend but they show that successive curing has not affected the total porosity values significantly (as shown on the MIP measurement done with mortar samples). The slight reduction on the porosity from 'A' curing condition to 'E' curing condition is thought to be due to the increased age of concretes since porosity decreases with time as a function of hydration. The porosity values of the eight mixes which were cured successively are within 7% of their mean and their standard deviation values in all cases are below 1.58. The mean and standard deviation of these mixes are shown in Table 9.2.

Table (9.2)

Mean and standard deviation of successively cured mixes

Mix no.	Mix code name	Mean porosity value	Standard deviation
1	QA /0.53	12.1	0.49
2	QAE/0.43	13.7	0.54
13	QB /0.56	9.7	0.38
16	QC /0.9	14.9	0.59
18	LC /0.95	16.1	1.07
19	LCE/0.9	24.9	0.91
20	PC /1.29	24.7	1.00
21	PCE/1.29	36.6	1.58

b) Effect of type of coarse aggregate

Since Pellite aggregates have higher porosity than limestone and limestone aggregates have higher porosity than quartz their concretes show higher porosities also. From Table 8.3 it can be seen that Pellite concretes have total porosity values between about 20% to 26% , Limestone concretes have porosity values between 12% to 17.5% and Quartzitic concretes have porosity values between 10% to 15% . The effect of type of coarse aggregate can be seen better in Figure 9.24 by comparing the following mixes: (7, 8, 9), (10, 11, 12) and (22, 23, 24).

c) Effect of water-cement ratio

Since the porosity of mortar increases by increasing W/C ratio, the total porosity of concrete is also slightly increased. This can be seen in Figure 9.25. Mixes of nearly the same age have been compared against each other. In this figure Quartz concrete shows 1% increase, Limestone concrete

shows 1.4% and Pellite concrete shows 0.7% increase in porosity for each 0.1 increase in W/C ratio.

d) Effect of air entraining

Since air entrainment increases porosity of mortars, the total porosity of concrete is also increased. This is shown in Figure 9.26. In this Figure comparison is made for mixes which have nearly the same age and close W/C ratios. For these mixes percentage increase of total porosity varies between about 9 to 83 per cent.

e) Effect of mix proportion

The effect of mix proportion on total porosity of concretes is dependent on the proportion of mortar to particular coarse aggregate and the porosities of mortar and the particular aggregate. Comparison of total porosities of mixes which have nearly the same age and W/C ratios are made in Figure 9.27. Changing mix proportion 'A' to 'B' or 'C' reduces porosity in the case of quartz and limestone concretes. This is because the volume of mortar which has a higher porosity is reduced in the mix proportion 'B' and 'C' for quartz and limestone concretes. (comparing mix number 1 to 13, 7 to 22 and 8 to 23 in Figure 9.27). On the other hand changing mix proportion 'A' to 'B' and 'C' for pellite concrete increases the total porosity since the pellite aggregate volume (which has higher porosity than mortar) is increased in mix proportion 'B' and 'C'. This can be seen by comparing mix number 9 with 24 in Figure 9.27.

9.3.1 Comparison of vacuum saturation porosity and calculated MIP porosity of concrete

Calculated total porosity values of concretes studied are tabulated in Table 9.3. These values are derived using calculated MIP porosities of mortar mixes (Table 8.2) and mortar :coarse aggregate proportion by volume in each concrete mix (calculated from mix proportion by mass and MIP's dry densities). The porosities of coarse aggregates calculated from their MIP porosities and proportion of each aggregate grade used in the mix (see Table 3.3) are as follow: -

Coarse aggregate	Calculated Porosity (%)
Quartz	4.0
Limestone	5.4
Pellite	25.2

For comparison purposes the vacuum saturation total porosity (from Table 8.3) is also given in the right hand column of Table 9.3. As it can be seen from this table the porosity values obtained by vacuum saturation are higher than MIP derived porosity values. This difference may be attributed to the volume of pores generated at the aggregate mortar interfaces which result from the localised bleeding of a concrete mix. This effect is more pronounced in case of air entrained concretes. The difference between calculated and measured porosity is also due to the existence of large pores with narrow entries (closed pores) which mercury can not penetrate[112,114]. In the light of these results the concrete porosity values obtained by the vacuum saturation technique will be used for studying the relationship between porosity and thermal conductivity of concrete in the following sections.

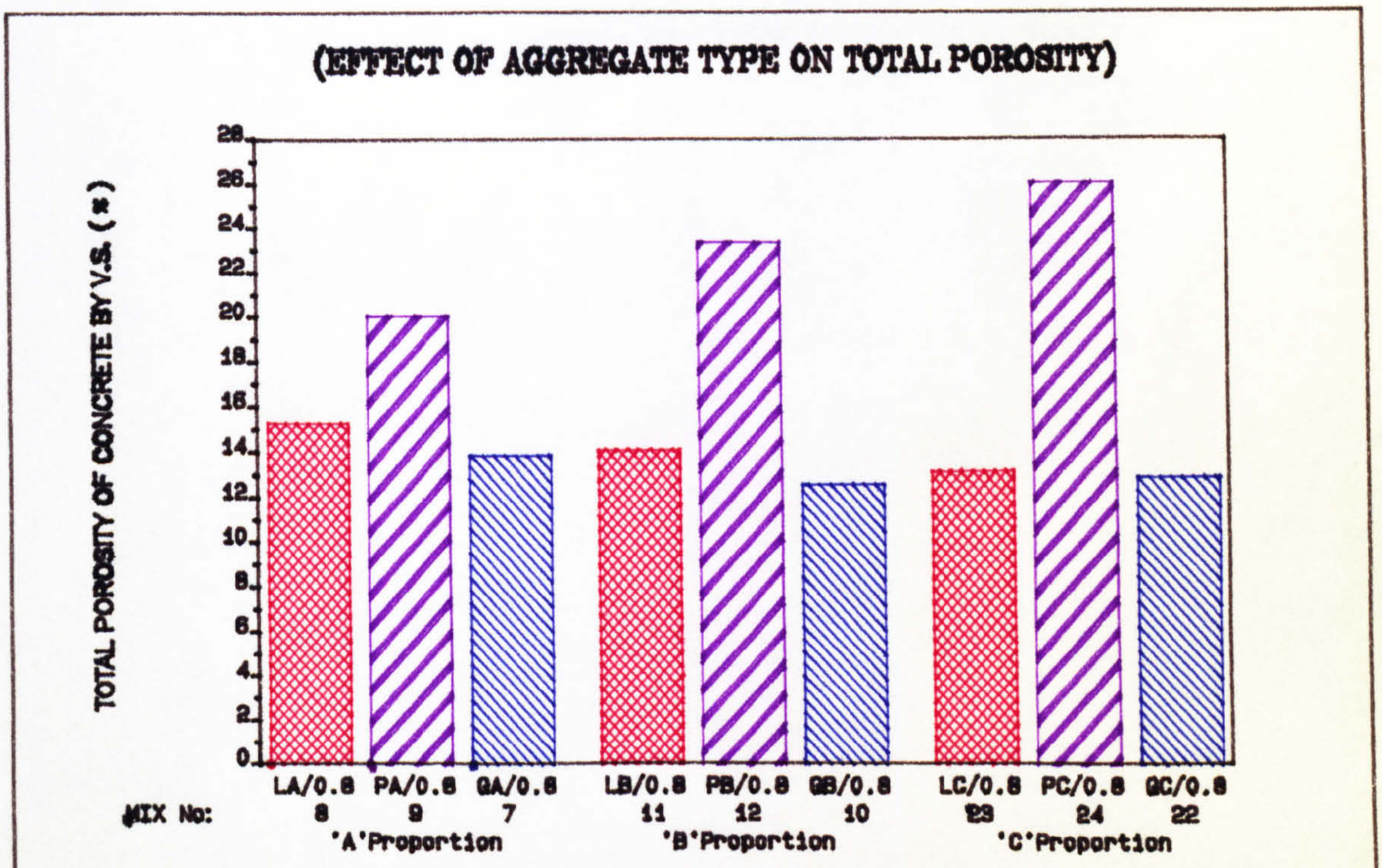

FIGURE (9.24) Bar chart representation of total porosity for selected concretes

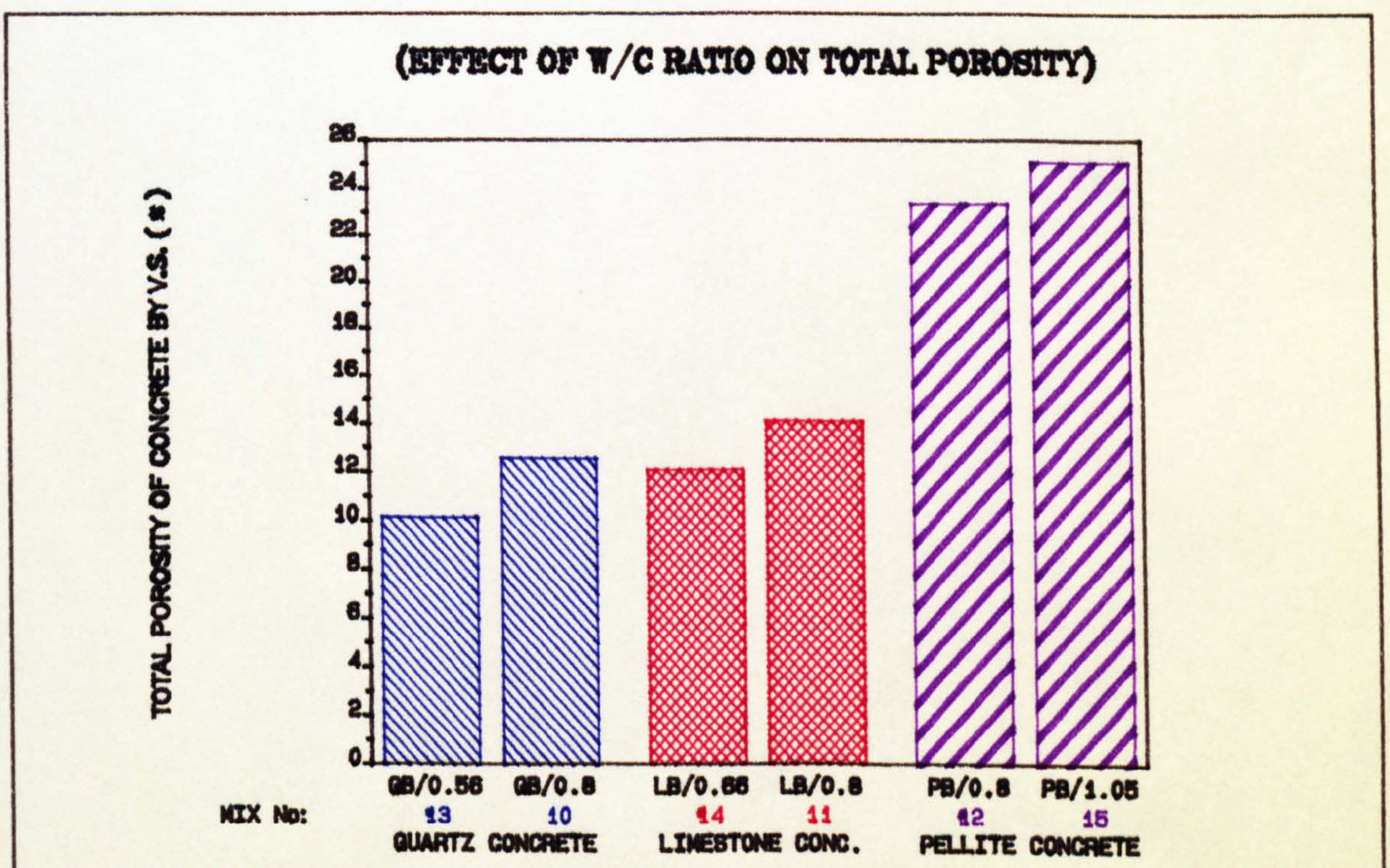

FIGURE (9.25) Bar chart representation of total porosity for selected concretes

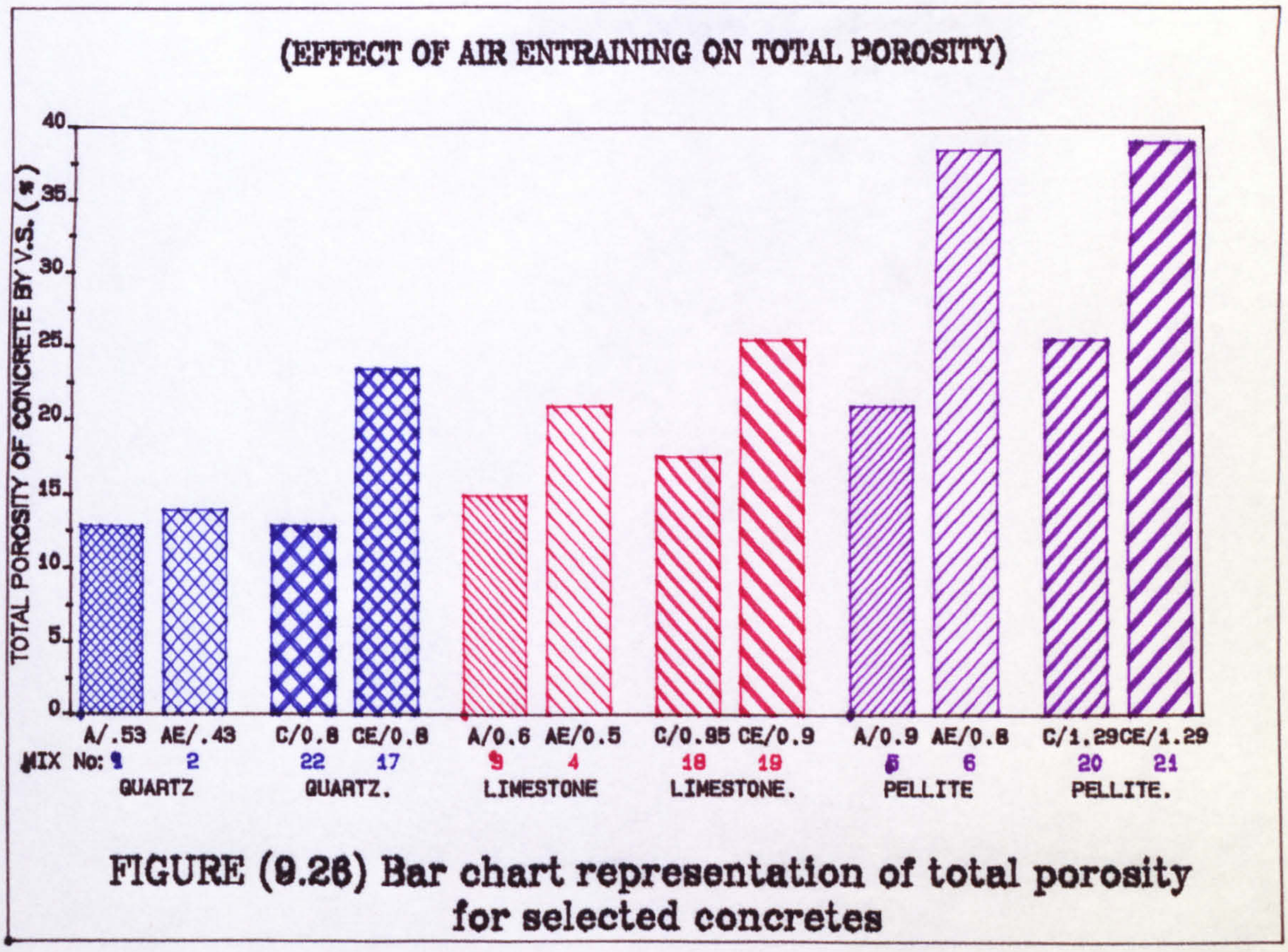

FIGURE (9.26) Bar chart representation of total porosity for selected concretes

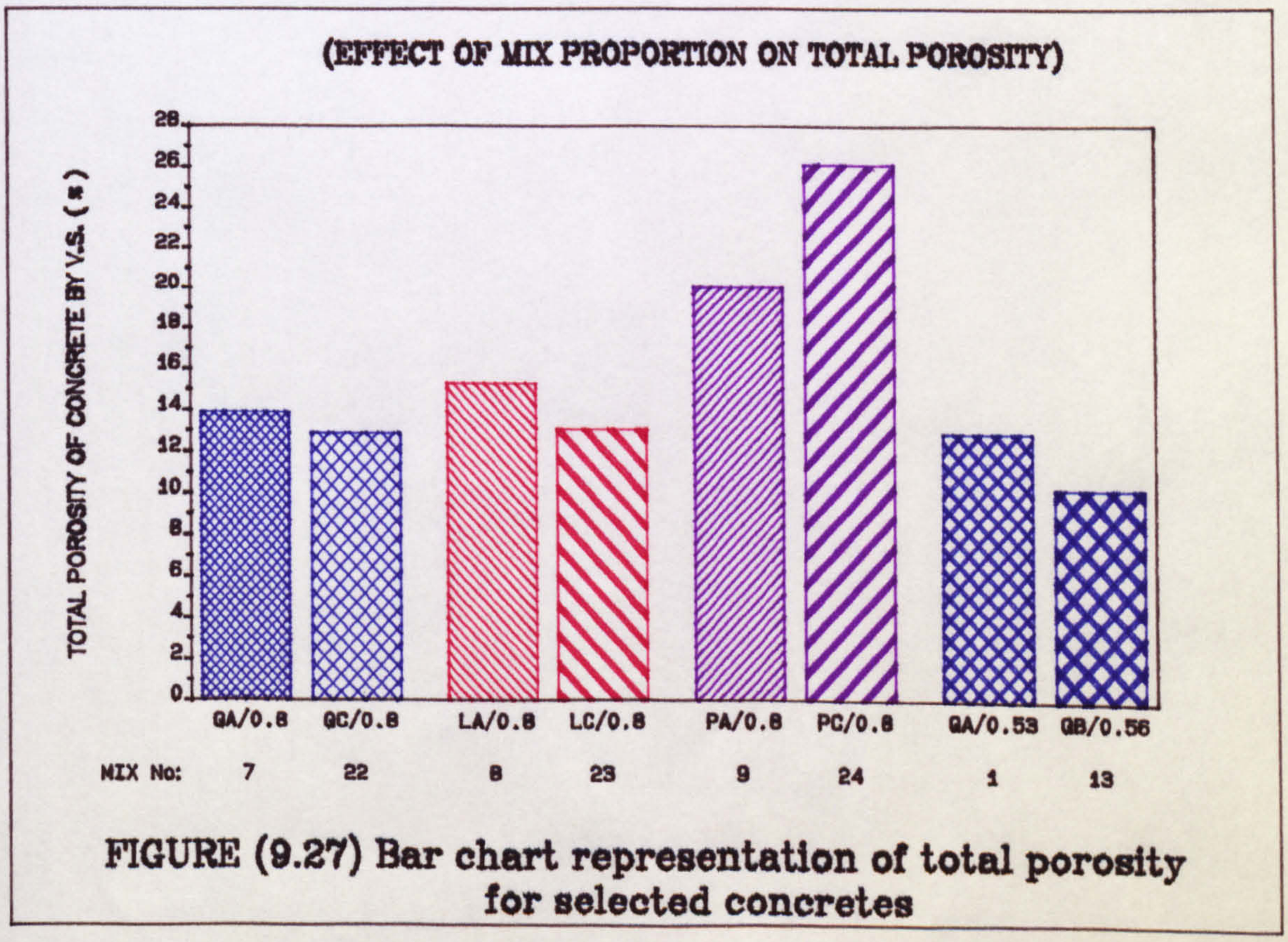

FIGURE (9.27) Bar chart representation of total porosity for selected concretes

Table (9.3)

Comparison of calculated MIP and vacuum saturation porosities of concretes.

Mix No.*	Concrete Code Name	MIP calculated Mortar Porosity (%)	Mortar :Agg (By vol.)	MIP calculated Total Porosity (%)	V.S. Total Porosity (%)
1A		16.5		10.7	12.9
1B		16.8		10.8	11.7
1C	QA/0.53	16.2	53.4 : 46.6	10.5	11.7
1D		16.1		10.5	12.2
1E		16.2		10.5	12.0
2A		20.9		13.5	14.0
2B		19.3		12.6	14.5
2C	QAE/0.43	21.6	56.1 : 43.9	13.9	13.5
2D		21.4		13.8	13.5
2E		21.6		13.9	13.1
3	LA/0.6	17.1	54.4 : 45.6	11.8	15
4	LAE/0.5	22.8	56.4 : 43.6	15.2	21
5	PA/0.9	22.7	48.9 : 51.1	24.0	21
6	PAE/0.8	23.9	50.0 : 50.0	24.6	38.5
7	QA/0.8	18.1	54.8 : 45.2	11.7	13.9
8	LA/0.8	18.1	54.4 : 45.6	12.3	15.3
9	PA/0.8	16.5	47.7 : 52.3	21.1	20.1
10	QB/0.8	19.6	44.0 : 56.0	10.9	12.6
11	LB/0.8	19.6	43.6 : 56.4	11.6	14.1
12	PB/0.8	16.2	35.7 : 64.3	22.0	23.4
13A		16.8		9.5	10.2
13B		16.5		9.4	9.4
13C	QB/0.56	16.0	42.9 : 57.1	9.1	9.4
13D		16.4		9.3	10.1
13E		16.6		9.4	9.6
14	LB/0.66	17.5	42.8 : 57.2	10.6	12.1
15	PB/1.05	20.8	37.5 : 62.5	23.6	25.1
16A		21.3		13.0	15.1
16B		18.3		11.5	15.7
16C	QC/0.9	20.5	52.3 : 47.7	12.6	14.8
16D		19.3		12.0	14.1
16E		18.3		11.5	14.6

(*) Letters after mix numbers indicate the curing conditions.

Table (9.3) (continued)

Mix No.*	Concrete Code Name	MIP calculated Mortar Porosity (%)	Mortar :Agg (By vol.)	MIP calculated Total Porosity (%)	V.S. Total Porosity (%)
17	QCE/0.8	23.8	54.1 : 45.9	14.7	23.5
18A		22.5		14.4	17.6
18B		20.3		13.2	16.9
18C	LC/0.95	21.3	52.6 : 47.4	13.8	15.6
18D		20.5		13.3	15.3
18E		22.3		14.3	15.2
19A		26.2		16.7	25.5
19B		25.4		16.3	25.3
19C	LCE/0.9	26.5	54.3 : 45.7	16.9	25.9
19D		24.9		16.0	24.3
19E		26.1		16.6	23.7
20A		20.0		22.8	25.5
20B		17.9		21.9	25.3
20C	PC/1.29	22.4	45.2 : 54.8	23.9	24.6
20D		21.4		23.5	25.0
20E		21.7		23.6	23.0
21A		22.9		24.1	39.0
21B		22.0		23.7	36.7
21C	PCE/1.29	22.9	45.8 : 54.2	24.1	35.8
21D		22.5		24.0	36.8
21E		20.5		23.0	34.7
22	QC/0.8	18.8	52.2 : 47.8	11.7	12.9
23	LC/0.8	18.8	51.8 : 48.2	12.3	13.1
24	PC/0.8	16.5	44.2 : 55.8	21.4	26.1

(*) Letters after mix numbers indicate the curing conditions.

- SUMMARY -

- The successive curing used for establishment of moisture correction factors does not significantly affect the total porosity of concretes.

- The total porosity values are more dependent upon type of coarse aggregate and mix proportions than W/C ratio of concretes.

- Air entrainment increases total porosity considerably (by as much as about 80% in some cases).

9.4 Thermogravimetry

The degree of hydration for the various mortar mixes calculated from calcium hydroxide content and from combined water are shown in Table 8.4.

This results indicate that the different concrete mixes are highly hydrated. The degree of hydration calculated from the calcium hydroxide content is on average 69.4 per cent. The variation are not wide enough to assess the influence of degree of hydration on thermal conductivity or porosity and pore size distribution.

The curing regimes which were used implied that hydration differences would not be substantial. As it is known after 90 days of curing most of the cement hydrates [133,136]. Samples were cured for at least 120 days under 'A' curing regime thus all of the samples had reached high degree of hydration before being cured under 'B' to 'E' condition.

Comparison of calcium hydroxide content to non-evaporable water results shows that the degree of hydration calculated from the amount of structural water is always lower than that calculated from calcium hydroxide. This is not unusual, since other investigators have found the same trends[108,142]. The important fact is that both results show that all samples have hydrated approximately to the same degree (the degree of hydration calculated from the structural water content is on average 67.8 per cent).

The results of carbonation measurements (Table 8.4) show that all mixes are slightly carbonated and that the degree of carbonation values seem higher than values reported

for OPC concretes hydrated to the same degree. However for the present study it should be remembered that specimens were exposed to 65% RH and 20°C for long periods. This condition has been found to provide optimal condition for carbonation [147]. Here again the differences of the degree of carbonation are not marked for different curing regimes.

The results also indicate that most concrete mixes have carbonated to the same extent upto the curing time at which thermal conductivity measurements, were carried out. Thus, it was not possible to assess the effect of carbonation on the λ-values measured in this work.

A correlation between the ratio of volume of hydrated cement to volume of aggregate phase and total porosity was explored but very poor correlation was found for different type of concretes studied.

9.5 Depth of carbonation

It is generaly known that concrete mix, age, curing of concrete and condition of exposure of concrete effect the depth of carbonation layer in concrete[142,143,147]. Table 8.5 shows that depth of carbonation is dependent upon the age of specimens (compare mix numbers 5 with 9 and 16 with 22), concrete mix (compare mix numbers 7, 8, 9, with 22, 23, 24) and condition of exposure of concrete (compare mix 16 with 22). However when the specimens are tested for thermal conductivity the depth of carbonation is very small in all cases with highest value for mix number 24 (i.e. 5 mm). This shows that for this investigation the effect of carbonation on λ is insignificant, as found with TG results. From Table 8.5 it can also be seen that pellite concretes have highest carbonation depth because of their high porosity and permeability. For the same reason limestone concretes have higher carbonation depth than quartz concretes.

9.6 Interpretation of SEM results

SEM morphologies on the fractured surfaces of the coarse aggregates, (at equal magnifications) are shown in Plates 9.1 to 9.9. It can be seen from these plates that quartz aggregates have very dense morphologies (see Plates 9.1 to 9.3). Limestones have a dense macro-structure as shown in the SEM photograph at low magnification (Plate 9.4) and a relatively higher microporosity as shown at high magnifications (Plates 9.5 and 9.6). This confirms the results obtained by MIP measurements which showed limestone to have a higher porosity in the pore diameter range of 0.01 to 1 micron (i.e. Figures 8.24 and 8.25). The median pore diameter was found to be about 0.6093 μm for quartz and about 0.2777 μm for limestone. Pellite aggregates on the other hand have a porous morphology. The open vitreous internal pore structure can be seen clearly in Plate 9.9. These open pores are discrete in nature with pore sizes ranging mostly from about 1 μm upto about 300 μm in diameter. The median pore diameter for Pellite was found to be about 1.3512 μm.

SEM observations on mature mortar samples are difficult to interpret because the morphological features of the various hydrates as seen by electron microscopy are very variable not only between different hydrated mortar samples but within the same mortar sample. However, no change in morphological structure of mortar could be observed due to effect of successive curing or increasing sand-cement ratios. Furthermore at high degree of hydration, it becomes extremely difficult to identify any morphological effects of increasing

the water-cement ratio as the microstructure is quite dense and massive.

Plates 9.10 - 9.12 show typical views of the morphology observed in the mortar samples investigated. Three main constituents can be identified, C-S-H gel ground mass of hydrated products (i.e. very small irregular cryptocrystalline particles, which may have the shapes of fibres, rolled foils, tubes and plane sheets), calcium hydroxide crystals and ettringite, $C_4A\bar{S}H_{12}$. Ettringite particles occur only sporadically in most of the fields examined. Mature cement paste consists of roughly 70 per cent of C-S-H gel, about 20 per cent of well-crystallized $Ca(OH)_2$, small percentages of ettringite, monosulphate and several minor substances[116].

Observations on air-entrained specimens at low levels of magnification show the marked influence of air entraining agent on the structure in comparison with specimen containing no air-entraining agent. This comparison is shown in Plate 9.13 and 9.14 for mix number 20 and 21. As can be seen in Plate 9.14, air-entrained mortar has well-dispersed spherical pores in its structure.

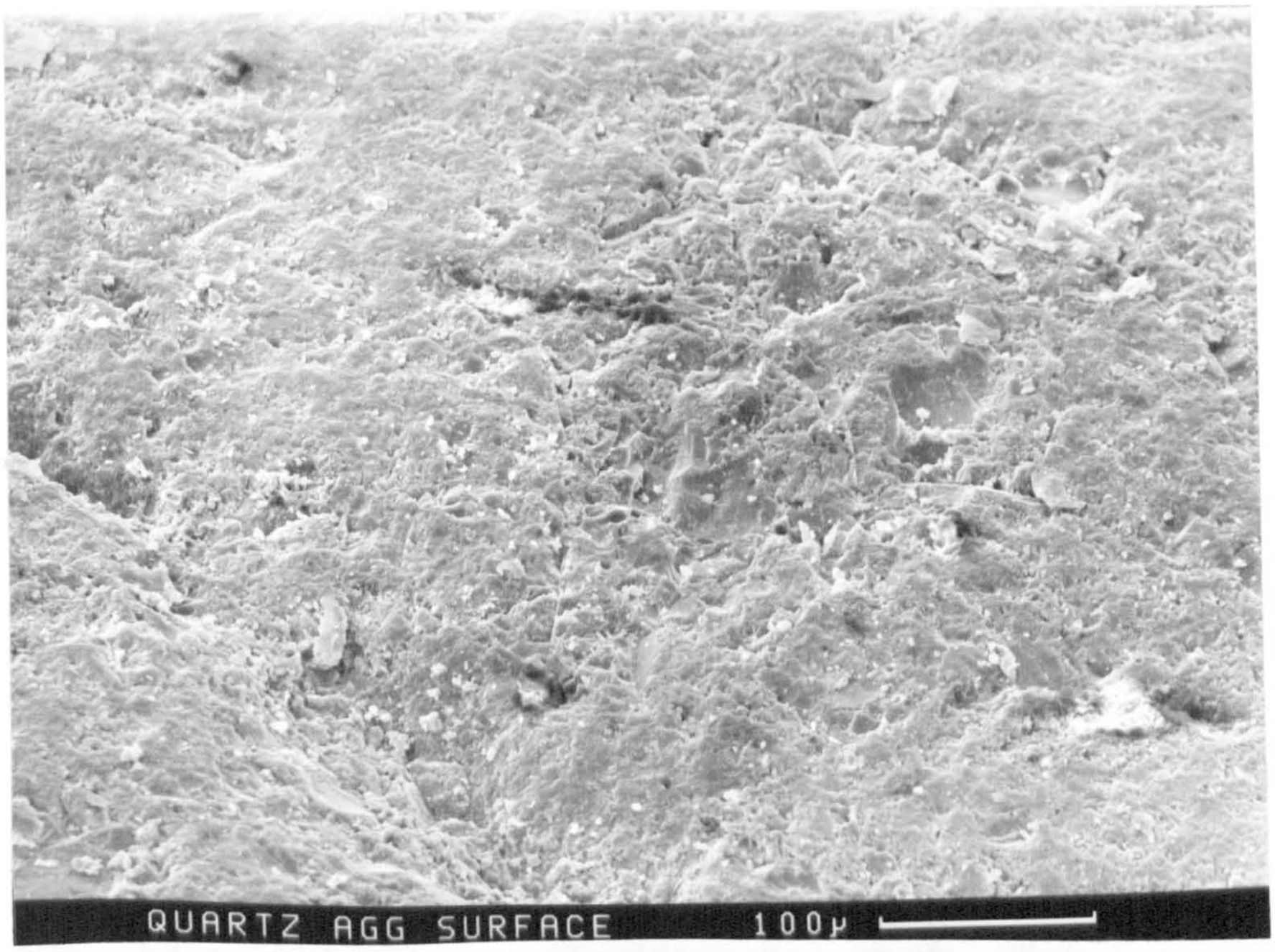

Plate 9.1 General view of the fracture surface of quartzitic aggregate magnification × 200

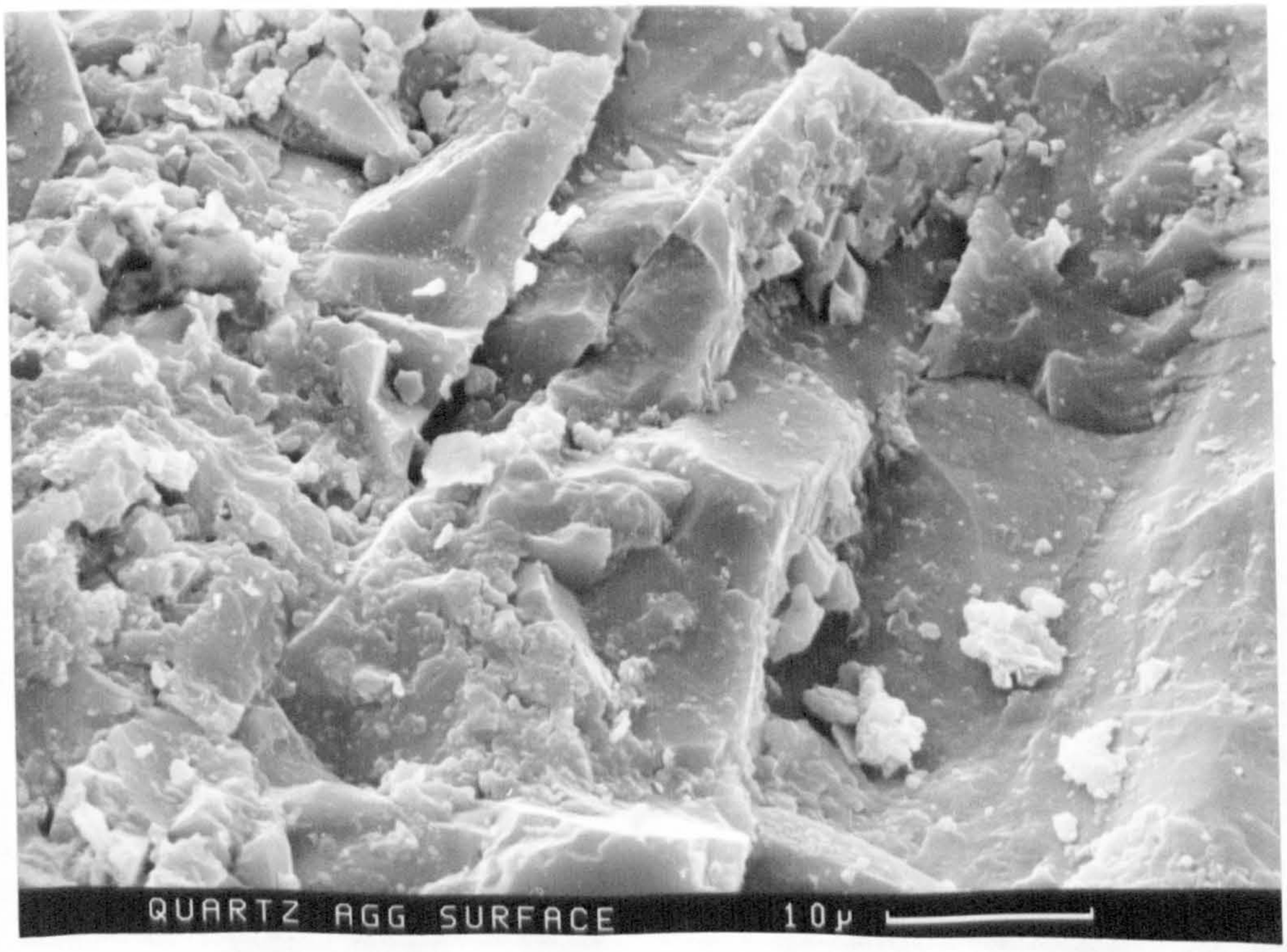

Plate 9.2 General view of the fracture surface of quartzitic aggregate magnification × 1900

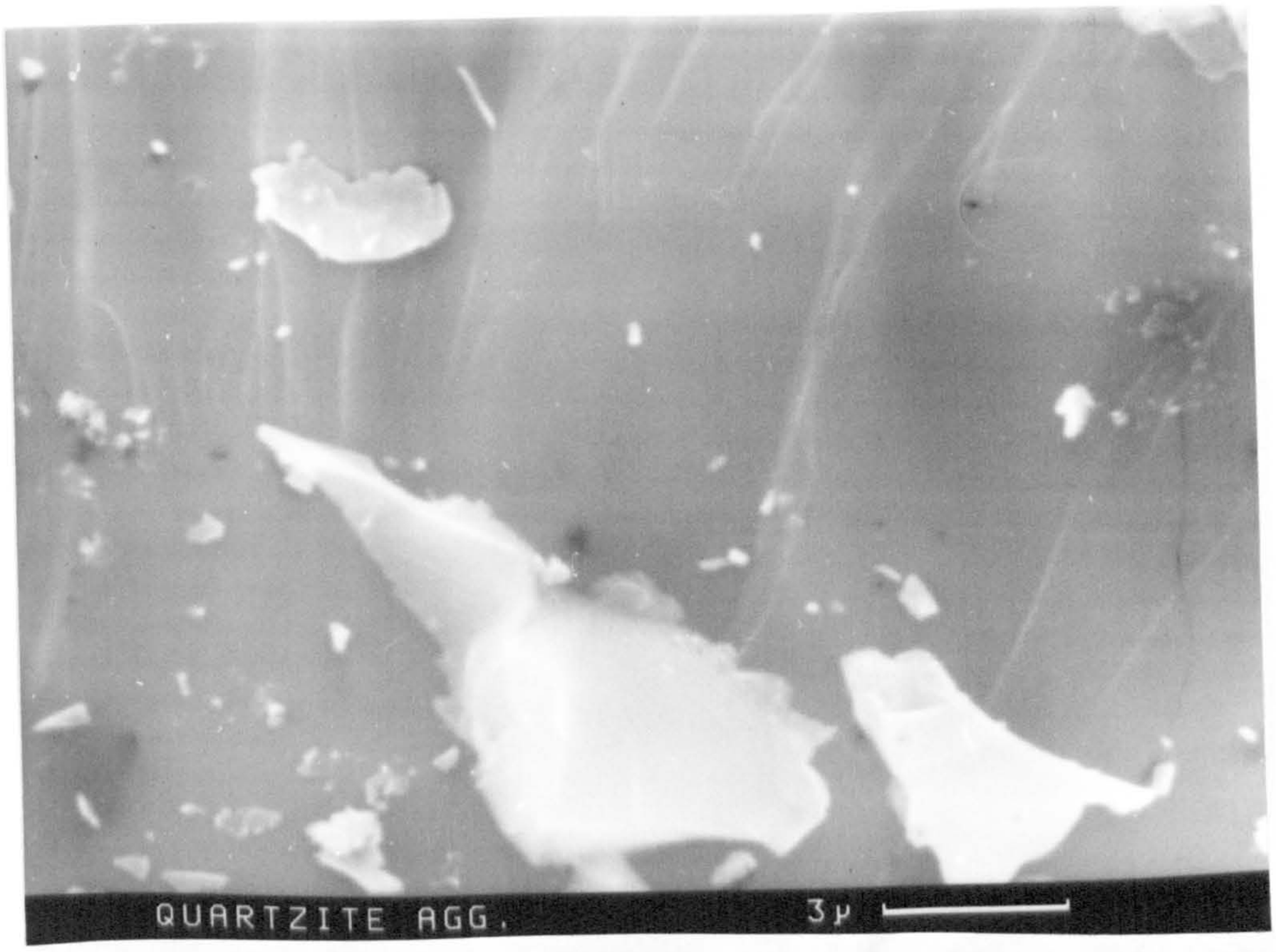

Plate 9.3 General view of the fracture surface of quartzitic aggregate magnification × 5750

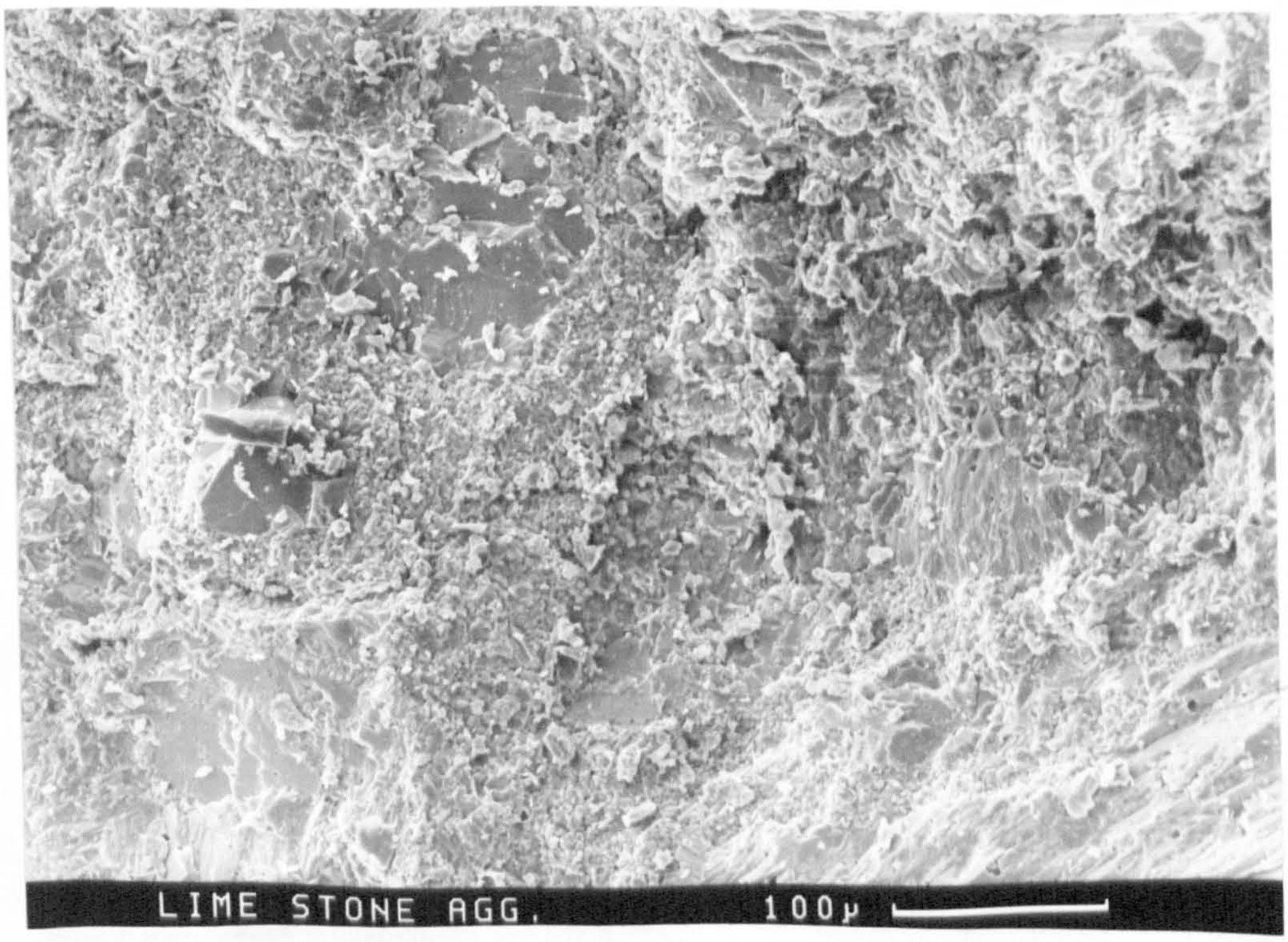

Plate 9.4 General view of the fracture surface of limestone aggregate magnification × 200

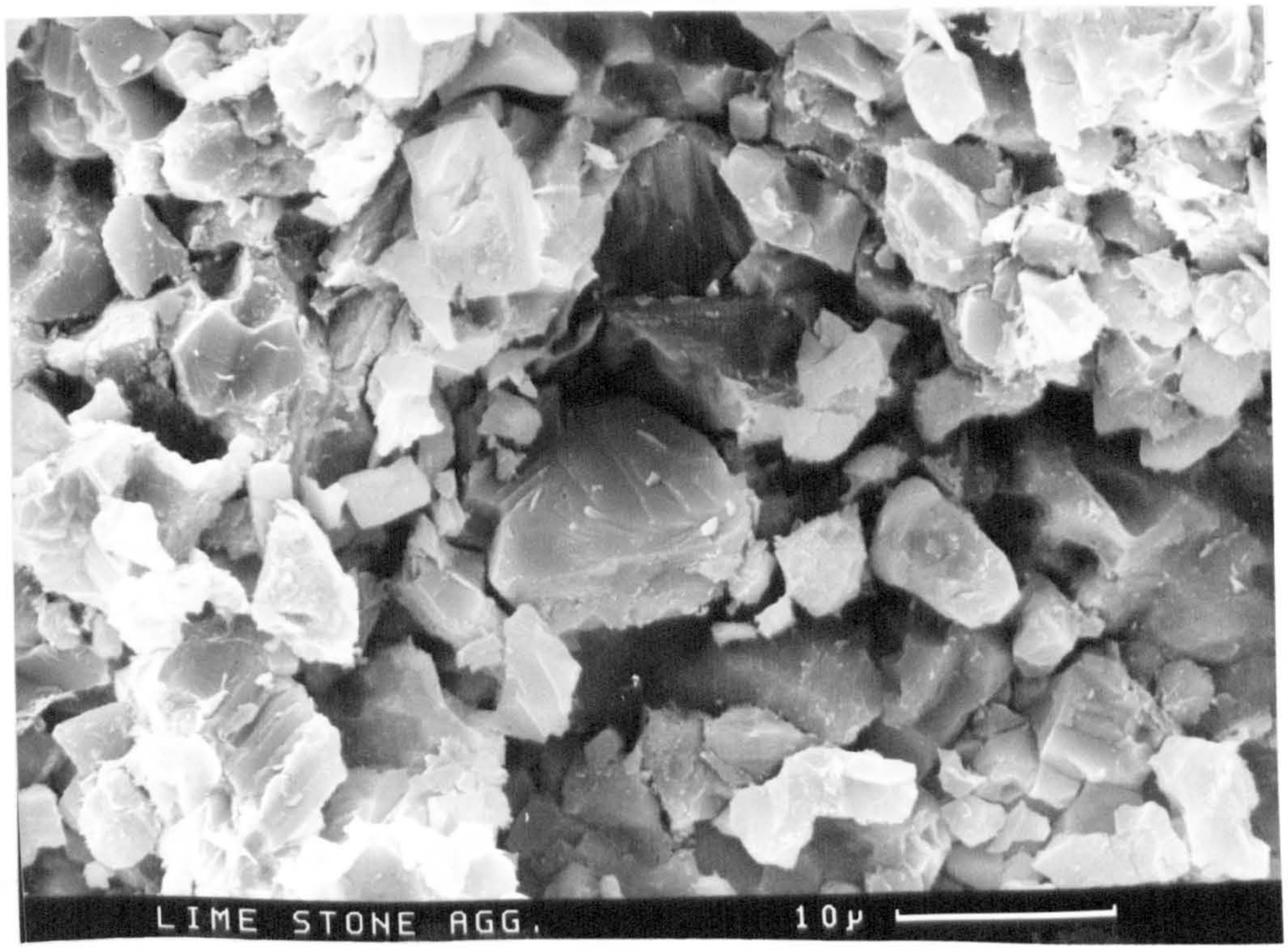

Plate 9.5 General view of the fracture surface of limestone aggregate magnification × 1900

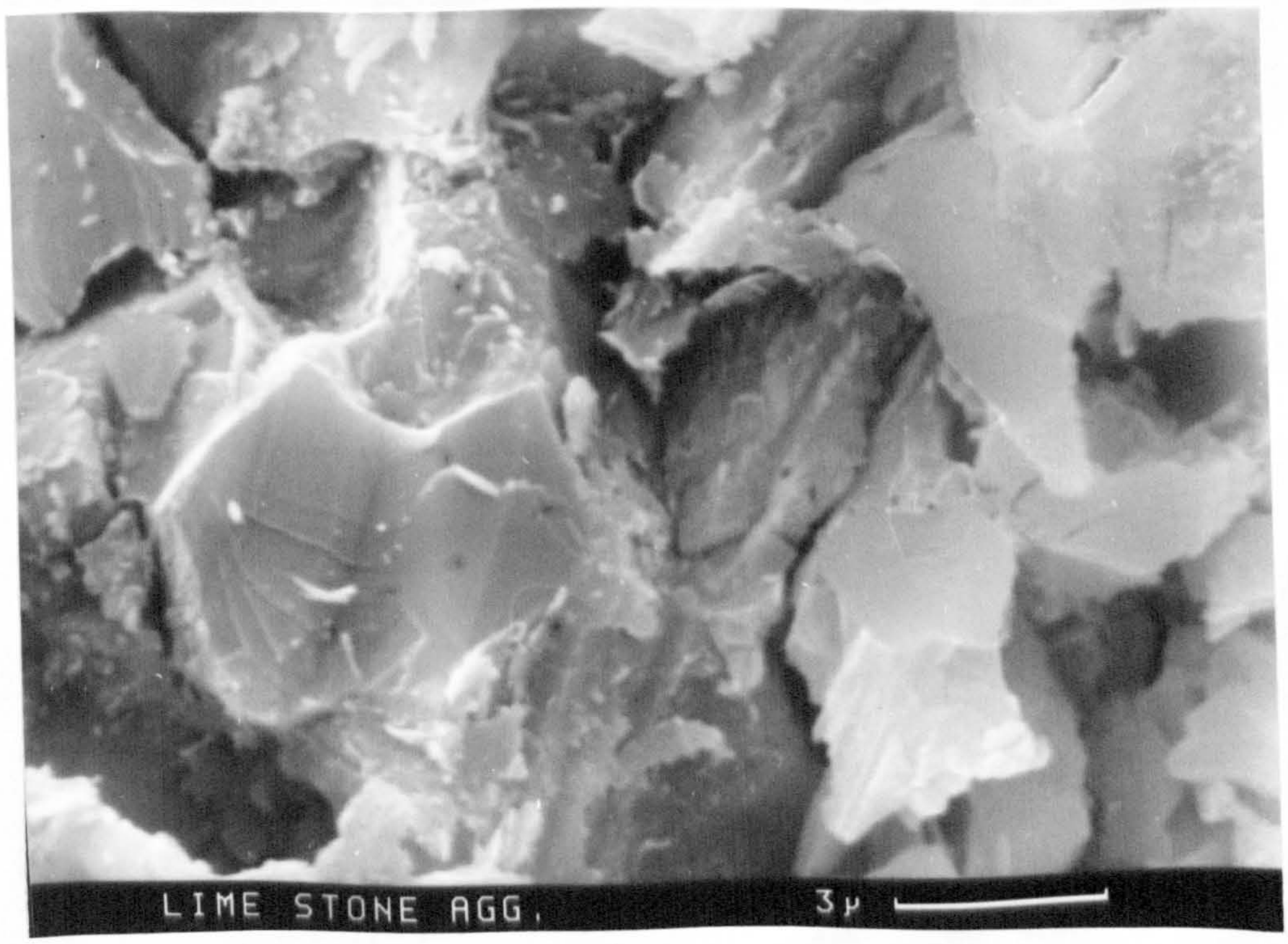

Plate 9.6 General view of the fracture surface of limestone aggregate magnification × 5750

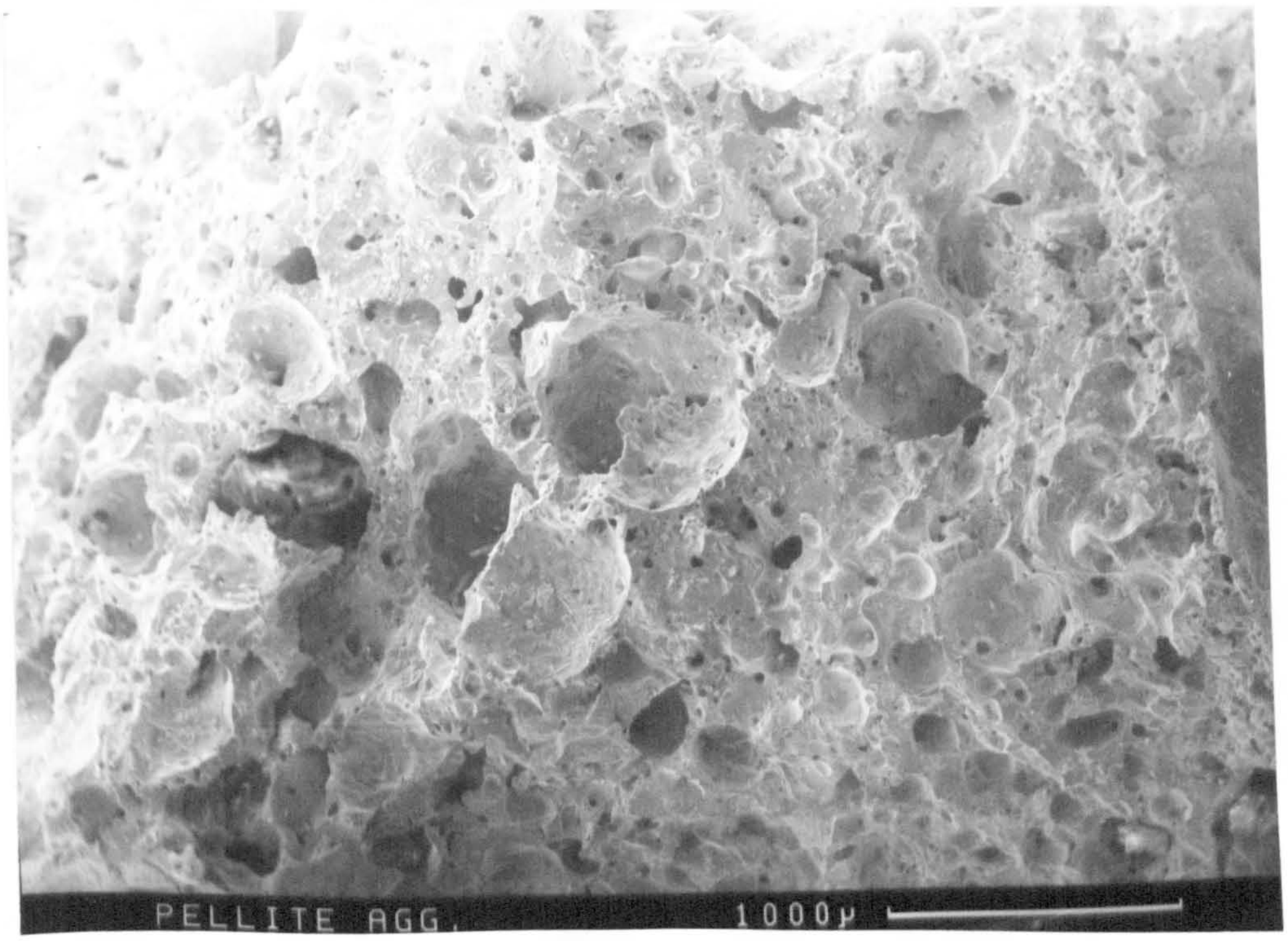

Plate 9.7 General view of the fracture surface of Pellite aggregate magnification × 27

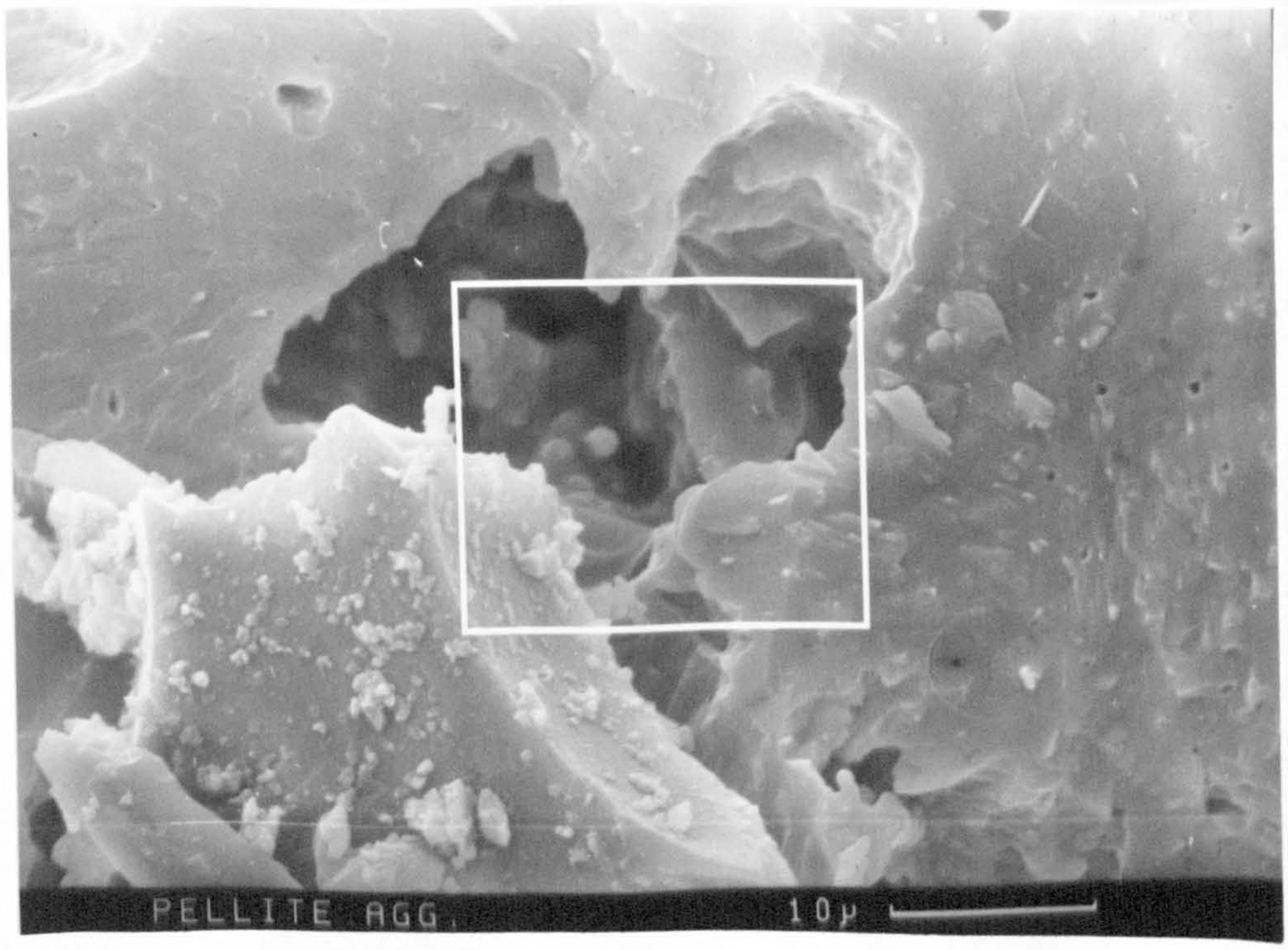

Plate 9.8 General view of the fracture surface of Pellite aggregate magnification × 1900

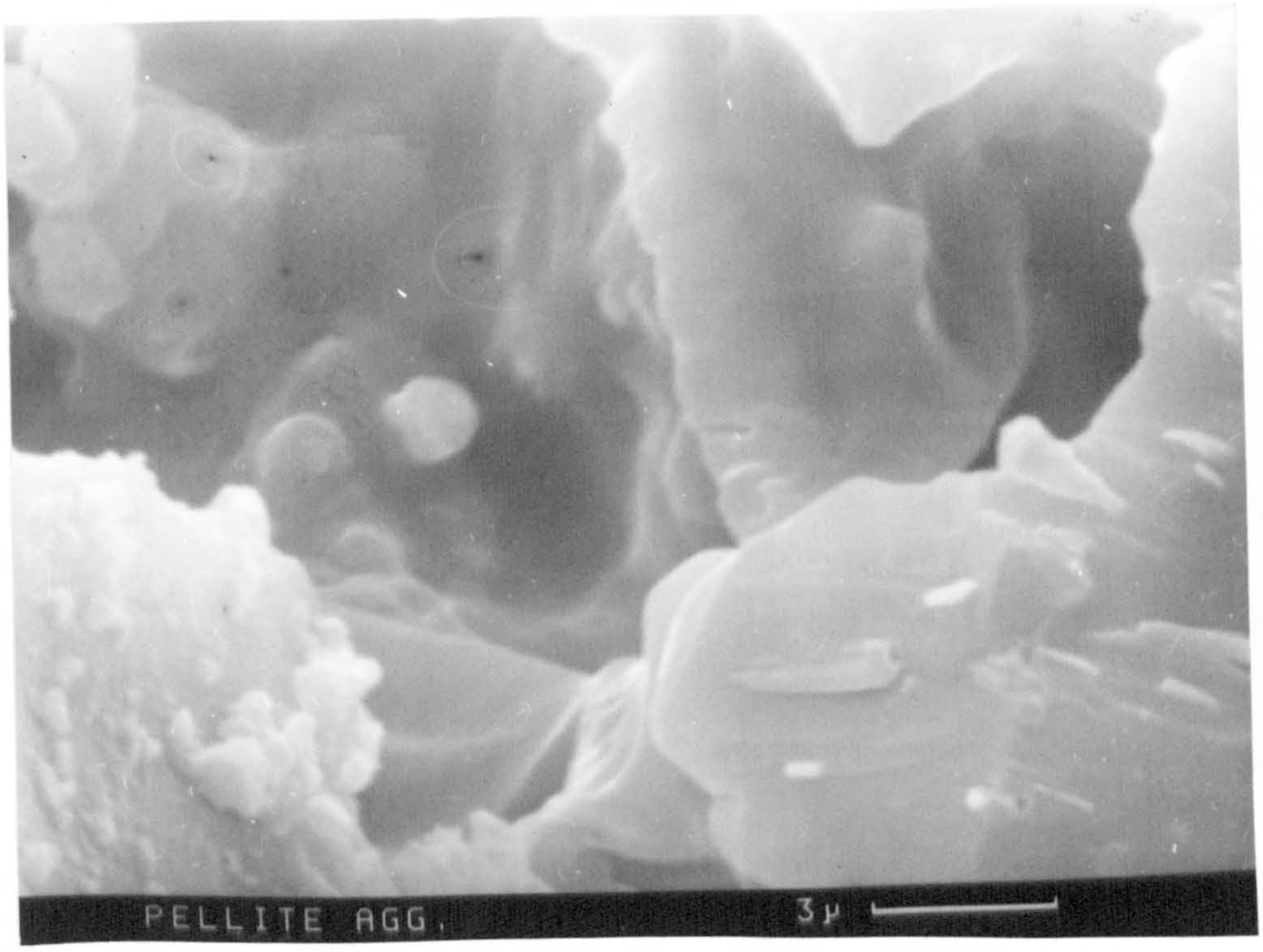

Plate 9.9 General view of the fracture surface of Pellite aggregate showing a close-up view of an area marked in Plate 9.8 magnification × 5750

Plate 9.10 SEM micrograph illustrating a typical fracture surface of mortar mix number 20 (Magnification × 1920). The C-S-H gel (honeycomb morphology) are visible in this micrograph.

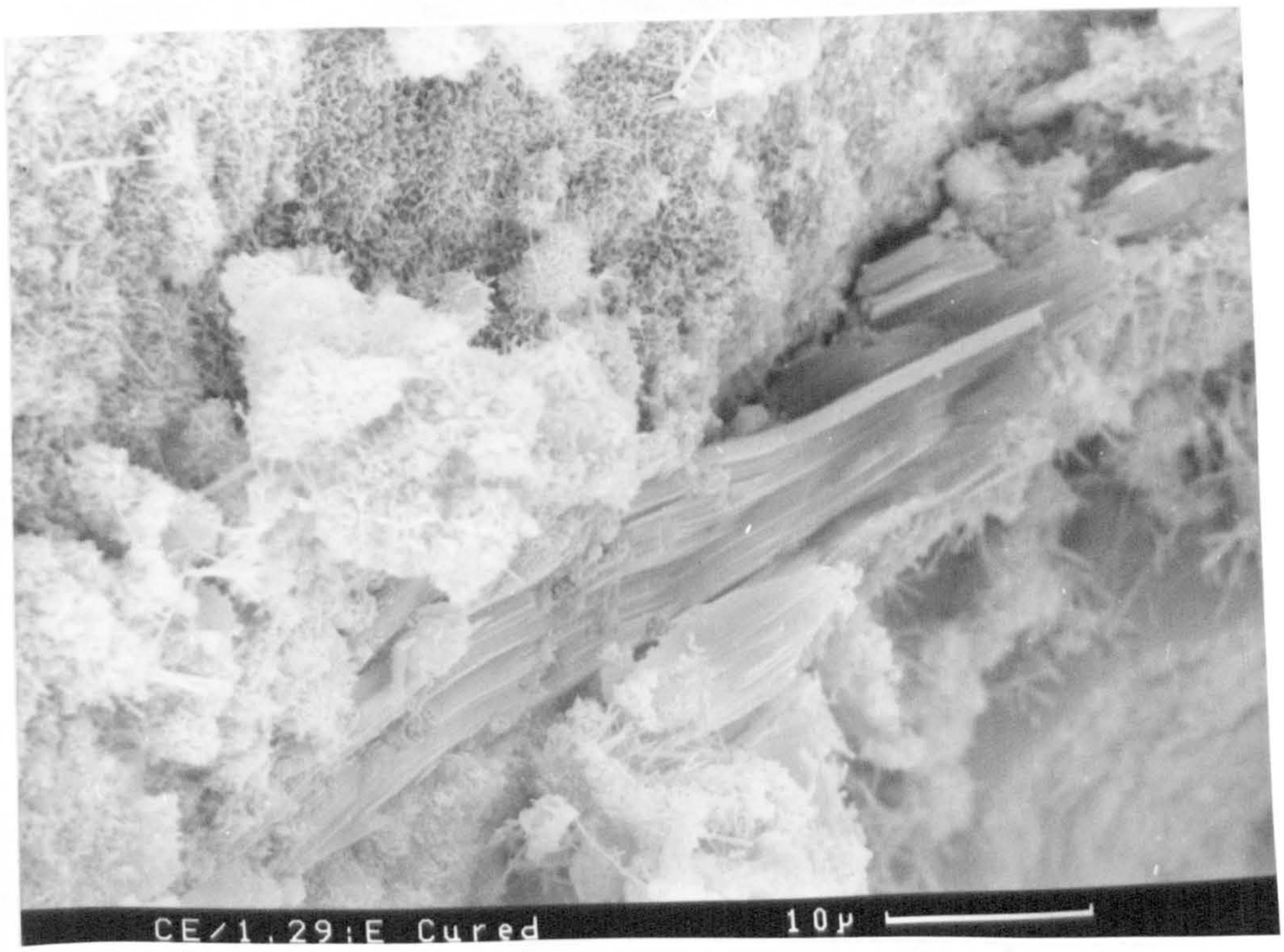

Plate 9.11 SEM micrograph illustrating a typical fracture surface of mortar mix number 21 (Magnification × 1900). The massive calcium hydroxide deposits grown through regions of C-S-H gel is clearly seen.

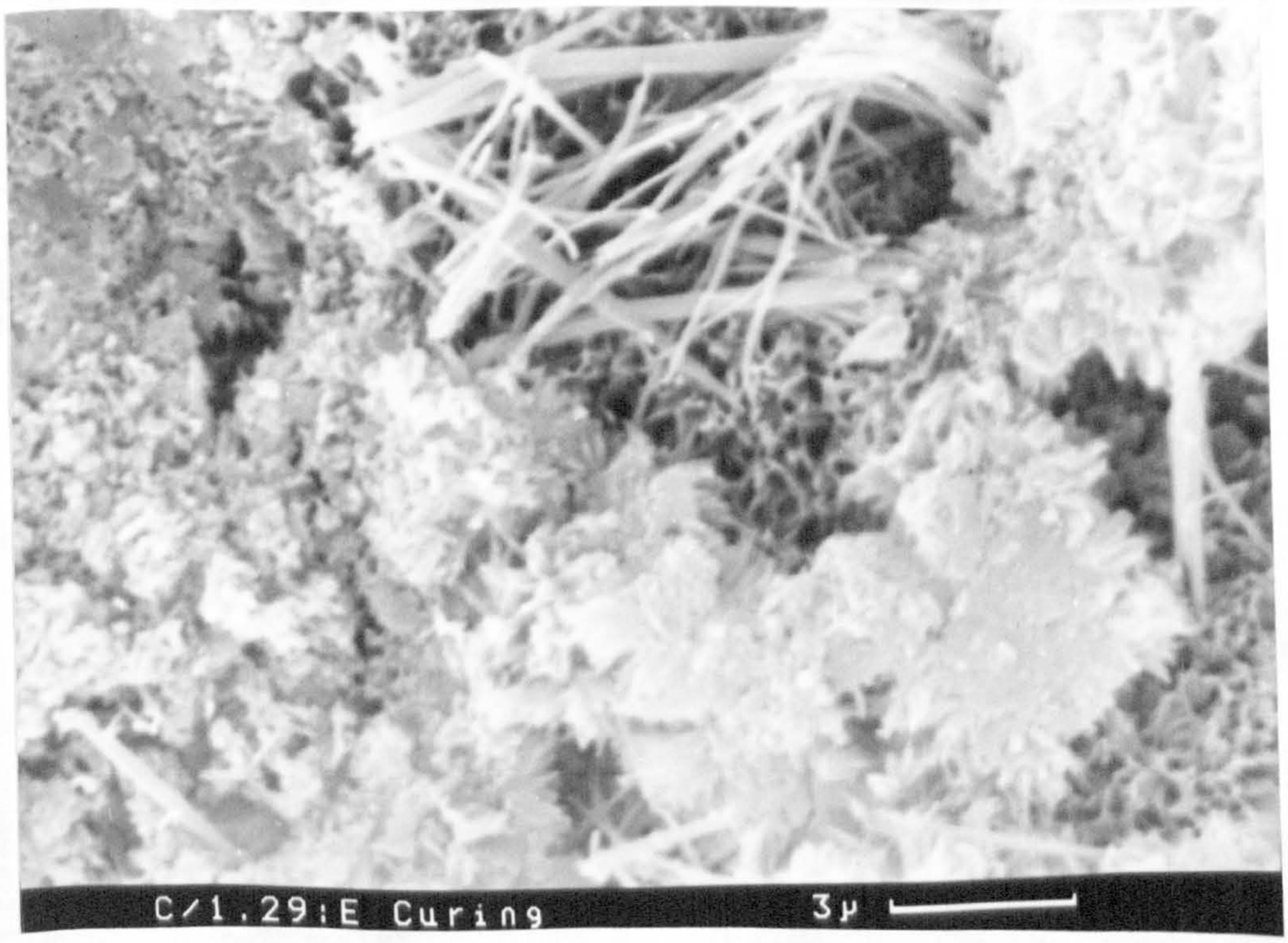

Plate 9.12 Finer structural details of mortar mix number 20 showing ettringite structure (Magnification × 5750).

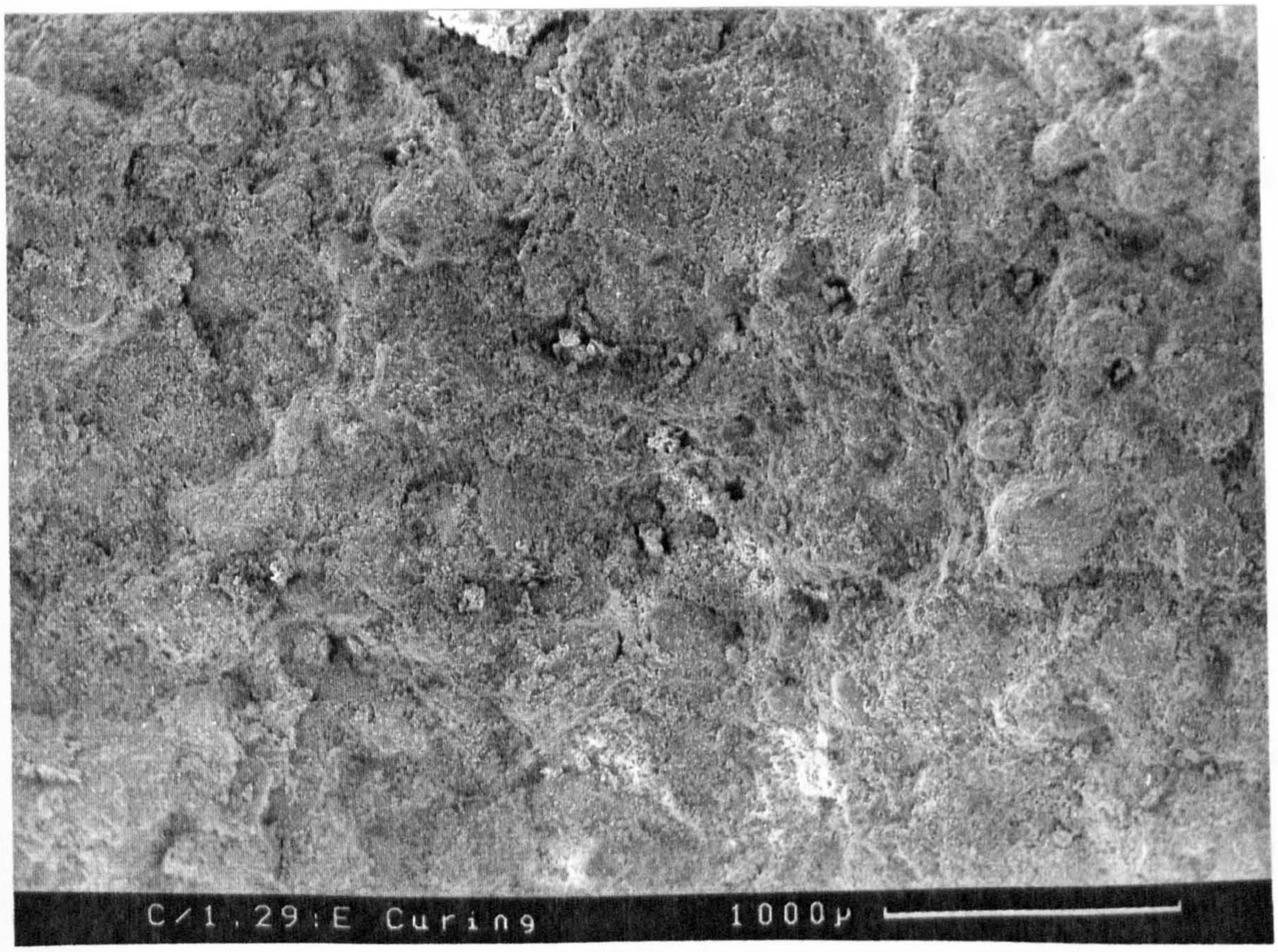

Plate 9.13 Coarser structural details of mortar mix number 20 (Magnification × 27).

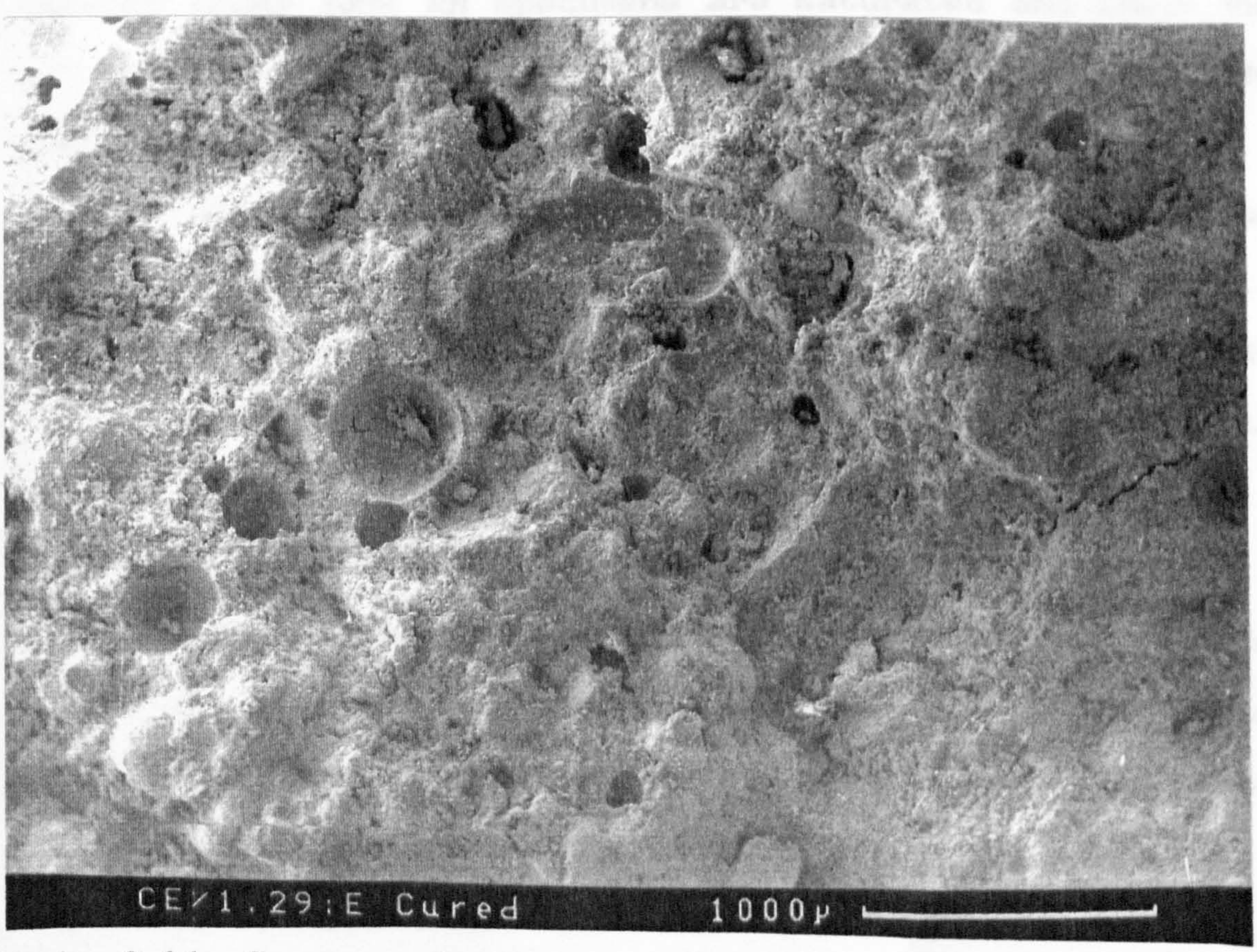

Plate 9.14 Coarser structural details of mortar mix number 21 showing a typical air - entrained mortar fracture surface (Magnification × 27).

9.7 Strength results

The compressive strength was carried out in this investigation as a supplement test since it is specified by British Standard[102,103] for judging the quality of concretes. The results of compressive strength in Table V.1 in Appendix V show good repeatability. The variability of strength as judged from standard deviation are quite low (maximum 2.00 MPa).

From Table 8.6 it can be seen that the strength of the mixes studied increases up to the 91 day period. The rate of increase is initially high but it slows down after 28 days of age. From Table 8.6 it can also be seen that at the curing condition of 20°C and 65% RH the strength values are higher than for saturated room curing condition. This is because under 100% RH specimens are saturated and their value of strength becomes lower than air dry specimens which exhibit some negative capillary pore pressure.

The effect of aggregate type on strength can be seen by comparing mix numbers 7-9, 10-12, and 22-24 in Table 8.6. Pellite concretes gives the lowest strength because of their high porosity. Limestone concrete gives higher strength than quartz concrete. The increase in compressive strength of concrete made with limestone aggregates could partially be attributed to the shape, surface roughness and intrinsic property of the limestone aggregates, i.e., the calcium carbonates surface reacts with the cement and probably improves the bond between aggregate and hydrated paste. As explained by Ramachandran et al[152], the effect could be due to the very fine limestone particles acting as a nucleating

agent and accelerates the hydration process. It is been reported [153-155] that certain carbonate (i.e. very fine limestone particles on the surface of aggregates) react with alkalis and improves the bonds at the aggregate cement matrix interface which leads to increase in the strength.

As expected air entrainment sharply reduces strength. This can be seen in Table 8.6 by comparing strength values of mix number's 1 with 2, 3 with 4, 5 with 6, 16 with 17, 18 with 19, and 20 with 21. This effect is more pronounced for pellite concretes because of the high porosity of aggregates.

The effects of increasing water-cement ratio are shown in Figures 9.28 to 9.30. The compressive strength of concrete reduces as water-cement ratio increases. This is to be expected since total porosity is increased as water-cement ratio is increased.

The correlation between compressive strength and porosity was statistically examined using strength values of 65% RH, 20°C cured specimens for 91 days and vacuum saturation total porosity values for the 24 concrete mixes studied. The regression equation developed is shown below:

$$fu = 115.816\ e^{-0.074P} \qquad \ldots (9.1)$$

with correlation coefficient, r = 0.921.

where :

fu = Compressive strength (MPa)

P = Vacuum saturation porosity

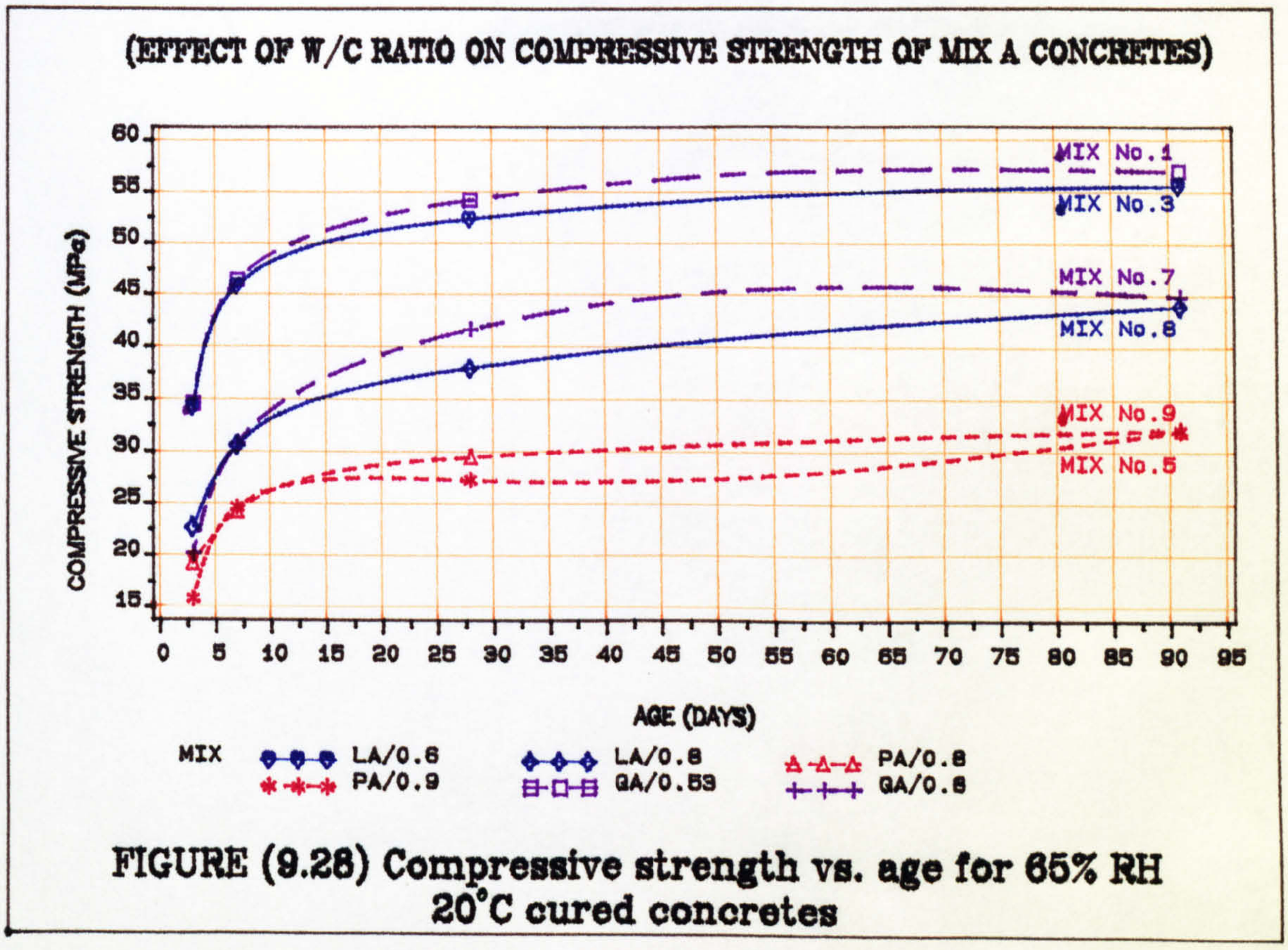

FIGURE (9.28) Compressive strength vs. age for 65% RH 20°C cured concretes

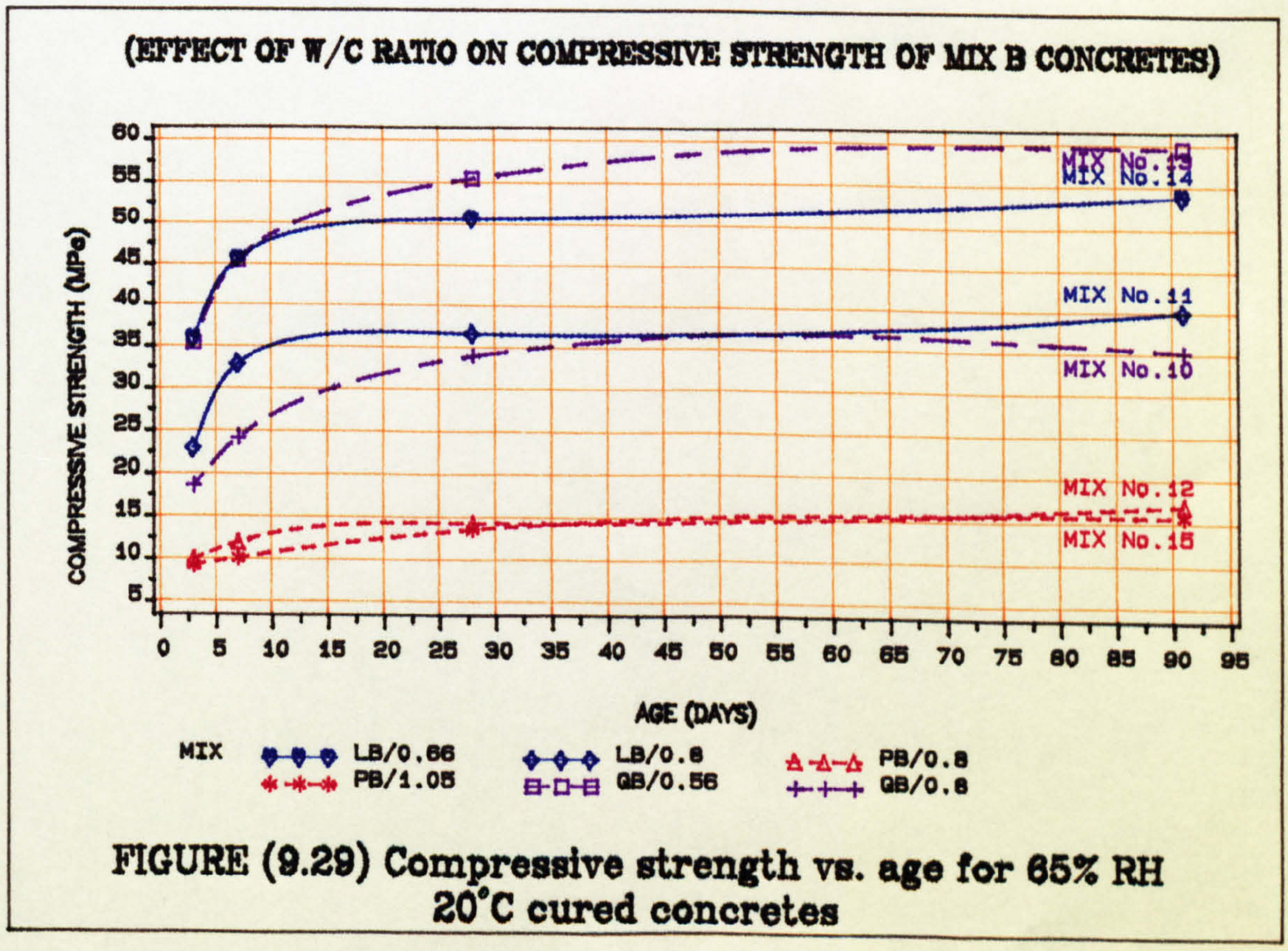

FIGURE (9.29) Compressive strength vs. age for 65% RH 20°C cured concretes

(EFFECT OF W/C RATIO ON COMPRESSIVE STRENGTH OF MIX C CONCRETES)

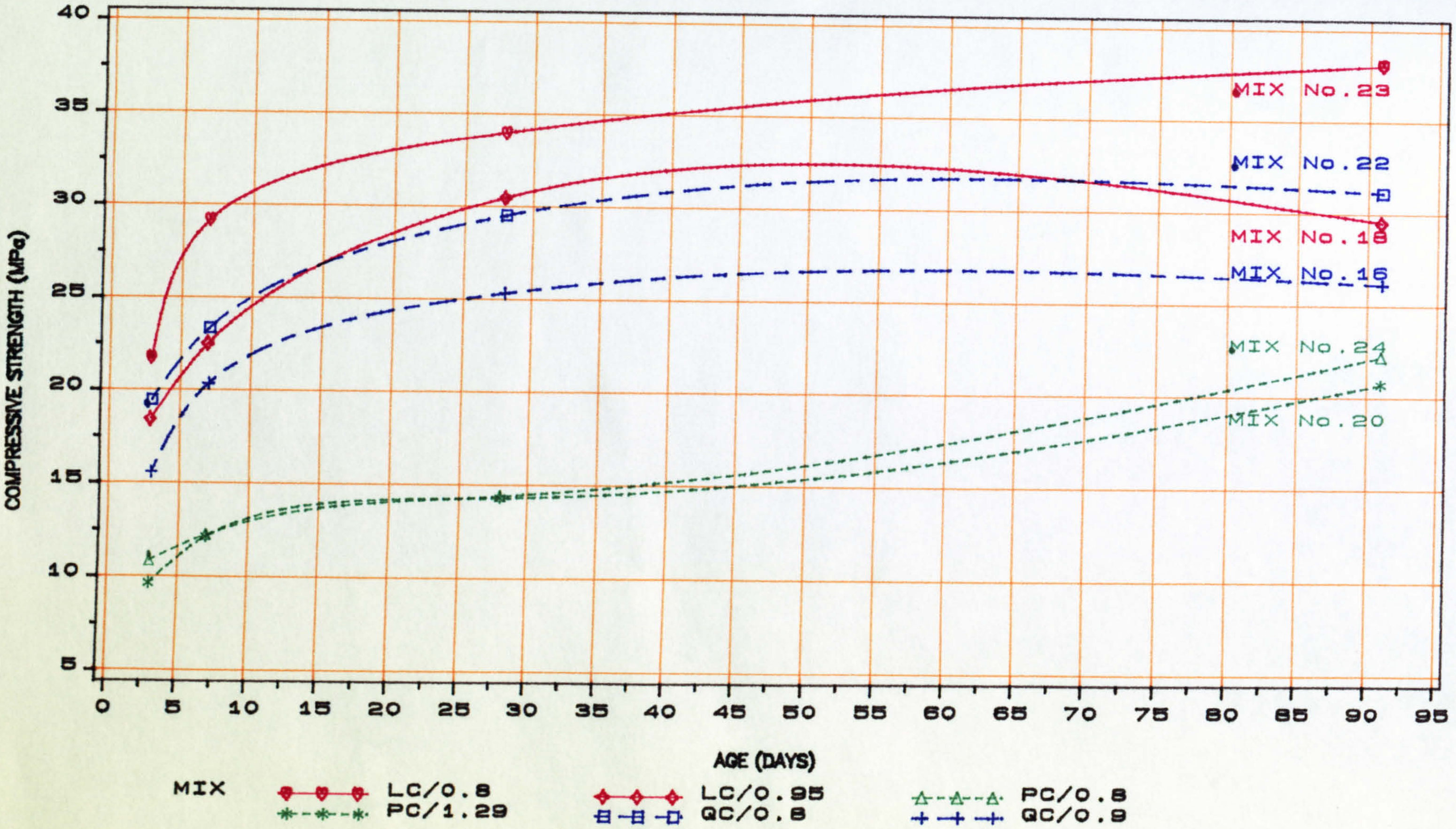

FIGURE (9.30) Compressive strength vs. age for 65% RH 20 C cured concretes

9.8 Relationships between thermal conductivity and parameters studied

The results discussed so far in sections 9.2 to 9.5 indicate that the degree of hydration and carbonation could not have affected the λ-values measured in this study because all the concrete mixes were highly hydrated and slightly carbonated to nearly the same level at the time of the thermal conductivity measurements. Furthermore, the effect of moisture content could be eliminated by adjusting measured λ-values to a common moisture content. Consequently, it was found that the main parameters which affect conductivity are density, porosity and pore size distribution.

In this section the latter parameters are correlated individually, with λ-values to examine the relation that each make with the thermal conductivity of the concretes studied.

As mentioned previously in section 2.3.1, in general, the thermal conductivity of a material increases as density increases but the relationship may become invalidated due to specific inherent properties such as total porosity, pore's internal characteristics and different order of crystallinity between the types of aggregates. This can be explored in Table 9.4 and Figures 9.31 and 9.32. Table 9.4 shows the thermal conductivity of concretes together with their mean dry densities in ascending order and their respective total porosities and median pore diameters. From the table it can be seen that as density increases, wherever the thermal conductivity reduces, then the porosity and / or the median pore diameter increases. An exception to this observation are mixes (17,4) and (1,14) whose decrease in thermal

conductivity is due to a change in coarse aggregate from quartzitic to limestone. This is because the mineral composition and order of crystallinity of the aggregates are different from each other.

A statistical regression analysis was carried out on the data given in Table 9.4. For the three individual aggregate concretes, density was correlated against thermal conductivity. Following this, density was correlated against thermal conductivity for all the data, irrespective of aggregate type. All the statistical equations developed were significant at α of 0.03 and in all cases, power and exponential equations gave the best correlation. The equations obtained together with their correlation coefficient, root mean square errors and coefficients of variation are listed below:

Pellite concrete:

$$\lambda = 2.3 \times 10^{-7} \quad \rho^{2.018} \qquad \text{...(9.2)}$$

$$\text{for } 1551 \leq \rho \leq 1902 \text{ kg/m}^3$$

$$r = 0.974 \ , \ \sqrt{MSE} = 0.043 \ , \ CV = 15.85$$

Limestone concrete:

$$\lambda = 8.7 \times 10^{-7} \quad \rho^{1.886} \qquad \text{...(9.3)}$$

$$\text{for } 1988 \leq \rho \leq 2291 \text{ kg/m}^3$$

$$r = 0.919 \ , \ \sqrt{MSE} = 0.046 \ , \ CV = 8.49$$

Quartz concrete:

$$\lambda = 2.4 \times 10^{-8} \quad \rho^{2.397} \qquad \text{...(9.4)}$$

$$\text{for } 2020 \leq \rho \leq 2341 \text{ kg/m}^3$$

$$r = 0.954 \ , \ \sqrt{MSE} = 0.040 \ , \ CV = 4.41$$

All 24 concretes:

$$\lambda = 0.034 \quad e^{0.002\rho} \qquad \text{...(9.5)}$$

$$\text{for } 1551 \leq \rho \leq 2341 \text{ kg/m}^3$$

$$r = 0.946 \ , \ \sqrt{MSE} = 0.174 \ , \ CV = 43.58$$

The descriptive statistics of these equations indicate that a very strong correlation exists between λ and density in each case.

The relationship obtained from Equation 9.5 is compared with 'standard' curve values proposed by Arnold[13] in Figure 9.31. All thermal conductivity data is expressed at 3% m.c. by vol. albeit using different factor correcting values (Jakobs for Arnold's data, Equation 5.3 for this work). It can be seen that the standard curve agrees reasonably well with experimental values at lower densities but as density increases the agreement is poor. This is especially pronounced for quartzitic concretes and highlights the need to include total porosity and a pore's characteristics when specifying a materials thermal properties.

Closer study of Table 9.4 shows that some of the mixes with similar densities have different λ-values (compare mix number 16 with 22, 8 with 23 and 3 with 23). This gives an indication of the effect that total porosity and median pore diameter have on thermal conductivity. Furthermore mixes 16 and 22, which have similar density and median pore diameters, exhibit different conductivities. This indicates that total porosity alone may be related to thermal conductivity. To investigate this possibility and establish

a general trend, a regression analysis was carried out on thermal conductivity and total porosity using data for Table 9.4.

Correlation between thermal conductivity and total porosity shows that, as expected, thermal conductivity decreases with increasing porosity. This is shown in the three dimensional scatter graph in Figure 9.32 and the graph plotting thermal conductivity versus total porosity in Figure 9.33. Regression analysis on the data for each type of concrete and for all the 24 concretes at 0.03 significant level are shown below. All these relations confirm the general concept that thermal conductivity reduces as porosity increases.

Pellite concrete:

$$\lambda = -0.001P^3 + 0.106P^2 - 2.945P + 27.363 \qquad \ldots(9.6)$$

$$\text{for } 20 \leq P \leq 39\%$$

$$r = 0.913 \ , \ \sqrt{MSE} = 0.074 \ , \ CV = 9.51$$

Limestone concrete:

$$\lambda = 5.196 \ P^{-0.395} \qquad \ldots(9.7)$$

$$\text{for } 12 \leq P \leq 25 \ \%$$

$$r = 0.907 \ , \ \sqrt{MSE} = 0.050 \ , \ CV = 9.10$$

Quartz concrete:

$$\lambda = 7.892 \ P^{-0.435} \qquad \ldots(9.8)$$

$$\text{for } 10 \leq P \leq 23 \ \%$$

$$r = 0.831 \ , \ \sqrt{MSE} = 0.075 \ , \ CV = 8.19$$

All 24 concretes:

$$\lambda = 54.286 \ P^{-1.239} \qquad \ldots(9.9)$$

$$\text{for } 10 \leq P \leq 39 \ \%$$

$$r = 0.866 \ , \ \sqrt{MSE} = 0.267 \ , \ CV = 67.06$$

The descriptive statistics of equation 9.9 show that the correlation between the thermal conductivity and porosity is relatively good for all the 24 concretes although it is slightly weaker than between thermal conductivity and density (r=0.946). Nevertheless it shows that strong correlation exists between thermal conductivity and total porosity.

To study any possible relation that the pore size distribution may have with thermal conductivity, the concrete's median pore diameter(calculated from MIP results) and thermal conductivity were statistically regressed (see Figure 9.34). The regression analysis on the data for each type of concrete and for all 24 concretes at 0.03 significant level are shown below:

Pellite concrete:

$$\lambda = -14.494\ MPD^3 + 46.422\ MPD^2 - 49.040\ MPD + 17.806 \quad \text{...(9.10)}$$

$$\text{for } 0.77 \leq MPD \leq 1.32\ \mu m$$

$$r = 0.773\ ,\ \sqrt{MSE} = 0.115\ ,\ CV = 14.78$$

Limestone concrete:

$$\lambda = -79.602\ MPD^3 + 126.413\ MPD^2 - 46.967\ MPD + 6.794 \quad \text{...(9.11)}$$

$$\text{for } 0.20 \leq MPD \leq 1.11\ \mu m$$

$$r = 0.719\ ,\ \sqrt{MSE} = 0.168\ ,\ CV = 9.67$$

Quartz concrete:

$$\lambda = 3.395\ e^{-0.654MPD} \quad \text{...(9.12)}$$

$$\text{for } 0.33 \leq MPD \leq 0.82\ \mu m$$

$$r = 0.814\ ,\ \sqrt{MSE} = 0.079\ ,\ CV = 8.56$$

All 24 concretes:

$$\lambda = 2.948\ e^{-1.185\ MPD} \qquad \text{...(9.13)}$$

$$\text{for} \quad 0.20 \leq MPD \leq 1.32\ \mu m$$

$$r = 0.741\ ,\ \sqrt{MSE} = 0.359\ ,\ CV = 34.32$$

where:

MPD = concrete median pore diameter in microns.

As expected, thermal conductivity reduces with increasing median pore diameter. The relatively good correlation indicates the existance of a relatively strong relation between median pore diameter and the thermal conductivity.

To examine the effect of pore characteristics on thermal conductivity using available variables (i.e. total porosity and median pore diameter) pair correlations between the ratio of median pore diameter and total porosity (and the inverse product of MPD and porosity) and thermal conductivity were also statistically examined. In all cases, the relation was found to be poor. This is because the dry density, which has the highest effect on thermal conductivity was not included.

It can be seen from Equations 9.5, 9.9 and 9.13 that the coefficient of determinations (i.e. r^2) are 0.89, 0.75 and 0.55 respectively. This means that the models are accounting respectively for 89% , 75% and 55% of the variability in the data and the remaining percentages (i.e. 11% ,25% and 45% respectively) can be explained by the other two main parameters which are not included in the models.

Therefore for this reason, and also because density, total porosity and median pore diameter can become inter-related, a much more accurate and reliable relation can be established by inclusion of the three main parameters studied, in correlation with the thermal conductivity values. This is attempted in the next section.

Table (9.4)

Summary of thermal conductivity, dry density, porosity and median pore diameter results for concretes studied

Mix No.	Concrete Code Name	λ @ 3% mc By Vol. (W/mK)	Mean Dry Density (kg/m^3)	Total Porosity (%)	Median Pore Diameter (Micron)	Predicted λ_3 Eqn. 9.14 (W/mK)
21	PCE/1.29	0.63	1551	39.0	1.32	0.56
6	PAE/0.80	0.65	1557	38.5	0.82	0.73
12	PB /0.80	0.65	1570	23.4	0.91	0.57
15	PB /1.05	0.69	1647	25.1	0.97	0.61
24	PC /0.80	0.85	1745	26.1	0.80	0.96
20	PC /1.29	0.82	1818	25.5	0.87	0.93
5	PA /0.90	0.91	1858	21.0	0.83	1.04
9	PA /0.80	0.99	1902	20.1	0.77	1.13
19	LCE/0.90	1.44	1988	25.5	1.11	1.47
17	QCE/0.80	1.99	2020	23.5	0.82	1.72
4	LAE/0.50	1.50	2033	21.0	0.27	1.32
2	QAE/0.43	2.17	2091	14.0	0.48	1.94
18	LC /0.95	1.81	2207	17.6	0.28	1.78
16	QC /0.90	2.61	2236	15.1	0.50	2.47
22	QC /0.80	2.70	2238	12.9	0.45	2.53
8	LA /0.80	1.81	2243	15.3	0.20	1.73
23	LC /0.80	1.96	2243	13.1	0.29	2.19
3	LA /0.60	1.75	2248	15.0	0.20	1.76
7	QA /0.80	2.56	2250	13.9	0.35	2.34
11	LB /0.80	1.73	2261	14.1	0.23	1.95
1	QA /0.53	2.76	2282	12.9	0.33	2.48
14	LB /0.66	1.89	2291	12.1	0.23	2.15
10	QB /0.80	2.52	2291	12.6	0.41	2.68
13	QB /0.56	2.86	2341	10.2	0.39	2.99

Notes on mix Code names:

Q stands for concretes made with Quartzitic coarse Agg.
L stands for concretes made with Limestone coarse Agg.
P stands for concretes made with Pellite coarse Agg.

	Cement	: Sand	: Coarse aggregate
A :	1	: 2.33	: 3.5 (Reference mix)
B :	1	: 2.33	: 5.6
C :	1	: 3.73	: 5.6

Third letter (E) Indicates Air-entrained mix.
(0.257 litre/100kg of Cement.)

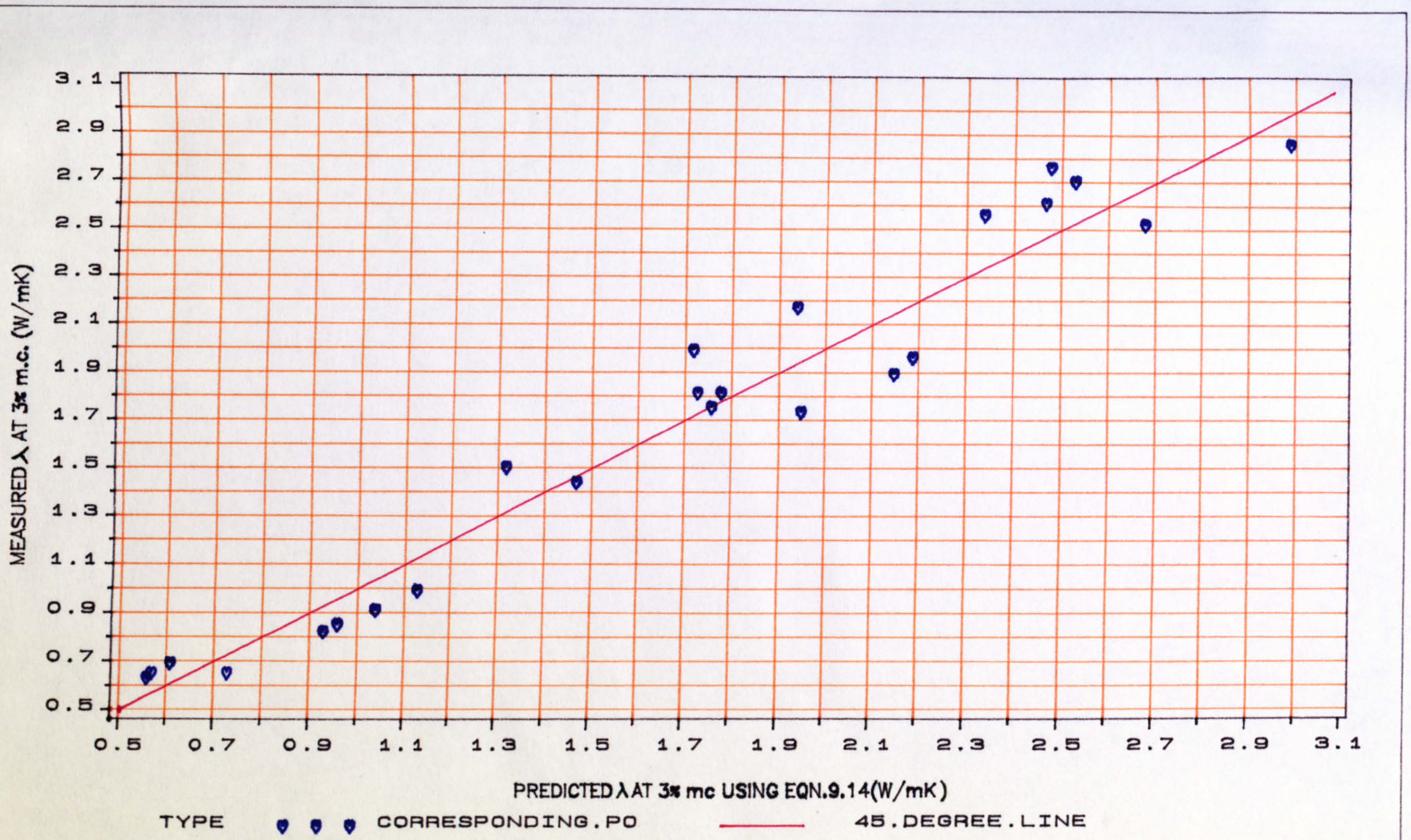

FIGURE (9.30A) Measured thermal conductivity vs. predicted thermal conductivity values

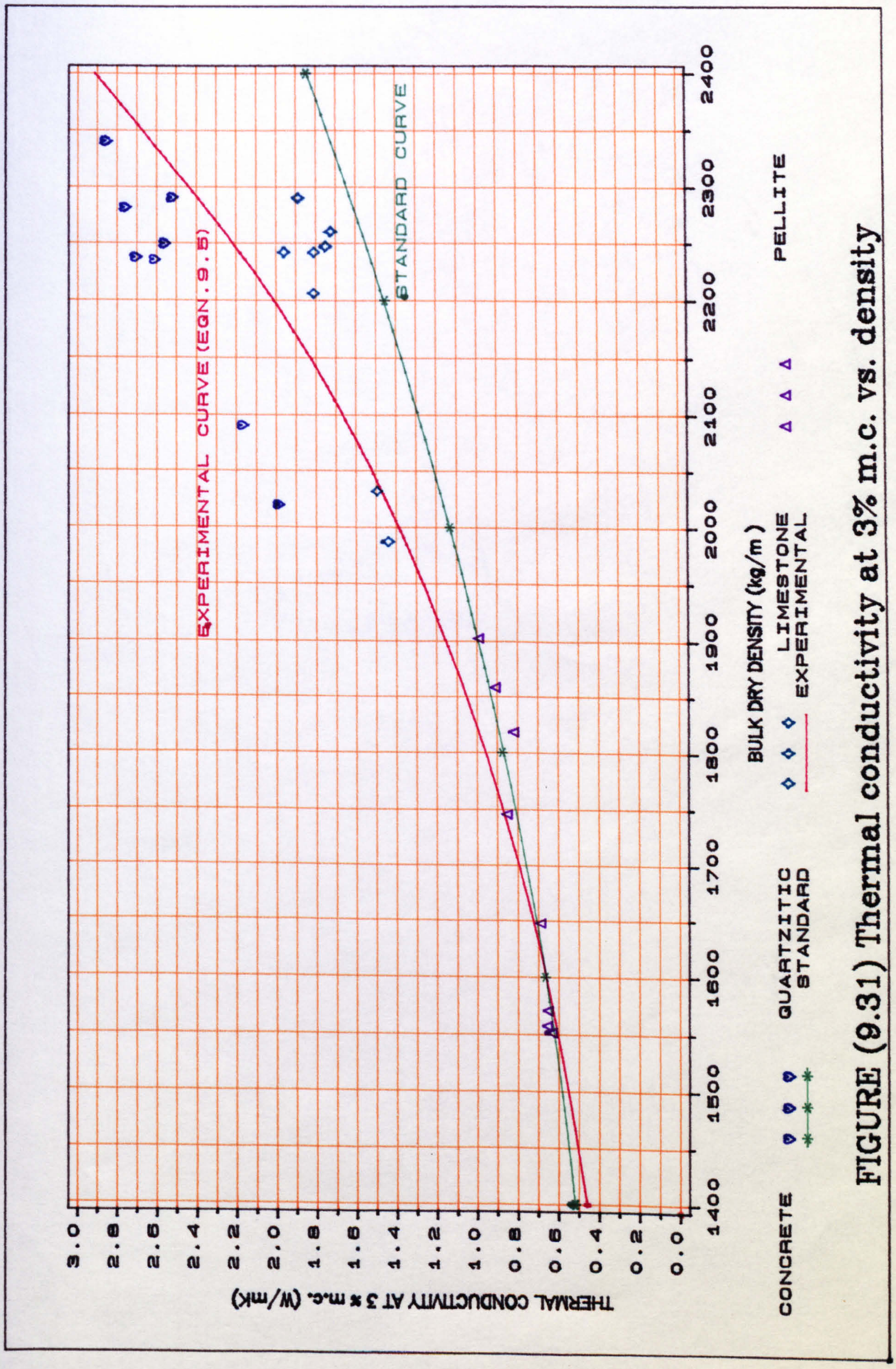

FIGURE (9.31) Thermal conductivity at 3% m.c. vs. density

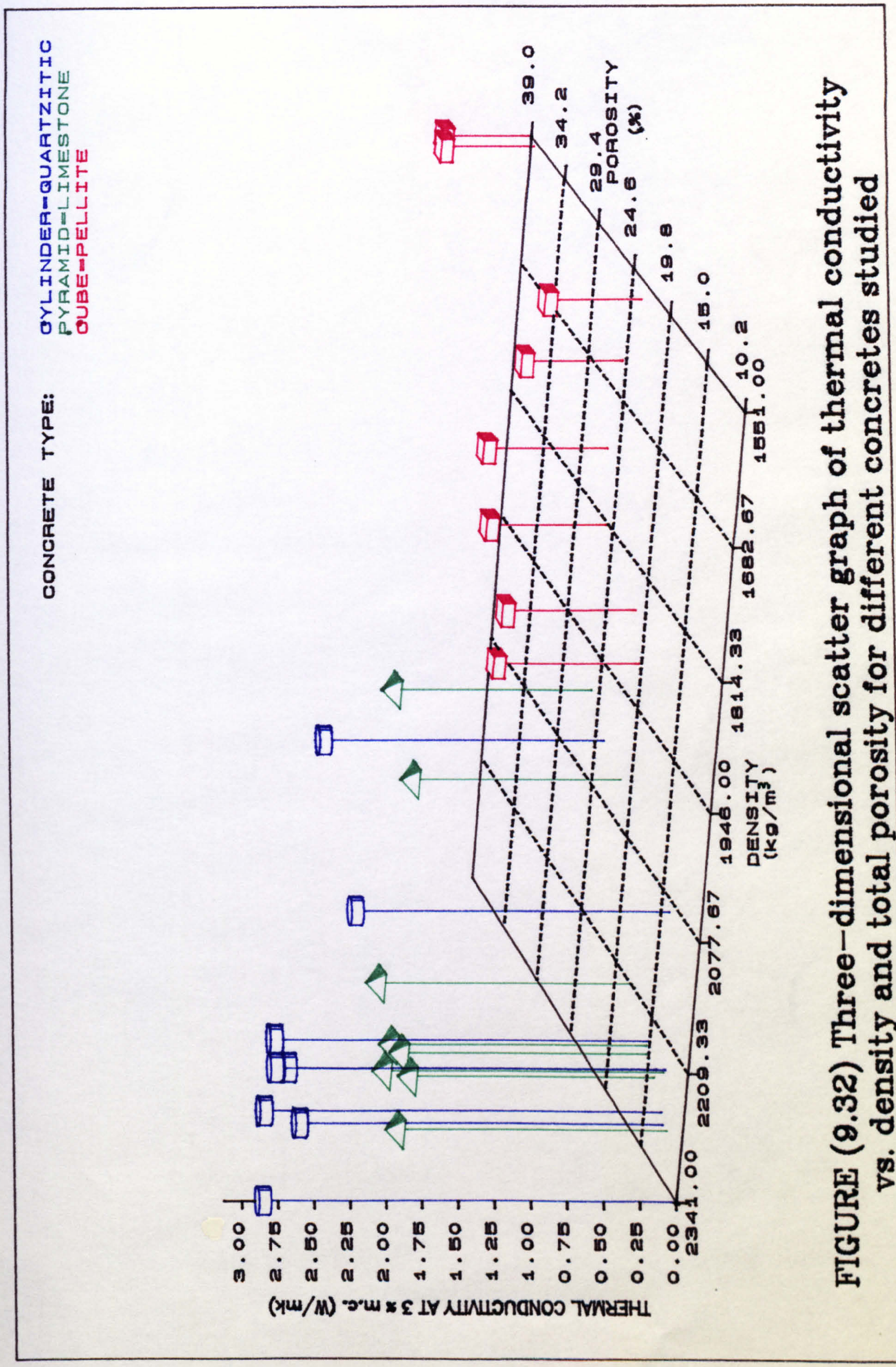

FIGURE (9.32) Three-dimensional scatter graph of thermal conductivity vs. density and total porosity for different concretes studied

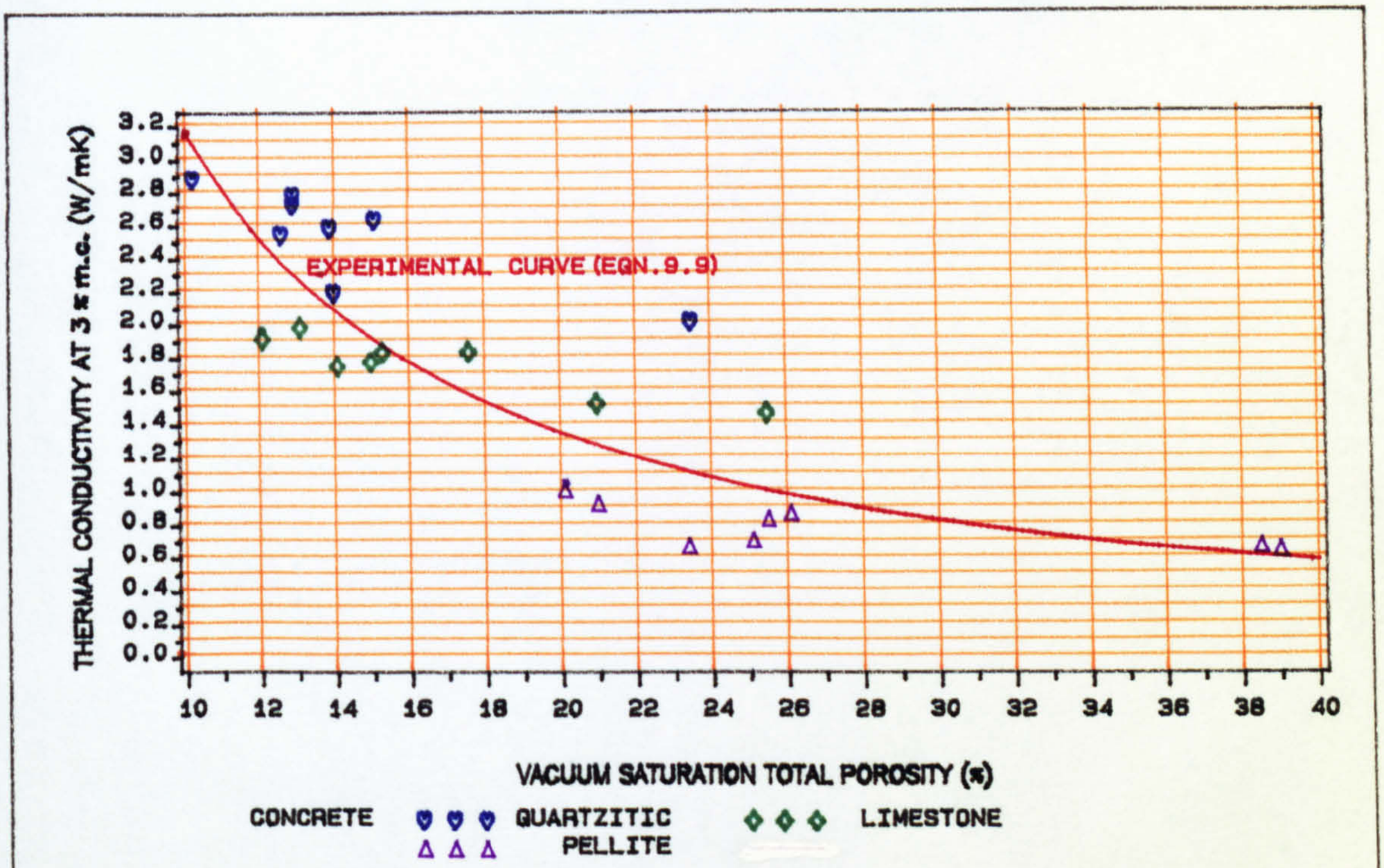

FIGURE (9.33) Thermal conductivity vs. total porosity for the 24 concretes studied

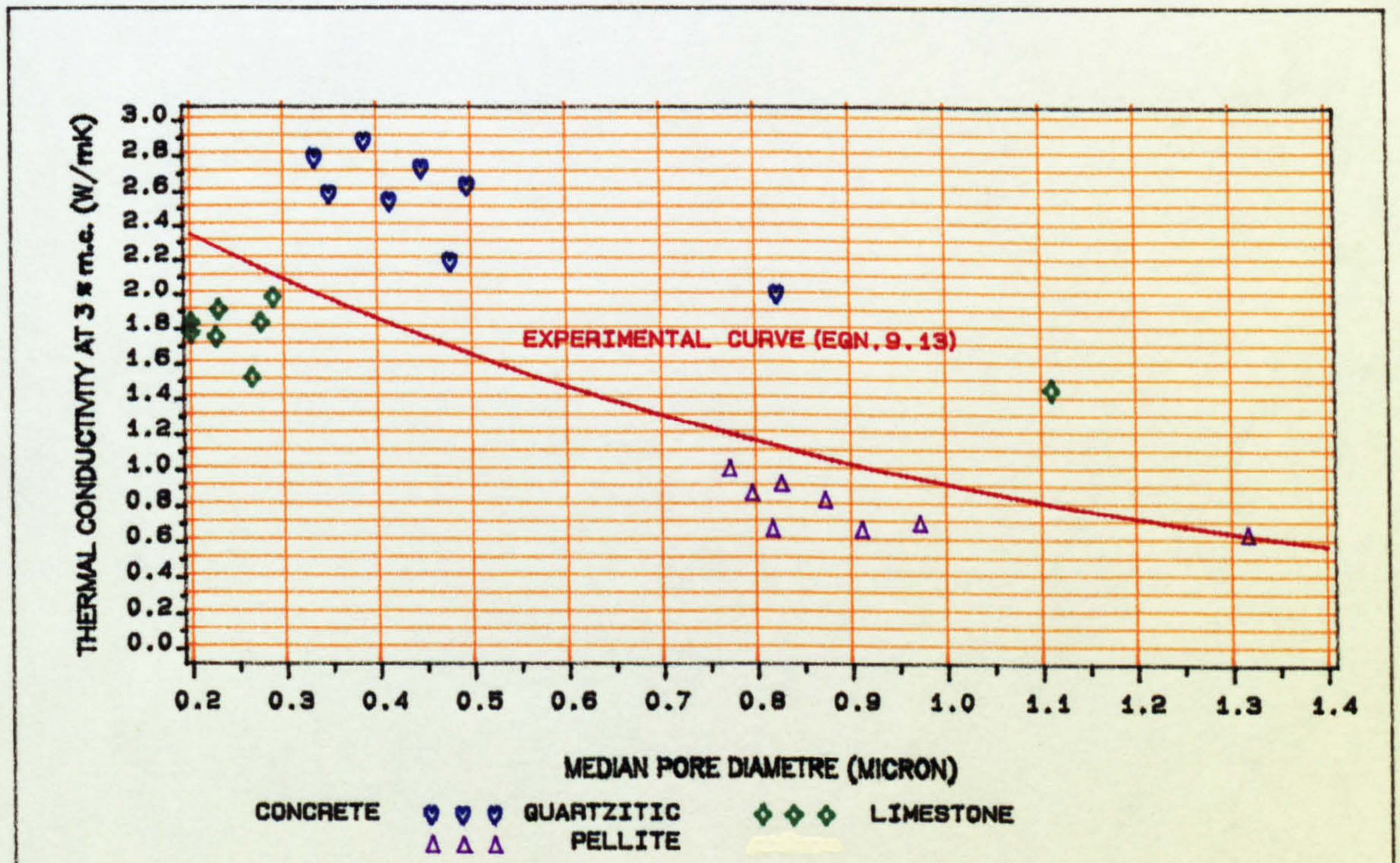

FIGURE (9.34) Thermal conductivity vs. median pore diametre for 24 concretes studied

9.9 Development of a model to predict the thermal conductivity of concretes

In order to develop models to predict the thermal conductivity of concretes at a standard moisture content (i.e. 3 per cent by volume) from the variables investigated, a multivariate statistical analysis was carried out on the data given in Table 9.4 using the Statistical Analysis System (SAS) package. The model that was developed, together with descriptive statistics is as follows:

$$\lambda = 1.766 \times 10^{-6}\rho^2 - 1139.668\left(\frac{MPD}{P}\right)^2 - 6.076 \times 10^{-3}\ \rho - 54.210\left(\frac{MPD}{P}\right) + 6.495 \times 10^{-2}\rho\left(\frac{MPD}{P}\right) + 5.467 \qquad \ldots(9.14)$$

Where:

ρ = dry density (kg/m^3) when $1551 \leq \rho \leq 2341$ kg/m^3

P = total porosity (%) when $10.2 \leq P \leq 39.0$ %

MPD = concrete median pore diameter (μm) when $0.20 \leq MPD \leq 1.32$ μm

Coefficient of correlation r = 0.962
Root mean square error = 0.295
Coefficient of variation = 0.14
F ratio = 44.4
Probability > F = 0.0001

The above model contains a term involving median pore diameter. Because this data is not readily obtainable without sophisticated equipment and trained personnel, in practical situations, a highly significant statistical model relating thermal conductivity to density and total porosity ought to be developed. An example of such a model is given below:

$$\lambda = 1.737 \times 10^{-3}\rho + 12.246\ \left(\frac{1}{P}\right) - 2.577 \qquad \ldots(9.15)$$

Coefficient of correlation r = 0.905
Root mean square error = 0.337
Coefficient of variation = 20.12
F ratio = 47.5
Probability > F = 0.0001

Where:

ρ = dry density (kg/m^3) when $1551 \leq \rho \leq 2341$ kg/m^3

P = total porosity (%) when $10.2 \leq P \leq 39.0$ %

The analysis revealed the following:

- The variables which can be used to predict the thermal conductivity of a concrete with a 97% confidence limit are density, porosity and median pore diameter. Carbonation depth was statistically rejected as a regressor because it was outside the mentioned confidence limit.

- When the three independent variables of density, porosity and median pore diameter are regressed against thermal conductivity (the dependent variable), the hypothesis tests on the regression coefficients indicate that density is the most important variable in the relationship and porosity the next.

- When the three independent variables are regressed against the dependent variable (thermal conductivity) a highly significant polynomial (quadratic response surface) model with a coefficient of correlation, r=0.959 is obtained. If the ratio of median pore diameter to porosity is used as one independent variable and density as the other, a slightly better correlation is obtained.

Three-dimensional surface graphs of the above models are shown in Figures 9.35 and 9.36. Figure 9.35 clearly shows the effect of density on thermal conductivity and how particularly pronounced it is at higher densities. This effect is also observed in Figure 9.36, where total porosity can be clearly seen to be inversed with thermal conductivity. The complex effect of porosity and pore size distribution

can be seen in clearer perspective in Figure 9.35. For higher densities as the ratio of MPD/P is increased (i.e. bigger pore diameters and lower total porosity) thermal conductivity is increased. For lower densities this effect is almost reversed particularly for very high MPD/P ratios (higher than about 0.30μ). This indicates that at low densities (i.e. not bigger than about 1950 kg/m^3), pore diameter has a pronounced effect on thermal conductivity while at higher densities, total porosity has more pronounced effect. Therefore if the effect of median pore diameter is not considered, the resultant model (e.g. Equation 9.15) would show an increase in λ-values for lower densities. Comparision of Figure 9.36 (which is generated from Equation 9.15) and Figure 9.35 (which is generated from Equation 9.14) clearly shows this trend.

Using the above models and knowing the dry density, total porosity and median pore diameter or solely dry density and total porosity, it is possible to predict the λ-value of a concrete with reasonable accuracy. In practice a concrete sample could be taken from an existing structure, its dry density and total porosity determined and its λ-value then predicted.

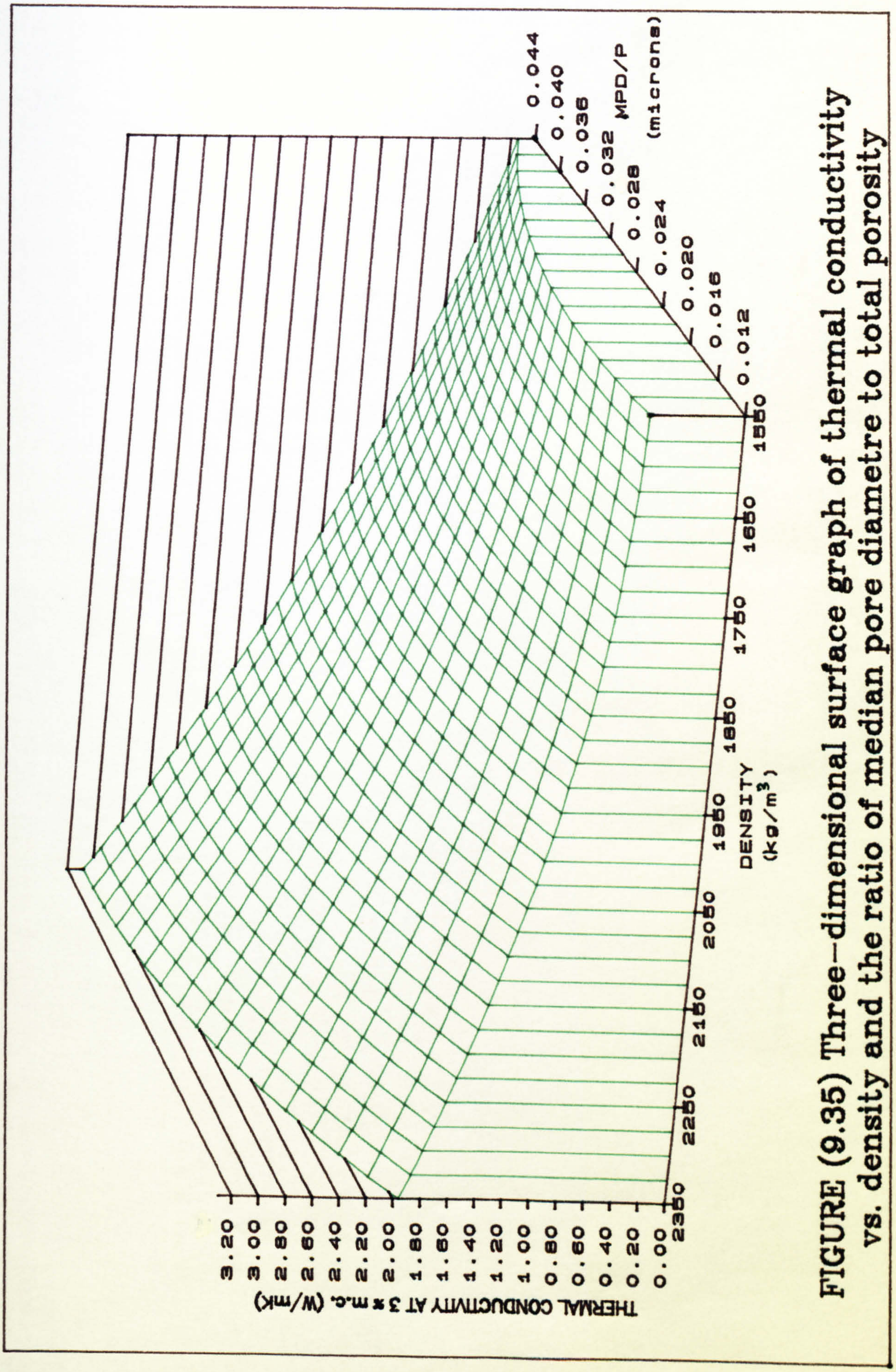

FIGURE (9.35) Three-dimensional surface graph of thermal conductivity vs. density and the ratio of median pore diametre to total porosity

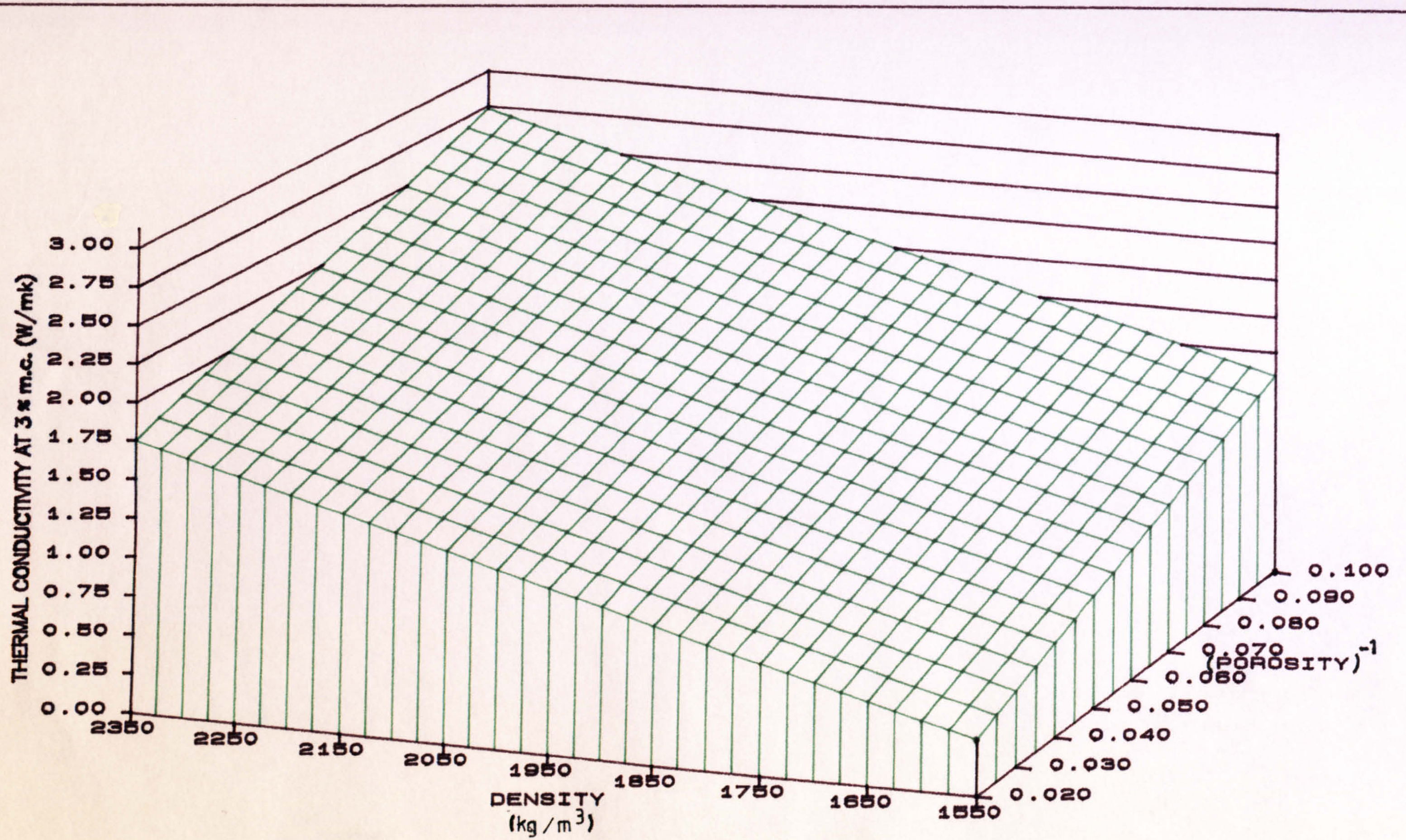

FIGURE (9.36) Three–dimensional surface graph of thermal conductivity vs. density and reciprocal of total porosity using Eqn.9.15.

9.10 Validation of experimental models given in the literature

In order to examine the accuracy of the equations given by Maxwell, Valore method 2 and Campbell-Allen & Throne (i.e. equations 2.21 to 2.23 in section 2.6), two pairs of mortar specimens and one pair of quartzitic sandstone specimen were prepared and their thermal conductivity measured in accordance with BS 874: 1988. The results of these tests are shown below:

Specimens slabs	Density (kg/m^3)	λ @ 3% m.c. by Vol.
Mortar A/0.8 (or B/0.8)	2007	1.50
Mortar C/0.8	1962	1.59
Quartzitic sandstone	2360	3.37

The reference system used for mortar slab A/0.8 (B/0.8) indicates that the specimen is made with a 1:2.33 cement to sand ratio and 0.8 W/C ratio. This mortar specimen corresponds to the mortar phase of concrete mix numbers 7 and 10 i.e. concretes QA/0.8 and QB/0.8. Likewise, mortar specimen coded C/0.8 indicates cement to sand ratio of 1:3.73 and W/C ratio of 0.8 which corresponds to the mortar phase of concrete mix number 22, i.e. concrete QC/0.8.

Knowing the λ-values of the mortar and aggregate phases and using information given in Table 9.3, models represented by equations 2.21 to 2.23 were then used to calculate the thermal conductivity of mix numbers 7, 10 and 22. For purposes of comparison the thermal conductivity of the same mixes was also calculated using derived Equation 9.14. The empirical λ-values obtained are tabulated and compared with the experimental results in Table 9.5. The

table shows that all the models quoted in the literature underestimate the thermal conductivity by approximately 5 to 19 per cent. Valore method 2 calculates values that are closest to experimental but these are still upto 16 per cent low.. The differences may be due to the inaccurately assumed λ values for the aggregate phase or the model assumption not realistically representing the matrix. This former point emphasises the limitations of these models since the thermal conductivity of the components should be measured independently. Finding a λ-value which exactly corresponds to the aggregate phase can be impossible in some cases (e.g. Pellite concretes).

Table (9.5)

Comparison of experimental models in the literature.

Mix no.	Concrete code name	λ at 3% m.c. by Vol. *				
		Experi-mental	Maxwell (Eqn. 2.19)	Valore method 2 (Eqn. 2.20)	Campbell-Allen and Thorne (Eqn. 2.21)	Eqn. 9.14
7	QA/0.8	2.56	2.19 [-17%]	2.22 [-15%]	2.15 [-19%]	2.34[-9%]
10	QB/0.8	2.52	2.38 [-6%]	2.41 [-5%]	2.36 [-7%]	2.68[+6%]
22	QC/0.8	2.71	2.30 [-18%]	2.33 [-16%]	2.28 [-19%]	2.53[-7%]

* Values in square brackets show the percentage difference from experimental values.

Attempts were made to prepare specimens from solid Limestone, and to measure their thermal conductivity according to BS 874: 1988. Despite many contacts with suppliers, reasonable limestone rocks could not be obtained and specimens prepared. This prevented the comparison of the emperical λ-values with the experimental results of mix numbers 8, 11 and 23 for limestone concretes.

The limited examination of experimental models that has been undertaken in this section indicates the viability of using the experimental models that have been developed (equations 9.14 and 9.15 in previous section) and how they improve the values of thermal conductivity obtained.

CHAPTER TEN

CONCLUSIONS AND RECOMMENDATIONS FOR FURTHER RESEARCH

10.1 Conclusions

The thermal, microstructural and engineering properties of lightweight and normal-weight concretes containing three different type of coarse aggregates have been investigated in the density range 1550 - 2350 kg/m^3 and porosity range 10 - 39 per cent. The results presented, provide significant contributions towards our understanding of the relationship between porosity and thermal conductivity and the main conclusions are summarised in the following paragraphs.

thermal conductivity and other parameters

1) One of the most important developments that the work has produced is an experimental model which, knowing dry density and total porosity (or median pore diameter), predicts the λ-value of concretes quite accurately. All that is required to make the prediction is a small sample of concrete from which dry density and total porosity (or median pore diameter) may be determined. Using these parameters, in the density range 1550 - 2350 kg/m^3, thermal conductivity can be modelled with reasonable accuracy.

Detailed examination of the models revealed that at densities below 1950 kg/m^3, median pore diameter has the greatest effect on thermal conductivity whilst at densities above 1950 kg/m^3, total porosity is the dominant parameter.

2) Multi-variate statistical analysis of the relationships that exist between thermal conductivity and a number of other parameters characterising the properties of concrete have shown that:

   a) the variables which can be used to predict the thermal conductivity of a concrete with a 97 % confidence limit are density, porosity and median pore diameter. The prediction is accurate to ±14 per cent of the measured values.

   b) when the three independent variables of density, porosity and median pore diameter are regressed against thermal conductivity, the hypothesis tests on the regression coefficients indicate that density is the most important variable in the relationship and that in general, porosity is the next.

3) The individual correlation between thermal conductivity and the three independent variables of dry density, total porosity and median pore diameter show that in general, the thermal conductivity of a concrete is directly related to density and inversely related to porosity and pore diameter. Single correlation gave the following numerical equations with density and porosity having the higher coefficients of correlation respectively.

$\lambda = 0.034\ e^{0.002\rho}$ for $1551 \leq \rho \leq 2341$ kg/m^3

$\lambda = 54.286\ P^{-1.239}$ for $10 \leq P \leq 39$ %

$\lambda = 2.948\ e^{-1.185MPD}$ for $0.20 \leq MPD \leq 1.32$ μm

4) Experimental models by other workers which were cited in the literature were evaluated using appropriate data to predict the thermal conductivity of selected concretes. Modelled values fell of thermal conductivity fell consistently below experimental and the literature models proved to be impractical to use since the thermal conductivity of the aggregate and mortar phase had to be measured separately. Limited examination of the models indicated the need for simplified expressions to predict thermal conductivity and this need supported the development work that has been done.

surface contact problems and thermal conductivity

5) The results of the investigation into the surface contact problem associated with fixing thermocouples to samples showed that the precise method of securing the thermocouples can significantly alter the measured conductivity value. By flattening or rolling the thermocouple's bead, the contact area with the surface of the specimen is increased and any air gap that exists is reduced. The contact resistance problem was found to be more profound on the higher conductive specimens and hence the choice of an appropriate method was important when testing dense concretes. The results of investigations using a concrete specimen with a density of 2275 kg/m^3, indicated that an increase in thermal

conductivity of about 35% can be expected when using foiled thermocouples. This method is now included in the latest edition of B.S.874 and is recommended for measuring the λ-value of high conductive masonry materials. The technique was used for all the measurements through out the project.

moisture content and thermal conductivity

6) Increasing the moisture content of a concrete at a fixed density increases its thermal conductivity. The relationship has been shown to be linear and dependent upon density.

Several heat transfer mechanisms are involved in the effect of moisture on thermal conductivity, including conduction through water contained in capillaries and pores, latent heat transfer due to evaporation and condensation, and transfer of mass due to vapour pressure differentials.

7) In order to provide a common basis for comparing the thermal conductivity values of concretes, they must be expressed at same standard moisture content. Until recently, moisture correction factors which are independent of density, such as those by Jakob, have been used. Thermal conductivity values when corrected to a standard moisture content using the Jakob factors have been shown to be in error by about 24 per cent in the density range 1550 to 2350 kg/m^3.

A general expression for the types of concrete investigated has been derived which relates the moisture factor to both density and moisture content by volume. The expression:

$$F = 1.174 - 8.449\times10^{-5}\rho + 35.688\times10^{-3}mc$$

is valid over the moisture content range 0 to 5 per cent and has been shown to give much better agreement with experimental data than the correction factors currently recommended for use, i.e. the Jakob's factors.

composition of concrete and thermal conductivity

8) The type of aggregate used to make a concrete contribute significantly to its characteristics. This is because concrete contain between about 44 to 64 per cent aggregate by volume. Therefore, variations in density and porosity of the aggregates will substantially influence the density and porosity of the concrete. The porosities of the aggregates studied ranged from 2 to as much as 25% by solid volume, but most importantly, the pore size distribution of the aggregates were mainly capillary pores. The work showed that these strongly influenced the resultant thermal conductivity.

Concretes made with quartzitic aggregate which was the densest and least porous gave the highest values of thermal conductivity while concretes made from porous, low density pellite aggregate gave the lowest value of thermal conductivity.

air entrainment and thermal conductivity

9) Air entrainment of up to 25% reduces the conductivity of concretes by as much as 50 per cent. This is due to an increase in total porosity, consequent reduction in density and also to a shifting of the mortar's pore sizes towards the macro range (i.e. 1 - 100 micron in diameter). This combination of factors reduces the rate of heat transfer through the concrete.

total porosity

10) The total porosity of the concretes studied was strongly influenced by a number of factors including the type of the aggregate, ratio of aggregate to mortar, amount of cement per unit volume and the water/cement ratio.

11) Total porosities obtained by vacuum saturation using concrete samples gave consistently higher values than porosities calculated from MIP measurements carried out on separate samples of mortar and aggregates. This difference was attributed to the volume of pores generated at the aggregate - mortar interfaces which result from localised bleeding in a concrete mix. The difference could also be due to the existence of large pores with narrow entries which mercury used during MIP can not penetrate whilst water as used by Vacuum Saturation can.

12) Compressive strength was found to be inversely related to the total porosity of the concrete. The relationship between total porosity and cube compressive strength was

found to be better expressed by an exponential equation of the form

$$fu = 115.816\ e^{-0.074P}$$

microscopic observation

13) Microscopic examination of aggregate particles revealed that quartz and limestone had a very dense pore structure while pellite was found to have open vitreous, discrete pore structure with a very porous micromorphology.

14) SEM micrographs of air entrained mortars showed a typical well-dispersed spherical macropore system. These observations were also confirmed by the MIP results.

10.2 Recommendations for further research

The work carried out in this investigation has revealed several areas where further research is necessary. It is therefore recommended that investigations should be made into the following:

1) From the results obtained in this investigation, several statistical models were established. However, more data on density, porosity, pore diameter sizes and type of aggregates are required to widen the scope of these models. In addition, the models need to be verified using results obtained by other investigators.

2) Because the gas permeability of a concrete is directly related to its pore characteristics, a study of the thermal conductivity of concretes of varying gas permeability might provide very useful data to replace the models proposed for the assessment of thermal conductivity.

3) It would be worth while to conduct a study into the effects of carbonation on thermal conductivity. This work could be done by accelerated carbonation using slabs of the same size as those needed for thermal conductivity measurements.

4) A study of the effect of mineral composition of the aggregate's granules on the thermal conductivity in conjunction with density, porosity and median pore diameter of granule aggregates can lead to establishing a simplified model for the thermal conductivity values of the aggregate phase. This would make the

experimental models cited in the literature more practical.

5) The moisture factor equation may possibly be improved by making additional measurements using relative humidities found in practice, i.e. in the region of 40 to 80 percent. The moisture factors may also be improved by using transient methods for measuring thermal conductivity especially on moist specimens to avoid moisture migration problems.

6) Finally, it would be worth while to conduct a study into the effectiveness of the use of heat flux meters for measuring thermal conductivity of concrete over a wide density range. The technique is now becoming an established method and may prove to be useful in measuring the thermal conductivity of concretes.

REFERENCES

1. British Standards 874: Pt. 2: Section 2.2:"Methods for determining thermal insulating Properties; Unguarded hot-plate method" British Standards institution, UDC 536. 212. 001. 4, 1988.

2. Jakob, M. , "Heat transfer" , Vol. 1, London, Chapman and Hall, 1949.

3. Biot, J.B., "Bibliothéque britannique" , Vol.27, P.310 1804.

4. Fourier, J.B.J. ,"Théorie analytique de la chaleur." , comprising some of his papers since 1807, English translation by Freeman, Cambridge, 1822.

5. British Standards 874 (1986), "Methods for determining thermal insulating properties.":

Part 1. Introduction, definitions and principles of measurement.

Part 2. Tests for thermal conductivity related properties.

Section 2.1 Guarded hot-plate method.

British Standards Institution UDC 536.21:43.08

Section 2.2 Unguarded hot-plate method[1].

Section 2.3 Heated -disc method for sheet materials.

Section 2.4 Heat-flow meter method.

Section 2.5 High-temperature guarded hot-plate method.

Section 2.6 Water calorimeter method.

Section 2.7 Hot-pipe method.

6. British Standards 874 :1973 and AMD 3006 (Aug.79), AMD 5173 (Oct. 86) " Methods for determining thermal insulating properties with definitions of thermal insulating terms.", British Standard Institution UDC 536. 21.

7. C.I.B.S.E. Guide A3, "Thermal properties of building structures.", C.I.B.S.E., London, 1986.

8. Jackob, M. and Hawkins, G.A. , " Elements of heat transfer.", John Wiley & Son Third edition, 1957.

9. Luikov, A. V., " Heat and mass transfer in capillary-porous bodies. " Pergammon Press Ltd. 1966.

10. Bayley, F.J., Owen, J.M. and Turner,A.B, et al, " Heat transfer " ,Nelson Publ. , 1972.

11. Simpson,A. and Stuckes, A.D., "Thermal conductivity of porous materials:1 theoretical treatment of conduction processes.", B.S.E.R. & T. Vol.7, No. 2, pp. 78-86, 1986.

12. Stephenson, M.E. and Mark, M., " Thermal conductivity of porous materials. ", ASHRAE Transactions No. 1739, pp.170-84, 1961.

13. Arnold, P.J. , " Thermal conductivity of masonary materials. ", Building Research Establishment, Current paper 1/70, Jan. 1970.

14. Krischer, O. and Rohnalter, H., "Wärmeleitung und damp diffusion in feuchten gütern (Heat conduction and vapour diffusion in damp materials.)", Düsseldorf, [VDI, Forschungsheft 402], 1940.

15. Loudon, A.G., " The effect of moisture content on thermal conductivity of autoclaved aerated concrete.", Amsterdam, Elsevier Scientific Publishing, pp. 131-41, 1983.

16. Krischer, O., " Heat conductivity and water vapour diffusion in materials for insulation against cold. ", Wärme und Kaltetechnik, Vol.43, No.1, pp.2-4, 1941.

17. Loudon, A.G., " The thermal and acoustic properties of lightweight concretes. ", Building Research Station, Design Series 45, 1967.

18. Stuckes, A.D. and Simpson, A., "The effect of moisture on the thermal conductivity of aerated concrete. ", B.S.E.R & T., Vol.6, No.2, pp. 49-53, 1985.

19. Stuckes, A.D., Tinker, J.A. and Simpson, A. , "The effect of moisture on the thermal conductivity of lightweight aggregate concrete.", B.S.E.R & T., Vol.7, No.1, pp.27-32, 1986.

20. Valore, R.C. , " Calculation of U-values of hollow concrete masonry. " , A.C.I. manual of concrete practice, 213 R-79, Part 1, 1983.

21. Valore, R.C., " Calculation of U-values of hollow concrete masonry. ", American Concrete Inst., Vol.2, No.2, pp.40-63, Feb. 1980.

22. Euchen, A. , " Forsch. Gebiete Ingenieurw.", B3, VDI - Forschungsheft, 353, 1932; Vol.11, No.6, 1940.

23. Russell, H.W. , " Principles of heat flow in porous insulators. ", Jrl. of Amer. Ceram. Soc. , Vol.18, pp.1-5.

24. Ribaud, M. ,Chal et Industr. Vol. 18, pp. 36-43, 1937.

25. Waddams, A.L. , Jrl. Soc. Chem. Ind., London, Vol. 63, P.357, 1944.

26. Francl, J. and Kingery, W. D. , Jrl. of Amer. Ceram. Soc. Vol.37, pp.99-107, 1954.

27. Loeb, A. L., " A theory of thermal conductivity of porous materials.", Jrl. Am. Ceram.Soc., Vol.37, No.2, pp.96-99, 1954.

28. Krischer, O. and Esdorn, H., " Heat transfer in damp porous substances of different structures.", Forschung auf dem Gebiete des ingenieurmesens, Vol. 22, No.1, 1956.

29. Kingery, W.D. and Klein, L. , Trans. Amer. Soc. Mech. Engrs. Vol.80, pp.705-10, 1958.

30. Sugawara, A. and Yoshizawa, Y., " An investigation on the thermal conductivity of porous materials and its application to porous rock. " , Austral. Jrl. Phys. , pp.469-80, 1961.

31. Gunst, E.V. and Zuilen, D.V. , " The influence of moisture content on the thermal conductivity of building materials.", Building Research Congress pp. 94-98, 1951.

32. Salmang, H. and Frank, H. , "Measuring thermal conductivity of refractory materials at high temperatures.", Sprechsaal, Vol.64, pp;127-29, 145-48, 165-67, 187-89, 205-8, 1931.

33. Jakob, M., "Heat transfer through ceramic materials.", Ceram. Abstr., Vol.7, No.7, P.454, 1928.

34. Herbst, H.," Gas permeability, resistance to pressure, thermal conductivity, thermal expansion, heat capacity and inclination to breaking of refractory brick dependence on porosity. ", Feuerungstech, Vol.22, No. 10, 1934, pp.115-16; Ceram. Abstr., Vol.14, No.3, P.72, 1935.

35. Green, A. T., "Comparison of temperature diffusivities and thermal conductivities of silica and fire-clay refractories. ", Trans. Ceram. Soc. (Engl.), Vol.26, No.3, pp.168-76; 1926-27, Ceram. Abstr., Vol.7, No.5, P.298, 1928.

36. Easter, G. J., "Pores in brick.", Jrl. Am. Ceram. Soc. Vol.11, No.10, pp.764-68, 1928.

37. Ganjian, E. , " The relation between porosity and thermal conductivity in engineering materials.", M.Sc. (Eng.) dissertation , Dept. of Civ. Eng. , Leeds University, 1986.

38. Tinker, J . A . , " The microstructure of selected lightweight aggregates and its relevance to the thermal conductivity of concrete blocks.", Proc. of the British masonry Society, pp.18-21, No. 2, April 1988.

39. Hanson, J.M., " Pelletised slag better insulation? " , Jrl. of CIBSE, 1982.

40. Davey, N. , " Concrete mixes for various building purposes ", Proc. of a symposioum on mix design and quality control of concrete, Cement and Concrete Assn. London, pp.28-41, 1954.

41. Mitchell, L.J. , " Thermal properties. ", A.S.T.M. Sp. Tech. Publicn. No.169, pp.129-135, 1956.

42. Rhodes, J.A. , " Thermal properties. ", A.S.T.M. Sp. Tech. Publicn. No.169B, pp.242-61, 1978.

43. Cammerer, W.F., "Conductibilité thermique de bétons et matériaux non faconnés dans l intervalle de température compries entre 200 et 900°C.", Bulletin de la society francaise de ceramique,No.98,pp.31-36,1973.

44. Kittel, C., "Interpretation of thermal conductivity of glasses. ", Phys. Rev., Vol.75, No.6, pp.972-74, 1949.

45. Van Geen, M.G. and Fiorato, A.E., " Thermal properties of masonry materials for passive-solar design. ", Portland Cement Association, Skokie, Report No.DOE/CE/30739-T1, 93p., Apr.1983.

46. Harada, T. , Takeda, J. , Yamane, S. and Furumura, F. " Strength, elasticity and thermal properties of concrete subjected to elevated temperatures. ", Int. Seminar on Conc. for nuclear reactors, Amer. Conc. Inst. Sp. Publicn., No.34.1, pp.377-406, 1972.

47. Eucken, A. , Physik. Zeitschr, Vol.12, P.1005, 1911.

48. Saare, E. and Jansson, I. , " Measurement of thermal conductivity of moist porous building materials. ", Lightweight concrete, RILEM, 1960.

49. Cabrera, J.G. , " The porosity of concrete. ", a paper presented to the Concrete Research Seminar, University of Leeds, July 1984.

50. Schuhmeister, Ber.K., Akad.Wien (Math Naturrur Klasse) Vol.76, P.283, 1877.

51. Austin, J. B. , " Factors influencing the thermal conductivity of non-metallic materials. ", Symp. on thermal insulating materials, ASTM , pp.3-67, 1939.

52. Speakman, J.B. and Chamberlain, N.H. , " The thermal conductivity of textile materials and fabrics. ", Jrl. Text. Inst., Vol.21, P.T29, 1930.

53. Baxter, S. , " The thermal conductivity of textile. ", Proc. Phys. Soc., Vol.58, P.105, 1946.

54. Maxwell, J. C. , " A treatise on electricity and magnetism.", 3rd Edit., Vol.1, Oxford Clarendon press, P.440, 1892.

55. Brailsford, A. D. and Major, K. G. , " The thermal conductivity of aggregates of several phases,including porous materials.",British Journal of Applied Physics, Vol.15, P.313, 1964.

56. Tinker, J.A. , " Modelling the thermal conductivity of multi-phase materials containing moisture.", Numerical Methods in thermal problems, Vol.5, Part 1, pp.669-80, 1987.

57. Reynolds, J. A. and Hough, J. M. , Proc. Phys. Soc., London, Vol.B70, P.769, 1957.

58. Pratt, A. W. , " Heat transfer in porous material ", Research, Vol. 15, No.5, pp.214- 244, May 1962.

59. Campbell - Allen, D. and Thorne, C. P. ," The thermal conductivity of concrete. " , Magazine of concrete research, Vol.15, No.43, pp.39-48, March 1963.

60. Huang, C.L.D. , "Multi-phase moisture transfer in porous media.", Proc. of the Multi-phase flow and heat transfer symp-workshop, publ. by Hemisphere publ. corp. , Washington D.C. and NY. , pp. 2429-2445, 1980.

61. Huang, C.L.D. , "Multi-phase moisture transfer in porous media subjected to temperature gradient.", International Jrl. of Heat and Mass transfer, Vol.22, No.9. pp.1295-1307, Sep. 1979.

62. Woodside, W. and Cliffe, J.B. ,"Heat and moisture transfer in closed systems of two granular materials." Soil Sci. , Vol.87, pp.75-82, 1959.

63. Philip, J.R. and De Vries, D.A. , "Moisture movement in porous materials under temperature gradients.", Trans. Am. Geophys. Union, Vol.38, pp.222-232, 1957.

64. Gurr, C.G. , Marshall, T.J. and Hutton J.T. ,"Movement of water in soil due to a temperature gradient." ,Soil Sci. , Vol.74, pp.335-345, 1952.

65. Powers, T. C. , "Structural and physical properties of hardened Portland cement paste. ", Journal of the American Ceramic Society, Vol.41, No.1, pp.1-6, 1958.

66. Lea, F. M. , "The chemistry of cement and concrete", 3rd edition, Edward Arnold publishers London, 1980.

67. Powers, T. C. and Brownyard, T. L. , "Studies of the physical properties of hardened portland cement paste.", Proc. American Concrete Institute, Vol.43, pp.101-132, 1947.

68. Powers, T. C., "Mechanisms of shrinkage and reversible creep of hardened cement paste.", Proc., International Conf. on the structure of concrete, London, pp.319-344 1965.

69. Feldman, R. F. and Sereda, P. J., "A model for hydrated portland cement paste as deduced from sorption length change and mechanical properties.", RILEM, Materials and structure, Vol.1, pp.509-519, 1968; Vol,2, pp.155-162, 1969.

70. Helmuth, R. F. and Verbeck, G. J. , "Structure and physical properties of cement paste.", 5th International Symposium on the Chemistry of Cement, Tokyo, Paper III-I, pp.1-32, 1968.

71. Diamond, S. , "A critical comparison of mercury porosimetry and capillary condensation pore size distributions of portland cement pastes.", Cement and Concrete Research, Vol.1, pp.531-545, 1971.

72. Winslow, D. N. and Diamond, S., "A mercury porosimetry study of the evalution of porosity in portland cement.", Jnl. of Materials, Vol.5, No.3, pp.564-585, 1970.

73. Cusens, A. R. and Cabrera, J. G. , " Developments in concrete and related materials.", Inst. Physc. Conf. No.89, pp.237-249, 1987.

74. British Standards Institution, B.S. 12:1989, "Portland Cements.", B.S.I., UDC 666-942, London, 1989.

75. British Standard Institution, B.S. 812, " Testing aggregates ",
Part 2 and Amendment 4615, "Methods for determination of physical properties.", B.S.I. London, 1984.
Part 101, "Guide to sampling and testing aggregates." B.S.I. London, 1984.

76. British Standard Institution, B.S. 3681: Part 2 , " Methods for sampling and testing of lightweight aggregates for concrete." B.S.I., London, 1973 (1983).

77. Emery, J.J. ,"Pelletised lightweight slag aggregates". Proceeding of the 2nd Inter. Congress on lightweight concrete, London, pp.36-46, Apr.14-15, 1980.

78. Margesson, R.D. and England, W.G. , "Processes for the pelletization of metallurgical slag." , U.S. Patent 3/594/142, 20 July 1971.

79. Cotsworth, R.P. , " Use of pelletized slag in concrete masonry units. ", Journal of Testing and Evaluation, Vol.6, No.2, pp.148-152, 1978.

80. British Standard Institution, B.S. 5075:
Part 2, "Specification for air entraining admixtures." B.S.I., London, 1982.
Part 3 , " Specifcication for super plastising admixtures.", B.S.I., London, 1985.

81. Sherriff, N. "Flowing concrete - An investigation into the parameters controlling the production of flowing concrete which is cohesive and non-segregating.", Cormix Technical Service Division, 10p., May 1975.

82. British Standard Institution, B.S. 882 and Amendment 5150, " Specification for aggregates from natural sources for concrete. ", B.S.I., London, 1986.

83. Cabrera, J. G. , " Design of concrete for minimum porosity.", 18th Concrete Research Seminar, University of Leeds, Concrete society, 1985.

84. Wainwright, P. J. , Cabrera, J. G. and Alamri, A. , "Durability aspects of cement mortars related to mix proportions and curing conditions. ", Proc. of the First Int. Conf. on Deterioration and Repair of Reinforced Concrete in the Gulf, Vol.1, Bahrain, 1985. pp. 453_465.

85. American Society for Testing and Materials, " Standard definitions of terms relating to concrete and concrete aggregate. " , C 125-66, Philadelphia, Pennsylvania, ASTM, 1966.

86. British Standard Institution, B.S. 1881, " Testing Concrete",
Part 105, "Method for determination of flow."
Part 106, "Methods for determination of air content of fresh concrete."

Part 116, "Method for determination of compressive strength of concrete cubes.", B.S.I., London, 1983.

87. Deutsche Normen, D I N 1048; "Testing methods for concrete; Part 1, Fresh concrete and Hardened concrete in separately made test specimens.", Vol.1, 2.2.

88. Cement and Concrete Association, " Concrete Practice " Printed by Brickell & Son Ltd., C & CA, 1975.

89. Soshiroda,T., "Segregation characteristics of concrete containing a high-range water-reducing admixture.", Symposium on Development in the use of super-plastizers, A.C.I. Special Publication, SP-68, pp.121-130, 1981.

90. Parrot, J.E. and Stuckes, A.D. "Thermal conductivity of solids.", Pion Ltd. ,P.4, 1975.

91. Ångström, A.J, Phil. Mag., Vol. 25, P.130, 1863.

92. British Standard Institution, B.S. 1972 and Amendment 4932, " Methods of test for thermal insulating materials.", B.S.I. London, 1967.

93. Spooner, D.C., " Results of a ' round robin ' thermal conductivity test organized on behalf of the British Standards Institution", Magazine of Concrete Research, Vol.32, No.111, June 1980.

94. Tye, R.P. and Spinney, S.C., " Thermal conductivity of concrete: measurement problems and effect of moisture.", Presented at the meeting of commission BI of institute international du Froid, Washington,14-15, Sep. 1976.

95. Tinker, J. A. , " Aspects of mix proportioning and moisture content on the thermal conductivity of lightweight aggregate concretes.", A thesis submitted to the University of Salford for the degree of Ph.D. in the department of Applied Acoustics, 1984.

96. CSTB REEF 58, "Hygrothermique et ventilation.", Centre Scientifique et technique des Batiment, Paris, 1975.

97. DIN 52612 , Part 2 , " Determination of thermal conductivity by means of the guarded hot-plate apparatus.", 1984.

98. UNI - CTI 7357, "Calcolo del fabbisogno termico per il riscaldamento degli edifici." , 1974.

99. Tinker, J.A., Cabrera, J.G. and Ganjian, E., " Thermal transfer in masonry materials - Moisture correction factors.", CIB 89 11th Inter. congress on quality for building users throughout the world, User Comfort theme I, Vol.III, June 19-23 1989.

100. Stuckes, A.D. and Simpson, A., " Moisture factors and thermal conductivity of concrete.", B.S.E.R. & T., Vol.7, No.2, pp.73-77, 1986.

101. Tinker, J.A. , Cabrera, J.G. and Ganjian, E. , "The effect of moisture on the thermal conductivity of lightweight and normal-weight concretes.", B.S.E.R. & T., in publication, 1991.

102. British Standard Institution , B.S. 5328 and Amendment 4970, "Methods for specifying concrete,including ready -mixed concrete.", 1981.

103. British Standard Institution , B.S. 8110, "Structural use of concrete.", Part 1: Code of practice for design and construction, 1985.

104. Collins, R. E. , "Flow of fluids through porous materials.", Reinhold Publ. Corporation, N.Y., 1976.

105. Neville, A. M. , "Properties of concrete.", Third edition, Reprinted by Longman Scientific & Technical, 1986.

106. Keulen, H. V. , "Determination of maximum water content." Proceedings of the RILEM/IUPAC International Symposium on pore structure and properties of materials, Prague, pp.C279-C292, 1973.

107. RILEM, CP11.3, "Absorption of water by immersion under vacuum.", Materials and Structures / Research and Testing, No.101, pp.393-394, 1984.

108. Lynsdale, C. J., "The influnence of super plasticisers on the engineering properties and performance of concrete.", A Ph.D. thesis submitted to the University of Leeds in the department of Civil Eng. , 1989.

109. Cabrera, J.G. and Lynsdale, C.J. , " Measurement of chloride permeability in super-plasticised OPC and pozzolanic Cement mortars. ", International conference on 'Measurements & Testing in Civil Engineering',Lyon, pp.279-291, 13-16, Sept. 1988.

110. Rootare, H. M. , "Review of mercury porosimetry.", Advanced experimental techniques in Powder Metallurgy, Vol.5 pp.225-252, 1970.

111. Brakel, J. V. , Modry, S. and Savata, M. , "Mercury porosimetry: State of the art.", Powder Technology, Vol.29, pp.1-12, 1981.

112. ORR, C. , " Application of mercury penetration to materials analysis.", Power Technology, Vol.3, pp.117-123, 1970.

113. Micromeritics Instruction Manual for Mercury Porosimeter Model Auto pore 9200, (version 2.02 software), 1982.

114. Ritter, H.L. and Drake, L.C. , "Pore size distribution in porous materials." Industrial and Engineering Chemistry, Vol.17, No.12, pp.782-786, 1945.

115. Winslow, D. N. , " The validity of high pressure mercury porosimetry. " , Journal of Colloid and Interface Science, Vol.67, No.1, pp.42-47, 1978.

116. Diamond, S., "Cement paste microstructure- An overview at several levels.", Proc. Conf. on Hyd. cement paste, Sheffield, pp.2-30, 1976.

117. Mehta, P. K. , "Hardened cement paste- microstructure and its relationship to properties.", Proc. 8th International Congr. on the chemistry of cement, Vol. 1, Brazil, pp.113-121, 1986.

118. Taylor, H.F.W., "Chemistry of cement hydration", Proc. 8th International Congr. on the Chemistry of Cement, Vol.1, Brazil, pp.82-109, 1986.

119. Diamond, S. , "Identification of hydrated cement constituents using a scanning electron microscope energy dispersive X-ray spectrometer combination." Cement and Concrete Research Vol.2, pp.617-632, 1972.

120. Diamond,S.,"The microstructure of cement in concrete." Proc. 8th International Congr. on the Chemistry of Cement, Vol.1, Brazil, pp.122-147, 1986.

121. Pratt, P. L. and Jennings, H. M. , "The microchemistry and microstructure of portland cement.", Ann. Rev. Mater. Sci. Vol.11, pp.123-149, 1981.

122. Ciach, T. D. and Swenson, E. G. , "Morphology and microstructure of hydrated portland cement and its constituents.", Cement and Concrete Research, Vol.1, Nos.1 to 5, pp.143-158, pp.159-176, pp.257-272, pp.367-384, pp.515-530, 1971.

123. Czernin, W., "Cement Chemistry and Physics for Civil Engineers.", 1st edition, Croshy Lockwood & Son Publ., London, 1962.

124. Taylor, H.F.W. , "The Chemistry of Cement." , Academic press, London and New York, 1964.

125. Powers, T. C., "Some physical aspects of the hydration of Portland cement.", Journal of the PCA Research and Development Laboratories, Vol.3, No.1, pp.47-56, 1961.

126. Lerch, W. , " The influence of gypsum on the hydration and properties of portland cement. ", Proceedings of the American Society for Testing Materials, Vol.46, pp.1252-1292, 1946.

127. McCarter, W. J. and Curran, P. N. , " The electrical response characteristics of setting cement paste. ", Magazine of Concrete Research, Vol.36, No.126, pp.42-49, 1984.

128. Mindess,S. and Young, J.F., "Concrete", Prentice-hall, Inc., Englewood Cliffs, New Jersey, U.S.A, 1981.

129. Midgley, H. G.,"The determination of calcium hydroxide in set Portland cements.", Cement & Concrete Research, Vol.9, pp.77-82, 1979.

130. Keattch, C. J. and Dollimore, D. , "An introduction to thermogravimetry", Heyden and Son Ltd., 2nd edition, 1975.

131. Longuet, P.,"The use of thermogravimetric measurements in cement chemistry.", Proceedings of the 5th Inter. Symp. on the chemistry of cement, Tokyo, Vol.I, Part I pp.239-251, 1968.

133. Bensted, J. , "Some applications of thermogravimetry to portland cement.", Il Cemento, Vol.77, No.3, pp.169 -182, 1980.

133. Cabrera J.G. and Plowman, C. , "Hydration and microstructure of High PFA content concrete.", Proceedings of the International CIRIA Conference on Rolled concrete for dams, London, June 1981.

134. Bye, G.C. , " Portland cement, composition, production and properties. " , Pergammon Press, Materials Engineering Practice Series, 1983.

135. Taplin, J. H. , " A method for following the hydration reaction in Portland cement paste. ", Australian Journal of Applied Science, Vol.10, pp.329-345, 1959.

136. Cabrera, J.G. , " Hydration of ordinary and super-plasticized cements.", First International Conf. of Material's Technology, American Ceramic Society, Anaheim, California, 1989 (to be published).

137. Stanton Redcroft, Instruction Manual for the Stanton Redcroft TG-750 thermobalance, London.

138. Cabrera, J. G. and Clease, P. , "Data retrieval from a thermogravimetric balance using a microcomputer", In preparation.

139. Verbeck, G. J. , " Carbonation of hydrated Portland cement.", ASTM SP Tech., Publication No.205, pp.17-36, 1958.

140. Leber, I. and Blakey, F. A. , " Some effects of carbon dioxide on mortars and concretes. " Journal of the American Concrete Institute, Vol.28, No.3, pp.295-308, 1956.

141. Hilsdorf, H.K., Kropp, J. and Gunter, M.,"Carbonation, Pore structure and durability.", Proceedings of the RILEM seminar on the durability of concrete structures under normal outdoor exposure, Hanover, pp.182-196, 1984.

142. Cabrera, J. G. , Cusens, A. R. and Ramezanianpour, A. "The effect of curing conditions on the carbonation of mortars containing cement, PFA, Silica fume and

Trass.", Proc. of the First Int.Conf. on Deterioration and repair of Reinforced concrete in the Gulf, Vol.2 Bahrain, 1985, pp. 183-200.

143. Wierig, H.J., "Long time studies on the carbonation of concrete under normal outdoor exposure.", Proceedings of the RILEM Seminar on the durability of concrete structure under normal outdoor exposure, Hanover, pp. 239-244, 1984.

144. Houst, Y.F. , Roelfstra, P.E. and Wittmann, F.H. , "A model to predict service life of concrete structure.", International conference on Materials Science and Restoration, Esslington, pp.181-186, 1983.

145. Lawrence, C. D. , " Durability of concrete: Molecular transport processes and test methods. ", Cement and Concrete Association, Technical Report 544, 1984.

146. Pihlayavaara, S. E. , " Some results of the effect of carbonation on the porosity and pore size distribution of cement paste. ", Materials and Structures, Vol.1, No.6, pp.521-526, 1968.

147. Ramezanianpour, A.A. , " Properties and durability of pozzolanic cement mortars and concretes.", A thesis submitted for the degree of Ph.D. in the department of civil engineering at the University of Leeds, 1987.

148. Cabrera, J.G., " The use of pulverized fuel ash to produce durable concrete.", Improvement of concrete durability, Thomas Telford Ltd. , pp. 19-36, 1985.

149. Gowripalan , N. , Cabrera , J.G. , Cusens , A.R. and Wainwright, P.G. , " Effect of curing on durability.", ACI Concrete Inter.: Design and Construction, Vol.12, No.2, pp.47-54, Feb. 1990.

150. Verbeck, G. , " Pore structure in hardened concrete." Tests and properties of concrete and aggregates, pp. 136-142.

151. Williamson,R.B., "Solidification of portland cement.", Report No. UC SESM 70 - 23, University of California, Berkeley, Dec. 1970.

152. Ramachandran, V.S. and Zhang chun-mei, " Cement with calcium carbonate additions. ", 8th International congress on the Chemistry of Cement, Brazil, pp.22-27, Sept. 1986.

153. Pagano, M.A. and Cady, P.D., "Chemical approach to the problem of alkali - reactive carbonate aggregates. ", Cement and Concrete Research, Vol. 12, pp. 1-12, 1982.

154. Tewfik, Moneer, F., Shoeb and Nabil, " Effect of some fillers on the properties of sulphur concrete.",Inter. Jrl. for Housing Science and its applications, Vol.4 , No.1, pp.39-46, 1980.

155. Dinku, A., " The influence of limestone aggregates and limestone fillers on the properties of concrete.", A thesis submitted for the degree of M.Phil. in the department of civil engineering at the University of Leeds, June 1990.

APPENDIX I

S L A B M O U L D

The steel mould that was used to cast 300 × 300 × 50mm thick concrete slabs in pairs is shown in the Figure below. The thickness can be adjusted from 10 to 60 mm.

The mould was fabricated from machined 19 mm mild-steel plate throughout with all component parts capable of being removed for cleaning and oiling.

All the steel faces in contact with concrete were coated in proprietary 'mould oil' before use.

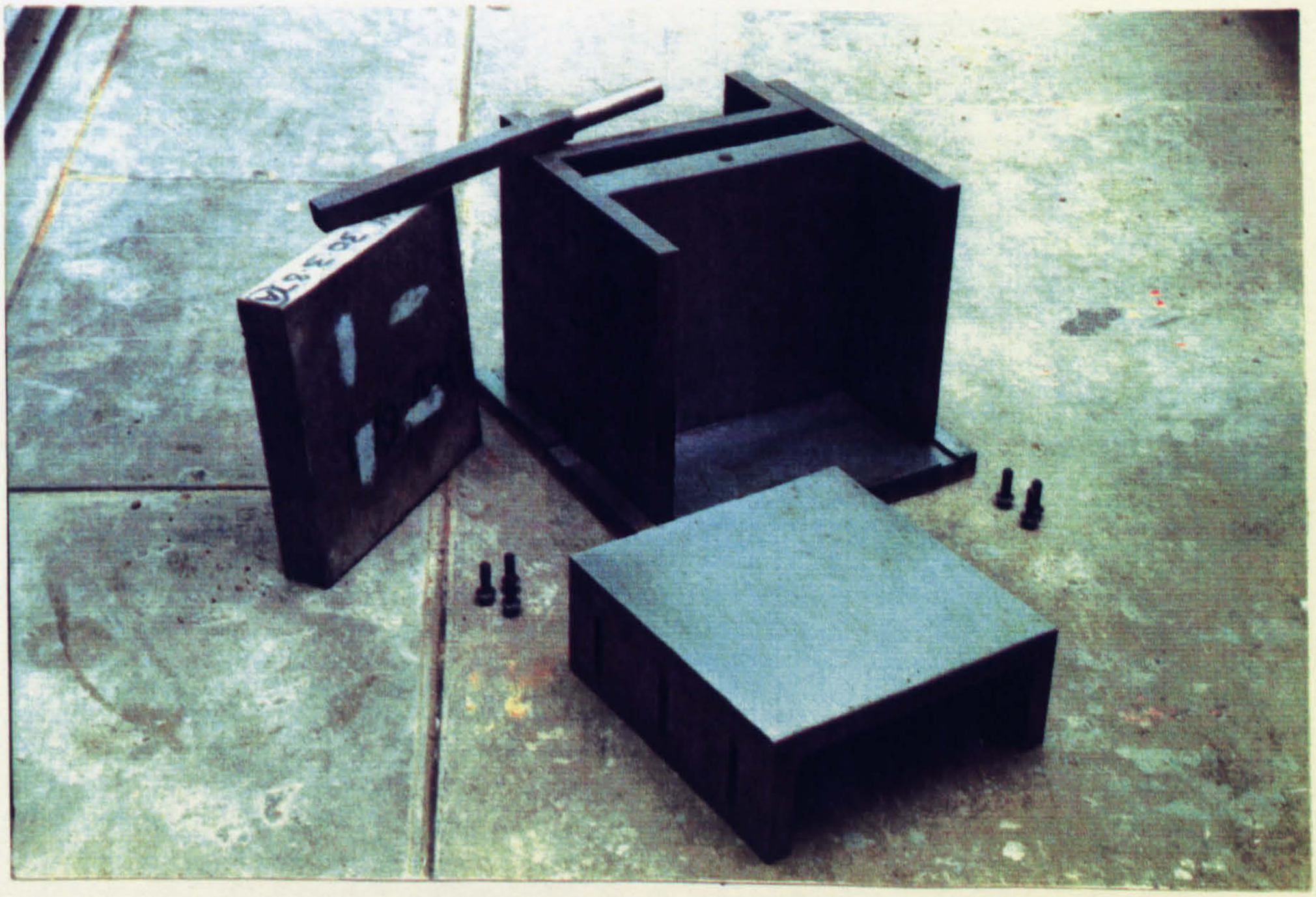

Fig.(I.1). Photograph of steel mould, square head rammer (used to compact the concrete slabs) and a typical concrete slabe.

APPENDIX II

FOIL-TYPE THERMOCOUPLES.

CONSTRUCTION AND CALIBRATION

Temperature measurements were made using 0.035mm foil-type thermocouples constructed from same batch of 0.2mm copper-constantan (type T) thermocouples. The construction of foil-type thermocouples is described below:

Thermocouple construction: Glass-fiber outer insulation is removed for 70mm from one end of a 2m length of thermocouple wire. Secondary insulation surrounding the fine copper and constantan wires is also removed for about 40mm. The bared wires are then twisted tightly at their tip and welded using an argon arc welder (Figure II.1).

When a satisfactory bead is formed, it is cleaned with alcohol to remove any deposits. The bead and about 20mm length of wire is then rolled out to a flatness of about 0.035mm thickness using a miniature roller as shown in Figure II.2.

Thermocouple calibration: The clibration of the thermocouples was performed using working temperature of 0°C to 40°C by measuring their outputs using a Data precision 3600 digital Volt meter with a resolution of 1μV.

The reference junction was kept at 0°C in a bath of well stirred ice and water. The water temperature was measured by a 0.1K resolution mercury in glass precision

thermometer. The hot junction of the thermocouples was maintained at 0, 10, 20 and 40 °C using Techne DB-40L Dri-Block Calibrator with temperature stability of ± 0.05 °C. Thermocouples with output value within ± 1μV of BS 4937: Part 5 reference tables were chosen to use in the plain hot-plate apparatus.

Fig.(II.1) Photograph of electric arc welder and argon gas bottle.

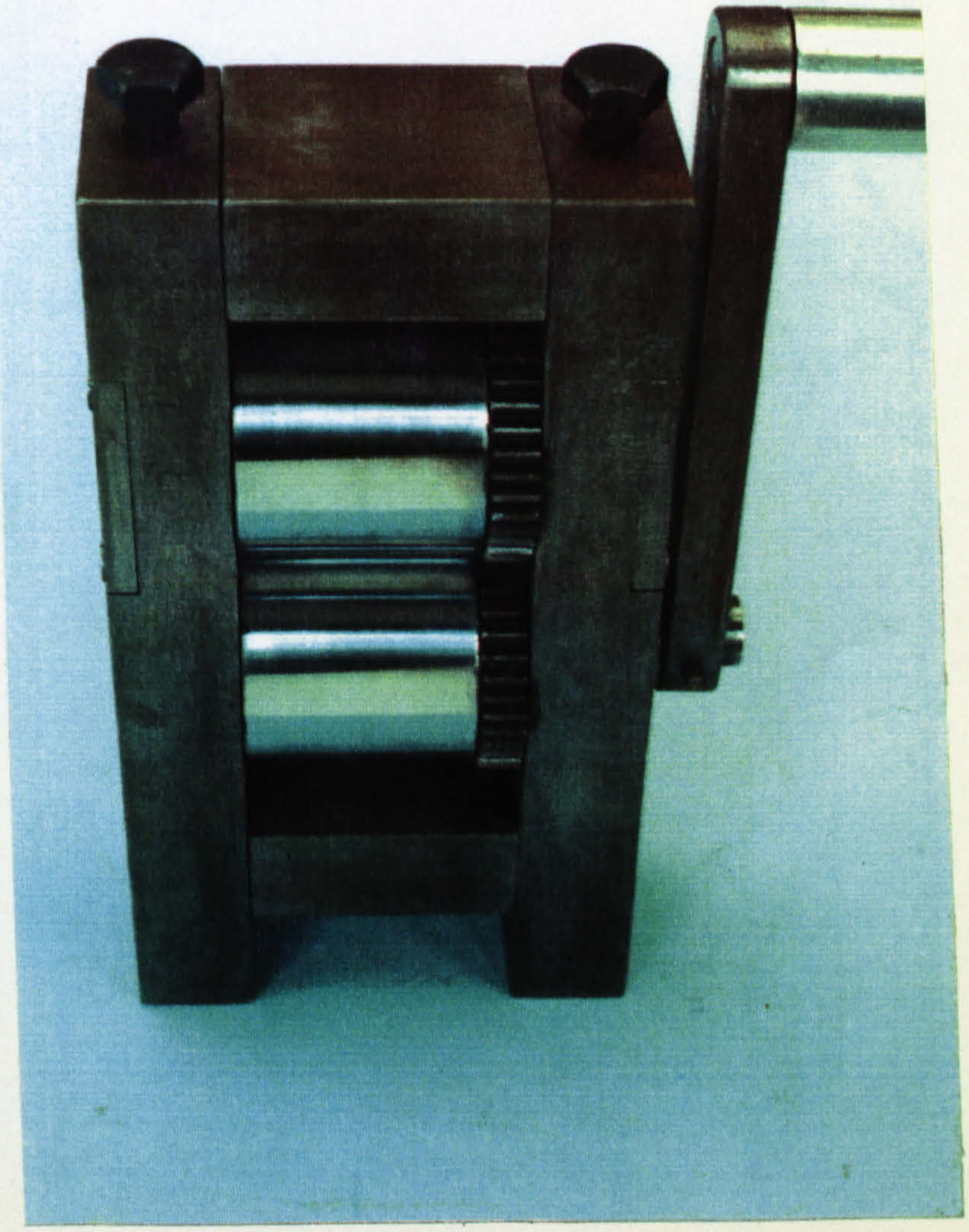

Fig.(II.2) Miniature roller designed to flatten the beads to .035mm thickness. The chrom plated drum rollers are 55mm in diameter, made of mild-steel.

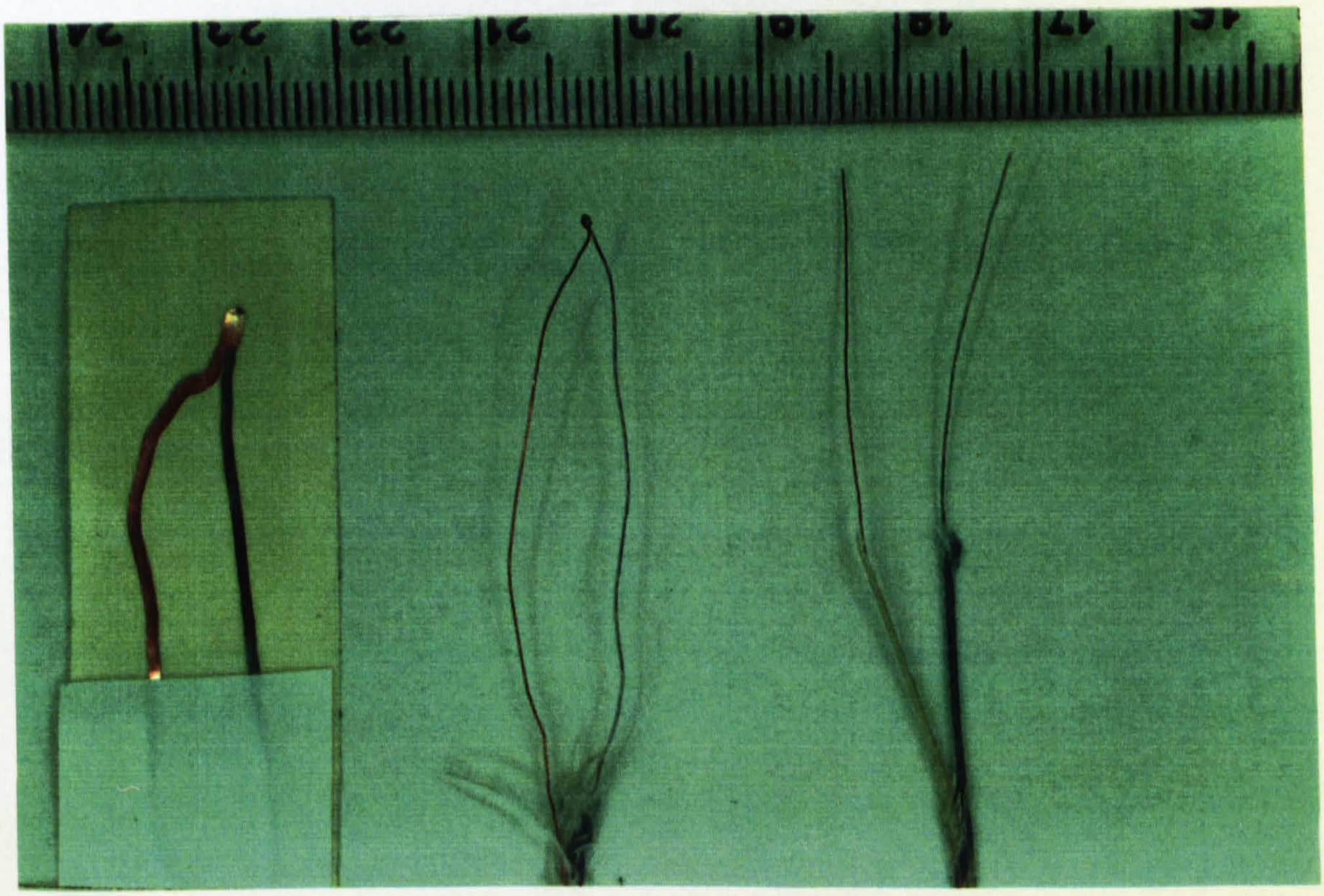

Fig.(II.3) Photograph of thermocouple's bare wires on the right, bead joined by arc welding in the centre and after flattening, calibrating and mounting on adhesive tape on the left.

APPENDIX III

SELECTED THERMAL CONDUCTIVITY PRINT-OUTS

TO DETERMINE CORRECTED K VALUE AT 1%,3% AND 5%.
RIG A. 50MM SLABS.
SLAB REF.
DATE

TEST - QCE08-A3

	RUN 1		RUN 2	RUN 3
AV CS TEMP A	10.131		10.13925	10.1715
AV CS TEMP B	9.3025		9.33025	9.372249
AV HS TEMP A	25.9865		25.98175	26.0105
AV HS TEMP B	26.83925		26.82675	26.86225
TEMP DIFF (DELTA) A	15.8555		15.8425	15.839
TEMP DIFF (DELTA) B	17.53675		17.4965	17.49
RANGE HS TEMPS B	26.82675	-	26.86225	
RANGE HS TEMPS A	25.98175	-	26.0105	
RANGE CS TEMPS A	10.131	-	10.1715	
RANGE CS TEMPS B	9.3025	-	9.372249	
VOLTAGE	44.198		44.198	44.197
CURRENT	2.6926		2.6926	2.6926
AV TEMP DIFF (DELTA)	16.67671			
AV SAMPLE TEMP	18.07948			
INITIAL K (W/MC)	1.952999		1.956119	1.956661
AV K (W/MC)	1.955259			
EDGE LOSS (W)	.7940338			
CORRECTED K (W/MC)	1.942214			
AV SLAB AREA	9.004404E-02			
THICKNESS SLAB A	.0491633			
THICKNESS SLAB B	.0495233			
DRY BULK DENSITY A	2013.842			
DRY BULK DENSITY B	2026.113			
MEAN DRY DENSITY	2019.977			
DEV FROM MEAN (%) A	-.303741			
DEV FROM MEAN (%) B	.303741			
MASS PRIOR TEST A	9.016			
MASS AFTER TEST A	9.012			
MASS OVEN DRY A	8.915			
MASS PRIOR TEST B	9.134			
MASS AFTER TEST B	9.13			
MASS OVEN DRY B	9.035			
MC (% WT)PRIOR TEST A	1.13292			
MC (% WT)PRIOR TEST B	1.095739			
MC (% WT)AFTER TEST A	1.088055			
MC (% WT)AFTER TEST B	1.05147			
% VOL MC CHANGE	9.002423E-02			
AV VOL MC % DURING TEST	2.205908			
K VALUE AT 1%=	1.864993			
K VALUE AT 3%=	1.993064			
K VALUE AT 5%=	2.121134			

APPENDIX IV

SELECTED TG AND DTG'S RESULTS

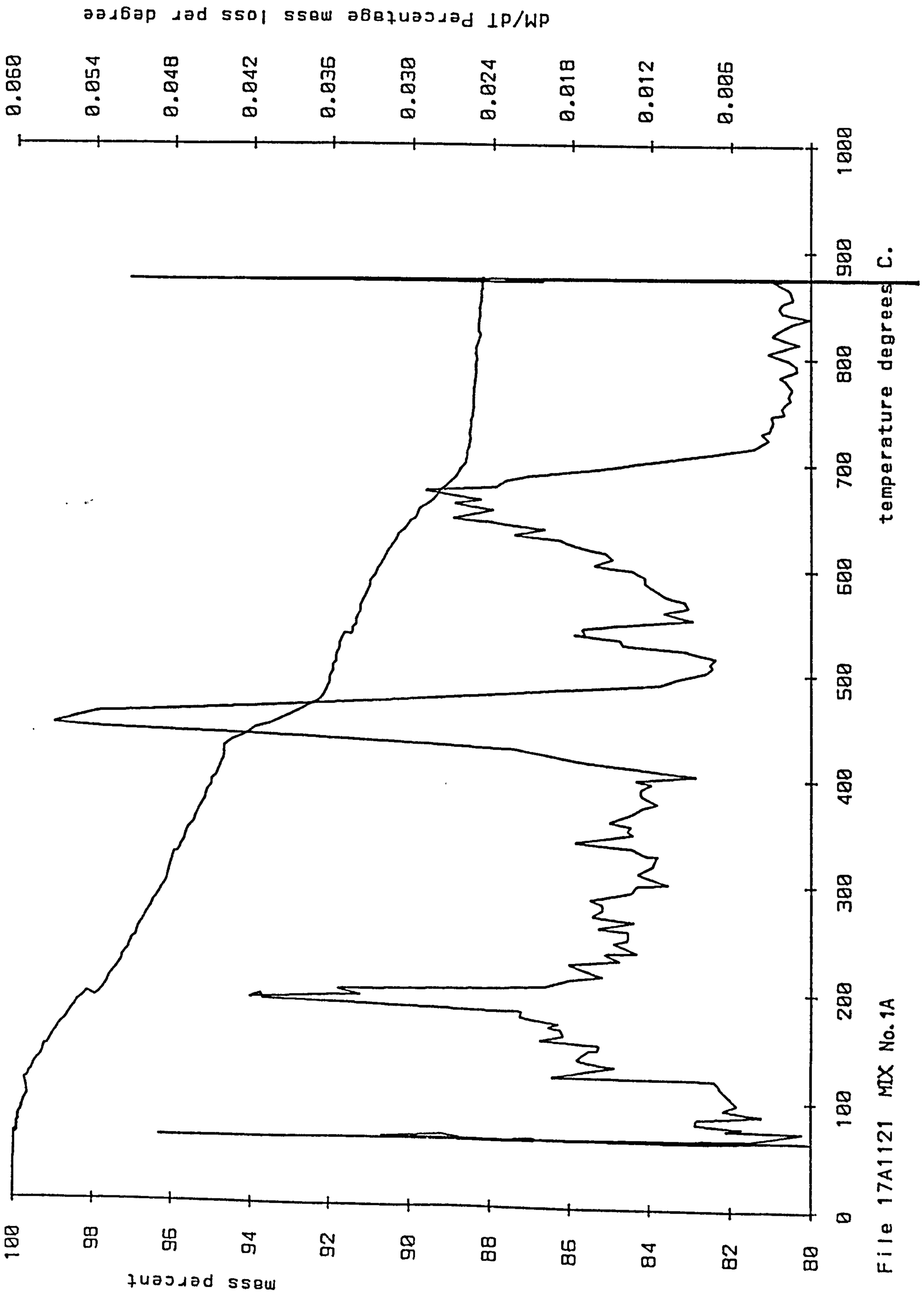

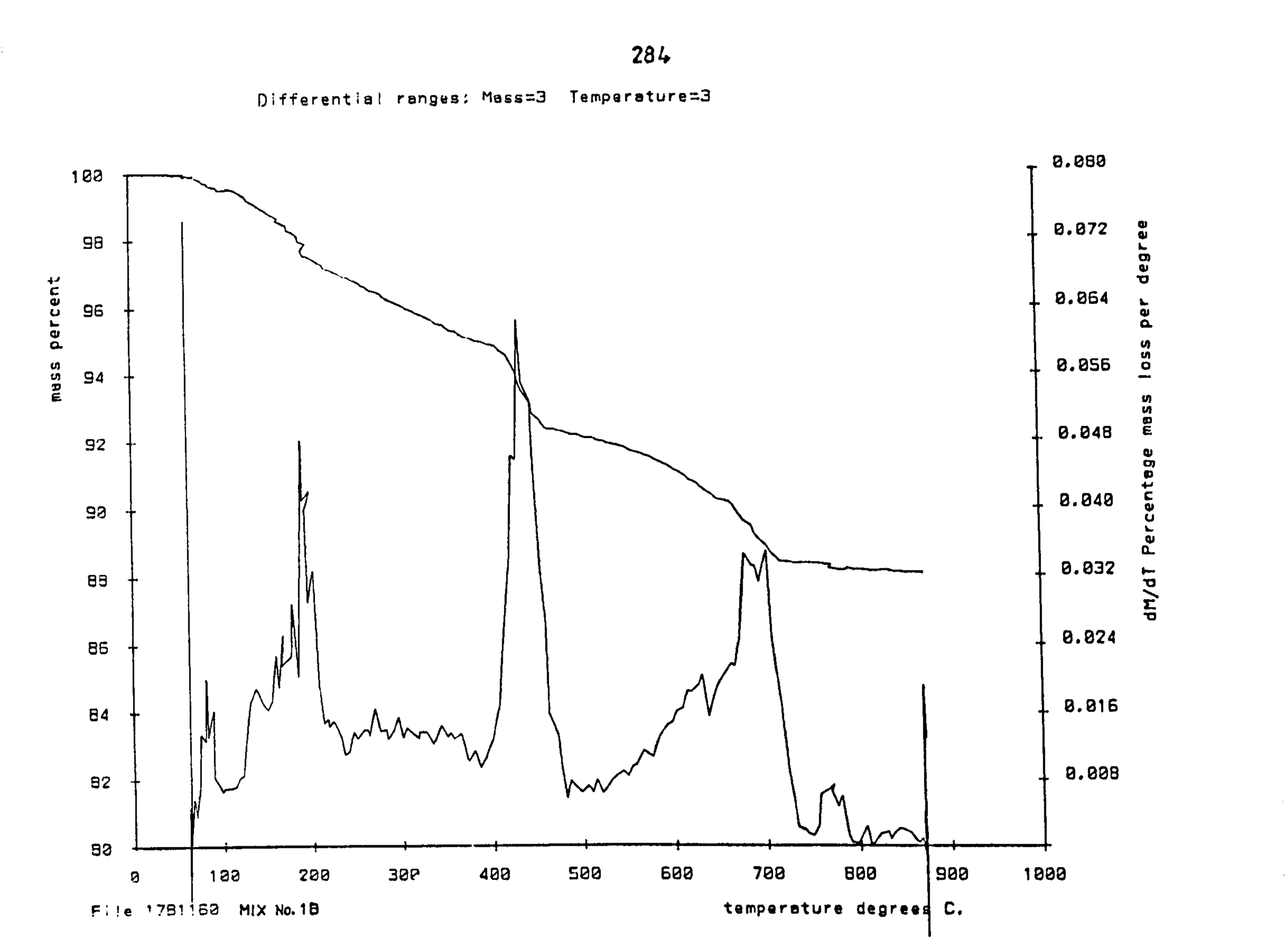
Differential ranges: Mass=3 Temperature=3
mass percent
100
98
96
94
92
90
88
86
84
82
80
0.080
0.072
0.064
0.056
0.048
0.040
0.032
0.024
0.016
0.008
dM/dT Percentage mass loss per degree
0
100
200
300
400
500
600
700
800
900
1000
File 1781160 MIX No.1B
temperature degrees C.

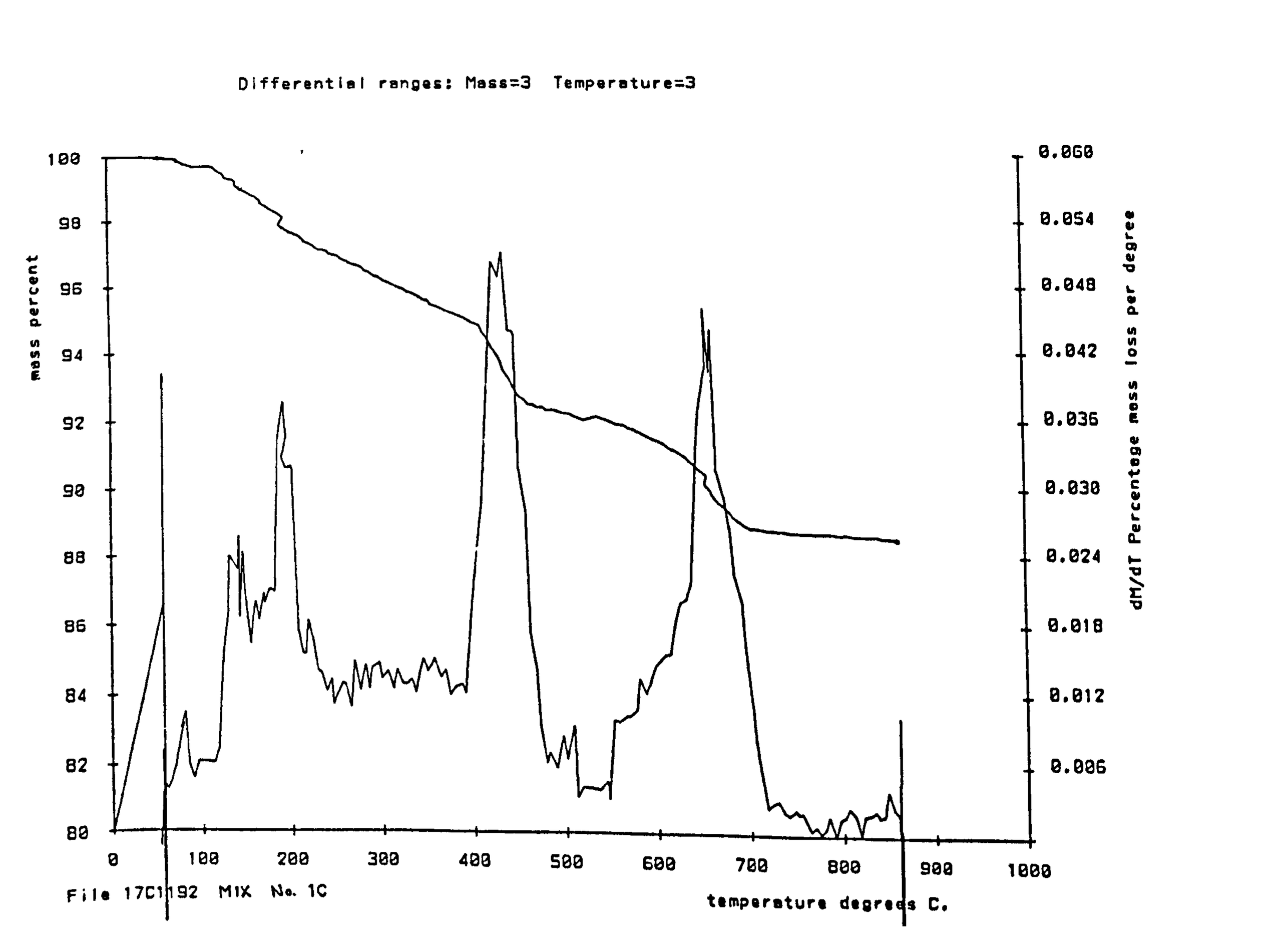
Differential ranges: Mass=3 Temperature=3
mass percent
100
98
96
94
92
90
88
86
84
82
80
0.060
0.054
0.048
0.042
0.036
0.030
0.024
0.018
0.012
0.006
dM/dT Percentage mass loss per degree
0
100
200
300
400
500
600
700
800
900
1000
File 17C1192 MIX No. 1C
temperature degrees C.

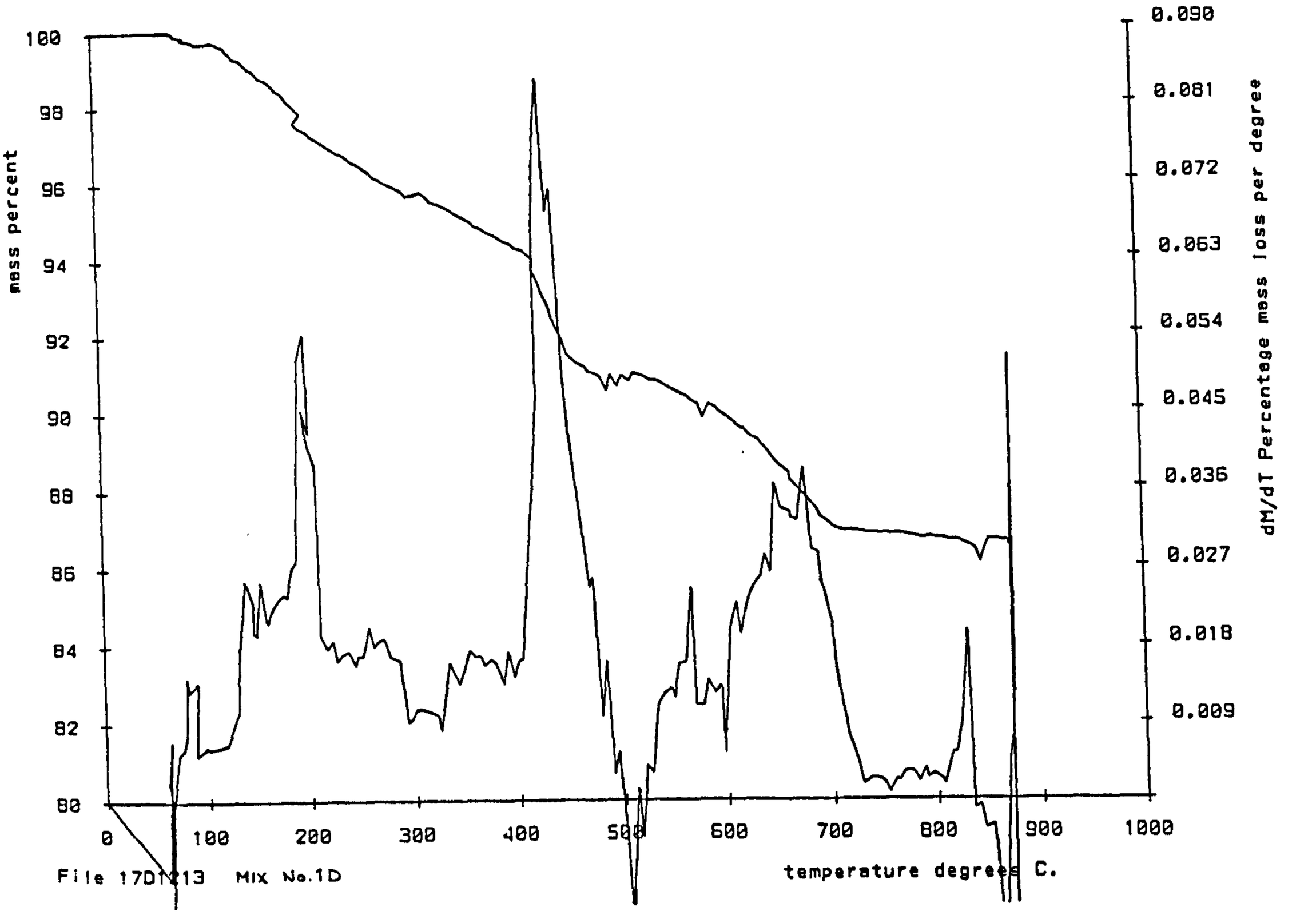
Differential ranges: Mass=3 Temperature=3
mass percent
100
98
96
94
92
90
88
86
84
82
80
0.090
0.081
0.072
0.063
0.054
0.045
0.036
0.027
0.018
0.009
dM/dT Percentage mass loss per degree
0
100
200
300
400
500
600
700
800
900
1000
temperature degrees C.
File 17D1213 MIX No.1D

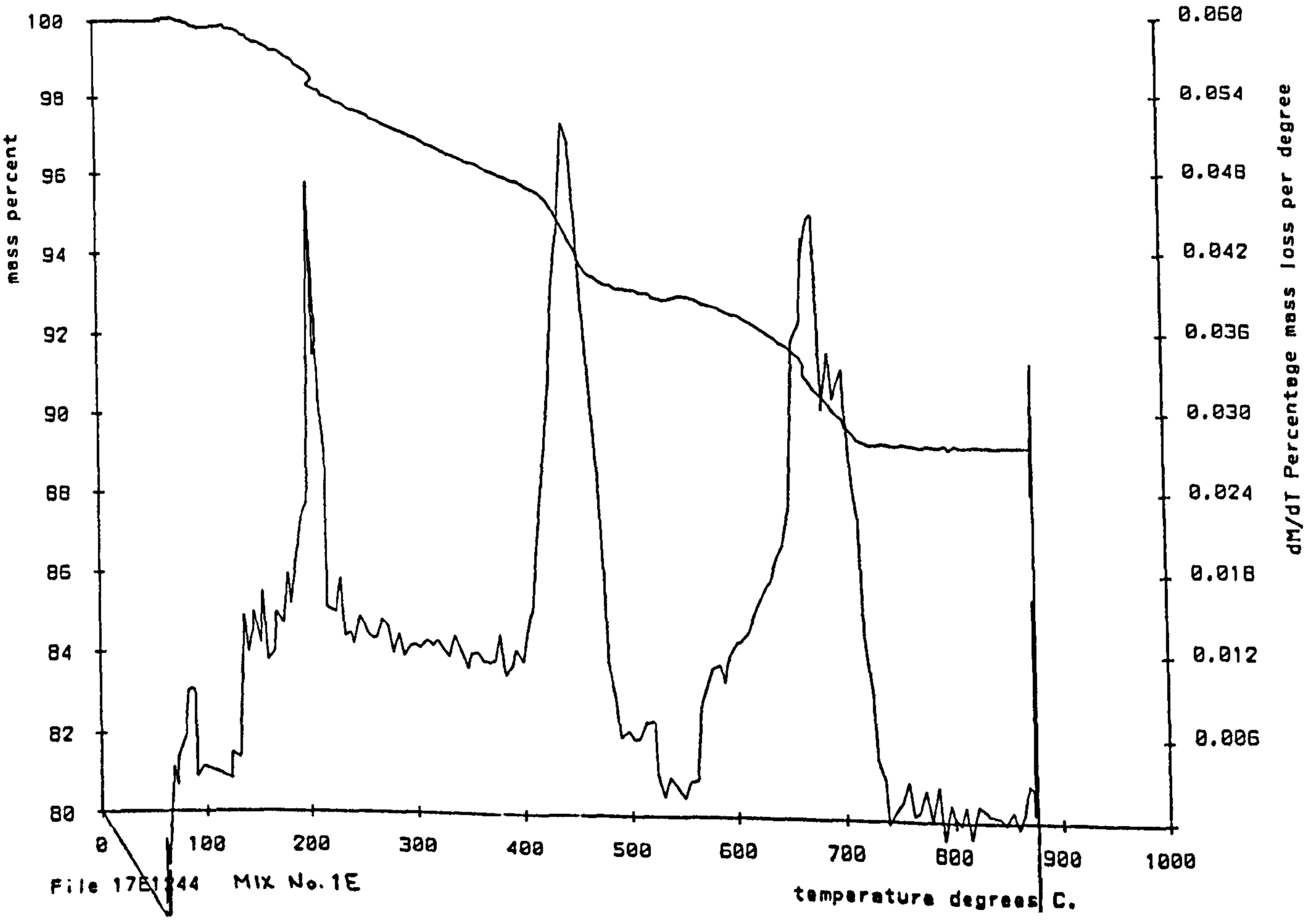
Differential ranges: Mass=3 Temperature=3
mass percent
100
98
96
94
92
90
88
86
84
82
80
0.060
0.054
0.048
0.042
0.036
0.030
0.024
0.018
0.012
0.006
dM/dT Percentage mass loss per degree
0
100
200
300
400
500
600
700
800
900
1000
temperature degrees C.
File 17E1244 MIX No.1E

APPENDIX V

CUBE COMPRESSIVE STRENGTH RESULTS

Table (V.1)

Cube compressive strength results for concretes

Mix no.	Concrete code name	Compressive strength (N/mm^2)*						
		Fog room curing				3 days fog room+65% RH 20°C curing		
		Age (days):				Age (days):		
		3	7	28	91	7	28	91
1	QA/0.53	34.7	42.8	52.1	57.0	45.8	55.1	57.7
		34.3	42.6	52.3	55.4	47.0	53.3	56.3
2	QAE/0.43	22.0	24.0	28.3	30.8	27.9	31.4	36.2
		24.3	24.6	27.5	31.6	31.5	34.8	37.0
		22.6				29.6	33.0	
		(1.19)				(1.80)	(1.70)	
3	LA/0.6	33.3	42.7	51.5	54.8	46.4	51.5	55.7
		35.4	43.7	51.5	55.4	45.1	53.0	55.4
		33.8						
		(1.10)						
4	LAE/0.5	20.0	23.2	27.5	29.8	24.5	28.9	31.3
		19.4	22.9	26.8	28.9	23.8	28.2	32.1
5	PA/0.9	16.0	22.8	36.7	38.2	24.2	27.6	32.5
		15.4	22.4	37.3	37.2	24.9	27.0	31.6
6	PAE/0.8	4.9	6.9	9.1	9.9	9.0	10.0	9.5
		4.1	6.7	9.0	11.3	8.1	8.6	9.4
		2.5			10.0	8.4	8.9	
		(1.22)			(.78)	(0.46)	(0.74)	
7	QA/0.8	20.4	25.8	41.0	44.2	30.3	42.2	45.5
		19.8	26.4	41.4	44.4	31.2	41.2	44.3
8	LA/0.8	22.3	28.1	36.8	44.4	30.2	37.4	43.6
		22.9	28.9	37.3	43.3	31.0	38.4	44.4
9	PA/0.8	18.9	26.1	34.1	33.9	23.8	31.2	32.6
		19.5	26.9	32.3	34.9	24.6	27.3	31.8
				32.0			30.0	
				(1.14)			(2.00)	
10	QB/0.8	19.4	24.0	34.0	34.8	23.7	33.4	34.0
		17.8	24.8	31.9	35.4	24.5	34.3	36.2
		18.3		33.0				35.3
		(.82)		(1.05)				(1.11)
11	LB/0.8	22.5	29.4	36.0	39.4	32.3	37.1	40.5
		23.1	28.6	36.7	40.3	33.3	36.1	39.5

(*) Values in brackets give standard deviations of the results.

Table V.1 (continued)

Mix no.	Concrete code name	Compressive strength (N/mm^2) *						
		Fog room curing				3 days fog room+65% RH 20°C curing		
		Age (days):				Age (days):		
		3	7	28	91	7	28	91
12	PB/0.8	9.7	11.6	12.9	16.6	11.8	15.0	17.2
		10.0	11.9	14.0	15.5	12.4	13.8	16.8
				13.8	16.4	11.4	14.0	
				(.59)	(.59)	(0.50)	(0.64)	
13	QB/0.56	35.2	45.0	51.6	57.7	45.9	55.0	58.8
		35.3	47.9	52.9	58.0	44.8	55.9	60.4
			45.5					
			(1.55)					
14	LB/0.66	35.6	43.5	47.0	48.6	46.1	49.9	52.8
		35.8	42.5	45.6	48.8	44.8	51.2	54.8
15	PB/1.05	9.0	10.4	10.9	12.2	9.9	13.3	16.2
		9.3	9.6	9.5	11.8	10.2	13.7	15.0
			9.9	10.5				15.8
			(.40)	(.72)				(0.61)
16	QC/0.9	15.9	19.2	23.6	25.9	21.1	25.1	25.8
		15.1	19.7	24.1	26.3	19.5	25.4	26.4
17	QCE/0.8	7.5	10.9	14.8	15.4	12.1	14.7	16.1
		7.9	10.5	15.0	15.8	11.3	15.1	15.6
18	LC/0.95	18.2	22.3	28.1	29.5	22.2	30.9	29.7
		18.6	22.7	28.8	29.3	22.8	30.0	29.3
19	LCE/0.9	6.8	9.7	11.6	12.0	9.8	12.8	13.5
		7.0	9.6	12.0	11.7	10.3	12.5	14.0
20	PC/1.29	10.1	12.5	11.6	18.0	12.0	14.4	20.6
		9.2	11.8	12.5	17.6	12.1	14.3	20.7
		9.6	12.1	12.1				
		(.45)	(.45)	(.45)				
21	PCE/1.29	2.4	3.1	4.2	4.3	3.6	4.3	4.4
		2.4	2.9	4.0	4.2	3.9	4.5	4.3
22	QC/0.8	19.6	23.3	29.7	31.3	23.3	29.4	31.1
		19.1	22.7	29.3	31.0	23.3	29.5	31.0
23	LC/0.8	21.7	26.7	33.9	37.8	29.5	33.8	38.5
		21.7	27.1	33.3	38.8	28.9	34.2	37.6
24	PC/0.8	10.8	12.0	13.9	20.9	12.4	14.7	23.1
		10.7	11.2	13.0	20.0	12.0	13.9	21.9
			11.4	13.2	20.3		14.5	21.6
			(.42)	(.47)	(.46)		(0.42)	(0.79)

(*) Values in brackets give standard deviations of the results.